

# **Radiocarbon analysis of atmospheric methane: A new setup to unravel regional methane sources**

Inaugural dissertation  
of the Faculty of Science,  
University of Bern

presented by

**Christophe Espic**

from Basadingen-Schlattingen

Supervisor of the doctoral thesis:  
Prof. Dr. Sönke Szidat

Department of Chemistry, Biochemistry and Pharmaceutical Sciences



This work is licensed under a Creative Commons Attribution 4.0 International License  
<https://creativecommons.org/licenses/by/4.0/>

**Radiocarbon analysis of atmospheric methane:  
A new setup to unravel regional methane sources**

Inaugural dissertation  
of the Faculty of Science,  
University of Bern

presented by

**Christophe Espic**

from Basadingen-Schlattingen

Supervisor of the doctoral thesis:

Prof. Dr. Sönke Szidat

Department of Chemistry, Biochemistry and Pharmaceutical Sciences

Accepted by the Faculty of Science.

Bern, 12 January 2022

The Dean

Prof. Dr. Zoltan Balogh

*“Science sans conscience n’est que ruine de l’âme”*

*François Rabelais*

# Summary

Methane ( $\text{CH}_4$ ) is the second most important anthropogenic greenhouse gas after carbon dioxide ( $\text{CO}_2$ ). The understanding of the past and future evolution of  $\text{CH}_4$  abundance in the atmosphere is a key factor in a context of climate change. Unfortunately, the complexity of natural and anthropogenic  $\text{CH}_4$  sources and sinks is a major hindrance to unraveling the present and future role of atmospheric  $\text{CH}_4$  on the climate.

A tool proposed for the distinction between biogenic and fossil  $\text{CH}_4$  sources is to measure the radiocarbon content ( $^{14}\text{C}$ ) of their emissions. As living plants and animals continuously exchange carbon with the environment through the processes of respiration and photosynthesis, their  $\text{CH}_4$  emissions contain present-day  $^{14}\text{C}$  levels. Conversely, fossil sources of  $\text{CH}_4$  such as natural gas seepage or fossil fuel burning are devoid of  $^{14}\text{C}$ , as their related  $\text{CH}_4$  emissions originate from very old organic matter containing no more  $^{14}\text{C}$ . Hence, the comparison of the  $^{14}\text{C}$  content of atmospheric  $\text{CH}_4$  of a polluted site and of free tropospheric air should allow the apportionment of regional biogenic and fossil sources of  $\text{CH}_4$ , which should in turn help developing effective mitigation strategies. Unfortunately, such measurements are expensive and time-consuming, as  $\text{CH}_4$  needs to be extracted and purified from large amounts of air. Hence, very few measurements of atmospheric  $^{14}\text{CH}_4$  have been published so far and none of them could lead to a source apportionment of regional  $\text{CH}_4$  sources.

The present thesis carries two main objectives. The first is technical, with the development of a setup allowing the preparation of pure atmospheric  $\text{CH}_4$  samples for  $^{14}\text{C}$  analysis. The second is scientific, with the collection, pretreatment and  $^{14}\text{C}$  measurement of air samples in Switzerland, the results of which are used to test the feasibility to apportion local and regional  $\text{CH}_4$  sources with the radiocarbon technique.

The procedure leading to atmospheric  $^{14}\text{CH}_4$  results is as follows: an air sample is first collected in the field by filling a bag with 60 L air using a small pump. The sample is then connected to the methane preconcentration and purification setup in the laboratory, which is composed of two parts: a preconcentration line, where  $\text{CO}_2$  and most of bulk air are removed from the sample; and a purification setup, which uses a preparative gas chromatography technique to extract and purify  $\text{CH}_4$  from all other carbon-containing gases. Pure  $\text{CH}_4$  is then combusted to  $\text{CO}_2$ , recovered in a small glass ampoule and its  $^{14}\text{C}$  content is measured with accelerator mass spectrometry. The main advantages of this setup are: efficiency, as its compactness limits the operation time and allows to prepare 3–4 samples per day; reliability, as the purity of  $\text{CH}_4$  is guaranteed by a chromatic purification; and flexibility, as  $\text{CO}_2$  is also recovered and the purification can be used as a standalone, offering the possibility to analyze high  $\text{CH}_4$  concentration samples.

We conducted biweekly  $^{14}\text{CH}_4$  and  $^{14}\text{CO}_2$  analyses of atmospheric air samples collected at three strategic sites in Switzerland. The  $^{14}\text{CH}_4$  results obtained from free tropospheric air collected at the Jungfrauoch Research Station confirm that  $^{14}\text{CH}_4$  releases from nuclear power plants kept increasing the global  $^{14}\text{C}$  content of atmospheric  $\text{CH}_4$  since the early 1970s, and address the lack of published  $^{14}\text{CH}_4$  values of clean background air since the early 2000s. Unfortunately, nuclear power plants discharging  $^{14}\text{C}$  are responsible for a very large scatter of  $^{14}\text{CH}_4$  values at the two other sampling sites, precluding any attempt to apportion fossil and biogenic sources of  $\text{CH}_4$ . Since atmospheric  $^{14}\text{CO}_2$  is much less sensitive to  $^{14}\text{C}$  emissions from nuclear power plants,  $^{14}\text{CO}_2$  measurements allowed to estimate recently added fossil fuel  $\text{CO}_2$  at Beromünster (rural site) and Bern (urban area). As expected from their respective geographical situation, the fossil fuel  $\text{CO}_2$  component is significantly larger in the city, because the sampling site is close to fossil sources such as the road traffic and domestic heating exhausts.

The preponderant influence of  $^{14}\text{C}$  emissions from nuclear activities on atmospheric  $^{14}\text{CH}_4$  levels motivated the conduction of a field study of atmospheric  $^{14}\text{CH}_4$  and  $^{14}\text{CO}_2$  near the Gösgen nuclear power plant during a revision period, when substantial  $^{14}\text{C}$  discharges were expected. The air samples collected and analyzed reveal an extremely large impact of sporadic  $^{14}\text{C}$  releases on atmospheric  $^{14}\text{CH}_4$  contents, with measured values up to 1800 times natural background levels at a distance of 6 km from the nuclear power plant. Although the Gösgen nuclear power plant emits little amounts of  $^{14}\text{CO}_2$  on average, considerable  $^{14}\text{CO}_2$  enhancements were also observed during the dispersion of the emission plume, emphasizing the large temporal variability of this  $^{14}\text{C}$  source. Unfortunately, the influence of  $^{14}\text{C}$  emissions from nuclear power plants on atmospheric  $^{14}\text{CH}_4$  and  $^{14}\text{CO}_2$  levels at a specific location are still simulated by supposing constant emissions in atmospheric studies. Thus, the observations made during the Gösgen study bring two key findings: First, they explain the very large scatter of  $^{14}\text{CH}_4$  values measured in Switzerland, which prevents from any meaningful  $^{14}\text{C}$  source apportionment of atmospheric  $\text{CH}_4$  in regions of nuclear activities under current conditions. Second, they indicate that when not correctly accounted for, sporadic discharges from nuclear power plants create significant biases in the estimation of the fossil fuel  $\text{CO}_2$  component at a sampling site.

Finally, we demonstrate the flexibility of the new setup with the participation in a laboratory intercomparison, which aimed at using the  $^{14}\text{C}$  method to apportion the biogenic and fossil fractions of blends of biogas and natural gas. The purification setup was very useful at separating individual subfractions of the gas mixtures and analyzing their respective  $^{14}\text{C}$  content, which provided some interesting additional information.

# Abbreviations

AGE	Automated graphitization equipment
AMS	Accelerator mass spectrometry
BWR	Boiling water reactor
CEP	Climate and Environmental Physics Institute (University of Bern)
CIS	CO <sub>2</sub> interface system
EF	Emission factor
F <sup>14</sup> C	Fraction modern ( <sup>14</sup> C)
FID	Flame ionization detector
GC	Gas chromatography
GHG	Greenhouse gas
GIS	Gas interface system ( <sup>14</sup> C measurement of CO <sub>2</sub> ampoules)
IRMS	Isotope-ratio mass spectrometry
MFC	Mass flow controller
MICADAS	MIni CARbon DAting System (AMS)
MPPS	Methane preconcentration and purification setup
NPP	Nuclear power plant
PBL	Planetary boundary layer
PP	Purged packed (inlet)
PRECON	Methane preconcentration setup (part of MPPS)
PURIF	Methane purification setup (part of MPPS)
PWR	Pressurized water reactor
RDT	Russian doll trap (CO <sub>2</sub> trap)
TCD	Thermal conductivity detector

# Contents

Summary.....	i
Abbreviations.....	iii
Contents.....	iv
1. Introduction.....	1
1.1 The greenhouse gas CH <sub>4</sub> .....	1
1.2 The atmospheric CH <sub>4</sub> budget.....	2
1.2.1 Methane formation pathways.....	2
1.2.2 Methane sources and sinks.....	2
1.3 Methane and the climate.....	4
1.3.1 A close relationship.....	4
1.3.2 Monitoring.....	5
1.3.3 Stable isotope measurements.....	6
1.3.4 Current status.....	7
1.4 Radiocarbon analysis.....	8
1.4.1 General.....	8
1.4.2 <sup>14</sup> C measurements.....	9
1.4.3 <sup>14</sup> C in the atmosphere.....	13
1.5 <sup>14</sup> C-based source apportionment of CH <sub>4</sub> .....	15
1.5.1 General.....	15
1.5.2 <sup>14</sup> C signature of CH <sub>4</sub> sources.....	16
1.5.3 Atmospheric <sup>14</sup> CH <sub>4</sub> .....	17
1.5.4 Global source apportionment of CH <sub>4</sub> .....	19
1.5.5 Regional source apportionment of CH <sub>4</sub> .....	19
1.6 Sample preparation for <sup>14</sup> CH <sub>4</sub> analysis.....	20
1.6.1 Requirements for a <sup>14</sup> C-AMS measurement.....	20
1.6.2 “Standard” procedure.....	21
1.6.3 Alternative approach.....	22
1.7 Aims of the thesis.....	23
2. Methane Preconcentration and Purification Setup (MPPS).....	25

Preamble .....	25
2.1 Introduction .....	27
2.2 Methods .....	29
2.2.1 Goals and strategy .....	29
2.2.2 Sampling .....	30
2.2.3 Methane preconcentration setup (PRECON) .....	30
2.2.4 Methane purification setup (PURIF) .....	33
2.2.5 Methane preconcentration and purification setup (MPPS) .....	36
2.2.6 Methane <sup>14</sup> C measurement .....	36
2.3 Results and discussion .....	36
2.3.1 Optimization and performance of the PRECON .....	36
2.3.2 Optimization and performance of the PURIF .....	38
2.3.3 Validation of the MPPS .....	40
2.4 Conclusion .....	42
3. Biweekly atmospheric <sup>14</sup> CH <sub>4</sub> and <sup>14</sup> CO <sub>2</sub> measurements at three sites in Switzerland .....	44
3.1 Introduction .....	44
3.2 Methods .....	45
3.2.1 Sites description .....	45
3.2.2 Air sampling .....	47
3.2.3 Sample pretreatment .....	48
3.2.4 <sup>14</sup> CH <sub>4</sub> and <sup>14</sup> CO <sub>2</sub> measurements .....	49
3.2.5 Regional fossil fuel CO <sub>2</sub> component .....	50
3.3 Results .....	52
3.3.1 Atmospheric <sup>14</sup> CH <sub>4</sub> at Jungfraujoch, Beromünster and Bern .....	52
3.3.2 Atmospheric <sup>14</sup> CO <sub>2</sub> at Jungfraujoch, Beromünster and Bern .....	53
3.3.3 Diurnal variability of <sup>14</sup> CH <sub>4</sub> and <sup>14</sup> CO <sub>2</sub> .....	54
3.3.4 Long-term biweekly <sup>14</sup> CO <sub>2</sub> measurements at Beromünster .....	55
3.3.5 Fossil fuel CO <sub>2</sub> component at Beromünster and Bern .....	57
3.4 Discussion .....	59
3.4.1 Atmospheric <sup>14</sup> CH <sub>4</sub> in Switzerland .....	59
3.4.2 Atmospheric <sup>14</sup> CO <sub>2</sub> — comparisons with <sup>14</sup> CH <sub>4</sub> .....	66

3.4.3	Diurnal variations and sampling duration.....	71
3.4.4	Long-term CO <sub>2ff</sub> at Beromünster – comparisons with an urban area.....	74
3.5	Conclusions and outlook.....	79
4.	Impact of a nuclear power plant on atmospheric <sup>14</sup> CH <sub>4</sub> and <sup>14</sup> CO <sub>2</sub> – a case study in Switzerland .....	81
4.1	Preamble.....	81
4.2	Methods.....	83
4.2.1	Site description.....	83
4.2.2	Sampling.....	84
4.2.3	Analyses .....	85
4.2.4	Evaluation and correction of the data.....	86
4.3	Results and discussion.....	87
4.3.1	Radioactive emissions at the stack.....	87
4.3.2	<sup>14</sup> CH <sub>4</sub> at the sampling sites .....	89
4.3.3	<sup>14</sup> CO <sub>2</sub> at the sampling sites .....	91
4.3.4	<sup>37</sup> Ar at site “Main”.....	92
4.3.5	Significance of the observed <sup>14</sup> C release event .....	93
4.3.6	Monitoring the <sup>14</sup> C emissions of NPPs.....	95
4.3.7	Implications for <sup>14</sup> CH <sub>4</sub> and <sup>14</sup> CO <sub>2</sub> source apportionments.....	97
4.4	Conclusion .....	99
5.	<sup>14</sup> C-AMS lab intercomparison.....	101
5.1	Introduction.....	101
5.2	Methods.....	102
5.2.1	Samples .....	102
5.2.2	Total combustion of the gas samples .....	102
5.2.3	Isolation of pure subfractions.....	103
5.2.4	<sup>14</sup> C measurements .....	103
5.3	Results and discussion.....	104
5.3.1	Composition.....	104
5.3.2	Radiocarbon content.....	106
5.3.3	Stable isotope composition.....	107

5.3.4 Biogenic carbon fraction .....	108
5.4 Conclusion .....	110
6. General conclusions and outlook .....	112
6.1 Summary of the achievements.....	112
6.2 Future technical developments.....	114
6.3 Further research.....	115
7. Bibliography.....	117
8. Appendices.....	142
8.1 Detailed performance parameters of the MPPS.....	142
8.2 $\Delta^{14}\text{CH}_4$ and $\Delta^{14}\text{CO}_2$ at Beromünster, Bern and Jungfrauoch.....	145
Acknowledgements .....	151
Declaration of consent.....	153
Curriculum vitae.....	154
Publications .....	154

# 1. Introduction

## 1.1 The greenhouse gas CH<sub>4</sub>

By absorbing and reflecting back to the surface a portion of the Earth's outgoing longwave radiation, greenhouse gases (GHG) are essential to life on Earth (Tyndall, 1861; Arrhenius, 1896). Without this natural effect, of which water vapor is the main contributor, the average surface temperature on Earth would be  $-18\text{ }^{\circ}\text{C}$  (Ahrens and Henson, 2015). This natural forcing has been however enhanced by a strong increase of anthropogenic GHG emissions since the onset of the industrial era. As reported by the Intergovernmental Panel on Climate Change (IPCC), GHGs contributed a global mean surface warming likely to be in the range of  $0.5\text{ }^{\circ}\text{C}$  to  $1.3\text{ }^{\circ}\text{C}$  over the period 1951 to 2010 (IPCC, 2013).

Paleo records such as air bubbles trapped in ice cores are invaluable witnesses of the climate of the past. They reveal that methane (CH<sub>4</sub>) mole fraction in the atmosphere fluctuated between 350 and 600 ppb during the glacial and interglacial cycles of the Quaternary period (Delmotte et al., 2004). More recently, they show a strong and fast rise of CH<sub>4</sub> mole fraction since the beginning of the industrial revolution, with current values about 2.5 times higher than preindustrial levels (see Figure 1.1). With a mole fraction over 1850 ppb, CH<sub>4</sub> is today the second most important anthropogenic GHG after CO<sub>2</sub> (Nisbet et al., 2019). Despite its low mole fraction with respect to the one of CO<sub>2</sub> ( $> 400\text{ ppm}$ ), CH<sub>4</sub> has a global warming potential 28–34 times higher than CO<sub>2</sub> on a timescale of 100 years, due to its strong absorption in the infrared (IPCC, 2013). Thus, CH<sub>4</sub> is responsible for more than 20% of the human-induced radiative forcing (Ciais et al., 2013).

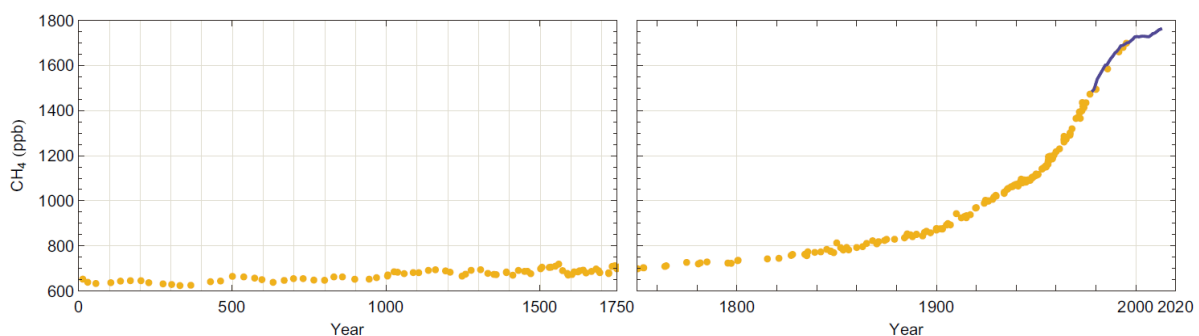


Figure 1.1 History of atmospheric CH<sub>4</sub> concentration, determined from air enclosed in ice cores and firn air (yellow dots) and from direct atmospheric measurements at the Cape Grim observatory (blue line). Sources: MacFarling Meure et al. (2006); IPCC (2013).

## 1.2 The atmospheric CH<sub>4</sub> budget

### 1.2.1 Methane formation pathways

Three different processes lead to the formation of CH<sub>4</sub> on Earth. Methane is either biogenic, i.e. the result of microbial activity, or thermogenic, i.e. the product of thermal degradation of organic matter, or pyrogenic, i.e. the result of an incomplete combustion of organic matter (Bréas et al., 2001; Stolper et al., 2015).

Biogenic CH<sub>4</sub> is formed through the process of methanogenesis, which is a form of anaerobic respiration of microbes, resulting in the degradation of organic matter (Stadtman, 1967; Whiticar, 1999). The two dominant methanogenic pathways are acetoclastic and hydrogenotrophic CH<sub>4</sub> production. Acetoclastic methanogenesis, also called “acetate fermentation”, follows the net reaction  $\text{CH}_3\text{COOH} \rightarrow \text{CH}_4 + \text{CO}_2$ . Hydrogenotrophic methanogenesis, also named “carbonate reduction”, can be represented by the general reaction:  $\text{CO}_2 + 8\text{H}^+ + 8\text{e}^- \rightarrow \text{CH}_4 + 2\text{H}_2\text{O}$ . As biogenic formation of CH<sub>4</sub> mainly occurs in anoxic environments, it mainly happens in flooded soils, at the bottom of water bodies lying over carbon-rich sediments and in the guts of ruminants and wild animals.

Methane is also produced by the thermally activated breakdown of larger organic molecules, which happens in deep sedimentary strata on geological timescales, under high pressure and temperature conditions (Galimov, 1988; Schoell, 1988). Thermogenic CH<sub>4</sub> is the main constituent and the most important source of natural gas.

Finally, pyrogenic CH<sub>4</sub> is emitted as the product of an incomplete combustion of biomass, biofuels and fossil fuels (Kirschke et al., 2013). The proportion of CH<sub>4</sub> produced during the burning of organic matter primarily depends on the availability of oxygen.

### 1.2.2 Methane sources and sinks

The sources of atmospheric CH<sub>4</sub> are very diverse and can be categorized by their formation process (i.e. biogenic, thermogenic or pyrogenic), or by their origin (i.e. natural or anthropogenic). Methane emissions are mainly biogenic (64–76%), thermogenic and pyrogenic sources contributing to 19–30% and 4–6%, respectively (Neef et al., 2010). It should be noticed that each formation type can be natural or anthropogenic and that individual sources can combine biogenic and thermogenic origins (Saunio et al., 2016). Therefore, the classification in categories and their relative contribution to the global budget of emissions are not straightforward, and differ among several authors.

Inventories of emissions by source category are presented in Figure 1.2, using blue levels for the natural sources and red levels for the anthropogenic sources. The main natural source is the wetlands, where CH<sub>4</sub> is anaerobically produced in flooded soils of the tropics and the boreal zone (Papa et al., 2010; Melton et al., 2013). Fresh waters (i.e. lakes, rivers, ponds and

estuaries) constitute another significant natural source. Methane produced in the carbon-rich sediments at the bottom of these water bodies is carried to the atmosphere by three major pathways of emission: ebullition, transport by the plants and diffusion through the water column (Bastviken et al., 2004; Walter et al., 2010). Natural geological sources are diverse, as their related CH<sub>4</sub> emissions have either a thermogenic or microbial origin. These sources refer to CH<sub>4</sub> produced in the Earth’s crust, which migrates along tectonic dislocations and degasses to the atmosphere, a phenomenon called “seepage” (Etiope et al., 2008). Geological sources are mainly onshore (e.g. sedimentary basins, mud volcanoes, gas seeps), the only offshore source being submarine seepage (Etiope, 2015). Finally, smaller natural sources include among others: wild animals (Crutzen et al., 1986), termites (Sanderson, 1996), hydrates (Milkov, 2005) and permafrost soils (Zhang et al., 2008).

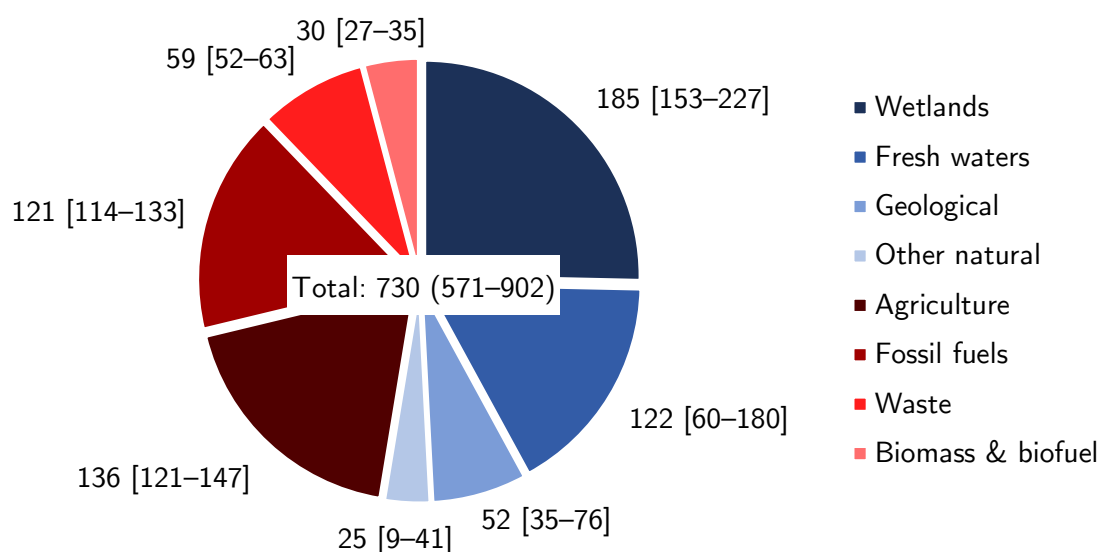


Figure 1.2 Natural (blue shades) and anthropogenic (red shades) sources of atmospheric CH<sub>4</sub>. The emissions, reported in Tg CH<sub>4</sub> yr<sup>-1</sup>, are the mean values from several emission inventories over the period 2003–2012. Ranges (in brackets) represent minimum and maximum values of the different inventories. Source: Saunio et al., 2016.

The anthropogenic sources of CH<sub>4</sub> are very diverse in nature, with agriculture (mainly ruminants, manure and rice paddies) as the largest contributor (Saunio et al., 2016). Fossil fuels is a source referring to fugitive CH<sub>4</sub> emissions during the exploitation, transport, distribution and usage of coal, oil and natural gas (Bréas et al., 2001). Although the fossil fuel source is dominantly of a thermogenic origin, the exploitation of shale gas causes the venting of CH<sub>4</sub> of a thermogenic or biogenic origin (Golding et al., 2013). Waste includes landfills and wastewater management, where CH<sub>4</sub> is produced by microbial decomposition of organic matter (Cho et al., 2012). The last anthropogenic source of CH<sub>4</sub> is pyrogenic, as it refers to an incomplete combustion of biomass and biofuels (Kirschke et al., 2013).

The primary sink for atmospheric CH<sub>4</sub> is its oxidation by hydroxyl radicals in the troposphere (90%) (Ehhalt, 1974). Other CH<sub>4</sub> sinks are its oxidation by methanotrophic bacteria in soils (4%), its escape to the stratosphere and subsequent reaction with chlorine and atomic oxygen radicals (3%), and atomic chlorine in the marine boundary layer (3%) (Allan et al., 2005; Kirschke et al., 2013).

The atmospheric CH<sub>4</sub> budget is the balance between its sources and sinks. Currently, the sum of the sources exceeds the sum of the sinks, and the CH<sub>4</sub> mole fraction is rising (Nisbet et al., 2019). Due to a relatively long lifetime of approximately 9 years in the atmosphere, CH<sub>4</sub> is considered as a well-mixed GHG (Prather et al., 2012).

## 1.3 Methane and the climate

### 1.3.1 A close relationship

In addition to being a potent GHG, CH<sub>4</sub> plays an important role in the atmospheric chemistry (Crutzen, 1995). The stratospheric sink of CH<sub>4</sub> is an important source of water vapor in the stratosphere, which increases the radiative forcing (Solomon et al., 2010). The oxidation of CH<sub>4</sub> in the troposphere by OH radicals leads to the formation of CO<sub>2</sub> and O<sub>3</sub>, two other GHGs (Crutzen, 1995). Through its reaction with OH radicals, CH<sub>4</sub> affects the oxidative capacity (cleansing power) of the atmosphere. As a result, increasing CH<sub>4</sub> emissions weaken the tropospheric OH sink, which in turn causes an increase of the CH<sub>4</sub> lifetime and thus its burden (IPCC, 2013). When all these effects are taken into account, the radiative forcing of CH<sub>4</sub> emissions goes from 0.48 (CH<sub>4</sub> concentration alone) to about 0.97 W m<sup>-2</sup> on an emission basis (IPCC, 2013). Finally, a recent reevaluation of the absorption of CH<sub>4</sub> in the shortwave (near-infrared) bands leads to a radiative forcing ~25% larger (0.61 Wm<sup>-2</sup>) than the value communicated by the IPCC in 2013.

The microbial production of CH<sub>4</sub> is highly sensitive to environmental factors such as the temperature, moisture and the organic content of the soils. Usually, enhanced temperature and humidity are synonym of higher CH<sub>4</sub> emissions (Le Mer and Roger, 2001). This is especially true for some natural sources of CH<sub>4</sub> such as wetlands and fresh waters, whose magnitude is closely linked to meteorological conditions (Warwick et al., 2002). Hence, the temporal variability of natural sources, particularly the wetlands, is the main driver of the inter-annual variability of the CH<sub>4</sub> growth rate (Bousquet et al., 2006; Dlugokencky et al., 2011; Melton et al., 2013; Jacob et al., 2016).

The climate is a very complex system with many present and future feedbacks difficult to evaluate (Heimann and Reichstein, 2008; Saunio et al., 2016; Dean et al., 2018). Atmospheric GHGs act as a positive forcing on the climate, the warming of which generates a positive feedback by increasing CH<sub>4</sub> emissions (Dean et al., 2018). The Arctic regions deserve a special attention, as they warm faster than the rest of the globe and store a large pool of carbon in

the permafrost (Walter et al., 2007; Tarnocai et al., 2009). Although it seems clear that a thawing permafrost should increase the emissions of CH<sub>4</sub> and CO<sub>2</sub> (Koven et al., 2011), the future contribution of the Arctic regions to CH<sub>4</sub> and CO<sub>2</sub> emissions remains unclear. Indeed, the repartition of the natural sources of CH<sub>4</sub> in these regions (wetlands, arctic lakes, permafrost) will be deeply altered in the course of this century (Lawrence et al., 2015). Hence, although most studies predict a future increase in CH<sub>4</sub> emissions from the Arctic regions in a warming climate, its quantification remains very uncertain (Walter et al., 2006; Schneider Von Deimling et al., 2012; Schuur et al., 2015; Thornton et al., 2015).

### 1.3.2 Monitoring

An understanding of the evolution of the global budget of atmospheric CH<sub>4</sub> and its main drivers requires the knowledge of the magnitude of individual sources and sinks. Although CH<sub>4</sub> is relatively well mixed in the atmosphere, small enhancements of its mole fraction are observed close to the sources. Thus, the monitoring of atmospheric CH<sub>4</sub> is used to estimate the global budget of CH<sub>4</sub> and to evaluate the distribution and strength of individual sources and sinks (e.g. Bousquet et al., 2006; Houweling et al., 2017).

Observations of atmospheric CH<sub>4</sub> became systematic in the late 1970s, with discrete air samplings and the use of gas chromatography to measure the mole fraction of CH<sub>4</sub> in the atmosphere (Blake et al., 1982). Since then, the growing number of stations and the development of optical detection methods improved the spatial and temporal coverage of CH<sub>4</sub> measurements (Dlugokencky et al., 2011). Today, CH<sub>4</sub> is monitored by four surface networks and their data are archived at the World Data Centre for Greenhouse Gases by the World Meteorological Organization (Kirschke et al., 2013; Saunio et al., 2016). To complement *in situ* observations and address their uneven spatial coverage, satellite data are also used since the beginning of the 2000s (Streets et al., 2013; Jacob et al., 2016). Remote sensing of CH<sub>4</sub> started first with SCIAMACHY (Frankenberg et al., 2006) and continued with GOSAT (Kuze et al., 2016).

Today, two modelling approaches are used to assess CH<sub>4</sub> fluxes, which are commonly referred to as “top-down” and “bottom-up” (Nisbet and Weiss, 2010). The top-down technique starts from atmospheric observations of CH<sub>4</sub> (satellites or surface stations) and uses chemistry transport models in an inverse approach to get a spatial and temporal estimate of the CH<sub>4</sub> emissions responsible for the concentrations measured (e.g. Streets et al., 2013; Jacob et al., 2016). In contrast, the bottom-up approach uses source-specific emission factors, process-based models and inventories of emissions, which are then extrapolated to larger scales (e.g. Hiller et al., 2014; Zhang and Chen, 2014). Both approaches are not fully independent, as atmospheric inversions require a prior knowledge of CH<sub>4</sub> emissions, which is usually provided by bottom-up inventories (Schwietzke et al., 2014; Jacob et al., 2016). Top-down modelling has the advantage to constrain global CH<sub>4</sub> emissions, but carries little information about individual

sources and emission processes that are usually not spatially resolved. Conversely, the bottom-up approach has the advantage to be process-based and closer to the sources, but no constraints apply to the sum of emissions when small-scale fluxes are extrapolated (IPCC, 2013).

Both approaches do not agree on the global budget of CH<sub>4</sub> emissions. With a mean value of 736 Tg CH<sub>4</sub> yr<sup>-1</sup> for the period 2003–2012, the bottom-up approach significantly overestimates the global CH<sub>4</sub> source, which is better constrained by top-down inversions to a mean value of 558 Tg CH<sub>4</sub> yr<sup>-1</sup> (Saunio et al., 2016). Although the two techniques agree relatively well on the magnitude of anthropogenic sources, the bottom-up approach significantly overestimates the contribution from natural sources (Kirschke et al., 2013). The problem is highlighted in Figure 1.2, where the contribution of individual sources is derived from emission inventories: First, natural sources are overrepresented, as top-down constraints report that about 60% of global emissions are anthropogenic (Saunio et al., 2016). Second, natural sources are associated with very large uncertainties, as individual studies do not agree well. Indeed, all techniques used to estimate CH<sub>4</sub> fluxes are challenged by the spatial and temporal variability of CH<sub>4</sub> emissions, which is not well represented due to the relatively low spatial and temporal coverage of satellite data, observational networks and emission inventories (Bousquet et al., 2006; Nisbet et al., 2014). In particular, some areas with expected high CH<sub>4</sub> emissions are still poorly observed, such as the tropical wetlands (Papa et al., 2010; Melton et al., 2013). For these regions, top-down atmospheric inversions lack of spatial and temporal coverage, which challenges the use of emission factors (Saunio et al., 2016). As a result, the main drivers of the observed growth rate of atmospheric CH<sub>4</sub> are still not well understood (Dlugokencky et al., 2009; Kirschke et al., 2013; Saunio et al., 2016; Nisbet et al., 2019).

### 1.3.3 Stable isotope measurements

One good tool to understand the production, removal and transport of CH<sub>4</sub> is to look at its stable isotopes ( $\delta^{13}\text{C}$  and  $\delta\text{D}$ ), because every process of formation or removal fractionates in a characteristic way, with a preference for the heavy or the light isotopes (Whiticar, 1999; Hoefs, 2009). Thus, stable isotope measurements allow making the distinction between biogenic, thermogenic and pyrogenic sources of CH<sub>4</sub> (Wahlen, 1993; Quay et al., 1999; Whiticar, 1999). As a result, biogenic formation of CH<sub>4</sub> leads to an isotopic composition strongly depleted in heavy isotopes, whereas thermogenic and pyrogenic sources are less depleted (Miller et al., 2002). Recently, a comprehensive isotope database was made available, compiling  $\delta^{13}\text{C}$  signatures of biogenic, thermogenic and pyrogenic CH<sub>4</sub> sources (Schwietzke et al., 2016; Sherwood et al., 2017). By virtue of recent technical improvements, high-resolution isotope measurements of atmospheric CH<sub>4</sub> have the potential to further constrain the CH<sub>4</sub> budget (Röckmann et al., 2016).

Although extensively used, stable isotope measurements do not allow differentiating all the types of CH<sub>4</sub> sources (Petrenko et al., 2008; Röckmann et al., 2016). For example, natural

emissions such as wetlands have a signature very close to agricultural emissions, because both types of sources are the result of methanogenesis. Moreover, stable isotope results have become more ambiguous to interpret recently, due to an increasing use of shale gas fracking as a new source of energy in the United States (Howarth et al., 2011). Indeed, fugitive emissions during fracking and gas transport constitute a new source of CH<sub>4</sub> to the atmosphere. However, unlike natural gas that is thermogenic, shale gas can be of thermogenic, microbial or of mixed origin (Golding et al., 2013). Thus, shale gas is associated with a wide range of isotopic compositions, making it undistinguishable from biogenic CH<sub>4</sub> based on stable isotopes alone.

### 1.3.4 Current status

Between 1999 and 2006, the growth rate of atmospheric CH<sub>4</sub> strongly decreased, leading to a quasi-stabilization of its concentration in the atmosphere (see Figure 1.1). In 2007, CH<sub>4</sub> started to rise again (Nisbet et al., 2014). This episode triggered a long-lasting debate among the scientific community, aiming at finding the culprits for the stabilization and the subsequent rise. Whilst Aydin et al. (2011) suggested a decline of the CH<sub>4</sub> emissions linked to fossil fuels, Kai et al. (2011) pointed out a weakening of microbial sources in the Northern Hemisphere. A few years later, Schaefer et al. (2016) proposed a decrease of thermogenic sources followed by an increase of biogenic CH<sub>4</sub> emissions, the latter being more consistent with agriculture than wetlands. Although stable isotopes were used in combination with inventories, monitoring and modelling, the interpretation of this episode was challenged by the relatively poor temporal and spatial resolution of observations and models (Nisbet et al., 2014).

Almost 15 years after the aforementioned conundrum, the scientific community is facing a new enigma: atmospheric CH<sub>4</sub> grew very rapidly in the period 2014-2017, at rates not observed since the 1980s (Nisbet et al., 2019). Once again, the causes of such a strong rise are not obvious and may comprise an increase of biogenic sources, such as tropical wetlands (Nisbet et al., 2016) or agriculture (Schaefer et al., 2016), an increase of emissions from oil and natural gas production (Hausmann et al., 2016), or a weakening of the main sink due to a reduction in the oxidative capacity of the atmosphere (Rigby et al., 2017).

These possible culprits are very different in essence, as some are natural and others anthropogenic. Furthermore, climate change has probably redistributed the relative strength of individual sources and sinks of CH<sub>4</sub>, as most of them are very sensitive to meteorological changes (Walter et al., 2006; Dean et al., 2018). A combination of these factors cannot be excluded, adding to the complexity of the situation (Nisbet et al., 2019).

Due to its relatively short lifetime and large warming potential, mitigation strategies of anthropogenic CH<sub>4</sub> emissions can be efficient on a relatively short-term (Dlugokencky et al., 2011; Schwietzke et al., 2016). Following the suggestions of Shindell et al. (2012), the 2015 UN Paris Agreement on Climate Change put a strong emphasis on a rapid cut of the CH<sub>4</sub> burden in the atmosphere (IPCC, 2018). Unfortunately, the strong rise of atmospheric CH<sub>4</sub> was not

taken into account in the pathway scenarios of the Paris Agreement, which challenges the target to keep the increase in the global average temperature to well below 2 °C above preindustrial levels (Rogelj et al., 2016; Nisbet et al., 2019).

Some mitigation strategies can even be cost-effective, such as the reduction of leaks during the transport and distribution of natural gas or the recollection of CH<sub>4</sub> produced in landfills (Dlugokencky et al., 2011). According to some recent publications, the contribution of fossil fuel CH<sub>4</sub> emissions might be substantially underestimated, offering the fossil fuel industry a greater potential for the mitigation of anthropogenic climate forcing (Schwietzke et al., 2016; Petrenko et al., 2017; Hmiel et al., 2020). In order to implement effective reduction plans at local, regional and global levels, there is an urgent need for a better understanding of the factors controlling the atmospheric CH<sub>4</sub> burden. We will see in the following sections that radiocarbon measurements of CH<sub>4</sub> might reveal a valuable additional tool, which has the unique capability to differentiate fossil and modern sources of CH<sub>4</sub> (Lowe et al., 1991; Quay et al., 1991).

## 1.4 Radiocarbon analysis

### 1.4.1 General

On Earth, carbon has three naturally occurring isotopes: <sup>12</sup>C (98.89%), <sup>13</sup>C (1.11%) and <sup>14</sup>C (~10<sup>-10</sup>%) (Schoor et al., 2016). The abundance of the stable isotopes <sup>12</sup>C and <sup>13</sup>C remained unchanged since their synthesis, whereas <sup>14</sup>C is constantly produced in the upper layers of the atmosphere. This happens when cosmic rays enter the atmosphere, as their interactions with air molecules lead to the generation of spallation products (Lal and Suess, 1968). Among them, the secondary thermal neutrons are then absorbed by nitrogen atoms and yield to the production of <sup>14</sup>C in the following reaction (Libby, 1946; Anderson et al., 1947):



<sup>14</sup>C is then quickly oxidized in the atmosphere to form <sup>14</sup>CO and eventually <sup>14</sup>CO<sub>2</sub> within a few months. Such as the other isotopes of carbon, <sup>14</sup>C enters the global carbon cycle that exchanges carbon among the different carbon reservoirs (atmosphere, biosphere, hydrosphere and lithosphere) via processes such as photosynthesis, respiration and dissolution in the oceans. Unlike <sup>12</sup>C and <sup>13</sup>C, the nucleus of <sup>14</sup>C is unstable and undergoes a spontaneous β<sup>-</sup>-decay with a half-life of 5730 ± 40 years (Godwin, 1962):



Thus, the concentration of <sup>14</sup>C in the atmosphere is the result of an equilibrium between its production rate and its exponential decay over time. All living plants and animals, which

actively exchange carbon with the environment, are in equilibrium with the  $^{14}\text{C}/^{12}\text{C}$  level of atmospheric  $\text{CO}_2$ . However, the balance is disrupted when an organism dies, as its incorporation of carbon stops and its  $^{14}\text{C}$  concentration decreases exponentially over time. This property allows  $^{14}\text{C}$  to be used as a tool for dating purposes (Arnold and Libby, 1949).

## 1.4.2 $^{14}\text{C}$ measurements

### 1.4.2.1 General

Owing to the very low  $^{14}\text{C}$  abundance in the environment, the methods required to measure the  $^{14}\text{C}$  content of a sample material need to be very sensitive. Gas proportional counting and liquid scintillation take advantage of the fact the  $^{14}\text{C}$  is a radioactive isotope to detect the beta particles emitted by the sample and assess its activity ( $\text{Bq kg}^{-1}$ ), which is proportional to the  $^{14}\text{C}/^{12}\text{C}$  ratio in the sample. The sensitivity of these techniques being inversely proportional to the half-life of the radionuclide measured, they are particularly well suited to the measurement of short-lived radionuclides with high activity (Synal, 2013).

Instead of assessing the radioactivity of a sample material, another approach is to measure directly the proportion of each isotope in the sample material using accelerator mass spectrometry (AMS). Thus, this method does not count beta particles but the amount of  $^{12}\text{C}$ ,  $^{13}\text{C}$  and  $^{14}\text{C}$  atoms in the sample. Consequently, the sensitivity of this technique does not depend on the half-life of the radionuclide of interest and is therefore better suited to the measurement of long-lived isotopes such as  $^{14}\text{C}$ . AMS systems allow dating organic samples of up to 50 kyr old (Synal et al., 2007).

Besides these two main  $^{14}\text{C}$  measurement methods, emerging technologies using a spectroscopic detection of  $^{14}\text{CO}_2$  and  $^{14}\text{CH}_4$  are developing (e.g. Galli et al., 2016; Karhu et al., 2019). These setups offer the advantages of being compact and having a great potential for future improvements. However, their low sensitivity does not make them suited to the measurement of atmospheric samples with natural  $^{14}\text{C}$  content yet.

The main benefit of AMS for radiocarbon measurements over the other methods aforementioned is the much higher sensitivity of the technique, which leads to a better accuracy and precision, a shorter measurement time and the possibility to analyze smaller sample masses (Synal, 2013). AMS was exclusively used in this work, as it is currently the most suitable technique available for environmental materials.

### 1.4.2.2 Accelerator mass spectrometry (AMS)

An AMS system consists of three main parts: an ion source, where the sample is introduced and negative ions are produced; a particle accelerator, which allows to dramatically increase the sensitivity of the method; and a mass spectrometry part, where the isotopes are separated and individually detected based on their respective mass. In this work, we used a MICADAS

AMS (see Figure 1.3), which is a compact system specifically designed for radiocarbon measurements (Synal et al., 2007; Szidat et al., 2014).

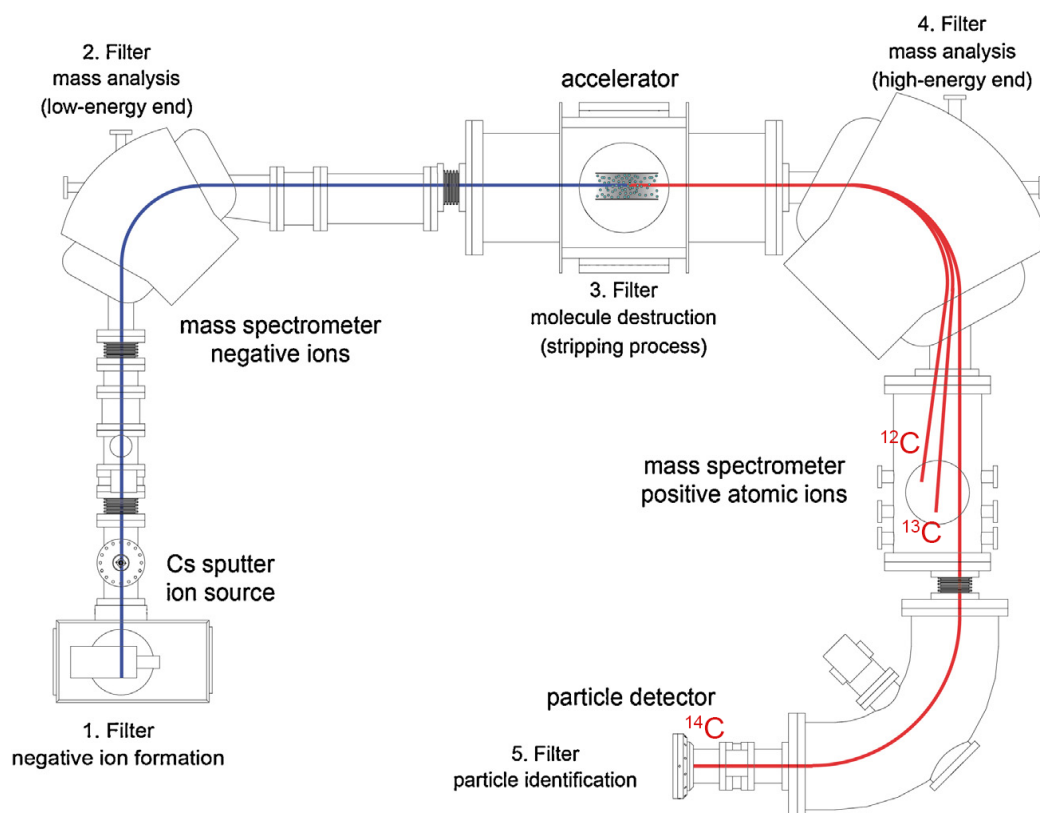


Figure 1.3 Layout of a typical MICADAS AMS system (Synal, 2013). Blue line: negatively charged ion beam ( $-1$ ). Red line: positively charged ion beam ( $+1$ ). See text for details.

The different sections of an AMS can be regarded as individual filter units, which combined allow reaching a very high sensitivity suited to original  $^{14}\text{C}/^{12}\text{C}$  ratios of  $10^{-12}$  to  $10^{-15}$  (Synal et al., 2007; Schulze-König, 2010). A cesium sputter ion source (Middleton, 1983) ionizes Cs vapors to  $\text{Cs}^+$  ions that are focused to a sample target. The sputtering of the sample material creates  $\text{C}^-$  ions, which are extracted from the ion source and accelerated toward the next unit of the AMS at a higher electric potential. The ion source acts as a first filter, since the isobar  $^{14}\text{N}$  does not form negative ions and is therefore not accelerated. The ion beam is then deflected by a dipole magnet playing the role of a mass selector, since the curvature radius of individual ions depends on their mass-to-charge ratio. The specificity of AMS systems lies in the presence of an acceleration unit, including a high voltage terminal and a stripper canal fed with  $\text{N}_2$ . Collisions with the stripper gas lead to a charge state conversion from  $\text{C}^-$  to  $\text{C}^+$  and cause a further acceleration of the ions by Coulomb repulsion. Moreover, the breakdown of large molecules via collisions with  $\text{N}_2$  leads to the suppression of isobaric interferences (mainly  $^{13}\text{CH}$  and  $^{12}\text{CH}_2$ ), which greatly improves the sensitivity of the  $^{14}\text{C}$  detection. After the acceleration

unit, a second magnet splits the ion beam for the individual detection of  $^{12}\text{C}$ ,  $^{13}\text{C}$  and  $^{14}\text{C}$  in Faraday cups and a gas ionization chamber, respectively.

The pretreatment of carbonaceous compounds for a radiocarbon measurement with an AMS requires first their transformation to  $\text{CO}_2$ , which is usually carried out via the combustion of the sample material in an elemental analyzer or in custom-made combustion systems (Szidat et al., 2004; Wacker et al., 2010b; Salazar et al., 2015). If the sample contains enough carbon ( $\geq 1$  mg C),  $\text{CO}_2$  is then reduced to elemental carbon with an automated graphitization equipment (AGE) and pressed into a target which can then be measured with the AMS (Němec et al., 2010).

The MICADAS AMS offers an alternative technique, which is a direct  $\text{CO}_2$  measurement in the hybrid gas ion source (Ruff et al., 2007). To do so, a gas interface system (GIS) is used (see Figure 1.4). A glass ampoule containing  $\text{CO}_2$  is introduced into a cracker unit where the ampoule is cracked and the  $\text{CO}_2$  released is manometrically quantified.  $\text{CO}_2$  is then flushed with helium into a small syringe and diluted to a fixed ratio of 1:20. The  $\text{CO}_2$ :He mixture is then transferred to the ion source through a small capillary at a constant flow rate and reaches a titanium target where it is sputtered by the  $\text{Cs}^+$  ions. The presence of a cracker magazine containing up to eight ampoules considerably reduces the operator input and the  $^{14}\text{C}$  measurement of a  $\text{CO}_2$  ampoule usually takes 20 min.

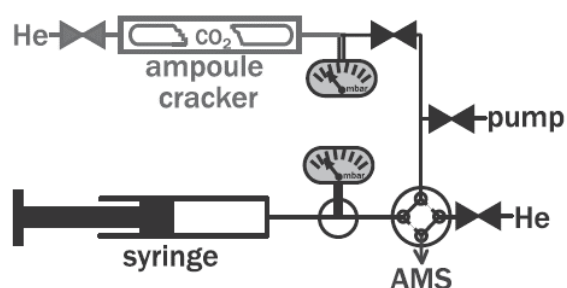


Figure 1.4 Gas interface system (GIS) used in combination with the MICADAS AMS for the measurement of gaseous  $\text{CO}_2$  samples (Wacker et al., 2013).

Performing direct gas measurements with an AMS offers two main advantages: First, an important gain in preparation time, as  $\text{CO}_2$  samples do not need to be graphitized prior to a  $^{14}\text{C}$  measurement. Second, the required sample size for a direct gas measurement is significantly lower than for solid targets. As the  $^{14}\text{C}$  analysis of graphite targets typically requires 1 mg C (Szidat et al., 2014), direct  $\text{CO}_2$  measurements can be performed on samples as small as 2–100  $\mu\text{g}$  C (Ruff et al., 2010; Fahrni et al., 2013). These two major benefits come at a cost, which is a reduced precision of the  $^{14}\text{C}$  results as opposed to the measurement of graphite samples (8–10‰ and 2‰, respectively). However, it will be shown later that for the determination of atmospheric  $^{14}\text{CH}_4$ , the advantages of a direct gas measurement largely outweigh the drawback of a lower measurement precision.

### 1.4.2.3 Corrections and units

Many different units have been used for reporting  $^{14}\text{C}$  results, which sometimes cause confusions as they do not all include the same corrections (Stenström et al., 2011). The choice of the unit usually depends on the field of application (dating, source apportionment, atmospheric measurements). As seen in section 1.3.3, isotopic fractionation occurs during chemical reactions and physical process, which affects the  $^{13}\text{C}/^{12}\text{C}$  ratio of a sample. Values are reported relative to a standard of known isotopic composition:

$$\delta^{13}\text{C} = \left[ \frac{\left( \frac{^{13}\text{C}}{^{12}\text{C}} \right)_{sample}}{\left( \frac{^{13}\text{C}}{^{12}\text{C}} \right)_{VPDB}} - 1 \right] \cdot 1000\text{‰} \quad \text{Equation 1.3}$$

With VPDB the Vienna Pee Dee Belemnite standard. As the effect mainly depends on the relative difference of mass between the two isotopes considered, isotopic fractionation affects the  $^{14}\text{C}/^{12}\text{C}$  ratio of a sample almost twice as much as its  $^{13}\text{C}/^{12}\text{C}$  ratio (Fahrni et al., 2017). To allow a decoupling of fractionation effects and radioactive decay, measured sample activities ( $A_S$ ) are corrected for isotopic fractionation to a value of  $\delta^{13}\text{C} = -25\text{‰}$  (normalization):

$$A_{SN} = A_S \cdot \left[ \frac{1 - \frac{25}{1000}}{1 + \delta^{13}\text{C}} \right]^2 \quad \text{Equation 1.4}$$

With  $A_{SN}$  the normalized specific activity of the sample. For absolute comparability,  $^{14}\text{C}$  results are reported relative to a standard of known activity. With a specific activity of  $226 \text{ Bq kg}^{-1}$ , the “absolute radiocarbon standard” represents the hypothetical  $^{14}\text{C}$  activity in the atmosphere in year 1950, if it would not have been influenced by anthropogenic perturbations (Mook and van der Plicht, 1999). This value corresponds to the activity of wood from 1890, corrected for decay to 1950 and normalized to  $\delta^{13}\text{C} = -25\text{‰}$ . Following the nomenclature from Stuiver and Polach (1977), Reimer et al. (2004) proposed to use the unitless quantity:

$$F^{14}\text{C} = \frac{A_{SN}}{A_{ON}} \quad \text{Equation 1.5}$$

With  $A_{ON}$  the specific activity of that hypothetical 1950 atmosphere decayed to the present (Donahue et al., 1990). Hence, a very old sample devoid of  $^{14}\text{C}$  has an  $F^{14}\text{C}$  of 0, whereas an  $F^{14}\text{C}$  of 1 refers to a “modern” sample with the reference year being 1950.

Practically, specific activities are not directly measured with an AMS as  $^{14}\text{C}/^{12}\text{C}$  and  $^{13}\text{C}/^{12}\text{C}$  ratios are measured instead. However, the specific activity of a sample is proportional to the ratio of  $^{14}\text{C}$  atoms to the total number of carbon atoms in the sample and thus using measured

$^{14}\text{C}/^{12}\text{C}$  ratios causes a minimal error (Donahue et al., 1990). Unfortunately, absolute ratios cannot be measured in an AMS system, as they would yield to an unacceptable precision. Indeed, the initial isotopic ratios of the sample material are altered during several steps of a measurement procedure, such as the sample preparation, the sputtering in the ion source or the stripping process (Wacker et al., 2010a; Synal, 2013). These fractionation effects are overcome by the measurement of a few standard samples of known isotopic composition together with the samples. Finally, the background activity of an AMS system is also accounted for with the measurement of “blank” samples (i.e. devoid of  $^{14}\text{C}$ ), as the mean blank value is subtracted to all the measured  $^{14}\text{C}/^{12}\text{C}$  ratios. As a result, Equation 1.5 can be rewritten as follows (Donahue et al., 1990; Stenström et al., 2011):

$$F^{14}\text{C} = \left[ \frac{\left(\frac{^{14}\text{C}}{^{12}\text{C}}\right)_{\text{sample}}}{0.7459 \cdot \left(\frac{^{14}\text{C}}{^{12}\text{C}}\right)_{\text{OXII}}} \right] \cdot \left[ \frac{1 + \delta^{13}\text{C}_{\text{OXII}}}{1 + \delta^{13}\text{C}_{\text{sample}}} \right]^2 \quad \text{Equation 1.6}$$

With OXII the NIST Standard Reference Material 4990C. OXII, sometimes written Oxa-II, is an oxalic acid standard prepared by fermentation of French beet molasses from 1977 (Cavallo and Mann, 1980; Stuiver, 1983). The factor 0.7459 corrects for the fact that the  $^{14}\text{C}$  activity in the atmosphere was significantly higher in 1977 than in 1950, which will be explained in the next section. The RAW data from a series of measurements (samples, standards and blanks) are processed in the data reduction program “BATS”, providing the  $F^{14}\text{C}$  results and their associated uncertainties (Wacker et al., 2010a).

For reporting  $^{14}\text{C}$  measurements of atmospheric  $\text{CH}_4$  and  $\text{CO}_2$ , the age-corrected  $\Delta^{14}\text{C}$  is usually preferred (Stuiver and Polach, 1977):

$$\Delta^{14}\text{C} = [F^{14}\text{C} \cdot e^{\lambda_c(1950-x)} - 1] \cdot 1000\text{‰} \quad \text{Equation 1.7}$$

With  $\lambda_c$  the Cambridge decay constant of radiocarbon ( $\lambda_c = 1/8267 \text{ yr}^{-1}$ ) and  $x$  the year of formation of the sample, which is typically the date of sample collection for  $^{14}\text{C}$  measurements of atmospheric  $\text{CH}_4$  and  $\text{CO}_2$  (Hammer et al., 2017). As for  $F^{14}\text{C}$  values, age-corrected  $\Delta^{14}\text{C}$  values do not change with time (i.e. the year of measurement), as both the standard and the sample decay at the same rate.

### 1.4.3 $^{14}\text{C}$ in the atmosphere

The concentration of  $^{14}\text{C}$  in the atmosphere primarily depends on the production rate of  $^{14}\text{C}$ . Although it is often considered as constant, small temporal and spatial variations have been observed through time, which are caused by variations in the cosmic ray flux, the strength of

the Earth’s magnetic field, the sun activity and the distribution of carbon among the various reservoirs (Stuiver and Quay, 1981; Stuiver and Braziunas, 1998; Beer et al., 2012).

The first noticeable anthropogenic perturbation of the  $^{14}\text{C}/^{12}\text{C}$  equilibrium occurred in the nineteenth century with the rapid increase of  $^{14}\text{C}$ -free  $\text{CO}_2$  emissions from the combustion of fossil fuels. As a result, the mole fraction of  $\text{CO}_2$  raised, which caused a dilution of  $^{14}\text{CO}_2$  in the atmosphere (Suess, 1955, 1958; Lal and Suess, 1968; Levin et al., 1989). This effect, named after Hans E. Suess who first noted its influence, is still today an important driver of atmospheric  $^{14}\text{CO}_2$  (Levin et al., 2013).

The second human-induced perturbation came along with the onset of nuclear tests in the 1950s, which peaked in the early 1960s until the ban of atmospheric nuclear tests in 1963. The so-called “bomb curve” or “bomb peak” shows that these nuclear explosions led to an almost doubling of atmospheric  $^{14}\text{CO}_2$  in the Northern Hemisphere (see Figure 1.5).

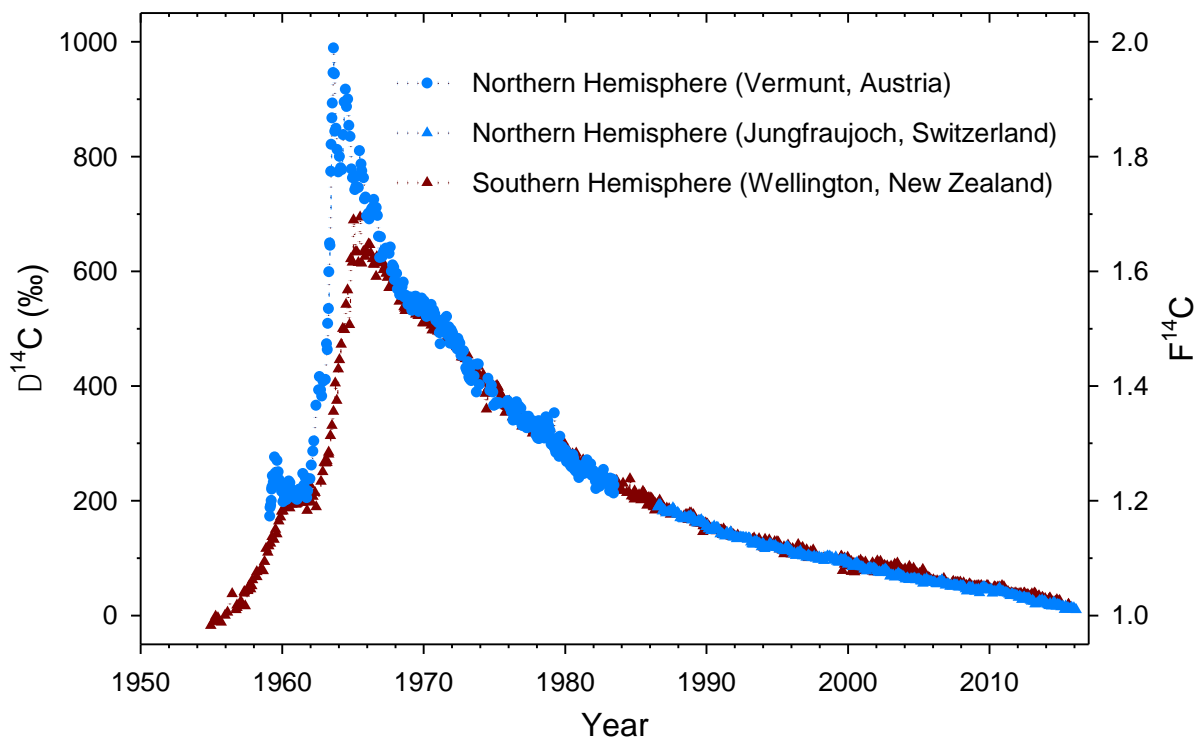


Figure 1.5 Atmospheric  $^{14}\text{CO}_2$  measurements (age-corrected  $\Delta^{14}\text{C}$  and corresponding  $F^{14}\text{C}$  values according to Equation 1.7 and Equation 1.6, respectively). Sources Northern Hemisphere: Levin et al. (1994) and Hammer and Levin (2017). Source Southern Hemisphere: Turnbull et al. (2017).

An analysis of the main features displayed by the bomb peak provides valuable information about the rate of repartition of  $^{14}\text{C}$  into different reservoirs, inter-hemispheric mixing, stratosphere-troposphere exchange processes and seasonal effects (Nydal and Lövseth, 1965; Manning et al., 1990; Turnbull et al., 2017). These observations are then used to infer atmospheric carbon exchange (Schuur et al., 2016). As an example, the fast decrease of

atmospheric  $^{14}\text{C}$  is explained by the relatively small size of this  $^{14}\text{C}$  reservoir, which contains about 2% of the total amount of  $^{14}\text{C}$  on Earth (Damon and Sternberg, 1989; Levin and Hesshaimer, 2000). Thus, atmospheric  $^{14}\text{C}$  is quickly distributed into much larger reservoirs such as the biosphere and the hydrosphere (Hesshaimer et al., 1994; Naegler and Levin, 2009). Finally, the  $^{14}\text{C}$  bomb spike is also used for precise dating of organic material, as atmospheric  $^{14}\text{C}$  quickly changed over a short period (Geyh, 2001; Brock et al., 2019).

When it comes to radiocarbon dating of organic matter, the original  $^{14}\text{C}$  of the material will depend on the atmospheric  $^{14}\text{C}$  level before its death. Thus, the history of natural and anthropogenic variations of atmospheric  $^{14}\text{C}$  is required for accurate dating. Proxies such as tree rings and varves are used for this purpose, leading to the production of regularly updated calibration curves (Reimer et al., 2013, 2020).

As we will see in Chapter 3, most of the excess  $^{14}\text{C}$  from the bomb peak has been redistributed in the environment and the  $^{14}\text{C}$  dilution from fossil  $\text{CO}_2$  emissions is today the main driver of the recent changes in atmospheric  $^{14}\text{C}$ . Indeed, with a downward trend of around 4-5‰ per year in the Northern Hemisphere, the  $^{14}\text{C}$  concentration in the atmosphere went back to its pre-bomb value.

## 1.5 $^{14}\text{C}$ -based source apportionment of $\text{CH}_4$

### 1.5.1 General

Source apportionment is a technique widely used in air pollution control and climate studies. The general principle is to identify the origin of particles or molecules in the atmosphere based on the specificity or “signature” of their different sources.  $^{14}\text{C}$ -based source apportionments exploit the fact that modern sources of carbon contain present-day  $^{14}\text{C}$  levels whereas old sources of carbon, such as the combustion of fossil fuels, are  $^{14}\text{C}$ -free. Hence, the  $^{14}\text{C}$  content of carbon-containing materials in the atmosphere provides information about the relative contribution of fossil and modern sources and mass balance models allow quantifying these contributions. This technique has been successfully used to apportion aerosols in the atmosphere (e.g. Szidat et al., 2004, 2006; Zhang et al., 2017), and also to estimate the relative contribution of fossil and modern sources of atmospheric  $\text{CO}_2$ . Measurements of  $^{14}\text{CO}_2$  were first performed at clean background sites, to unravel the global or continental proportion of fossil fuel  $\text{CO}_2$  in the atmosphere (e.g. Stuiver and Quay, 1981; Levin et al., 1985). More recently, the comparison of  $^{14}\text{CO}_2$  levels at polluted sites and background sites has allowed regional source apportionments of  $\text{CO}_2$  (e.g. Levin et al., 2003; Berhanu et al., 2017).

As described in section 1.2.1,  $\text{CH}_4$  is the result of successive transformations of atmospheric  $\text{CO}_2$ . Thus, the  $^{14}\text{C}$  content of  $\text{CH}_4$  is closely related to the one of  $\text{CO}_2$  and an analog method could be applied to apportion  $\text{CH}_4$  sources (Graven et al., 2019). To do so, it is first necessary

to assess the typical  $^{14}\text{C}$  signature of  $\text{CH}_4$  sources, but also the  $^{14}\text{CH}_4$  content of background air.

### 1.5.2 $^{14}\text{C}$ signature of $\text{CH}_4$ sources

As for oil and coal, the formation of natural gas is a process that takes several millions of years (see section 1.2.1). As a consequence, the emissions of  $\text{CH}_4$  linked to natural gas or the incomplete combustion of fossil fuels are considered as devoid of  $^{14}\text{C}$  (i.e.  $F^{14}\text{C} = 0$ ). Although marine gas hydrates can originate from biogenic or thermogenic processes, the current level of knowledge shows that they are strongly depleted in  $^{14}\text{C}$  and are therefore usually considered as fossil  $\text{CH}_4$  sources (Winckler et al., 2002; Kessler et al., 2008). Shale gas emissions are also  $^{14}\text{C}$ -free, which allows them to be distinguished from other modern biogenic sources as it strips away the ambiguity caused by their wide range of associated stable isotope signatures (see section 1.3.3).

Biogenic sources, such as rice paddies or ruminants, emit  $\text{CH}_4$  from recently assimilated organic material (Graven et al., 2019). As a consequence, their  $^{14}\text{C}$  content is similar to the one of atmospheric  $\text{CO}_2$ , which has been confirmed by  $^{14}\text{CH}_4$  measurements conducted by Wahlen et al. (1989). However, some other sources such as biomass burning show a large diversity of  $^{14}\text{CH}_4$  concentration (Wahlen et al., 1989). Indeed, the  $^{14}\text{C}$  content of a tree reflects averaged atmospheric  $^{14}\text{CO}_2$  content over its growing period. This delay can lead to a large variety of  $^{14}\text{CH}_4$  emissions, especially for organic matter incorporating  $\text{CO}_2$  during the period of the bomb peak (see Figure 1.5). To account for this effect, Lassey et al. (2007a) introduced the term “biospheric lag time”, which is the time lapse between the carbon being fixed by photosynthesis and being released as  $\text{CH}_4$ .

Besides modern and fossil sources of  $\text{CH}_4$ , some large sources release carbon of an intermediate age measurable with the radiocarbon technique ( $< 50$  kyr old). For such sources, measuring their  $^{14}\text{CH}_4$  content provides valuable information about the carbon cycle and carbon dynamics, as it allows a distinction between the decomposition of fresh organic matter or a release of ancient carbon which was previously preserved from decomposition (Walter et al., 2006; Garnett et al., 2013). Although several studies showed that the wetlands usually emit  $\text{CH}_4$  from the decomposition of recent organic matter (Wahlen et al., 1989; Chanton et al., 1995), Zimov et al. (1997) and later Walter et al. (2008) discovered that some arctic lakes release  $\text{CH}_4$  from Pleistocene-aged carbon, highlighting the concern about new additional  $\text{CH}_4$  sources that do not belong to the short carbon cycle. Radiocarbon measurements have led to the discovery of other sources of possible intermediate age such as peatlands (Chanton et al., 2008; Garnett et al., 2013; Leith et al., 2014) or some sediments from the Arctic Ocean (Sapart et al., 2017). For these intermediate age sources, the knowledge of their true  $^{14}\text{CH}_4$  signature before mixing in the atmosphere is essential for accurate  $\text{CH}_4$  source apportionments (Manning et al., 1990; Graven et al., 2019). Considering them as modern sources would yield to an

overestimation of their strength, whereas assigning them as fossil emissions might lead to an underestimation of their magnitude.

### 1.5.3 Atmospheric $^{14}\text{CH}_4$

Unlike atmospheric  $^{14}\text{CO}_2$ , which has been continuously monitored since the mid-1950s, measurements of atmospheric  $^{14}\text{CH}_4$  are scarce, which is mainly due to its very low concentration in the atmosphere and hence the labor-intensive methods required for its analysis. The first radiocarbon measurements of atmospheric  $\text{CH}_4$  were conducted by Willard Frank Libby in 1949 and 1950 before the atmospheric bomb tests and were published later (Ehhalt, 1974; Ehhalt and Schmidt, 1978). More systematic measurements at remote sites started in the late 1980s in the Northern and the Southern Hemisphere (Lowe et al., 1988; Wahlen et al., 1989; Quay et al., 1991; Levin et al., 1992). Recently, Petrenko et al. (2008) developed an extraction system for  $^{14}\text{CH}_4$  measurements of ancient air trapped in polar ice, allowing reconstructing a history of atmospheric  $^{14}\text{CH}_4$  (Petrenko et al., 2017; Hmiel et al., 2020).

Lassey et al. (2007a) presented a composite record of atmospheric  $^{14}\text{CH}_4$  measurements supplied by the authors aforementioned (see Figure 1.6). Assuming that the  $^{14}\text{C}$  content of the biospheric source of  $\text{CH}_4$  reflects atmospheric  $^{14}\text{CO}_2$  with a lag time of 6 years and an attenuation caused by an averaging of the bomb peak over time, they also simulated the theoretical  $^{14}\text{CH}_4$  history (plain lines). Although the observations are roughly consistent with the simulated values until the late 1970s, atmospheric  $^{14}\text{CH}_4$  has not followed the decline of  $^{14}\text{CO}_2$  as it kept rising since. The explanation lies in the strong growth of the nuclear sector with associated  $^{14}\text{CH}_4$  emissions from an increasing number of nuclear power plants (NPPs), which overcompensated the decline of the bomb  $^{14}\text{C}$  tail (Lassey et al., 2007a; Zazzeri et al., 2018). Although NPPs cannot be considered as a significant  $\text{CH}_4$  source (van der Zwaan, 2013), they are a considerable source of  $^{14}\text{CH}_4$ , which has been estimated to account for 20–40% of the total  $^{14}\text{CH}_4$  burden in the atmosphere in the 1990s (Quay et al., 1999).

The composite record presented in Figure 1.7 focuses on the recent history of atmospheric  $^{14}\text{CH}_4$  measurements at remote sites and highlights some interesting features (Lassey et al., 2007b): First, the quality of the measurements has quickly improved, resulting in less scatter and lower uncertainties. Second, a linear increase of  $^{14}\text{CH}_4$  of almost 1 pMC per year fits relatively well to the observed values for the period 1986–2000, which can be almost solely imputed to the NPP source (Lassey et al., 2007a). Finally, the graph underlines the scarceness of recent measurements, with most of the measurements being performed between 1987 and 1995. The most recent published  $^{14}\text{C}$  measurement of atmospheric  $\text{CH}_4$  was carried out in 2009 by Townsend-Small et al. (2012). However, their air samples collected at Mount Wilson Observatory over a single day yielded to  $^{14}\text{CH}_4$  results ranging from +262‰ to +340‰ (127–135 pMC). Hence, these results are not representative of background  $^{14}\text{CH}_4$ .

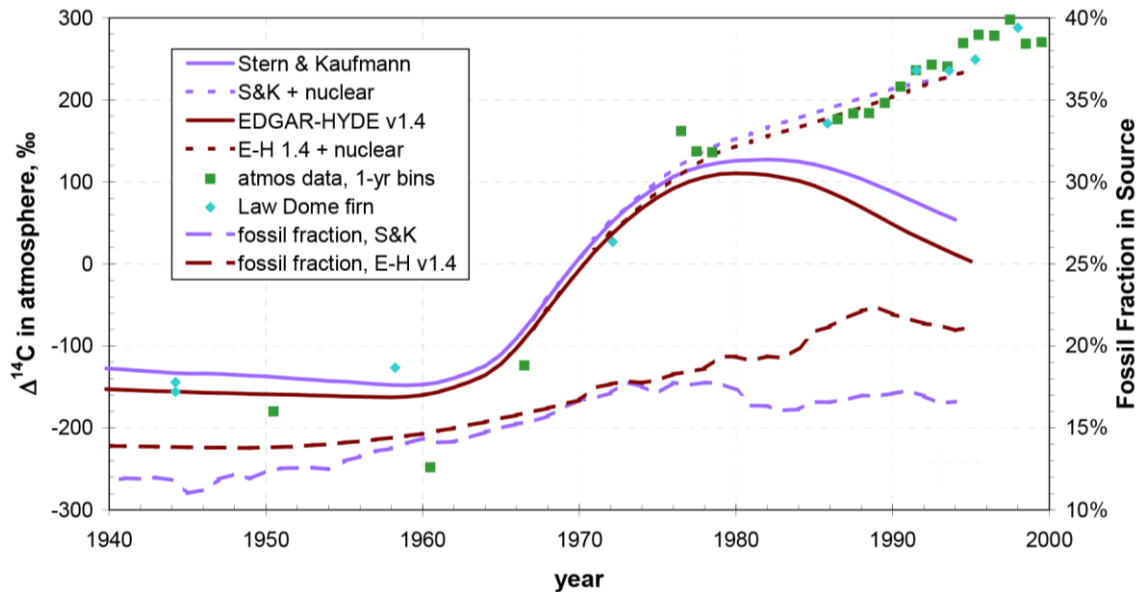


Figure 1.6 Comparison of background  $^{14}\text{CH}_4$  results (squares and diamonds) with simulated  $^{14}\text{CH}_4$  values. Plain lines: Simulations accounting for a 6-yr biospheric lag time. Dotted lines: Simulations accounting for a 6-yr biospheric lag time and the contribution from NPPs. Dashed lines: Simulations of the fossil fraction of the  $\text{CH}_4$  source. Source: Lassey et al. (2007a).

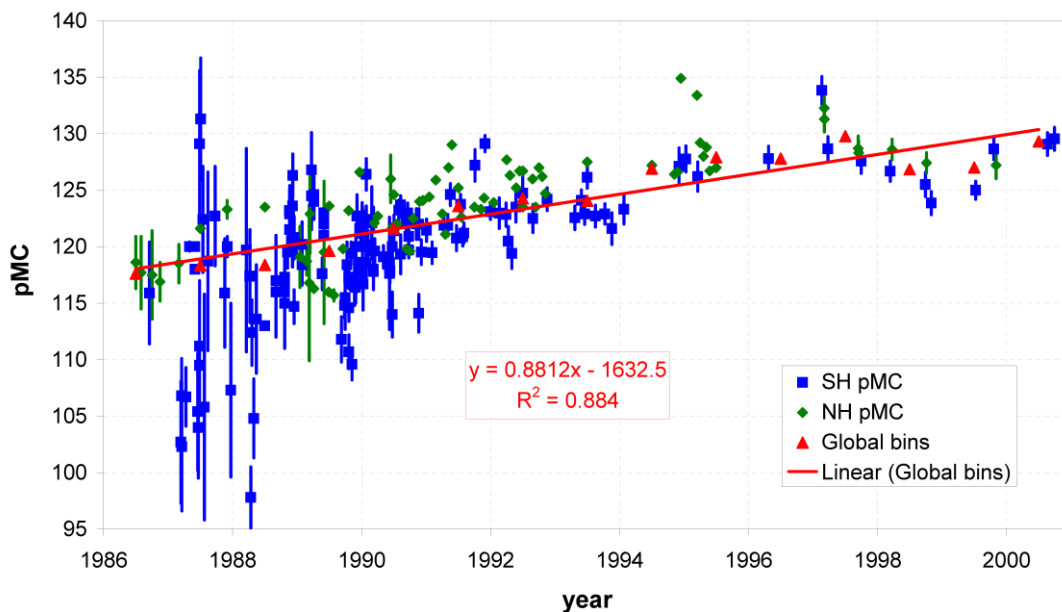


Figure 1.7 Compiled data of atmospheric  $^{14}\text{CH}_4$  measurements performed in the Southern Hemisphere (blue squares) and the Northern Hemisphere (green diamonds). The y-axis is reported in percent Modern Carbon (pMC), with  $\text{pMC} = F^{14}\text{C} \cdot 100\%$ . Source: Lassey et al. (2007b).

Although the impact of nuclear power production was already visible in the late 1980s, atmospheric  $^{14}\text{CH}_4$  values were still between fossil sources (0 pMC) and an estimated biogenic source of  $131 \pm 3$  pMC (Lowe et al., 1988). Until recently, atmospheric  $^{14}\text{CH}_4$  was still rising and  $^{14}\text{CO}_2$  is today still decreasing. Hence, the  $^{14}\text{C}$  content of atmospheric  $\text{CH}_4$  is higher than

all its natural and anthropogenic sources and all types of emissions tend to decrease the atmospheric  $^{14}\text{CH}_4$  concentration.

### 1.5.4 Global source apportionment of $\text{CH}_4$

By releasing  $^{14}\text{C}$ -free  $\text{CH}_4$  into the atmosphere, fossil  $\text{CH}_4$  sources dilute the  $^{14}\text{C}$  content of atmospheric  $\text{CH}_4$ . Assuming a simple model of  $\text{CH}_4$  sources, which classifies them either as “modern” or “fossil”, a measure of atmospheric  $^{14}\text{CH}_4$  provides a direct estimate of the relative strength these two types of sources (Lowe et al., 1988; Manning et al., 1990). The authors usually report the “fossil fraction”, which is the fraction of the global  $\text{CH}_4$  source that has a fossil origin (Lowe et al., 1988; Lassey et al., 2007b). Neglecting that intermediate age sources also contribute to a dilution of atmospheric  $^{14}\text{CH}_4$  implies that the fossil fractions reported are upper estimates (Manning et al., 1990).

The five samples of various origins collected prior to the nuclear tests and reported by Ehhalt (1974) showed a  $^{14}\text{C}$  content of 80% the one of modern wood, which allowed the author to estimate a fossil contribution of  $\text{CH}_4$  sources of maximum 20%. Although his determination seems robust, as he did not have to account for any bias caused by atom bomb tests or releases of  $^{14}\text{CH}_4$  from NPPs, the samples were collected in industrial areas and might have been contaminated by local fossil emissions. With a similar approach, the fossil fraction has been reported to be 32% (Lowe et al., 1988),  $21 \pm 3\%$  (Wahlen et al., 1989),  $18 \pm 9\%$  (Quay et al., 1999) and 17–25% (Manning et al., 1990). From the  $^{14}\text{C}$  results shown in Figure 1.7, Lassey et al. (2007b) estimated a fossil fraction of  $30.0 \pm 2.3\%$  for 1986–2000. While these estimations are derived from reliable  $^{14}\text{CH}_4$  results from clean background sites, the authors needed to correct for the bomb peak and the global impact of the NPP source, which explains the large uncertainties reported.

Today, continuous measurements of  $^{14}\text{CH}_4$  at background sites do not exist, which explains why there is no recent estimate of the fossil fraction of the global  $\text{CH}_4$  source using radiocarbon analysis. Background  $^{14}\text{CH}_4$  values in Europe could also provide interesting information concerning the evolution of the contribution of NPPs (Levin et al., 1992; Zazzeri et al., 2018).

### 1.5.5 Regional source apportionment of $\text{CH}_4$

The knowledge of the global  $\text{CH}_4$  budget (see Figure 1.2) is valuable for a good understanding of the role of  $\text{CH}_4$  in the climate system. However, it is not very helpful for the development of abatement strategies, as the latter can only be realistically implemented at local or regional scales. It is therefore crucial to identify the main  $\text{CH}_4$  sources in regions where emissions are high, in order to deploy efficient mitigations policies targeting large emitters. A few authors used measurements of  $\text{CH}_4$  concentration and fluxes in combination with statistical tools and correlations with other gas species to apportion regional sources of  $\text{CH}_4$  (Cambaliza et al., 2015; Assan et al., 2018). Using high-frequency stable isotope analysis of atmospheric  $\text{CH}_4$  at

the Cabauw tower in the Netherlands, Röckmann et al. (2016) were able to distinguish pollution events (natural gas and landfills) from agricultural emissions.

As discussed previously, radiocarbon analysis comes in as a more straightforward and complementary tool, which has the unequivocal ability to distinguish  $^{14}\text{C}$ -free emissions (natural gas, shale gas) from biogenic sources of  $\text{CH}_4$ . It could also help validate the effectiveness of abatement strategies targeting fossil fuel  $\text{CH}_4$  emissions by measuring the evolution of the fossil fraction of  $\text{CH}_4$  emissions over time (Graven et al., 2019). A  $^{14}\text{C}$ -based regional source apportionment of atmospheric  $\text{CH}_4$  could be carried out in a similar way as it has been performed for  $\text{CO}_2$ , by comparing the  $^{14}\text{CH}_4$  content of clean background air and polluted sites (Graven et al., 2019). Unfortunately, such a technique has not been successfully implemented yet for two main reasons: First, NPPs do not only contribute to a global enhancement of atmospheric  $^{14}\text{CH}_4$ , but their sporadic discharges are also responsible for a large scatter of measured  $^{14}\text{CH}_4$  values in air samples collected in countries with NPPs (Kunz, 1985; Eisma et al., 1995). This issue precluded Levin et al. (1992) and later Townsend-Small et al. (2012) to apportion  $\text{CH}_4$  sources using  $^{14}\text{CH}_4$  analysis. Second, radiocarbon analysis is an expensive technique that requires labor-intensive pretreatment methods. This is particularly the case for  $\text{CH}_4$ , as its low concentration in the atmosphere implies that  $\text{CH}_4$  has to be extracted from large volumes of air to run an analysis. Hence, the vast majority of  $^{14}\text{CH}_4$  studies focus on methane-rich environments and measure close to major sources such as wetlands or gas leaks (see section 1.5.2).

Despite the challenges associated with  $^{14}\text{C}$  analyses of atmospheric  $\text{CH}_4$ ,  $^{14}\text{CH}_4$  measurements at polluted sites are too few to withdraw definitely the possibility of a  $\text{CH}_4$  source apportionment using radiocarbon. Once again, the paramount importance of measurements at clean background sites is emphasized: similarly to the estimation of the fossil component of  $\text{CO}_2$  in air (Berhanu et al., 2017), the calculation of the regional fossil fraction of the methane sources relies strongly on the knowledge of background atmospheric  $^{14}\text{CH}_4$ . Indeed, an underestimation of background  $^{14}\text{CH}_4$  would yield to an underestimation of fossil sources. To test the approach of a regional  $^{14}\text{C}$  source apportionment of  $\text{CH}_4$ , a setup for the extraction of pure  $\text{CH}_4$  from atmospheric air is required.

## 1.6 Sample preparation for $^{14}\text{CH}_4$ analysis

### 1.6.1 Requirements for a $^{14}\text{C}$ -AMS measurement

Owing to the very low abundance of  $^{14}\text{C}$  in the atmosphere, we showed in section 1.4.2 that the use of an AMS is today mandatory for  $^{14}\text{C}$  measurements of organic materials. A radiocarbon measurement of  $\text{CH}_4$  comes as a real technical challenge, since  $^{14}\text{CH}_4$  has an extremely low mole fraction of  $10^{-18}$  to  $10^{-20}$  in the atmosphere. Thus, the amount of  $\text{CH}_4$  necessary for a  $^{14}\text{C}$  measurement is the bottleneck of the method, as it dictates the size of the

samples collected in the field and hence the complexity of the extraction and purification methods. As described in section 1.4.2, the typical amount of carbon required for a conventional measurement (solid target) is 1 mg C, which approximately corresponds to 2 mL pure CH<sub>4</sub>. With a CH<sub>4</sub> mole fraction usually below 2 ppm, a conventional <sup>14</sup>C analysis of atmospheric CH<sub>4</sub> involves more than 1000 L air (Wahlen et al., 1989; Moriizumi et al., 1998), although some authors could measure smaller samples of a few hundred liters (Klouda et al., 1986; Lowe et al., 1991; Townsend-Small et al., 2012).

Besides the challenges brought by the need to extract CH<sub>4</sub> from large volumes of air, another crucial parameter for the quality of a <sup>14</sup>CH<sub>4</sub> analysis is the purity of CH<sub>4</sub> before its radiocarbon measurement. In an ideal situation, all other carbon-containing gases need to be quantitatively removed during the sample pretreatment, which are mainly CO (~100 ppb) and CO<sub>2</sub> (~415 ppm) in the case of atmospheric air. With a mole fraction more than 200 times higher than the one of CH<sub>4</sub>, CO<sub>2</sub> is the main contaminant of a concern. However, CO cannot be always overlooked as its concentration in the vicinity of its sources is significantly enhanced (Pack et al., 2015).

### 1.6.2 “Standard” procedure

Because of its high volatility and low concentration in air, CH<sub>4</sub> is difficult to separate from other gaseous compounds. For those reasons, commercial setups do not exist and the research groups performing <sup>14</sup>CH<sub>4</sub> measurements developed custom-made extraction lines (e.g. Kessler and Reeburgh, 2005; Petrenko et al., 2008; Pack et al., 2015). The gaseous compounds are usually separated based on their different physical properties. With a boiling point of -78 °C and -89 °C, respectively, less volatile compounds such as CO<sub>2</sub> or N<sub>2</sub>O condense at -196 °C and are therefore trapped in liquid nitrogen traps. As its boiling point is -162 °C, CH<sub>4</sub> has a still relatively large vapor pressure of 13 mbar at -196 °C, which is the reason why atmospheric CH<sub>4</sub> (< 2 ppm) does not condense in liquid nitrogen traps.

The simplified schematic shown in Figure 1.8 highlights the usual main steps involved in the preparation of CH<sub>4</sub> samples for radiocarbon measurements. Typically, CH<sub>4</sub> is cryogenically separated from the other gases in air in a stepwise process: the sample is flushed through a purification line where CO<sub>2</sub> is first removed from the gas mixture in a liquid nitrogen trap. Although not systematically performed (Garnett et al., 2016), CO is then combusted to CO<sub>2</sub> and subsequently trapped as CO-derived CO<sub>2</sub>. The temperature of this first combustion oven is set low enough to keep CH<sub>4</sub> unaffected. Then, CH<sub>4</sub> is combusted to CO<sub>2</sub> at a higher temperature before being collected in another liquid nitrogen trap. Finally, CH<sub>4</sub>-derived CO<sub>2</sub> is graphitized and its <sup>14</sup>C content is measured with an AMS. Small variations around this general method include the use of Sofnocat or Schütze reagent to quantitatively oxidize CO to CO<sub>2</sub> at ambient temperature (Lowe et al., 1991; Petrenko et al., 2008).

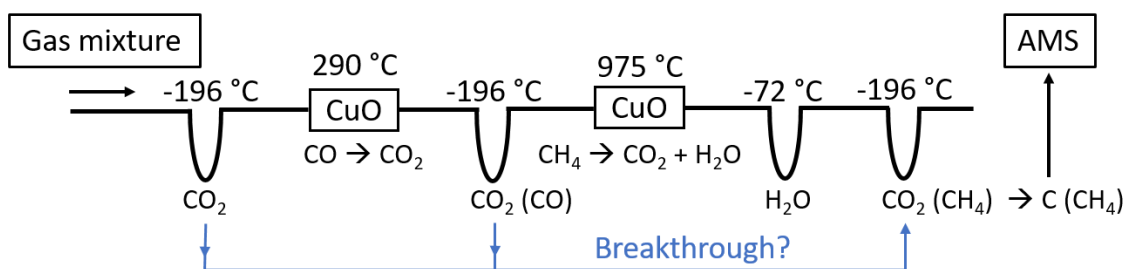


Figure 1.8 Typical procedure for the preparation of  $^{14}\text{CH}_4$  samples from a gas mixture (atmospheric air or  $\text{CH}_4$ -enriched gas sample). Typical combustion temperatures are reported. In brackets: original molecule in the gas mixture. In blue: potential drawback of the procedure.

The combustion of CO and  $\text{CH}_4$  to  $\text{CO}_2$  reduce their volatility and allow a collection of the  $\text{CO}_2$  subfractions of different origins in individual traps. However,  $\text{CH}_4$ -derived  $\text{CO}_2$  is now undistinguishable from CO-derived  $\text{CO}_2$  and the original  $\text{CO}_2$  in the gas mixture. Although the setups are usually optimized to avoid possible contamination, there is no guarantee that a defective trap cannot lead to a  $\text{CO}_2$  breakthrough to the  $\text{CH}_4$ -derived  $\text{CO}_2$  trap (Pack et al., 2015).

Some of these extraction lines were used to purify low concentration  $\text{CH}_4$  samples like atmospheric  $\text{CH}_4$  (Lowe et al., 1991; Townsend-Small et al., 2012) or air bubbles trapped in ice cores (Petrenko et al., 2008). However, most of these setups are not suited to the measurement of atmospheric  $^{14}\text{CH}_4$ , as they are designed to accept smaller sample volumes with larger  $\text{CH}_4$  concentrations such as natural waters or sediments (Kessler and Reeburgh, 2005; Pack et al., 2015; Garnett et al., 2016).

### 1.6.3 Alternative approach

About 20 to 30 years ago, a few research groups developed a preparation line that includes a purity check of  $\text{CH}_4$  prior to the  $^{14}\text{C}$  analysis (Wahlen et al., 1989; Eisma et al., 1994; Moriizumi et al., 1998). To do so, they combined a  $\text{CH}_4$  preconcentration line using adsorbents to trap  $\text{CH}_4$  with a preparative gas chromatography technique (pGC) to purify  $\text{CH}_4$  before its combustion to  $\text{CO}_2$ . With this technique, the potential contamination from the breakthrough of  $\text{CO}_2$  from other traps is eliminated, as  $\text{CH}_4$  is combusted to  $\text{CO}_2$  after its purification in the GC column. Unfortunately, the preconcentration of  $\text{CH}_4$  from very large amounts of air requires big traps and considerable amounts of adsorbent, which results in laborious cleaning procedures and time-consuming sample preparation. This drawback is probably the main reason why such setups are not used anymore for  $^{14}\text{CH}_4$  measurements.

## 1.7 Aims of the thesis

The climate is changing and it is a well-known aspect of the human race that the principles of precaution and prevention do not weigh much in view of other economic challenges. Climate change is not affecting humans evenly and often more effort is put into finding proofs of the human responsibility instead of looking for solutions to mitigate climate change and reduce its impact on the most exposed and vulnerable societies. To guide decision makers in their quest of efficient action plans, it is crucial to provide them with robust and accurate information concerning the main actors of climate change, their possible evolution and the consequences for nature and human societies. Among the culprits of climate change, CH<sub>4</sub> plays a unique role as one of the main contributors to global warming. Climate feedbacks could trigger the release of enormous amounts of CH<sub>4</sub> and the future evolution of its sources is still not well understood. However, the relatively low lifetime of CH<sub>4</sub> in the atmosphere with respect to the one of CO<sub>2</sub> makes CH<sub>4</sub> a good candidate to implement powerful mitigation plans on relatively short timescales via the reduction of anthropogenic CH<sub>4</sub> emissions. In order to enable the development of meaningful local and regional abatement strategies, efficient tools need to be available to unravel the main sources of CH<sub>4</sub>. Among them, radiocarbon measurements of CH<sub>4</sub> have the unique ability to distinguish fossil and modern sources of CH<sub>4</sub>. Thus, measuring the radiocarbon content of atmospheric CH<sub>4</sub> can be used as a source apportionment tool and provides a valuable complementary information. Unfortunately, radiocarbon measurements of CH<sub>4</sub> remain scarce and time consuming, especially when coping with low concentration methane samples.

In this framework, the research presented in this thesis has two main objectives. First, the development of an analytical setup, which allows the preparation of pure environmental CH<sub>4</sub> samples for radiocarbon analysis. Second, the preparation and radiocarbon measurement of atmospheric CH<sub>4</sub> samples, for a better understanding of CH<sub>4</sub> sources.

At first, the development of a new analytical setup for the preparation of pure atmospheric CH<sub>4</sub> samples is presented (Chapter 2). The system combines a preconcentration line with a preparative gas chromatography technique to isolate pure environmental CH<sub>4</sub> samples for <sup>14</sup>C measurements.

In Chapter 3, we present a new dataset of atmospheric <sup>14</sup>CH<sub>4</sub> and <sup>14</sup>CO<sub>2</sub> measurements performed on samples collected biweekly at three different sites in Switzerland: the Beromünster tall tower (rural area), the University of Bern (urban area) and the Jungfraujoch Research Station (free tropospheric air).

In Chapter 4, we report on a study aiming at better understanding the impact of nuclear power plants on atmospheric <sup>14</sup>CH<sub>4</sub>, which took place during the revision of the Gösgen nuclear power plant on June 2, 2019. The consequences for the use of <sup>14</sup>CH<sub>4</sub> and <sup>14</sup>CO<sub>2</sub> in environmental studies are discussed.

In Chapter 5, we show our results of a European  $^{14}\text{C}$  intercomparison of biogas and biofossil gas mixtures, which has the objective to compare the biogenic carbon fraction of five samples obtained by the participating laboratories. Although we cannot report the results of the other participants, as they are not yet available, this intercomparison highlights the versatility of the new setup.

Chapter 6 summarizes the major results reported in this thesis and presents some propositions of system adaptations for the handling of high concentration methane samples. Finally, further research directions are proposed for the next coming years.

## 2. Methane Preconcentration and Purification Setup (MPPS)

### Preamble

The development of a new sample preparation setup for  $^{14}\text{CH}_4$  analysis came along with some requirements such as throughput, reliability and versatility. These requirements, together with some financial and practical considerations, were the main factors driving our choices.

As  $^{14}\text{C}$  measurements of atmospheric  $\text{CH}_4$  are expensive and time-consuming,  $^{14}\text{CH}_4$  measurements remain very scarce and the interpretation of  $^{14}\text{CH}_4$  results suffers from the small datasets available. As shown in section 1.4.2.2, the MICADAS AMS offers the possibility of a direct  $\text{CO}_2$  measurement, skipping the graphitization step and allowing the analysis of sample sizes of 50  $\mu\text{g C}$  or smaller. This feature is particularly interesting for an atmospheric  $^{14}\text{CH}_4$  determination, as samples of only 50 L air are sufficient for such analysis. Hence, a direct gas measurement with the AMS offers two main advantages: First, it eases the sample collection in the field, as a regular atmospheric  $^{14}\text{CH}_4$  analysis typically requires 1000 L air (see section 1.6.1). Second, the preparation of smaller samples drastically facilitates the preconcentration and purification procedures, as it allows building a smaller setup requiring less time for its cleaning and running. Hence, the sample throughput has the potential to be greatly improved compared to more conventional extraction lines. Although a direct  $\text{CO}_2$  measurement comes at the cost of a reduced measurement precision (see section 1.4.2), the benefits largely outweigh this disadvantage. Furthermore and unlike for dating purposes, the  $^{14}\text{C}$  results will be primarily used for a  $\text{CH}_4$  source apportionment, for which the precision of the measurement is not the only limiting factor (see Chapter 3).

As  $^{14}\text{CH}_4$  measurements performed during a field campaign are usually rather few and cannot be systematically repeated by lack of time or sample material, it is of paramount importance to get reliable results. To avoid the potential contamination issues described in section 1.6.2, a systematic quality check is a prerequisite. Similar to the setups used by Wahlen et al. (1989) or Eisma et al. (1994), we decided to implement a preparative gas chromatography technique to purify  $\text{CH}_4$  before its combustion to  $\text{CO}_2$ . However, this technique brings some other challenges, such as the necessity to decrease the sample size dramatically before the purification step with the GC. Thus, atmospheric  $\text{CH}_4$  needs to be preconcentrated beforehand, which involves the use of cryogenic traps filled with adsorbents, as liquid nitrogen alone is not sufficient to trap  $\text{CH}_4$  (see section 1.6.2). The porous polymer HayeSep D was first considered as the best candidate, since it offers a high selectivity of  $\text{CH}_4$  over bulk air (Eyer et al., 2014). However, separating  $\text{CH}_4$  from  $\text{O}_2$  and  $\text{N}_2$  with this adsorbent necessitates to work at a stable temperature of  $-130\text{ }^\circ\text{C}$  (Sapart et al., 2011), which has been tested in the field with and

isopentane bath<sup>1</sup>. Unfortunately, expensive cooling systems such as cryofingers are necessary to keep a stable temperature during the preconcentration of large volumes of air (Mohn et al., 2010; Eyer et al., 2016). For this reason, we chose activated carbon over HayeSep D as it is cheaper, safer, offers acceptable selectivity and can be simply operated at liquid nitrogen temperature (Bräunlich, 2000).

Our initial thoughts led us to a first idea of a portable CH<sub>4</sub> preconcentration setup, which would allow the collection of preconcentrated air samples in small glass bulbs directly in the field. Although Palonen et al. (2017) developed a portable CH<sub>4</sub> sampling system for radiocarbon analysis, it is not suited to low concentration environments such as background air. Indeed, the setups adapted to the preconcentration of atmospheric air require large equipment (compressors, pumps, electricity supply), severely limiting access to remote locations. With the need of only 50 L air for a <sup>14</sup>CH<sub>4</sub> measurement, we decided to perform the preconcentration in the laboratory. Thus, minimal equipment is sufficient to collect samples in the field, giving the flexibility to sample at any location or to perform a simultaneous collection of samples at different sites. Moreover, this strategy allows carrying out the sample preparation in a more controlled way in the laboratory, with a greater ability to solve system failures and limit the risks of a field campaign catastrophe. As we will see throughout this thesis, versatility was also considered all over the development steps, with for example the option to simultaneously prepare CH<sub>4</sub> and CO<sub>2</sub> samples, or the recent adaptation of the setup for the preparation of medium to high concentration CH<sub>4</sub> samples from aqueous environments (Bantle, 2021).

In summary, the new setup presented in this chapter uses the advantages of recent technological breakthroughs for the measurement of small <sup>14</sup>C samples to develop a smaller, faster and more versatile CH<sub>4</sub> preconcentration and purification setup. This chapter was published in the journal Radiocarbon:

Espic, C., Liechti, M., Battaglia, M., Paul, D. Röckmann, T., Szidat, S., 2019. Compound-specific radiocarbon analysis of atmospheric methane: A new preconcentration and purification setup. *Radiocarbon* 61(5), 1461-1476.

---

<sup>1</sup> Personal communication from Célia Sapart.

# COMPOUND-SPECIFIC RADIOCARBON ANALYSIS OF ATMOSPHERIC METHANE: A NEW PRECONCENTRATION AND PURIFICATION SETUP

C. Espic<sup>1,2</sup>, M. Liechti<sup>1</sup>, M. Battaglia<sup>1,2</sup>, D. Paul<sup>3</sup>, T. Röckmann<sup>3</sup>, S. Szidat<sup>1,2\*</sup>

<sup>1</sup>Department of Chemistry and Biochemistry, University of Bern, Bern, Switzerland.

<sup>2</sup>Oeschger Centre for Climate Change Research, University of Bern, Bern, Switzerland.

<sup>3</sup>Institute for Marine and Atmospheric Research (IMAU), Utrecht University, Utrecht, the Netherlands.

\*Corresponding author. Email: szidat@dcb.unibe.ch.

## ABSTRACT

Methane contributes substantially to global warming as the second most important anthropogenic greenhouse gas. Radiocarbon measurements of atmospheric methane can be used as a source apportionment tool, as they allow distinction between thermogenic and biogenic methane sources. However, these measurements remain scarce due to labor-intensive methods required. A new setup for the preparation of atmospheric methane samples for radiocarbon analysis is presented. The system combines a methane preconcentration line with a preparative gas chromatography technique to isolate pure methane samples for a compound-specific radiocarbon analysis. In order to minimize sample preparation time, we designed a simplified preconcentration line for the extraction of methane from 50 L atmospheric air, which corresponds to 50  $\mu\text{g C}$  as required for a reliable radiocarbon analysis of methane-derived  $\text{CO}_2$  gas measurement with accelerator mass spectrometry. The system guarantees a quantitative extraction of methane from atmospheric air samples for  $^{14}\text{C}$  analysis, with a good repeatability and a low processing blank. The setup was originally designed for the measurement of samples with low methane concentrations, but it can also be adapted to apportion sources from environmental compartments with high methane levels such as freshwaters or wetlands.

**Keywords:** methane, radiocarbon, extraction, preparative GC, source apportionment.

## 2.1 Introduction

Since the beginning of the industrial revolution, the concentration of methane ( $\text{CH}_4$ ) in the atmosphere has increased by a factor of 2.5, which is mainly due to anthropogenic emissions (Dlugokencky et al., 2011). With a mole fraction higher than 1.8 ppm,  $\text{CH}_4$  is today the second most important anthropogenic greenhouse gas after  $\text{CO}_2$ . Although the global budget of atmospheric  $\text{CH}_4$  is quite well constrained, individual sources remain poorly quantified and not well understood (Saunois et al., 2016). The spatial and temporal variability of  $\text{CH}_4$

emissions from natural sources are a major hindrance to forecasting and mitigation strategies (Bousquet et al., 2006; Saunio et al., 2016), and a warming climate could alter the strength of these emissions dramatically (Dean et al., 2018).

The sources of atmospheric CH<sub>4</sub> are evaluated by top-down measurements and bottom-up inventories (e.g. Hiller et al., 2014; Jacob et al., 2016), but as a result of the natural variability of CH<sub>4</sub> emissions, these approaches usually do not agree well (Nisbet and Weiss, 2010). To improve this approach, stable and clumped isotopes of methane are also widely studied, because many CH<sub>4</sub> sources have a specific isotopic signature (Quay et al., 1999; Stolper et al., 2015; Sapart et al., 2017).

The radiocarbon (<sup>14</sup>C) content of atmospheric CH<sub>4</sub> is of growing interest, since it can be used as a tool for a CH<sub>4</sub> source apportionment (Wahlen et al., 1989; Lassey et al., 2007b; Petrenko et al., 2008; Townsend-Small et al., 2012; Petrenko et al., 2017). Indeed, “contemporary” or “modern” CH<sub>4</sub> sources (e.g. agriculture, biomass burning) contain present-day <sup>14</sup>C levels, whereas “old” or “fossil” CH<sub>4</sub> sources (e.g. fossil fuels, geologic CH<sub>4</sub>) are <sup>14</sup>C-free. Intermediate age sources such as arctic lakes or peatlands can also be dated, providing valuable information about carbon dynamics in such environments (Zimov et al., 1997; Walter et al., 2006; Garnett et al., 2011). These radiocarbon measurements can be performed by accelerator mass spectrometry (<sup>14</sup>C-AMS), but this task is challenging given the large amounts of CH<sub>4</sub> required and its very low concentration in the atmosphere.

Methane is usually separated from other trace gases in a stepwise process (Lowe et al., 1991; Brenninkmeijer and Röckmann, 1996; Röckmann, 1998; Kessler and Reeburgh, 2005; Petrenko et al., 2008; Pack et al., 2015): First CO<sub>2</sub> is cryogenically removed, then CO is oxidized to CO<sub>2</sub> and also cryogenically removed, before CH<sub>4</sub> can finally be oxidized and isolated as CO<sub>2</sub> as well. Alternatively, molecular sieves or soda lime are used to scrub CO<sub>2</sub> (Palonen et al., 2017; Garnett et al., 2019). However, for these simplified processes, cross contamination of CO<sub>2</sub> from one fraction to the next remains an issue difficult to monitor and overcome (Pack et al., 2015).

Some laboratories use a preparative gas chromatography technique to separate CH<sub>4</sub> from CO<sub>2</sub> and other trace gases. This technique has been applied for stable isotope measurements of CH<sub>4</sub>, where only small samples are necessary for such analysis (e.g. Miller et al., 2002; Bock et al., 2010; Brass and Röckmann, 2010). It has also been used in combination with an AMS, for radiocarbon measurements of repeated injections of high concentration methane samples (McIntyre et al., 2013). Although a preparative gas chromatography technique warrants that pure CH<sub>4</sub> is measured, its application for <sup>14</sup>C measurements of atmospheric CH<sub>4</sub> is not straightforward as the required sample volumes are of several orders of magnitude larger for radiocarbon analysis.

Here, we present a new methane preconcentration and purification setup (MPPS) that allows the preparation of pure atmospheric CH<sub>4</sub> samples for <sup>14</sup>C measurements. The system combines

a methane preconcentration setup (PRECON) with a purification setup which applies preparative gas chromatography to obtain pure CH<sub>4</sub> samples from the atmosphere (PURIF).

## 2.2 Methods

### 2.2.1 Goals and strategy

Our research aims at enabling the extraction of CH<sub>4</sub> from various kinds of environments (e.g. atmosphere, fresh waters and wetlands) and performing <sup>14</sup>C measurements to deepen the knowledge of CH<sub>4</sub> sources and the carbon cycle. The strategy adopted for the collection, preparation and radiocarbon measurements of environmental CH<sub>4</sub> samples is shown in Figure 2.1.

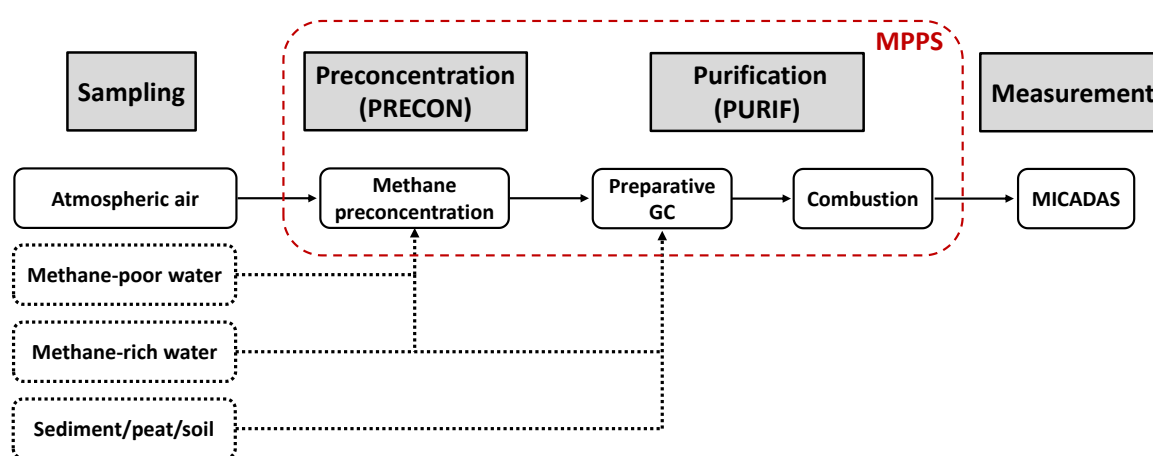


Figure 2.1 Strategy for <sup>14</sup>CH<sub>4</sub> measurements. Red dashed box: methane preconcentration and purification setup (MPPS), which represents the essential part of this work. Black dotted line: connection of samples from other CH<sub>4</sub> sources that will be measured in the future.

The procedure can be divided in four main steps: field sampling, preconcentration, purification and <sup>14</sup>C measurement. As shown by the black dashed lines in Figure 2.1, the possibility to measure CH<sub>4</sub> from aquatic and terrestrial environments will be implemented soon. However, the system has been developed and optimized for <sup>14</sup>C measurements of atmospheric CH<sub>4</sub>, as this task remains the biggest challenge given the low concentration of CH<sub>4</sub> in air (< 2 ppm) and the overwhelming presence of CO<sub>2</sub> (> 400 ppm). First, 50–100 L of atmospheric air are collected in an aluminum bag which is brought to the lab, where it is connected to a methane preconcentration line (PRECON), to dramatically decrease the sample size by removing CO<sub>2</sub> and most of the bulk air (i.e. N<sub>2</sub>, O<sub>2</sub> and Ar). The preconcentrated sample is then transferred to a GC column, where CH<sub>4</sub> is chromatographically purified and subsequently trapped as pure CH<sub>4</sub>. The purity can be checked by re-injection of the trapped CH<sub>4</sub> into the GC. It is then combusted to CO<sub>2</sub>, manometrically quantified and flame-sealed in a glass ampoule. Finally, the <sup>14</sup>C measurement of the CH<sub>4</sub>-derived CO<sub>2</sub> is performed with a MICADAS AMS (Szidat et al., 2014).

The individual steps involved in a  $^{14}\text{C}$  measurement of atmospheric  $\text{CH}_4$  are described in the following subsections, with a special emphasis on the PRECON and the PURIF analytical setups.

## 2.2.2 Sampling

It is necessary to extract  $\text{CH}_4$  from 50 to 100 liters of air, as its concentrations are less than 2 ppm in atmospheric background air and the target amount for reliable  $^{14}\text{C}$  gas measurements is 50  $\mu\text{g C}$ . Therefore, atmospheric air samples are collected by pumping 50–100 L air (STP) into an aluminum bag (100 L PE-AL-PE, Tesseraux, Germany) using a small membrane pump (N838ANE, KNF, Germany).

## 2.2.3 Methane preconcentration setup (PRECON)

### 2.2.3.1 Description

A new methane preconcentration setup was developed in our laboratory. It facilitates a drastic reduction of the size of atmospheric air samples from 50–100 L down to 10–15 mL by removing most of the bulk air and  $\text{CO}_2$ , while preserving the original  $\text{CH}_4$  content. This setup (see Figure 2.2a) is coupled to a methane purification setup (see Figure 2.2b), which will be described in the next section. The main components are three cryogenic traps cooled to liquid nitrogen temperature ( $-196\text{ }^\circ\text{C}$ ), of which the first (Russian doll trap, RDT) removes  $\text{CO}_2$ , while the second (charcoal trap, CT1) and the third (CT2) allow two successive  $\text{CH}_4$  preconcentration steps.

The line consists of 1/4" stainless steel (SS) tubing with Swagelok connections (Swagelok, USA) and a central part between V2 and V7 made of 12 mm OD glass with grease-free Rotulex joints. These two parts are connected using Ultra-Torr (UT) fittings on the glass side and SS tube adapters on the metal side (Swagelok, USA). The gas flow rates in the line, all given in normal conditions (1013 mbar,  $0\text{ }^\circ\text{C}$ ), are regulated by two mass flow controllers MFC1 (SLA5850S,  $0\text{--}5\text{ L min}^{-1}$ , Brooks, USA) and MFC2 (SLA5850S,  $0\text{--}150\text{ mL min}^{-1}$ , Brooks, USA). MFC1 and MFC2 regulate the flow for the first and second preconcentration step, respectively. The absolute pressure along the line is monitored by four pressure sensors (P1–P3: PBMN Industrial Low Pressure,  $0\text{--}2\text{ bar}$ ; P4: PBMN flush,  $0\text{--}2\text{ bar}$ , Baumer, Switzerland).

An aluminum bag (sample bag), which contains an atmospheric air sample collected in the field, is connected to the preconcentration line. The sample is dried in the trap ‘Drierite’, a plastic tube (24 mm ID,  $L = 160\text{ mm}$ ) filled with 70 g of Drierite<sup>TM</sup> ( $\text{CaSO}_4$ , 10–20 mesh, Sigma-Aldrich, USA) which turns from blue to pink when it should be regenerated ( $60\text{ min}$ ,  $210\text{ }^\circ\text{C}$ ). V1 allows to switch to a nitrogen supply to clean the system ( $\text{N}_2$ , purity = 99.999%, Carbagas, Switzerland).

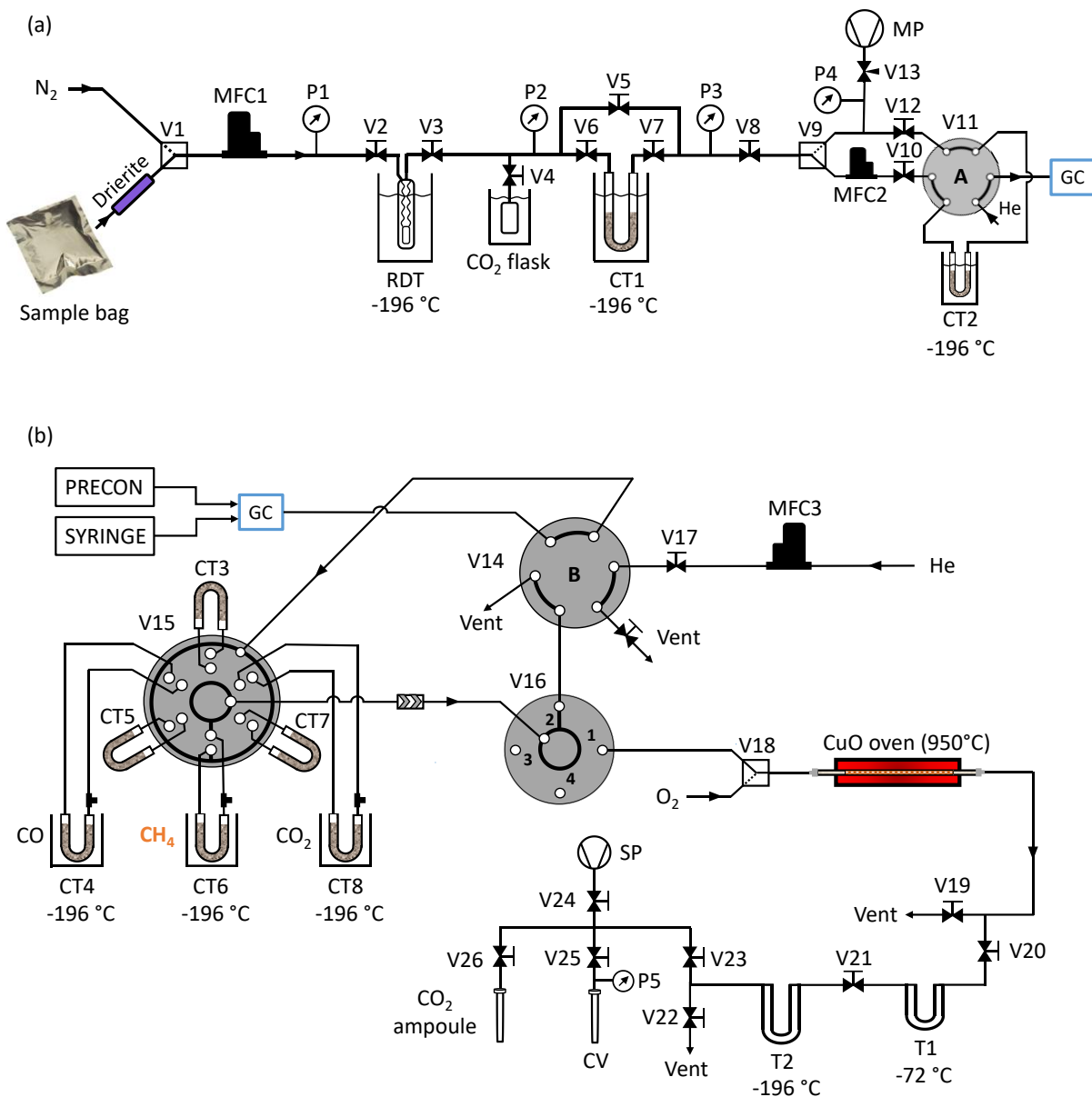


Figure 2.2 a) Methane preconcentration setup (PRECON). The traps RDT, CT1 and CT2 are used for CO<sub>2</sub> removal, first and second CH<sub>4</sub> preconcentration steps, respectively. b) Methane purification setup (PURIF), shown when trapping pure CO, CH<sub>4</sub> and CO<sub>2</sub> provided from either a syringe injection or the PRECON.

RDT is a custom-made “Russian doll” glass trap of a concentric design, similar to the one described by Brenninkmeijer and Röckmann (1996). When immersed into liquid nitrogen, the undulations of its inner part and three nested glass fiber thimbles (Whatman 33 x 94 mm and 25 x 100 mm, GE Healthcare, USA) at its bottom section ensure a very efficient trapping of CO<sub>2</sub> and other lower volatility gases through the mechanisms of condensation and adsorption. This configuration allows an efficient removal of substantial amounts of CO<sub>2</sub> at high flow rates. Atmospheric CO<sub>2</sub>, which has been scavenged from the air sample and trapped in RDT, can be recovered after the end of the preconcentration by cryogenically transferring it into the

glass bottle ‘CO<sub>2</sub> flask’. An automated graphitization equipment (Němec et al., 2010) is then used for the production of solid targets for <sup>14</sup>CO<sub>2</sub> measurements.

CT1 is a custom-made U-shaped glass trap (13 mm ID) filled with 12 g activated charcoal (Fluka 05112, grain size 0.3–0.5 mm, 0.41 g/cm<sup>3</sup>, Sigma-Aldrich, USA). P2 and P3 are used to monitor the pressure drop across the trap and the stability of the system throughout the first preconcentration step. A bypass allows excluding this trap from the flow path when necessary.

The second CH<sub>4</sub> preconcentration step is achieved in CT2, a custom-made 1/8” OD SS U-shaped trap (2.16 mm ID, L = 40 cm) filled with 0.5 g charcoal. The trap is connected to the valve V11, an electrically actuated 2-position 6-port valve with 1/8” fittings (VICI, USA), which is used in “load” mode when CH<sub>4</sub> is preconcentrated into CT2 (as shown in Figure 2.2a) or in “injection” mode when the sample in CT2 is transferred to the GC column of the PURIF.

The sample is pumped from the aluminum bag through the preconcentration line with a membrane pump MP (MZ 2C NT, Vacuubrand, Germany), which is well suited for the handling of high gas flow rates in the line. The pump has an ultimate vacuum of 7 mbar and is also used for cleaning purposes, as it can easily tolerate the removal of potential moisture in the line. Finally, V13 is a needle valve which allows to stop pumping the line gently when required.

### 2.2.3.2 Procedure

#### *Cleaning*

Before the preconcentration of an air sample, the line and particularly the traps are cleaned thoroughly to remove any contamination from the previous sample or from eventual leaks in the line. First, RDT is cleaned at 95 °C (hot water bath) in a N<sub>2</sub> flow of 1.5 L min<sup>-1</sup> for 3 min, to remove water vapor and other condensable gases that could remain adsorbed onto the glass fiber thimbles. In this step, CT1 is bypassed and the impurities are directly removed by the pump. As CT1 contains a significant amount of charcoal, care is taken to ensure that CH<sub>4</sub> previously adsorbed is comprehensively eliminated. To do so, CT1 is heated to 95 °C, evacuated for 10 min and then flushed with N<sub>2</sub> (20 min, 1.5 L min<sup>-1</sup>). The trap is then pressurized to slightly above ambient pressure with N<sub>2</sub> and closed. Finally, CT2 is heated to 95 °C and evacuated for 3 min, flushed for three additional minutes with 50 mL min<sup>-1</sup> N<sub>2</sub>, pressurized to ~1.2 bar and closed.

#### *First preconcentration*

A N<sub>2</sub> flow of 1.5 L min<sup>-1</sup> is established in the line with CT1 bypassed and V9 positioned toward the pump. The sample bag is then opened and V1 is switched to connect the sample to the line. RDT is cooled to -196 °C to scrub CO<sub>2</sub>, and after 1 min, CT1 is included into the flow path by cooling it to -196 °C, opening its inlet (V6) and outlet (V7) and closing the bypass (V5). At that time, CT1 starts trapping CH<sub>4</sub> and the flow integrator of MFC1 is initiated to

determine the total volume of air. During the 40 minutes of sample transfer at a flow rate of  $1.5 \text{ L min}^{-1}$ , the pressures in the lines are monitored (P1, P2 and P3) to avoid a pressure rise due to a leak or a shortcoming of the pump that could trigger  $\text{O}_2$  condensation (Brenninkmeijer, 1991). The pressure in the line is usually very stable, with typical values at gauges P2 and P3 of 205 mbar and 85 mbar, respectively. When the pressure at P1 drops below 200 mbar, indicating that the sample has been almost totally transferred to CT1, the inlets of RDT and CT1 are closed and V1 is switched to the  $\text{N}_2$  bottle. CT1 is evacuated until the pressure at its outlet is stable (i.e.  $\text{P3} = 10\text{--}12 \text{ mbar}$ ). The liquid nitrogen bath is then replaced by a dry ice/ethanol slurry ( $-72 \text{ }^\circ\text{C}$ ) for 5 min 30 sec to desorb and pump away excess air trapped together with  $\text{CH}_4$  into CT1. As shown below, there is no loss of  $\text{CH}_4$  when bulk air is removed from the trap at  $-72 \text{ }^\circ\text{C}$ . V8 is then closed, and the dry ice/ethanol bath is replaced with an ambient temperature water bath to manometrically quantify the amount of gas still trapped in the enclosed volume delimited by V6 and V8. Typical sample volumes after the first preconcentration step are 80–100 ml, which is too high to be directly transferred to the GC column for the  $\text{CH}_4$  purification.

#### *Second preconcentration*

The second preconcentration step, which aims at further reducing the sample volume by removing excess air, is executed in a similar way and transfers the sample from CT1 to CT2. To do so, V9 is switched toward CT2 and the line until V8, including CT2, is evacuated. The valve to the pump V13 is then closed and CT2 is cooled to  $-196 \text{ }^\circ\text{C}$ . CT1 is heated to  $95 \text{ }^\circ\text{C}$  to desorb  $\text{CH}_4$  together with excess air and all gases are then transferred to CT2 at a flow rate of  $20 \text{ mL min}^{-1}$  (MFC2) by opening V8. When the pressure after CT2 starts rising (P4), which indicates a breakthrough of air at CT2, V13 is opened to pump away excess air. When P3 drops below 50 mbar, CT1 is flushed with  $20 \text{ mL min}^{-1} \text{ N}_2$  through CT2 for 15 min to guarantee that all the  $\text{CH}_4$  adsorbed onto CT1 is carried to CT2. The transfer is stopped by closing V8 and CT2, still at  $-196 \text{ }^\circ\text{C}$ , is evacuated for 1 min. CT2 is then heated to  $-72 \text{ }^\circ\text{C}$  for exactly 1 min 30 sec to desorb and remove excess air.

#### *Transfer to the PURIF*

The preconcentrated air sample, still trapped in CT2, is carried to the GC column by first switching V11 to position B (injection), which enables the He carrier gas from the GC to flush CT2 to the column. The dry ice/ethanol bath under CT2 is then removed, the trap is heated to  $95 \text{ }^\circ\text{C}$  to comprehensively desorb  $\text{CH}_4$  and other trapped gases and the GC run is started immediately afterwards.

## 2.2.4 Methane purification setup (PURIF)

### 2.2.4.1 Description

The methane purification setup (PURIF) is schematically shown in Figure 2.2b. Small ( $< 10 \text{ mL}$ )  $\text{CH}_4$ -containing gas mixtures are chromatographically purified and pure  $\text{CH}_4$

subfractions are recovered as CH<sub>4</sub>-derived CO<sub>2</sub> in a glass ampoule. Although the setup mainly aims at preparing pure CH<sub>4</sub> samples for subsequent <sup>14</sup>C analysis, this preparative GC technique allows even compound-specific radiocarbon analyses of CH<sub>4</sub>, CO, CO<sub>2</sub> and eventually C<sub>2</sub>H<sub>6</sub>. The gas sample is first chromatographically separated before pure CH<sub>4</sub> is isolated in an individual trap. It is then transferred to a CuO oven where CH<sub>4</sub> is converted into CO<sub>2</sub>, quantified manometrically and finally flame-sealed in a glass ampoule. The system can handle two different types of sample feed: (1) a manual syringe injection into the GC inlet (SYRINGE) and (2) an on-line injection of a preconcentrated air sample (PRECON).

The GC (7890B, Agilent, USA) is equipped with a purged packed (PP) inlet, a packed column (ShinCarbon ST 80/100, 2 mm ID, L = 2 m, Restek, USA) and a thermal conductivity detector (TCD). The PP inlet was modified such that the injection valve V11 of the PRECON was included into the flow path of the He carrier gas which feeds the inlet (see Figure 2.2a). The column is thus constantly flushed with He (purity = 99.999%, Carbagas, Switzerland), and the flow is regulated by the electronic pneumatic control module of the GC. Hence, the option is kept to either perform a direct syringe injection of a gas mixture through the septum of the inlet (V11 in “load” mode, as shown in Figure 2.2a) or to transfer a preconcentrated sample from CT2 (PRECON) to the column (V11 in position “inject”). The column was chosen for its ability to handle large injection volumes at low bleeding and high efficiency of separating permanent gases and hydrocarbons. According to the physical properties of the packing material, the gases are mainly separated according to their volatility. Therefore, bulk air (O<sub>2</sub>, N<sub>2</sub> and Ar) elutes first, followed by CO, CH<sub>4</sub>, CO<sub>2</sub> and finally trace gases of lower volatility. The oven is kept at 40 °C for 4 min and is then heated to 250 °C with a temperature ramp of +10 °C/min. The column is finally cleaned at 280 °C for three additional minutes. The PP inlet is operated in constant pressure mode (20 psig), which causes a gradual decrease of the He carrier gas flow rate from 14 mL min<sup>-1</sup> down to 9 mL min<sup>-1</sup> as the temperature of the oven rises and the He viscosity increases consequently.

All the tubing is 1/8” SS with Swagelok fittings. The exhaust of the TCD is connected to V14, a 2-position 6-port valve (VICI, USA). When V14 is in position B, as shown in Figure 2.2b, the gases eluting from the column are carried to V15, a 6-position selector valve (EUTA-2ST6MWE-CU, VICI, USA). The trapping consists of 6 identical custom-made 1/8” OD SS U-shaped traps (2.16 mm ID, L = 35 cm), each of which filled with 0.4 g charcoal and connected to a port of V15. Although V15 was chosen for its small internal volume, intermediary traps are used to ensure a minimal cross contamination when V15 is switched from one collecting trap to the next. Each trap is also equipped with a septum injector nut (VICI, USA) holding a 6 mm septum (TCSO, Trajan, Australia) and connected to a union tee, allowing the collection of pure CH<sub>4</sub> (in He) aliquots with a syringe (Pressure-Lok Series A-2, 2 ml, VICI, USA).

V16 is a 4-position dead-end selector (EUTA-2SD4MWE-CU, VICI, USA). An external He supply (V14 in position A), flow-regulated by MFC3 (SLA5850S, 0–50 mL min<sup>-1</sup>, Brooks, USA) is used to either clean the 6 traps (V16 in position 2) or to transfer CH<sub>4</sub> to the combustion oven (V16 in position 1). The methane combustion line consists of a quartz tube (4 mm ID, L = 40 cm) filled with 5.4 g copper oxide wires (0.5 mm diameter, Elementar, Germany) in its central part and connected on both ends to the SS line by means of UT fittings. The quartz tube stands in the middle of a custom-made combustion furnace heated to 950 °C.

The recovery part, where CH<sub>4</sub>-derived CO<sub>2</sub> is quantified and sealed in an ampoule, is an adaptation of the THEODORE system described by Szidat et al. (2004). T1 and T2 are helicoidally-shaped 1/8" SS lines cooled to -72 °C and -196 °C when trapping the combustion products H<sub>2</sub>O and CO<sub>2</sub>, respectively. The line is evacuated with a scroll pump SP (IDP-3, Agilent, USA) which allows to evacuate the line down to 1 x 10<sup>-1</sup> mbar. The amount of CO<sub>2</sub> recovered after CH<sub>4</sub> combustion is quantified with the pressure sensor P5 (PBMN Industrial Low Pressure, 0–1 bar, Baumer, Switzerland) in the calibrated volume (CV) of 7.94 cm<sup>3</sup>. The CH<sub>4</sub>-derived CO<sub>2</sub> is finally flame-sealed into a glass ampoule (4 mm OD, L = 6–7 cm).

#### 2.2.4.2 Procedure

When not in use, the recovery part remains evacuated to minimize contamination and to shorten the cleaning procedure preceding a sample processing. For similar reasons, CT3 to CT8 are always kept pressurized with He. The combustion oven is gradually heated to 950 °C while flushing with 20 mL min<sup>-1</sup> He. Meanwhile, the GC column is baked out to remove any potential contamination and enable the TCD to reach a stable condition. The charcoal U-traps CT3 to CT8 are flushed one by one for 3 min each, and an overpressure (1.5 bar) is applied in each trap to prevent any external contamination. Just before the sample injection, the six traps are immersed into liquid nitrogen and are again individually pressurized to 1.5 bar with He. The valve V14 is then switched to position B and V16 to position 2 (see Figure 2.2b), so that the gases eluting from the GC column are transferred to the selected trap.

As stated above, the purification setup can either be used as a stand-alone unit, by directly injecting a gas mixture, or together with the PRECON. In the first case, the sample is injected with a syringe through the septum of the PP inlet and the GC run is started immediately after. When used together with the PRECON, the GC method is started just after heating the second preconcentration trap CT2 to 95 °C.

CT4, CT6 and CT8 are used to trap CO, CH<sub>4</sub> and CO<sub>2</sub>, respectively. The GC effluent is directed through the traps CT3, CT5 and CT7 between the peaks of the three target gases to avoid any cross contamination between the carbon-containing gases eluting from the column. The selector valve V15 is switched to the position of the chosen trap 30 s before the onset of the peak at the TCD and 45 s after the TCD signal has reached baseline to account for the

transfer time between the detector and the traps (around 12 s) and to ensure a comprehensive trapping of the pure subfractions. After the elution and adsorption of CO<sub>2</sub> on CT8, V14 is switched to position A so that the GC flow is disconnected from the trapping part to avoid any low volatile gas eluting from the column to be adsorbed in a trap.

The six traps are heated to 95 °C to desorb CH<sub>4</sub>, CO and CO<sub>2</sub>, the combustion line is flushed (35 mL min<sup>-1</sup> He, 2 min) to a vent (V22) and T1 and T2 are cooled down to -72 °C and -196 °C, respectively. CT6 is selected and CH<sub>4</sub> is combusted in a He flow of 10 mL min<sup>-1</sup> for 10 min and the CH<sub>4</sub>-derived CO<sub>2</sub> is trapped in T2. When the combustion is completed, remaining He in T2 is pumped away and the CH<sub>4</sub>-derived CO<sub>2</sub> is manometrically quantified in the calibrated volume CV before it is flame-sealed in a glass ampoule, ready for a <sup>14</sup>C-AMS gas measurement.

### 2.2.5 Methane preconcentration and purification setup (MPPS)

When the PRECON and the PURIF are used together for <sup>14</sup>C measurements of atmospheric CH<sub>4</sub> samples, time can be saved by handling both setups simultaneously. During preconcentration of the sample, the PURIF is started up and cleaned. If a second sample needs to be processed, the cleaning of the PRECON is started (RDT, CT1 and CT2) while the first sample is purified in the GC column. A single preconcentration followed by a purification lasts ~3 hours, two samples can be prepared for <sup>14</sup>C measurements in ~5.5 hours so that three samples may be handled in one working day.

### 2.2.6 Methane <sup>14</sup>C measurement

The CH<sub>4</sub>-derived CO<sub>2</sub> ampoules are measured using the ampoule cracker of the gas handling system of the MICADAS at the University of Bern. The precision achieved during <sup>14</sup>C measurements of CO<sub>2</sub> samples amounting 50–80 µg C is typically 1% for a modern sample. Two standards, a <sup>14</sup>C-free CO<sub>2</sub> blank and the NIST Standard Reference Material 4990C (Oxa-II, F<sup>14</sup>C = 1.3407 ± 0.0005), are measured before and after the samples for blank subtraction, standard normalization and correction of isotopic fractionation (Szidat et al., 2014).

## 2.3 Results and discussion

### 2.3.1 Optimization and performance of the PRECON

The PRECON was tested and optimized using a “pressurized air sample” from a commercially available pressurized air bottle (C017E5R, Druckluft, Carbagas, Switzerland), with measured concentrations of 426 ppm CO<sub>2</sub> and 2.10 ppm CH<sub>4</sub>. It does contain neither water vapor nor CO, as these gases were removed when atmospheric air was pressurized into the bottle. A cavity ring-down spectroscopy analyzer (G2401, PICARRO, USA) was connected to the exhaust of the membrane pump to control the concentrations of CO, CO<sub>2</sub>, CH<sub>4</sub> and H<sub>2</sub>O during

the different steps of the procedure. Finally, the preconcentrated samples were transferred to the GC and the TCD was used to assess the performance of the preconcentration.

The RDT removes over 99.8% CO<sub>2</sub> for atmospheric air samples up to a total volume of 400 L without any CO<sub>2</sub> breakthrough. As the preconcentrated sample is subsequently purified in the GC column, the scavenging of CO<sub>2</sub> does not need to be quantitative. Hence, the usage of a single RDT is sufficient and simplifies the system operation compared to the setups from others, which apply multiple successive traps for this purpose (Wahlen et al., 1989; Brenninkmeijer and Röckmann, 1996; Kessler and Reeburgh, 2005; Petrenko et al., 2008).

No measurable CH<sub>4</sub> breakthrough (< 2‰) was observed in the first preconcentration trap (CT1, 12 g charcoal, 13 mm ID) for air samples up to 200 L, corresponding to a total amount of 210 µg C (CH<sub>4</sub>) successively trapped, which is four times the targeted sample size. During the preconcentration of larger air volumes, the trapping efficiency drops gradually over time and reaches 50% CH<sub>4</sub> breakthrough after 430 L air. Thus, this trap should not be used for sample sizes over 200 L, as isotopic fractionation may occur and would make eventual CH<sub>4</sub> stable isotope measurements useless (Wahlen et al., 1989; Kessler and Reeburgh, 2005).

The dimensions of the second preconcentration trap CT2 (0.5 g charcoal, 2.16 mm ID) were chosen as a downscaling of CT1 to further remove excess air while trapping the total amount of CH<sub>4</sub> transferred from CT1. From an original air volume of 60 L, the sample size is typically 80–100 ml after the first preconcentration step in CT1 and 10–15 ml after the second step in CT2, corresponding to successive CH<sub>4</sub> enrichment factors of approximately 650 and 8, respectively. Thus, CH<sub>4</sub> is enriched to a concentration of 8–12‰ after the two preconcentration steps, which is in agreement with the values obtained by Bergamaschi et al. (1998) for a similar procedure. The enrichment factor is lower in CT2, which can be explained by the higher O<sub>2</sub>/N<sub>2</sub> ratio in the sample in CT1 compared to the original ratio in atmospheric air. This O<sub>2</sub> enrichment after the first preconcentration step is due to its lower volatility compared to N<sub>2</sub>, which causes a more efficient adsorption of O<sub>2</sub> onto the charcoal. This discrimination over N<sub>2</sub> is further enhanced in CT2, resulting in a larger proportion of the sample trapped in CT2. However, the slightly oversized CT2 prevents any CH<sub>4</sub> loss during the preconcentration, and the final sample volume (10–15 ml) is still appropriate for a chromatographic separation in the GC column of the PURIF.

The performance of the PRECON was also evaluated by TCD measurements during the preconcentration of 60 L of the pressurized air sample, with known concentrations of CO, CH<sub>4</sub> and CO<sub>2</sub>. The results are detailed in the next section, together with the performance of the PURIF (see Figure 2.3 below).

## 2.3.2 Optimization and performance of the PURIF

### 2.3.2.1 Separation

The main physical parameters that influence the quality of the chromatographic separation are the carrier gas flow rate and the temperature of the oven. The GC method optimization was carried out with a standard gas mixture (79% N<sub>2</sub>, 12% CO<sub>2</sub>, 5% O<sub>2</sub>, 2% CO and 2% CH<sub>4</sub>) that contains higher concentrations of the main trace gases, as the TCD is not sensitive enough for the detection of low concentration compounds. The chromatogram of the syringe injection of 2 mL standard gas mixture, corresponding to approximately 20 µg C (CH<sub>4</sub>), is shown in Figure 2.3. Methane is well separated from CO and CO<sub>2</sub> even when using a temperature ramp to shorten the method.

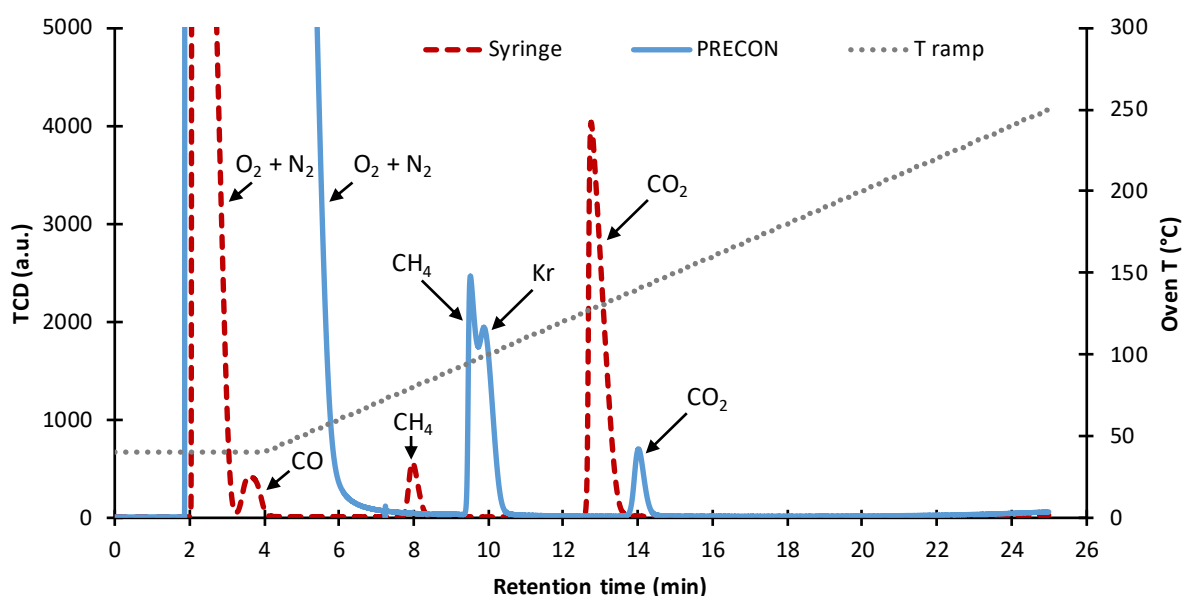


Figure 2.3 Chromatographic separation of a gas mixture. Dashed red line: injection into the PP inlet of 2 mL standard gas mixture (79% N<sub>2</sub>, 12% CO<sub>2</sub>, 5% O<sub>2</sub>, 2% CO and 2% CH<sub>4</sub>). Blue line: on-line injection from the PRECON of the preconcentration of 60 L pressurized air sample (2.10 ppm CH<sub>4</sub>, 426 ppm CO<sub>2</sub>). Grey dotted line: oven temperature program.

An overload of the column causes a broadening and tailing of the peaks, as the column is not designed for such large gas volumes. The effect is enhanced when larger samples are injected, which causes further peak broadening and reduced retention times. This behavior does not affect the collection of pure CH<sub>4</sub>, as the peaks of CO, CH<sub>4</sub> and CO<sub>2</sub> are still well separated. However, it causes a poor separation of CO from bulk air, which is partially counterbalanced by the low oven temperature of 40 °C for the first four minutes of the run. Unfortunately, these two peaks start to overlap for samples bigger than 2 mL. A longer column combined with a cooling of the oven could solve this issue if <sup>14</sup>C measurements are of interest, but it would come at the cost of an extended time for the chromatographic separation and the column

cleaning. As atmospheric CO is very low in concentration and hard to separate from ambient air due to a similar volatility to O<sub>2</sub> (Brenninkmeijer, 1993), the required modifications are currently not considered.

Figure 2.3 additionally shows the result of the preconcentration and chromatographic purification of 60 L of the pressurized air sample, when the PRECON and PURIF are jointly used. It should first be noticed that the retention times of the gases are 1–1.5 min longer compared to a direct injection. This is partly due to the sample transfer time between CT2 and the PP inlet, but also to a strongly reduced carrier gas flow rate when the preconcentrated sample in CT2 is heated, as it expands and creates an overpressure in the PP inlet. Fortunately, the shift of the retention times is reproducible and can be accounted for when the pure subfractions are collected in their respective traps. The sample volume after preconcentration is around 10–15 mL, resulting in a strong broadening of the bulk air peak. The TCD signal slowly drops to the baseline after the elution of O<sub>2</sub> and N<sub>2</sub>, which is mainly caused by the dead volumes in the line between CT2 and the PP inlet of the GC.

The PRECON greatly decreased the amount of CO<sub>2</sub> from the air sample. However, the GC results show that the PURIF remains a mandatory step for getting reliable <sup>14</sup>CH<sub>4</sub> results, as the CO<sub>2</sub> amount after preconcentration is ~20% the amount of CH<sub>4</sub>. The residual CO<sub>2</sub> originates from an incomplete scavenging of CO<sub>2</sub> in RDT along with some CO<sub>2</sub> production in CT1 when it is heated to 95 °C (Bräunlich, 2000).

Although CH<sub>4</sub> is well separated from other carbon-containing gases, it unfortunately co-elutes with krypton (Kr), a noble gas that shows concentrations of ~1 ppm in the atmosphere and similar physical properties with CH<sub>4</sub>. Since both separations in the charcoal traps of the PRECON and in the GC column are based on physical adsorption using carbon molecular sieves, Kr is preconcentrated together with CH<sub>4</sub> in the PRECON and co-elutes with CH<sub>4</sub>. This issue was already documented by Schmitt et al. (2013). A full chromatographic separation may only be possible at the cost of cooling the GC oven or using a longer column, which would dramatically extend the whole procedure. As CH<sub>4</sub> is ultimately combusted and recovered as CO<sub>2</sub> in a glass ampoule, however, Kr is removed in this latter step. Consequently, co-eluting Kr impedes the ability to precisely quantify the amount of CH<sub>4</sub> preconcentrated, but the manometric quantification of the CH<sub>4</sub>-derived CO<sub>2</sub> can still be used to assess the yield and performance of the whole procedure involving PRECON and PURIF.

### 2.3.2.2 Trapping

Methane trapping efficiency after its chromatographic separation was measured by connection of the outlet of the CH<sub>4</sub> trap (CT6) to the flame ionization detector (FID) of the GC, which is more sensitive to hydrocarbons than the TCD. Up to 2 ml pure CH<sub>4</sub>, which corresponds to an amount of ~1000 µg C, could be trapped at –196 °C for 50 minutes, while the trap was

flushed with a He flow rate of  $35 \text{ mL min}^{-1}$  to the FID without any detectable breakthrough. This result yields to a trapping efficiency of  $>99.99\%$ .

The  $\text{CH}_4$  trap is heated to  $95 \text{ }^\circ\text{C}$  when  $\text{CH}_4$  is transferred to the combustion oven. This temperature allows a comprehensive desorption of  $\text{CH}_4$  from the charcoal and thus prevents any isotopic fractionation (Bräunlich, 2000). The traps CT4 and CT8 were also successfully tested for their ability to trap and desorb CO and  $\text{CO}_2$ , respectively.

### 2.3.2.3 Combustion

The choice of CuO as a catalyst for the conversion of  $\text{CH}_4$  to  $\text{CO}_2$  was based on several aspects: it is cheap, easy to use, regenerate or replace and shows a good oxidation efficiency of hydrocarbons without any need of an additional oxidant, which simplifies the isolation of pure  $\text{CH}_4$ -derived  $\text{CO}_2$  (Dumke et al., 1989; Kessler and Reeburgh, 2005). A long and thin quartz tube allows a comprehensive combustion of  $\text{CH}_4$  while the oven cleaning is facilitated, which minimizes cross contamination from a sample to the next. Methane combustion efficiency was assessed by connection of the outlet of T2 to the FID. As  $\text{CH}_4$  is not trapped in T2, an empty tube cooled to  $-196 \text{ }^\circ\text{C}$  without any adsorbent, a potential incomplete combustion of  $\text{CH}_4$  can be detected by the FID. Aiming at a time-efficient method, the highest He carrier flow granting a complete combustion of  $\text{CH}_4$  was sought. This is achieved at a flow rate of  $10 \text{ mL min}^{-1}$  and breakthroughs of  $0.2\%$  and  $1.8\%$  are observed for flow rates of  $20 \text{ mL min}^{-1}$  and  $35 \text{ mL min}^{-1}$  He, respectively.

## 2.3.3 Validation of the MPPS

### 2.3.3.1 Performance

The constant contamination is a model of the procedural blank of a system (Brown and Southon, 1997; Salazar et al., 2015), which assumes that a constant amount of carbon with a fixed  $F^{14}\text{C}$  value is added to the recovered  $\text{CH}_4$ -derived  $\text{CO}_2$  when an air sample is preconcentrated and purified. It can be evaluated by processing  $\text{CH}_4$  standards of known mass and  $^{14}\text{C}$  content through the whole procedure. We use a modern methane standard that was produced through the reduction of  $\text{CO}_2$ , which was released by the combustion of tree leaves. The pure modern methane standard was measured with the MICADAS after combustion of  $\text{CH}_4$  to  $\text{CO}_2$  and shows a  $F^{14}\text{C}$  of  $1.024 \pm 0.003$ , which is consistent with the results from the direct  $^{14}\text{C}$  measurements of the  $\text{CH}_4$  with gas proportional counting (GPC) at the GPC Radiocarbon Lab at the Physics Institute of the University of Bern (Loosli et al., 1980). In order to ease the handling of small volumes, the modern methane standard was diluted to  $10\%$   $\text{CH}_4$  in He. The  $\text{CH}_4$  contained in the standard gas mixture was used as a fossil  $\text{CH}_4$  standard, as it is totally depleted in  $^{14}\text{CH}_4$  (i.e.  $F^{14}\text{C} = 0$ ). Different amounts of these two gases were injected with a septum injector nut at the preconcentration line before the RDT into a  $\text{N}_2$  flow of  $60 \text{ L}$  in total and the preconcentration and purification steps were performed as usually. The procedural blank (constant contamination) of the MPPS was determined to be

$0.35 \pm 0.10$   $\mu\text{g C}$  with an  $F^{14}\text{C}$  of  $0.35 \pm 0.18$  (see Table 2.1). These values were calculated using the statistical model developed by Salazar et al. (2015). The cross contamination from the previous sample, which is  $0.4 \pm 0.2\%$ , most likely originates from an imperfect cleaning of the charcoal traps.

*Table 2.1 Quality assurance parameters of the Methane Preconcentration and Purification Setup (MPPS), with average uncertainty ( $1\sigma$ ) and standard deviation (Std dev) of all measurements (both calculated referring to a single analysis). See appendix 8.1 for detailed results.*

Quality parameter	Value	Uncertainty	Std dev	<i>n</i>
Constant contamination mass ( $\mu\text{g C}$ )	0.35	0.10	–	22
Constant contamination $F^{14}\text{C}$	0.35	0.18	–	22
Cross contamination (%)	0.4	0.2	–	2
Repeatability* ( $F^{14}\text{C}$ )	1.539	0.012	0.010	6
Accuracy <sup>#</sup> : measurement ( $F^{14}\text{C}$ )	1.018	0.008	0.009	3
Accuracy: reference value ( $F^{14}\text{C}$ )	1.024	0.003	–	–
MPPS yield (%)	101.2	1.4	–	13

\*Determined from repeated analysis of 60 L of the pressurized air sample.

<sup>#</sup>Determined from repeated analysis of the modern methane standard.

The system repeatability was determined from several preconcentration, purification and  $^{14}\text{CH}_4$  measurement of 60 L pressurized air sample (see Table 2.1). The MPPS exhibits a good repeatability, as the standard deviation of the  $F^{14}\text{C}$  for all  $\text{CH}_4$  analyses of the pressurized air sample is 0.010, which is comparable to the average  $F^{14}\text{C}$  measurement uncertainty of a single analysis (0.012). To assess the system accuracy, repeated  $^{14}\text{C}$  measurements of the modern methane standard that was processed through the MPPS were compared to the modern methane standard  $F^{14}\text{C}$  reference value. The results, presented in Table 2.1, show that the mean  $F^{14}\text{C}$  from the repeated measurements ( $F^{14}\text{C} = 1.018 \pm 0.008$ ) is statistically indistinguishable from the reference value ( $F^{14}\text{C} = 1.024 \pm 0.003$ ). The overall yield of the setup was calculated from the comparison of the amount of  $\text{CH}_4$ -derived  $\text{CO}_2$  recovered in a glass ampoule with its corresponding theoretical amount of  $\text{CH}_4$  injected into the PRECON (see Table 2.1). The samples used for this evaluation were collected in aluminum bags at the Beromünster tall tower, Switzerland, as described by Berhanu et al. (2017). The yield of the MPPS is  $101.2 \pm 1.4\%$ , indicating a quantitative recovery of  $\text{CH}_4$  during the preconcentration and purification steps.

The chromatographic purification of  $\text{CH}_4$  after preconcentration is an essential step, as it guarantees the reliability of the  $^{14}\text{C}$  results. Such an approach has been previously employed by some other groups (e.g. Wahlen et al., 1989; Eisma et al., 1994). However, their systems were used for the purification of much larger air volumes and thus required more traps and a long and labor-intensive procedure limiting their throughput. The simplified preconcentration line presented here drastically reduces the sample preparation time for a  $^{14}\text{CH}_4$  measurement,

as three samples can be readily prepared within a working day. Hence, the MPPS is suited to the monitoring of atmospheric  $^{14}\text{CH}_4$ .

### 2.3.3.2 Versatility

According to the research strategy depicted in Figure 2.1, the two systems presented in this work can be adapted to handle  $\text{CH}_4$  collected from many diverse environments (e.g. aquatic, wetland, marine etc.), where  $\text{CH}_4$  concentrations can be much higher than in atmospheric air. As methanogenesis is often intense in the carbon-rich sediments at the bottom of some lakes and ponds, typical concentrations in the samples collected can be high enough so that a few milliliters contain enough  $\text{CH}_4$  for a radiocarbon analysis (Rinta et al., 2015). If so, the sample does not require preconcentration and the PURIF can be used alone as it can handle direct injections of gas mixtures up to 10 mL.

For intermediate concentration methane sources, such as arctic lakes or peatlands, gas samples are usually extracted with headspace techniques (Walter et al., 2008; Garnett et al., 2011). A methane  $^{14}\text{C}$  analysis of such samples often involves the extraction from gas samples of a few hundred milliliters. In this case, using the whole PRECON might be an overkill; hence, it may be possible to adapt the PRECON to use the second preconcentration step with CT2 alone before performing the  $\text{CH}_4$  purification.

Finally,  $\text{CH}_4$  dissolved in low concentration waters can be extracted with membrane contactors (Matsumoto et al., 2013; Sparrow and Kessler, 2017), resulting in extracted gas volumes similar to the ones required for atmospheric air sampling. Thus, these samples can be handled as the atmospheric air samples by combination of the whole PRECON and the PURIF.

## 2.4 Conclusion

A new methane preconcentration and purification setup was developed for the preparation of atmospheric  $\text{CH}_4$  samples for  $^{14}\text{C}$  measurements. The system requires only ~50 liters of atmospheric air, which can be collected in an aluminum bag or pressurized in a gas bottle. A preparative gas chromatography technique is used for  $\text{CH}_4$  isolation, which confirms that methane has been successfully separated from any other carbon-containing gases such as CO or  $\text{CO}_2$  that could dramatically bias the  $^{14}\text{CH}_4$  results. A procedural blank of  $0.35 \pm 0.10 \mu\text{g C}$  with an  $F^{14}\text{C}$  of  $0.35 \pm 0.18$  was determined, which is low compared to the typical amounts of  $\text{CH}_4$  purified and measured. Methane is quantitatively extracted from the original air sample and isolated as pure  $\text{CH}_4$  for the AMS  $^{14}\text{C}$  measurement, which shows a good accuracy and repeatability. The system is therefore well suited to the radiocarbon analysis of atmospheric  $\text{CH}_4$ . Since methane is not combusted before purification,  $\text{CH}_4$  aliquots can be collected for stable isotope measurements. Combined with  $^{14}\text{C}$  results, they should provide complementary information.

## **Acknowledgements**

We are grateful to the funding of the Dr. Alfred Bretscher Scholarship. Carina van der Veen and Henk Snellen (IMAU, Utrecht) assisted during the early steps of the setup development. Markus Leuenberger, Thomas Wagner and Peter Düring (Climate and Environmental Physics, University of Bern) provided the methane modern standard, the air samples from Beromünster, the PICARRO and the pressurized air bottle. We further thank Robert Eichler (Paul Scherrer Institute) for the oven furnace and Gary Salazar for the assistance with the MICADAS and the evaluation of the data.

# 3. Biweekly atmospheric $^{14}\text{CH}_4$ and $^{14}\text{CO}_2$ measurements at three sites in Switzerland

## 3.1 Introduction

With a mole fraction of 1858 ppb and 407 ppm in the atmosphere in 2018 (Nisbet et al., 2019), methane ( $\text{CH}_4$ ) and carbon dioxide ( $\text{CO}_2$ ) are the two major greenhouse gases (GHGs) contributing to about 20% and 65% of the anthropogenic radiative forcing, respectively (Etminan et al., 2016). The situation is of concern for atmospheric  $\text{CH}_4$ , which recently experiences an unexpected strong growth rate (Nisbet et al., 2019). The lack of understanding of the evolution of atmospheric  $\text{CH}_4$  is mainly attributed to the complexity of natural and anthropogenic  $\text{CH}_4$  sources, which are associated to various mechanisms of formation and emissions and a high sensitivity to the climate (Bousquet et al., 2006; Dlugokencky et al., 2011; Saunio et al., 2016; Nisbet et al., 2019). Moreover, the variations of the strength of  $\text{CH}_4$  sinks may also play a significant role in the recent growth of atmospheric  $\text{CH}_4$  burden (Rigby et al., 2017; Turner et al., 2017). By virtue of its relatively short atmospheric lifetime ( $< 10$  years), abatement strategies of anthropogenic  $\text{CH}_4$  emissions have been proposed as an option to mitigate climate change on a short term (Shindell et al., 2012; IPCC, 2018). Their implementation could be cost-efficient and socially acceptable, as there is a great potential for the reduction of fugitive emissions from the natural gas, oil and coal extraction and supply (Schwietzke et al., 2016; Nisbet et al., 2019). In contrast to  $\text{CH}_4$ , the growth rate of atmospheric  $\text{CO}_2$  is more predictable as it is largely determined by the strength of anthropogenic fossil fuel  $\text{CO}_2$  emissions (Gregg et al., 2008; IPCC, 2013). However, uncertainties in the global carbon budget remain when reporting inventories of  $\text{CO}_2$  emissions (Marland, 2008), and in the future evolution of the land and ocean sinks (Heimann and Reichstein, 2008; Le Quéré et al., 2016).

As discussed in Chapter 1, the  $^{14}\text{C}$  analysis of atmospheric  $\text{CH}_4$  and  $\text{CO}_2$  is a useful tool to distinguish biogenic and fossil sources, the latter being devoid of  $^{14}\text{C}$ . This technique has been applied to atmospheric  $\text{CH}_4$ , to estimate the fossil fraction of the global  $\text{CH}_4$  source (Ehhalt, 1974; Wahlen et al., 1989; Quay et al., 1999; Lassey et al., 2007b). Very few studies focused on using atmospheric  $^{14}\text{CH}_4$  measurements to apportion  $\text{CH}_4$  sources at local and regional scales (Levin et al., 1992; Townsend-Small et al., 2012). Unfortunately,  $^{14}\text{CH}_4$  discharges from nuclear power plants (NPPs) were responsible for a very large temporal and spatial variability of atmospheric  $^{14}\text{CH}_4$  results, which precluded any attempt to estimate the relative strength of local  $\text{CH}_4$  sources (Kunz, 1985; Eisma et al., 1994, 1995; Zazzeri et al., 2018). Conversely,  $^{14}\text{CO}_2$  has been successfully used as a tracer for recently added fossil fuel  $\text{CO}_2$  in the atmosphere at local and regional scales (Turnbull et al., 2006; Levin et al., 2008; Berhanu et al., 2017; Wenger et al., 2019).

In Switzerland, CH<sub>4</sub> is responsible for less than 11% of the total GHG emissions, whereas CO<sub>2</sub> contributes to about 81% (FOEN, 2017). Methane emissions are largely dominated by anthropogenic sources (>95%), of which almost 85% are related to the agricultural sector (Hiller et al., 2014; Henne et al., 2016). In contrast, the combustion of fossil fuels from the energy sector contributes to more than 77% of the total CO<sub>2</sub> emissions. These contributions by source category are based on emission inventories, which are associated with large uncertainties, particularly for CH<sub>4</sub>.

The new methane preconcentration and purification setup (MPPS), described in details in Chapter 2, was developed and optimized for the preparation of atmospheric CH<sub>4</sub> samples for <sup>14</sup>C analysis. Owing to its relatively compact design, three samples can be readily prepared within a working day, which makes the system well suited to the monitoring of atmospheric <sup>14</sup>CH<sub>4</sub>. In addition to the extraction of pure CH<sub>4</sub>, the setup allows the simultaneous recovery of CO<sub>2</sub>, which is analyzed for its <sup>14</sup>C content as well. In this chapter, we present a new dataset of biweekly measurements of atmospheric <sup>14</sup>CH<sub>4</sub> and <sup>14</sup>CO<sub>2</sub> conducted at three strategic sites in Switzerland: the Beromünster tall tower, located in a rural area; the University of Bern, a polluted urban site; and the Jungfrauoch High Altitude Research Station, a background site representative of free tropospheric air. The atmospheric <sup>14</sup>CH<sub>4</sub> and <sup>14</sup>CO<sub>2</sub> results are compared and serve as a basis for a discussion on their usability for source apportionments of fossil emissions in Switzerland and abroad. Finally, we update the series of biweekly <sup>14</sup>CO<sub>2</sub> measurements performed at Beromünster, which started in 2013 and were reported for the period 2013–2015 by Berhanu et al. (2017). This series of measurements is used for an estimation of the fossil fuel CO<sub>2</sub> component at Beromünster, which is then compared to the one determined at Bern.

## 3.2 Methods

### 3.2.1 Sites description

The selection of the three sampling sites, shown in Figure 3.1, was based on a combination of strategic and practical considerations. The main objective was to collect air from a rural area (Beromünster), a polluted urban area (Bern), and a free tropospheric background site used as a reference (Jungfrauoch).

- **Beromünster:** The Beromünster tall tower is located on a gentle hill, in an agricultural area in central Switzerland (47°11'23" N, 8°10'32" E, 797 m a.s.l.). Since 2012, the tower is part of a GHG observation network of four continuous carbon measurement sites (CO<sub>2</sub>, CH<sub>4</sub> and CO), which belong to the CarboCount CH project (Oney et al., 2015). In addition to the continuous monitoring of GHG mole fractions, air samples are collected on a biweekly basis at Beromünster since July 2013, for <sup>14</sup>CO<sub>2</sub> analysis at the University of Bern (Berhanu et al., 2017). Owing to the height of the

tower (212 m), regional CH<sub>4</sub> and CO<sub>2</sub> signals were simulated to come from nearly the entire Swiss Plateau. The prevailing wind direction at Beromünster is SW and sometimes NE, channeling between the Jura mountain range and the Alps. A detailed characterization of the site with respect to local meteorological conditions, temporal variations of the GHGs and main influences can be found elsewhere (Oney et al., 2015; Satar et al., 2016).

- **Bern:** The sampling of air took place at the Department of Chemistry and Biochemistry of the University of Bern, located in an urban area of the Swiss Plateau (46°57'11" N, 7°25'46" E, 554 m a.s.l.). An air inlet was placed along the outer wall of the building at a height of 6 m. Care was taken to keep the inlet away from air exhausts of the University heating and ventilation systems, as they can be strong point sources of CO<sub>2</sub> (Levin et al., 2008).
- **Jungfraujoch:** The Sphinx laboratory of the High Altitude Research Station Jungfraujoch is situated in the Bernese Alps, on a mountain saddle between the mountains Mönch and Jungfrau (46°32'51" N, 7°59'6" E, 3580 m a.s.l.). Owing to its high elevation, the station is usually situated over the planetary boundary layer (PBL), allowing the sampling of free tropospheric air (Levin et al., 2008; van der Laan-Luijkx et al., 2013). It is therefore considered as a background site, providing valuable information about the well-mixed atmosphere at hemispheric scales (Gloor et al., 2000; Satar et al., 2016). Since 1986, two-weekly integrated atmospheric CO<sub>2</sub> samples have been collected for <sup>14</sup>CO<sub>2</sub> analysis (Levin et al., 1989; Levin and Kromer, 2004).

Along with the location of the sampling sites (in blue), the position of the five Swiss NPPs is reported in Figure 3.1 (in black). As Mühleberg and Leibstadt hold a boiling water reactor (BWR), their <sup>14</sup>C emissions are mostly in the form <sup>14</sup>CO<sub>2</sub>. In contrast, Gösgen and Beznau I/II are equipped with a pressurized water reactor (PWR), with associated <sup>14</sup>C emissions dominantly as <sup>14</sup>CH<sub>4</sub> (Kunz, 1985; Uchrin et al., 1997; Yim and Caron, 2006).



Figure 3.1 Geographical map of Switzerland, with the sampling sites (in blue) and the five nuclear power plants (in black). Gösgen and Beznau I/II hold a PWR (emitting mostly  $^{14}\text{CH}_4$ ), whereas Mühleberg and Leibstadt hold a BWR (emitting mostly  $^{14}\text{CO}_2$ ).

### 3.2.2 Air sampling

The air sampling for  $^{14}\text{CH}_4$  and  $^{14}\text{CO}_2$  analyses started first at Beromünster (August 2018), followed by Bern (October 2018) and Jungfrauoch (December 2018). At the three sites, an air sample was collected every second week, on Thursday morning (Jungfrauoch and Beromünster) and Friday morning (Bern). The sampling was usually performed between 06:00 and 10:00 UTC at Jungfrauoch and Bern, and between 09:00 and 13:00 UTC at Beromünster.

At Jungfrauoch, two samples were collected from an air inlet placed on the terrace of the Sphinx observatory, facing the wind direction to mitigate potential contamination from the station. A small membrane pump was used to successively fill two 100 L PE-Al-PE bags (Tesseraux, Germany) at a flow rate of  $\sim 1.6 \text{ L min}^{-1}$  (STP) over a 60 min interval for each sample. The second sample bag was used as a backup and for quality control, by checking its tightness over time. The samples were collected as early as possible in the morning, to minimize the impact of uplifted air masses from the PBL that sometimes occurs in spring and summer (Collaud Coen et al., 2011).

At Beromünster, a similar procedure was already implemented since 2013, with the biweekly sampling of air in a 100 L aluminum bag for  $^{14}\text{CO}_2$  analysis (Berhanu et al., 2017). There, three air samples were successively collected from the inlet at the highest sampling height of the tower (212.5 m), at a flow rate of  $9 \text{ L min}^{-1}$  for 6–8 min. The triplicates were used to assess

the reliability of the CO<sub>2</sub> extraction and the <sup>14</sup>C measurement results, and from November 2017 onwards, only one sample was collected and measured every second week. Since August 2018, an additional 200 L aluminum bag was filled immediately after the first sample collection, for combined <sup>14</sup>CH<sub>4</sub> and <sup>14</sup>CO<sub>2</sub> analyses in our laboratory. During each sampling, CH<sub>4</sub> and CO<sub>2</sub> mole fractions were measured with a cavity ring-down spectroscopy analyzer (G2401, PICARRO, USA).

The sampling procedure at the University of Bern was simplified, as it did not require the filling of a sample bag. Hence, the air inlet was directly connected to the methane preconcentration and purification setup (MPPS) described in Chapter 2, and 60 L atmospheric air were transferred to the setup over a period of 40 min.

In addition to the biweekly collection of air samples aforementioned, an overnight sampling was conducted simultaneously at the three sites between March 20 and March 21, 2019. The main objective was to assess the daily variability of <sup>14</sup>CH<sub>4</sub> and <sup>14</sup>CO<sub>2</sub> at the three locations. Hence, a sample was collected every 3 hours, each sampling lasting 15 min at Beromünster, and 1 h at Jungfrauoch as well as at Bern.

### 3.2.3 Sample pretreatment

#### 3.2.3.1 CH<sub>4</sub> extraction

Every second Friday, one day after the collection at Jungfrauoch and Beromünster, the three samples from Jungfrauoch, Beromünster and Bern were processed through the MPPS for the isolation of CH<sub>4</sub> and CO<sub>2</sub> fractions. The extraction and purification of CH<sub>4</sub> with the MPPS is described in Chapter 2. In brief, CH<sub>4</sub> undergoes first two successive preconcentration steps in a custom-made cryogenic line. It is then isolated using a preparative gas chromatography technique. The pure CH<sub>4</sub> subfraction is then combusted to CO<sub>2</sub> and flame-sealed in a small glass ampoule. The setup was designed at a relatively small scale, to reduce the sample preparation time. Thus, it is suited to the extraction of 10–200 µg C of CH<sub>4</sub>-derived CO<sub>2</sub> from atmospheric air samples, which roughly corresponds to the sampling of 10–200 L air. Methane was always extracted from 60 L air (0 °C, 1 atm), which yielded to the recovery of 55–75 µg C, depending on the CH<sub>4</sub> mole fraction in each sample. Such a volume allowed to keep the recovered amount well over the procedural blank of the setup ( $0.35 \pm 0.10$  µg C with an F<sup>14</sup>C of  $0.35 \pm 0.18$ ), and ensured optimal conditions for the <sup>14</sup>CH<sub>4</sub> measurement. Methane mole fractions were not directly measured in the samples collected at Bern, but they could be estimated from the amount of CH<sub>4</sub> extracted from 60 L air. To do so, the amounts of CH<sub>4</sub> recovered after the processing of Beromünster samples, with measured mole fractions during the sampling, were used as a calibration for an estimation of the CH<sub>4</sub> mole fractions in the samples collected at Bern.

### 3.2.3.2 CO<sub>2</sub> extraction

The CO<sub>2</sub> extraction from the samples collected at Beromünster was conducted cryogenically at the Climate and Environmental Physics institute from the University of Bern (CEP). The procedure, detailed in Berhanu et al. (2017), yields to the recovery of 20–30 mL CO<sub>2</sub> (STP) into a 50 mL glass flask, with an extraction efficiency over 99%. Prior to <sup>14</sup>CO<sub>2</sub> analysis, the stable isotope composition of the extracted CO<sub>2</sub> ( $\delta^{13}\text{C}$ ) was also measured by isotope-ratio mass spectrometry (IRMS), which has an accuracy and precision better than 0.1‰ (Leuenberger et al., 2003).

Together with the extraction of CH<sub>4</sub>, CO<sub>2</sub> was also recovered from the sampling of 60 L air with the MPPS. During the general procedure of CH<sub>4</sub> preconcentration, CO<sub>2</sub> is first scrubbed from the sample and trapped into a liquid nitrogen cooled “Russian Doll” glass trap (“RDT”, see Figure 2.2). The design of the trap allows a removal of more than 99.8% CO<sub>2</sub>, together with N<sub>2</sub>O and some bulk air. Hence, in parallel to the chromatographic separation of CH<sub>4</sub>, CO<sub>2</sub> was recovered in a 55 mL glass flask (“CO<sub>2</sub> flask” in Figure 2.2). To do so, RDT was first evacuated to remove remaining bulk air. RDT was then heated to ~90 °C to release CO<sub>2</sub> and subsequently immersed in a dry ice/ethanol slurry (–72 °C) to freeze out any remaining water vapor in the line. Finally, the expanded CO<sub>2</sub> was collected in the flask cooled to –196 °C. Unfortunately, the large internal volume of RDT (~500 mL) and the presence of three nested glass fiber thimbles in its inner part hampered the evacuation of RDT when immersed in liquid nitrogen. Indeed, Brenninkmeijer and Röckmann (1996) noted that for such traps the comprehensive removal of bulk air is not possible as long as the trap is still cooled to –196 °C. Thus, some remaining air in RDT was expanded together with CO<sub>2</sub>, which significantly slowed down the transfer of CO<sub>2</sub> to the flask. Consequently, the CO<sub>2</sub> recovery was not comprehensive (~70% of the original amount in RDT) and some bulk air was trapped together with CO<sub>2</sub> in the flask (~20%). As we were concerned about isotopic fractionation, which could happen during such a process involving desorption and diffusion (Brenninkmeijer and Röckmann, 1996), the recovery steps were kept identical for all the samples after some optimization tests.

### 3.2.4 <sup>14</sup>CH<sub>4</sub> and <sup>14</sup>CO<sub>2</sub> measurements

The <sup>14</sup>C analysis of CH<sub>4</sub>-derived CO<sub>2</sub> was performed as a direct AMS gas measurement, using the ampoule cracker of the gas interface system to transfer the CH<sub>4</sub>-derived CO<sub>2</sub> samples to the AMS as shown in Figure 1.4. The total procedural blank of  $0.35 \pm 0.10 \mu\text{g C}$  with an  $F^{14}\text{C}$  of  $0.35 \pm 0.18$  and a cross contamination of  $0.4 \pm 0.2\text{‰}$  were considered for correction for the report of final <sup>14</sup>C results and their associated uncertainties (1 $\sigma$ ).

The extracted CO<sub>2</sub> fractions stored in the glass flasks were not directly measured as gas samples with the AMS, since the typical amounts of CO<sub>2</sub> recovered (~15 mL) were large enough to allow a conventional <sup>14</sup>C measurement of solid targets. The general procedure for the preparation of graphite targets for <sup>14</sup>C-AMS is described in section 1.4.2.2. In short, the

CO<sub>2</sub> flasks were connected to a gas interface and a portion of the CO<sub>2</sub> was graphitized with an automated graphitization equipment, yielding to the production of solid targets with carbon masses of 1 mg. A sequence of measurements with the AMS consisted of up to 34 sample targets, together with three targets of the primary NIST standard oxalic acid II (SRM 4990C) and two targets of fossil CO<sub>2</sub> (Carbagas, Gümliigen), which were used for standard normalization, blank subtraction, and correction for isotope fractionation (Szidat et al., 2014).

### 3.2.5 Regional fossil fuel CO<sub>2</sub> component

The general procedure followed for the determination of the fossil fuel CO<sub>2</sub> component at Beromünster and Bern is similar to the one previously described by several authors (Levin et al., 1989, 2003; Zondervan and Meijer, 1996; Turnbull et al., 2006; Berhanu et al., 2017). Owing to its long atmospheric lifetime, CO<sub>2</sub> is relatively well mixed in the troposphere (IPCC, 2013). However, small CO<sub>2</sub> enhancements are observed at regional scales close to the sources. Thus, the CO<sub>2</sub> mole fraction measured (CO<sub>2meas</sub>) at a site is assumed to be composed of three major components: a free troposphere background (CO<sub>2bg</sub>), a regional biospheric component comprising respiration and photosynthesis (CO<sub>2bio</sub>), and a fossil fuel component (CO<sub>2ff</sub>):

$$\text{CO}_{2\text{meas}} = \text{CO}_{2\text{bg}} + \text{CO}_{2\text{bio}} + \text{CO}_{2\text{ff}} \quad \text{Equation 3.1}$$

Each of these components has a specific <sup>14</sup>C signature. Here, and for the rest of the chapter, age-corrected Δ<sup>14</sup>C will be used instead of F<sup>14</sup>C values (see Equation 1.7), for the sake of consistency with the majority of studies on atmospheric GHGs. Therefore, the components of Equation 3.1 have an associated <sup>14</sup>C signature described as Δ<sup>14</sup>CO<sub>2meas</sub>, Δ<sup>14</sup>CO<sub>2bg</sub>, Δ<sup>14</sup>CO<sub>2bio</sub>, and Δ<sup>14</sup>CO<sub>2ff</sub>, respectively. An isotopic mass balance is formulated as follows:

$$\begin{aligned} \text{CO}_{2\text{meas}} \cdot (\Delta^{14}\text{CO}_{2\text{meas}} + 1) &= \text{CO}_{2\text{bg}} \cdot (\Delta^{14}\text{CO}_{2\text{bg}} + 1) \\ &+ \text{CO}_{2\text{bio}} \cdot (\Delta^{14}\text{CO}_{2\text{bio}} + 1) \\ &+ \text{CO}_{2\text{ff}} \cdot (\Delta^{14}\text{CO}_{2\text{ff}} + 1) \end{aligned} \quad \text{Equation 3.2}$$

As fossil fuels are devoid of radiocarbon (i.e. Δ<sup>14</sup>CO<sub>2ff</sub> = -1000‰), the last term of Equation 3.2 is zero. Furthermore, we assume that Δ<sup>14</sup>CO<sub>2bio</sub> ≈ Δ<sup>14</sup>CO<sub>2bg</sub> as the major component of CO<sub>2bio</sub> is autotrophic respiration, corresponding to a young reservoir of carbon in equilibrium with atmospheric CO<sub>2</sub> (Levin et al., 2003). Combining Equation 3.1 and Equation 3.2 leads to the determination of the fossil fuel CO<sub>2</sub> component:

$$\text{CO}_{2\text{ff}} = \frac{\text{CO}_{2\text{meas}} \cdot (\Delta^{14}\text{CO}_{2\text{bg}} - \Delta^{14}\text{CO}_{2\text{meas}})}{\Delta^{14}\text{CO}_{2\text{bg}} + 1} \quad \text{Equation 3.3}$$

This formulation is very convenient, as it shows that the fossil fuel CO<sub>2</sub> component at a polluted site can be estimated from CO<sub>2meas</sub> and Δ<sup>14</sup>CO<sub>2meas</sub> measured *in situ*, and from the

corresponding  $\Delta^{14}\text{CO}_{2\text{bg}}$  value measured at a background site during the same period. However, Equation 3.3 does not include the correction for two small biases. First, NPPs release substantial amounts of  $^{14}\text{CO}_2$ , which create large-scale gradients in atmospheric  $\Delta^{14}\text{CO}_2$  (Graven and Gruber, 2011). At Beromünster, Berhanu et al. (2017) simulated that the emissions from NPPs account for a mean enhancement in  $\Delta^{14}\text{CO}_{2\text{meas}}$  of +1.6‰. The second bias is due to heterotrophic respiration, which represents the respiration from soil organisms other than the plants (Hanson et al., 2000). Carbon in soils spans a large range of residence times, depending on many factors such as the type of soil and the geographical location (Hahn et al., 2006; Bloom et al., 2016). Following Turnbull et al. (2006) who assumed that soils organisms decompose organic matter that has a mean terrestrial carbon residence time of 10 years, the  $^{14}\text{C}$  content of their respiration is not in equilibrium with present-day atmospheric  $^{14}\text{CO}_2$  but is instead similar to the  $^{14}\text{C}$  content of atmospheric  $\text{CO}_2$  10 years before. Owing to the decrease of atmospheric  $^{14}\text{CO}_2$  over time (see Figure 1.5), the effect of heterotrophic respiration has been simulated to lead to an underestimation of  $\text{CO}_{2\text{ff}}$  of 0.2 to 0.5 ppm in the Northern Hemisphere, with the largest biases expected during summertime when the respiration of soils is larger (Turnbull et al., 2006). Equation 3.4 includes the corrections for the biases aforementioned.

$$\text{CO}_{2\text{ff}} = \frac{\text{CO}_{2\text{meas}} \cdot (\Delta^{14}\text{CO}_{2\text{bg}} - \Delta^{14}\text{CO}_{2\text{meas}} + \beta_{NPP})}{\Delta^{14}\text{CO}_{2\text{bg}} + 1} + \beta_h \quad \text{Equation 3.4}$$

With  $\beta_{NPP}$  the correction for the impact of NPPs (e.g. 1.6‰ at Beromünster) and  $\beta_h$  the correction for heterotrophic respiration, which is a simple harmonic function oscillating seasonally between 0.2 ppm in winter and 0.5 ppm in summer (Turnbull et al., 2009; Berhanu et al., 2017). The fossil fuel  $\text{CO}_2$  components reported in this chapter for Beromünster was calculated from Equation 3.4 using  $\Delta^{14}\text{CO}_2$  from the Jungfraujoch background site as a reference for  $\Delta^{14}\text{CO}_{2\text{bg}}$  (Levin et al., 2013).

As  $\text{CO}_2$  mole fractions were not measured at Bern during the collection of samples, another formulation was used for the estimation of  $\text{CO}_{2\text{ff}}$ , which does not require the knowledge of  $\text{CO}_{2\text{meas}}$  but  $\text{CO}_{2\text{bg}}$  instead (Riley et al., 2008; Turnbull et al., 2009):

$$\text{CO}_{2\text{ff}} = \frac{\text{CO}_{2\text{bg}} \cdot (\Delta^{14}\text{CO}_{2\text{bg}} - \Delta^{14}\text{CO}_{2\text{meas}})}{\Delta^{14}\text{CO}_{2\text{meas}} + 1} + \beta_h \quad \text{Equation 3.5}$$

With  $\text{CO}_{2\text{bg}}$  the  $\text{CO}_2$  mole fraction continuously measured at Jungfraujoch by the CEP. The bias caused by  $^{14}\text{C}$  releases from NPPs was not included in the calculation of  $\text{CO}_{2\text{ff}}$  at Bern, as it has not been simulated at that site. Hence, the actual  $\text{CO}_{2\text{ff}}$  at Bern might sometimes be larger than the reported values using Equation 3.5.

## 3.3 Results

### 3.3.1 Atmospheric $^{14}\text{CH}_4$ at Jungfraujoch, Beromünster and Bern

Figure 3.2 shows the  $^{14}\text{CH}_4$  results of air samples collected on a biweekly basis at Jungfraujoch (blue circles), Beromünster (grey squares) and Bern (orange triangles). The samples collected at Jungfraujoch were usually associated with the lowest and most stable  $\Delta^{14}\text{CH}_4$  results, with a mean value of  $368\text{‰}$  in 2019. When excluding the two unusually elevated results of June 13 ( $478\text{‰}$ ) and July 25 ( $535\text{‰}$ ), the reason for which will be discussed in section 3.4.1.1, the average  $\Delta^{14}\text{CH}_4$  was  $354 \pm 15\text{‰}$  at the background site.

The picture is very different at Beromünster, with extremely large variations and a measured  $\Delta^{14}\text{CH}_4$  between  $332$  and  $2984\text{‰}$ , the latter value corresponding to a  $^{14}\text{CH}_4$  concentration almost 3 times higher than background  $^{14}\text{CH}_4$  concentrations. Excluding the measurement of January 24 (outside  $3\sigma$ ), the mean  $\Delta^{14}\text{CH}_4$  at Beromünster was  $481 \pm 218\text{‰}$  in 2019.

At Bern, the measured atmospheric  $\Delta^{14}\text{CH}_4$  ranged between  $313$  and  $728\text{‰}$ , with a mean value of  $415 \pm 108\text{‰}$  in 2019. Although the amplitude of the variations was lower than at Beromünster, the  $\Delta^{14}\text{CH}_4$  values at Bern were 35% of the time significantly higher than the corresponding background values from Jungfraujoch. When not elevated, the  $\Delta^{14}\text{CH}_4$  values measured at Bern were close or slightly lower than background values from Jungfraujoch.

Although the results of the three sampling sites do not reveal a trend or seasonality, the episodes with elevated  $\Delta^{14}\text{CH}_4$  content were usually observed at Beromünster and Bern jointly, sometimes also at Jungfraujoch (June 13 and July 25).

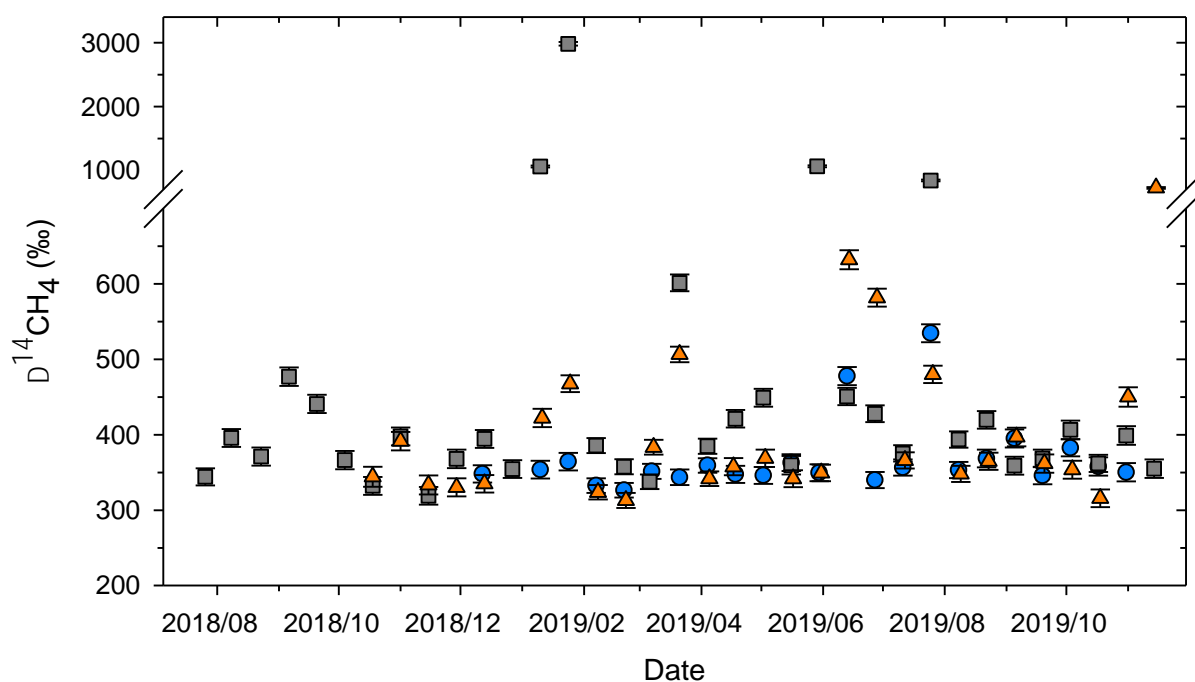


Figure 3.2 Biweekly atmospheric  $\Delta^{14}\text{CH}_4$  measurements at Jungfrauoch (blue circles), Beromünster (grey squares) and Bern (orange triangles). Note the break and change of scale in the vertical axis to display 4 extreme values measured at Beromünster. A total procedural blank of  $0.35 \pm 0.10 \mu\text{g C}$  with an  $F^{14}\text{C}$  of  $0.35 \pm 0.18$  and a cross contamination of  $0.4 \pm 0.2\%$  are considered (see Table 2.1). The error bars refer to  $1\sigma$  uncertainties. See Table 8.4 in appendix for individual results.

### 3.3.2 Atmospheric $^{14}\text{CO}_2$ at Jungfrauoch, Beromünster and Bern

The  $^{14}\text{CO}_2$  results of the biweekly collection of air samples at Jungfrauoch, Beromünster and Bern are presented in Figure 3.3. During the early stages of the biweekly sampling, the extraction procedure for  $\text{CO}_2$  was still under optimization and there was a lack of available recovery flasks, which explain the larger uncertainties and some missing data points, respectively. Since February 2019,  $\Delta^{14}\text{CO}_2$  was systematically measured at the three sites. At Jungfrauoch (blue circles),  $\Delta^{14}\text{CO}_2$  was relatively stable and usually higher than at the two other sites, with a mean value of  $-0.9 \pm 4.6\%$  in 2019.

At Beromünster (grey squares),  $\Delta^{14}\text{CO}_2$  was on average lower than at Jungfrauoch, with a mean value of  $-6.8 \pm 7.0\%$  in 2019. The variations in the signal at Beromünster were larger than at Jungfrauoch, with a maximum difference of  $25.7\%$  in 2019.

Apart from a high  $\Delta^{14}\text{CO}_2$  of  $+38.1\%$  measured on 14 June 2019, atmospheric  $\text{CO}_2$  at Bern (orange triangles) was systematically depleted in  $^{14}\text{C}$  in comparison to the corresponding values measured at the two other sites. The mean  $\Delta^{14}\text{CO}_2$  at Bern was  $-31.4\%$  when ignoring the outlier of June 14, which is  $30\text{--}35\%$  lower than the mean value at Jungfrauoch. The measurements at Bern showed the largest range of values, with a minimum of  $-90.1\%$  on

March 21 and a maximum of +38.1‰ on June 14. Although the dataset is too short to distinguish trends and seasonality, the  $^{14}\text{CO}_2$  content at the three sites did not show any marked difference between winter and summer.

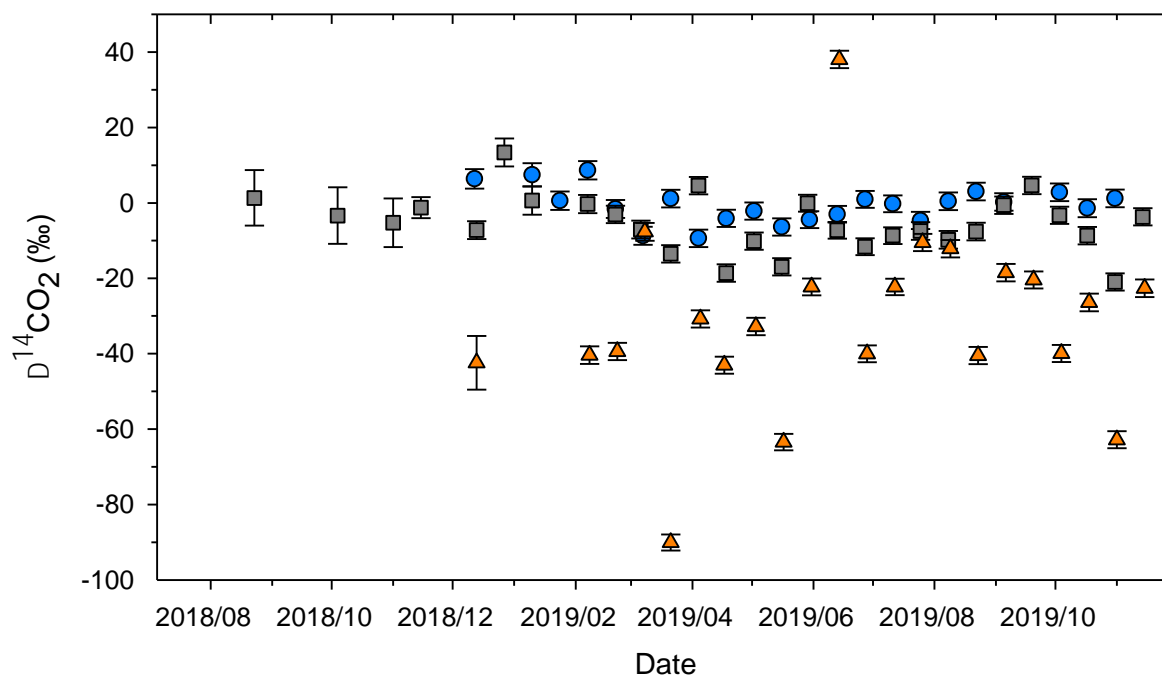


Figure 3.3 Biweekly atmospheric  $\Delta^{14}\text{CO}_2$  measurements at Jungfrauoch (blue circles), Beromünster (grey circles) and Bern (orange triangles). The vertical error bars refer to  $1\sigma$  uncertainties. See Table 8.5 in appendix for individual results.

### 3.3.3 Diurnal variability of $^{14}\text{CH}_4$ and $^{14}\text{CO}_2$

The  $\Delta^{14}\text{CH}_4$  and  $\Delta^{14}\text{CO}_2$  results of the overnight air sampling conducted at Jungfrauoch (blue circles), Beromünster (grey squares) and Bern (orange triangles) from 20 to 21 March 2019 are shown in Figure 3.4. Due to a defective sampling bag, the first sample collected at Bern could not be analyzed (March 20, 12:00 UTC). The  $\Delta^{14}\text{CH}_4$  values measured at Jungfrauoch were very stable over the 24 hours sampling period, with a mean  $\Delta^{14}\text{CH}_4$  of 344‰ and a standard deviation of all  $^{14}\text{CH}_4$  analyses (7‰) lower than the uncertainty of a single measurement (11‰). The values were significantly higher at Beromünster and Bern, with a mean  $\Delta^{14}\text{CH}_4$  of 596 and 519‰, respectively. For these two sites, the temporal variations were noticeably larger than at Jungfrauoch, and Beromünster showed the largest fluctuations with values ranging between 545 and 661‰.

The  $\Delta^{14}\text{CO}_2$  results, depicted in Figure 3.4b, differ strongly from the  $\Delta^{14}\text{CH}_4$  results previously described. First, the  $^{14}\text{C}$  content of  $\text{CO}_2$  was well below the  $^{14}\text{C}$  content of  $\text{CH}_4$  and showed lower discrepancies among the three sites, with  $\Delta^{14}\text{CO}_2$  values comprised between a minimum of -90.1‰ (Bern) and a maximum of 4.2‰ (Jungfrauoch). In contrast to  $\Delta^{14}\text{CH}_4$ , the highest  $\Delta^{14}\text{CO}_2$  values were systematically measured at Jungfrauoch, with a mean value of -0.4‰ at

the background site. At Beromünster,  $\Delta^{14}\text{CO}_2$  varied between  $-22.6$  and  $-4.8\text{‰}$ , with an average depletion of  $12.4\text{‰}$  compared to Jungfraujoch and no clear diurnal cycle. With an average value of  $-37.0\text{‰}$  over the 24 hours of sampling,  $\Delta^{14}\text{CO}_2$  was considerably lower at Bern and showed marked temporal variations. Two episodes of  $\Delta^{14}\text{CO}_2$  decrease were observed during early morning and early evening, with a minimum of  $-90.1\text{‰}$  at 06:00 UTC.

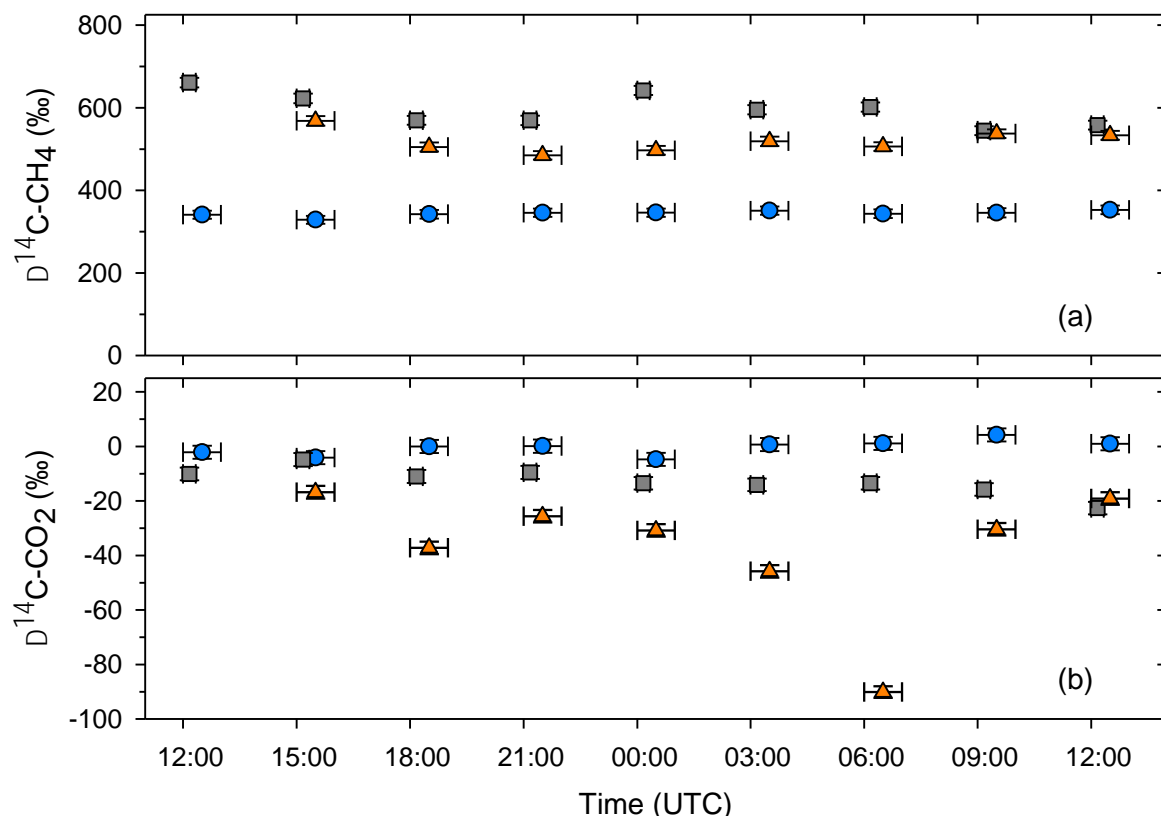


Figure 3.4 Overnight sampling of atmospheric air at Jungfraujoch (blue circles), Beromünster (grey squares) and Bern (orange triangles) from March 20 to March 21, 2019. The horizontal error bars illustrate the sampling duration (15 min at Beromünster, 60 min at Jungfraujoch and Bern). The vertical error bars refer to the  $1\sigma$  uncertainties. See Table 8.6 and Table 8.7 in appendix for individual results. (a)  $^{14}\text{CH}_4$  results. (b)  $^{14}\text{CO}_2$  results.

### 3.3.4 Long-term biweekly $^{14}\text{CO}_2$ measurements at Beromünster

Figure 3.5 shows biweekly  $^{14}\text{CO}_2$  measurements of air samples collected from the highest inlet (212 m) of the Beromünster tall tower, spanning a period of 6 years between July 2013 and July 2019 (grey squares). This new dataset is an update of the  $^{14}\text{CO}_2$  measurements reported for the period 2013–2015 by Berhanu et al. (2017). The blue curve is a fit of two-weekly integrated  $\Delta^{14}\text{CO}_2$  at Jungfraujoch, which were analyzed at the low-level counting facility of the Institute of Environmental Physics, Heidelberg University, Germany (Hammer and Levin, 2017; ICOS RI, 2019). The construction, relevance and validity of the Jungfraujoch fit are discussed in section 3.4.4.1.

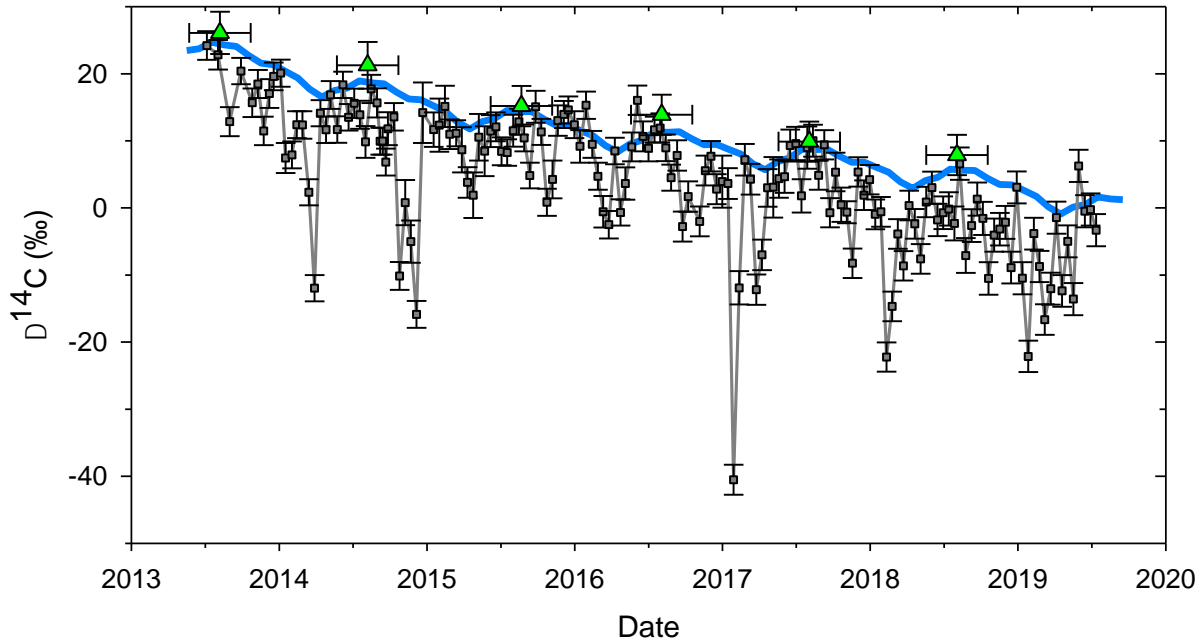


Figure 3.5 In grey:  $\Delta^{14}\text{CO}_2$  at Beromünster, determined from biweekly point samplings (squares). The lines are used to guide the eye. In blue: 3-components fit of two-weekly integrated  $\Delta^{14}\text{CO}_2$  at Jungfraujoch (Hammer and Levin, 2017; ICOS RI, 2019). In green: Mean annual  $\Delta^{14}\text{C}$  of leaf samples collected each year in June, August and October at three locations in Switzerland (FOPH, 2019). The error bars refer to the  $1\sigma$  uncertainties.

The  $\Delta^{14}\text{CO}_2$  differences between Beromünster and the clean air reference from Jungfraujoch were between  $+6.0\text{‰}$  (June 6, 2016) and  $-49.3\text{‰}$  (January 26, 2017), with a mean value of  $-6.5\text{‰}$  over the period 2013–2019. The Beromünster signal showed a relatively clear seasonality, with the occurrence of strong  $\Delta^{14}\text{CO}_2$  depletions usually observed in winter and early spring. Finally, the  $\Delta^{14}\text{CO}_2$  signal at Beromünster revealed a mean downward trend of  $-3.7\text{‰}$  per year, closely following the corresponding annual decrease of  $-3.6\text{‰}$  at Jungfraujoch (blue curve) over the same period.

In addition to the aforementioned air samplings, leaf samples were collected each year in June, August and October at three rural sites remote from fossil fuels and NPP sources, and their mean  $^{14}\text{C}$  content was used as annual reference values for undisturbed  $\Delta^{14}\text{CO}_2$  (green triangles). These results are published by the Swiss Federal Office for Public Health (<https://www.bag.admin.ch/bag/en/home.html>) in annual reports (e.g. FOPH, 2019). As the leaves uptake atmospheric  $\text{CO}_2$  over their growing season, reported mean annual values average atmospheric  $^{14}\text{CO}_2$  from May to October (horizontal error bars). The mean annual  $^{14}\text{C}$  contents of the leaf samples were systematically slightly higher than the corresponding background values modeled at Jungfraujoch (blue curve), although both values could not be statistically distinguished.

A laboratory intercomparison reported a small bias between atmospheric  $^{14}\text{CO}_2$  measurements at Heidelberg and the LARA laboratory in Bern (Hammer et al., 2017), which needed to be accounted for when comparing  $^{14}\text{C}$  results of both laboratories. Consequently,  $2.1 \pm 0.5\text{‰}$  were subtracted from all the  $\Delta^{14}\text{C}$  results obtained at the LARA, namely the Beromünster samples (grey squares) and the leaf samples (green triangles).

### 3.3.5 Fossil fuel $\text{CO}_2$ component at Beromünster and Bern

Figure 3.6a shows the  $\text{CO}_2$  mole fractions measured at Beromünster during each sample collection for  $^{14}\text{CO}_2$  analysis (grey squares). Globally, the  $\text{CO}_2$  mole fractions measured at Beromünster follow the seasonal cycles and the annual trend of  $+2.3 \text{ ppm yr}^{-1}$  measured at Jungfraujoch (blue circles) over the period 2013–2019. However, spikes of  $\text{CO}_2$  were regularly observed at Beromünster, particularly in winter, with  $\text{CO}_2$  peaking at 458 ppm on 26<sup>th</sup> of January 2017, which is about 12% higher than the corresponding background value measured at Jungfraujoch.

The fossil fuel  $\text{CO}_2$  component ( $\text{CO}_{2\text{ff}}$ ) at Beromünster, derived from Equation 3.4, is presented in Figure 3.6b. The values are corrected for the biases induced by NPPs ( $\beta_{\text{NPP}} = +1.6\text{‰}$ ) and heterotrophic respiration ( $\beta_h$  oscillates seasonally between 0.2 ppm in February and 0.5 ppm in August). The red shaded area shows  $\text{CO}_{2\text{ff}} \pm \sigma$ , with typical  $1\sigma$  uncertainties of 1.3 ppm calculated by error propagation, using an uncertainty of 1.2‰ for  $\beta_{\text{NPP}}$  (Berhanu et al., 2017) and 50% for  $\beta_h$  (Turnbull et al., 2006). Over the sampling period 2013–2019,  $\text{CO}_{2\text{ff}}$  at Beromünster varied between a minimum of  $-1.5 \text{ ppm}$  (May 29, 2019) and a maximum of 23.3 ppm (January 26, 2017), with a mean value of 3.7 ppm. Although the signal does not show clear seasonal and annual trends, elevated values were usually observed in winter.

The biogenic  $\text{CO}_2$  component at Beromünster ( $\text{CO}_{2\text{bio}}$ ), calculated using Equation 3.1, is shown in Figure 3.6c. The green shaded area shows  $\text{CO}_{2\text{bio}} \pm \sigma$ , with typical  $1\sigma$  uncertainties of 1.7 ppm calculated by error propagation.  $\text{CO}_{2\text{bio}}$  ranged between  $-10.2$  and 25.7 ppm, with a mean value of  $+1.7 \text{ ppm}$ . Again,  $\text{CO}_{2\text{bio}}$  did not show any clear seasonal trend, but the lowest  $\text{CO}_{2\text{bio}}$  values were usually observed in summer and the highest values in winter.

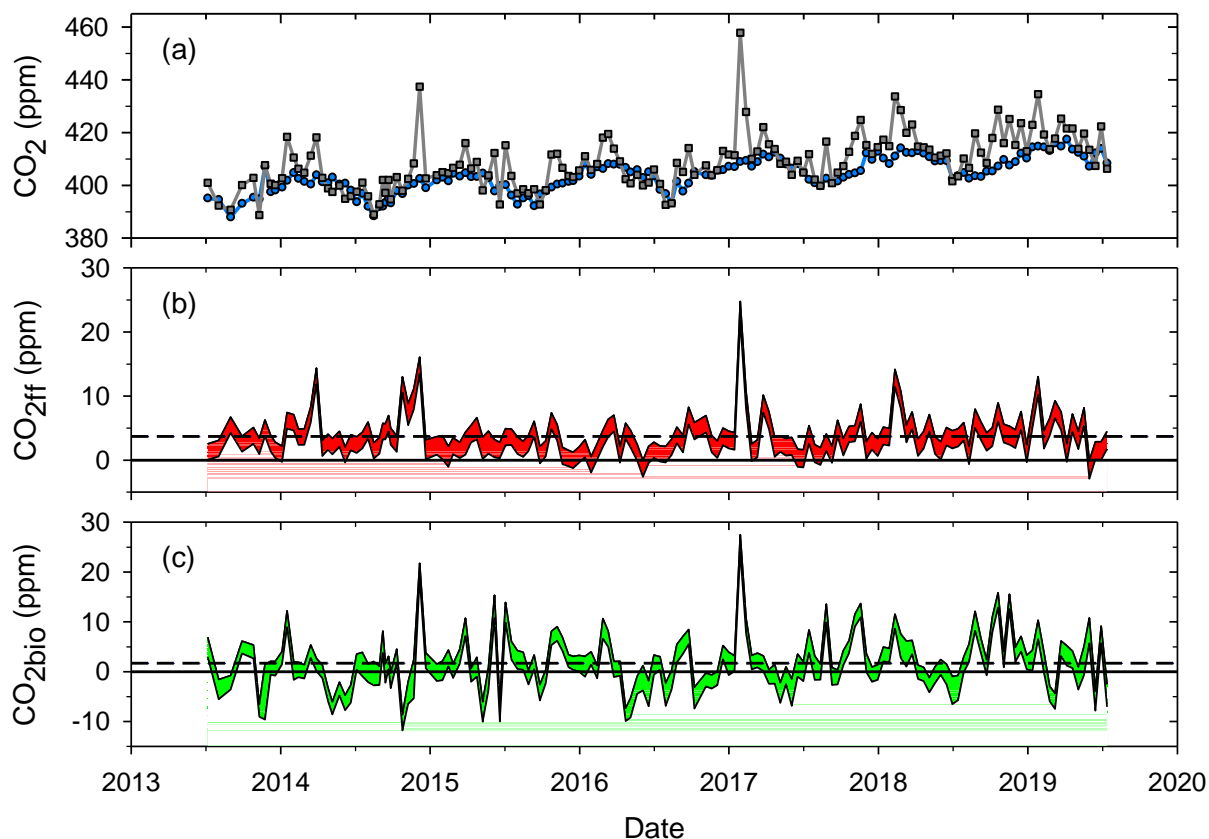


Figure 3.6 Source apportionment of the fossil fuel and biogenic  $\text{CO}_2$  components at Beromünster using radiocarbon analysis. (a)  $\text{CO}_2$  mole fractions measured at Beromünster during each sample collection (grey squares) and corresponding background daily averages measured at Jungfraujoch (blue circles). (b) Fossil fuel  $\text{CO}_2$  component ( $\text{CO}_{2\text{ff}}$ ) calculated from Equation 3.4, with a mean  $\text{CO}_{2\text{ff}}$  of 3.7 ppm (dashed line). (c) Biogenic  $\text{CO}_2$  component ( $\text{CO}_{2\text{bio}}$ ), calculated as the result of the subtraction of  $\text{CO}_{2\text{bg}}$  and  $\text{CO}_{2\text{ff}}$  from  $\text{CO}_{2\text{meas}}$  (see Equation 3.1), with a mean  $\text{CO}_{2\text{bio}}$  of 1.7 ppm (dashed line). The colored areas in panels (b) and (c) represent the  $1\sigma$  confidence bands (see text for details).

The estimation of  $\text{CO}_{2\text{ff}}$  at Bern is based on the  $\Delta^{14}\text{CO}_2$  results of the air samples collected at Bern in 2019 and extracted with the MPPS (see Figure 3.3), and therefore covers a much shorter time window than at Beromünster. To preserve comparability between background  $\Delta^{14}\text{CO}_2$  and  $\Delta^{14}\text{CO}_2$  measured at Bern, the samples collected at Jungfraujoch the day preceding the sampling at Bern were used as  $\Delta^{14}\text{CO}_{2\text{bg}}$  for the calculation of  $\text{CO}_{2\text{ff}}$ , as their  $\text{CO}_2$  content was also extracted with the MPPS (see Figure 3.7a). The fossil fuel  $\text{CO}_2$  component at Bern, reported in Figure 3.7b, ranged between  $-15.9$  and  $41.8$  ppm, with a mean value of  $15.2$  ppm. The  $^{14}\text{CO}_2$  content measured at Bern on June 14 ( $\Delta^{14}\text{CO}_2 = 38\text{‰}$ ) was significantly higher than the corresponding background value observed at Jungfraujoch, yielding to an erroneous determination of  $\text{CO}_{2\text{ff}}$  ( $-15.9$  ppm) that was not included in the calculation of the mean  $\text{CO}_{2\text{ff}}$ .

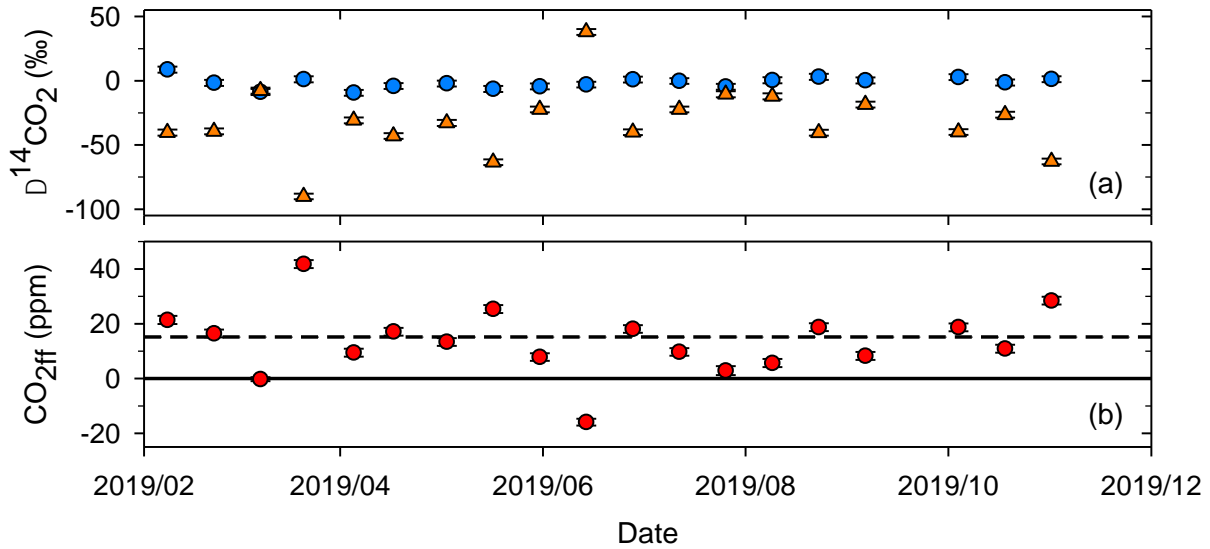


Figure 3.7 Fossil fuel  $\text{CO}_2$  component ( $\text{CO}_{2\text{ff}}$ ) at Bern. (a)  $\Delta^{14}\text{CO}_2$  measured at Jungfraujoch (blue circles) and Bern (orange triangles). (b)  $\text{CO}_{2\text{ff}}$  calculated from Equation 3.5, using the  $\text{CO}_2$  mixing ratios measured at Jungfraujoch (see Figure 3.6a) and  $\Delta^{14}\text{CO}_2$  measured at Jungfraujoch and Bern. From the biweekly measurements between February and November 2019,  $\text{CO}_{2\text{ff}}$  showed a mean value of 15.2 ppm (dashed line).

## 3.4 Discussion

### 3.4.1 Atmospheric $^{14}\text{CH}_4$ in Switzerland

#### 3.4.1.1 Mainly influenced by NPPs

The  $\Delta^{14}\text{CH}_4$  values reported in Figure 3.2 clearly indicate the presence of one or several strong sources enriched in  $^{14}\text{CH}_4$ , as the values vary from background levels at Jungfraujoch to highly enriched values at Beromünster and Bern. Eisma et al. (1994) reported a similar range of  $^{14}\text{CH}_4$  values at a measurement site in The Netherlands, which they attributed to releases of  $^{14}\text{CH}_4$  from NPPs, although they could not systematically link the results to the  $^{14}\text{C}$  emissions of specific NPPs.

The stable  $\Delta^{14}\text{CH}_4$  values measured at Jungfraujoch, with a mean  $\Delta^{14}\text{CH}_4$  of 354‰ in 2019, confirm that this site is a suitable reference for background  $\Delta^{14}\text{CH}_4$  in Switzerland. However, as pointed out by several studies, the PBL is particularly high in spring and summer, and frequently allows the intrusion of polluted air masses to Jungfraujoch at the end of the morning and in the afternoon (Baltensperger et al., 1997; Collaud Coen et al., 2011; Ketterer et al., 2014). This effect is presumably at the origin of the two elevated  $\Delta^{14}\text{CH}_4$  values measured on June 13 and July 25, with a  $^{14}\text{CH}_4$  content almost 14% higher than previously measured at that site. To mitigate the risk of sampling polluted air at Jungfraujoch, van der Laan-Luijckx et al. (2013) usually collect flasks early morning, at around 07:00 local time. Unfortunately, it

was not logistically possible to collect samples at Jungfraujoch before 9:30 local time for this study. Although it should not be of a concern for the majority of the biweekly samplings, spring and summer results should be taken with caution, as a combination of a convective PBL and a strong  $^{14}\text{CH}_4$  release from NPPs may result in an enhanced  $^{14}\text{CH}_4$  content at Jungfraujoch.

Unlike atmospheric  $^{14}\text{CO}_2$  level, which started to decrease in the early 1960s, the concentration of atmospheric  $^{14}\text{CH}_4$  has been increasing since then due to the expansion of nuclear facilities (Wahlen et al., 1989; Manning et al., 1990; Levin et al., 2010). Radiocarbon measurements of atmospheric  $\text{CH}_4$  in the late 1980s revealed a value of  $228 \pm 8\text{‰}$  in the Northern Hemisphere (Wahlen et al., 1989), with a strong increase of about  $+13.5\text{‰}$  per year (Quay et al., 1991). A few years later, Lassey et al. (2007b) reported a mean annual increase of  $8.8\text{‰}$  over the period 1986–2001, based on a composite record of 230 individual atmospheric  $^{14}\text{CH}_4$  measurements. Zazzeri et al. (2018) estimated that global  $^{14}\text{CH}_4$  emissions from nuclear activities have probably decreased since 2011, as a consequence of the shutdown of some PWRs in Europe and Japan after the Fukushima accident. Our findings at Jungfraujoch, with a mean  $\Delta^{14}\text{CH}_4$  of  $354\text{‰}$  in 2019, seem to confirm a stabilization and potential decrease of atmospheric  $\Delta^{14}\text{CH}_4$ . Indeed, the results are substantially lower than a hypothetical value over  $450\text{‰}$  in 2019, if the annual increase reported by Lassey et al. (2007b) would have remained constant until today. However, we did not find any other recent ( $< 15$  years) measurement of background atmospheric  $^{14}\text{CH}_4$  to confirm these findings.

Although the variations of  $\Delta^{14}\text{CH}_4$  at Beromünster and Bern seem randomly distributed over time, episodes with elevated values were usually observed simultaneously at both sites. Moreover, the two elevated  $\Delta^{14}\text{CH}_4$  values measured at Jungfraujoch on June 13 and July 25 were also associated with high values recorded at Bern and Beromünster. These results seem to indicate a common source of  $^{14}\text{CH}_4$  affecting the three sites. The Gösgen NPP is an obvious candidate as the main  $^{14}\text{CH}_4$  source, since it holds a PWR and is located only 25 km NW from Beromünster where the highest  $^{14}\text{CH}_4$  contents were measured. As an example among others, the wind was blowing from the northeast at the sampling site when Beromünster recorded an extreme  $\Delta^{14}\text{CH}_4$  value of  $2984\text{‰}$  on 24 January 2019 (see Figure 3.1). According to CGER METEX, which allows a simulation of air trajectories, the air masses passed over Gösgen 5 hours before reaching Beromünster. Hence, the Gösgen NPP might be the main contributor to the variations of  $\Delta^{14}\text{CH}_4$  observed at the three sites, with the distance to the  $^{14}\text{CH}_4$  source and the wind direction being the main factors determining the magnitude of the impact at the respective sampling sites.

While the highest  $\Delta^{14}\text{CH}_4$  values measured at Beromünster were usually linked to a direct contribution from the Gösgen NPP, back trajectories from other days with moderately elevated values could not provide evidence of an input from Gösgen. In fact, the actual situation is probably more complex, as the sampling at Beromünster was performed at the top of a tall

tower situated on a hill, with a signal known to be influenced by the entire Swiss Plateau (Oney et al., 2015; Satar et al., 2016). As the prevailing wind directions at Beromünster are NW and SE, which are not in the direction of Gösigen, other Swiss NPPs such as Beznau I/II might significantly influence the  $^{14}\text{CH}_4$  concentration measured at the sampling site (Berhanu et al., 2017). Indeed, Eisma et al. (1995), who also sampled air from a tall tower, determined that the  $^{14}\text{CH}_4$  content measured was highly influenced by the wind direction. Finally, a probable contribution from France should not be overlooked: First, since France holds 58 PWR-type NPPs and is the largest emitter of  $^{14}\text{C}$  in Europe (IAEA, 2017; Zazzeri et al., 2018). Second, because air masses in Switzerland are frequently advected from France by the westerly winds (Oney et al., 2015; Berhanu et al., 2017).

### 3.4.1.2 Source apportionment of fossil $\text{CH}_4$

The Keeling plot in Figure 3.8 indicates a lack of correlation between  $\Delta^{14}\text{CH}_4$  measured at Beromünster or Bern and the  $\text{CH}_4$  mixing ratio in the corresponding air sample. Indeed, although NPPs are negligible sources of GHGs (van der Zwaan, 2013), they constitute a significant source of  $^{14}\text{CH}_4$ , which has been estimated to contribute to  $26 \pm 8\%$  of the global budget of atmospheric  $^{14}\text{CH}_4$  in the 1990s (Quay et al., 1999). Unfortunately, their  $^{14}\text{C}$  emissions are not constant and reveal large temporal variations (Kunz, 1985; Eisma et al., 1995). As a consequence, any potential decrease of  $\Delta^{14}\text{CH}_4$  caused by emissions of fossil  $\text{CH}_4$  is hidden by the large scatter of  $\Delta^{14}\text{CH}_4$  values induced by sporadic discharges from NPPs. Townsend-Small et al. (2012) faced similar problems when analyzing polluted air from Los Angeles. Indeed, they did not find any relationship between  $\text{CH}_4$  concentration and  $\Delta^{14}\text{CH}_4$ , despite the fact that the observed variations of  $\Delta^{14}\text{CH}_4$  were significantly smaller than in the present study.

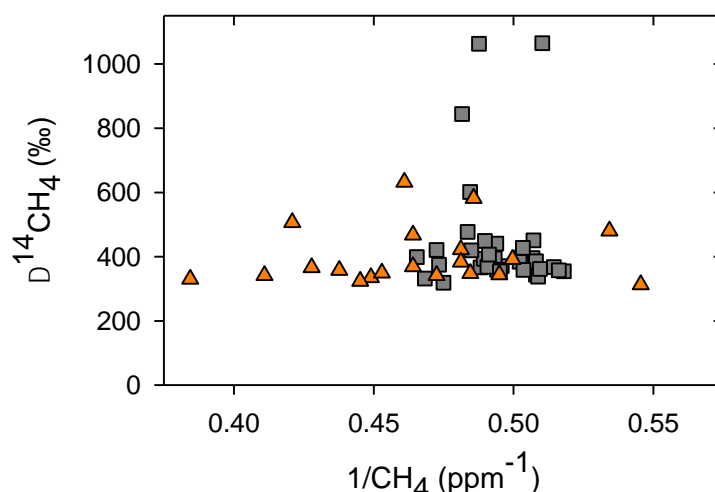


Figure 3.8 Keeling plot of  $\Delta^{14}\text{CH}_4$  measurements at Beromünster (grey squares) and Bern (orange triangles). The extreme  $\Delta^{14}\text{CH}_4$  value of 2984‰ measured on 24<sup>th</sup> of January 2019 is not displayed, as it was not associated with a particularly high  $\text{CH}_4$  mixing ratio.

In the late 1980s and early 1990s, some authors used  $^{14}\text{CH}_4$  measurements at background sites to estimate the fossil fraction of the global methane source (Lowe et al., 1988; Manning et al., 1990; Quay et al., 1991). Determining the main sources of  $\text{CH}_4$  at regional scales would offer the advantage to allow the deployment of efficient mitigation strategies (Dlugokencky et al., 2011; Graven et al., 2019; Nisbet et al., 2019). Here, we use a simple model for the estimation of a regional fossil fuel  $\text{CH}_4$  component ( $\text{CH}_{4\text{ff}}$ ) and biogenic  $\text{CH}_4$  component ( $\text{CH}_{4\text{bio}}$ ) based on  $^{14}\text{CH}_4$  results, similar to the model previously described for the determination of the fossil  $\text{CO}_2$  component (see section 3.2.5). The situation was different at the end of the 1980s, as biogenic sources of  $\text{CH}_4$  were enriched in  $^{14}\text{C}$  with respect to atmospheric  $\text{CH}_4$  (Lowe et al., 1988). Today, biogenic sources of  $\text{CH}_4$  have a  $^{14}\text{C}$  signature similar to atmospheric  $^{14}\text{CO}_2$  (Palstra and Meijer, 2014) and the release of  $^{14}\text{CH}_4$  from nuclear facilities rose atmospheric  $\Delta^{14}\text{CH}_4$  to a mean value of 354‰ at Jungfraujoch (see Figure 3.2). By analogy with Equation 3.1, the  $\text{CH}_4$  mixing ratio measured at a site ( $\text{CH}_{4\text{meas}}$ ) can be expressed as the sum of a background component ( $\text{CH}_{4\text{bg}}$ ), a biogenic component ( $\text{CH}_{4\text{bio}}$ ) and a fossil component ( $\text{CH}_{4\text{ff}}$ ). A mass balance is then formulated for  $\text{CH}_4$  and  $^{14}\text{CH}_4$ :

$$\text{CH}_{4\text{meas}} = \text{CH}_{4\text{bg}} + \text{CH}_{4\text{bio}} + \text{CH}_{4\text{ff}} \quad \text{Equation 3.6}$$

$$\begin{aligned} \text{CH}_{4\text{meas}} \cdot (\Delta^{14}\text{CH}_{4\text{meas}} + 1) &= \text{CH}_{4\text{bg}} \cdot (\Delta^{14}\text{CH}_{4\text{bg}} + 1) \\ &+ \text{CH}_{4\text{bio}} \cdot (\Delta^{14}\text{CH}_{4\text{bio}} + 1) \\ &+ \text{CH}_{4\text{ff}} \cdot (\Delta^{14}\text{CH}_{4\text{ff}} + 1) + \alpha_{NPP} \end{aligned} \quad \text{Equation 3.7}$$

With  $\alpha_{NPP}$  an additional term accounting for the contribution of NPPs to  $\Delta^{14}\text{CH}_4$  measured at the site. Unfortunately,  $\Delta^{14}\text{CH}_{4\text{meas}}$  is usually higher than  $\Delta^{14}\text{CH}_{4\text{bg}}$  at Beromünster and Bern, indicating that  $\alpha_{NPP}$  prevails. Calculating  $\text{CH}_{4\text{ff}}$  at Beromünster and Bern from the  $\Delta^{14}\text{CH}_4$  results displayed in Figure 3.2 is therefore meaningless, because  $\alpha_{NPP}$  was regularly large and would require a precise assessment. Nonetheless, the model remains useful for testing the sensitivity of the  $^{14}\text{C}$  method by assuming no contribution from NPPs (i.e.  $\alpha_{NPP} := 0$ ). With the knowledge that fossil emissions are devoid of  $^{14}\text{C}$  (i.e.  $\Delta^{14}\text{CH}_{4\text{ff}} = -1000\text{‰}$ ) and that biogenic emissions have a  $^{14}\text{C}$  content close to background  $^{14}\text{CO}_2$  (i.e.  $\Delta^{14}\text{CH}_{4\text{bio}} \approx \Delta^{14}\text{CO}_{2\text{bg}}$ ) (Palstra and Meijer, 2014),  $\text{CH}_{4\text{ff}}$  can be written as:

$$\text{CH}_{4\text{ff}} = \frac{\text{CH}_{4\text{bg}} \cdot (\Delta^{14}\text{CH}_{4\text{bg}} - \Delta^{14}\text{CO}_{2\text{bg}})}{\Delta^{14}\text{CO}_{2\text{bg}} + 1} - \frac{\text{CH}_{4\text{meas}} \cdot (\Delta^{14}\text{CH}_{4\text{meas}} - \Delta^{14}\text{CO}_{2\text{bg}})}{\Delta^{14}\text{CO}_{2\text{bg}} + 1} \quad \text{Equation 3.8}$$

Hence,  $\text{CH}_{4\text{bg}}$ ,  $\text{CH}_{4\text{meas}}$ ,  $\Delta^{14}\text{CH}_{4\text{bg}}$ ,  $\Delta^{14}\text{CO}_{2\text{bg}}$  and  $\Delta^{14}\text{CH}_{4\text{meas}}$  need to be measured or approximated to allow an estimation of  $\text{CH}_{4\text{ff}}$ . Owing to the disequilibrium between  $\Delta^{14}\text{CH}_{4\text{bg}}$  and  $\Delta^{14}\text{CH}_{4\text{bio}}$  ( $\approx \Delta^{14}\text{CO}_{2\text{bg}}$ ), the first term of Equation 3.8 cannot be neglected. Hence, the main practical difference with the estimation of  $\text{CO}_{2\text{ff}}$  reported in Equation 3.3 is that  $\text{CH}_4$  mole fractions at the sampling site and at the background site need both to be measured. By setting  $\text{CH}_{4\text{ff}} = \phi_{\text{ff}} \cdot (\text{CH}_{4\text{meas}} - \text{CH}_{4\text{bg}})$  and  $\text{CH}_{4\text{bio}} = (1 - \phi_{\text{ff}}) \cdot (\text{CH}_{4\text{meas}} - \text{CH}_{4\text{bg}})$ , with  $\phi_{\text{ff}}$  the

fraction of added  $\text{CH}_4$  of fossil origin, the relation between  $\Delta^{14}\text{CH}_{4\text{meas}}$  and the fossil and biogenic components is as follows:

$$\Delta^{14}\text{CH}_{4\text{meas}} = \frac{\text{CH}_{4\text{bg}}(\Delta^{14}\text{CH}_{4\text{bg}} + 1)}{\text{CH}_{4\text{meas}}} + \frac{(1 - \phi_{\text{ff}})(\text{CH}_{4\text{meas}} - \text{CH}_{4\text{bg}})(\Delta^{14}\text{CO}_{2\text{bg}} + 1)}{\text{CH}_{4\text{meas}}} - 1 \quad \text{Equation 3.9}$$

Equation 3.9 shows that  $\Delta^{14}\text{CH}_{4\text{meas}}$  at a site mainly depends on the amount of excess  $\text{CH}_4$  ( $\text{CH}_{4\text{meas}} - \text{CH}_{4\text{bg}}$ ) and the fraction of added  $\text{CH}_4$  of fossil origin ( $\phi_{\text{ff}}$ ). In 2019, the mean  $\text{CH}_{4\text{bg}}$  measured at Jungfraujoch was about 1900 ppb, and  $\text{CH}_4$  mole fractions measured at Beromünster and Bern were on average 6% and 12% higher than at the background site, respectively. By setting  $\Delta^{14}\text{CH}_{4\text{bg}} = 354\text{‰}$ ,  $\Delta^{14}\text{CH}_{4\text{bio}} = \Delta^{14}\text{CO}_{2\text{bg}} \approx 0\text{‰}$  (see section 3.3.2), allowing  $\text{CH}_{4\text{meas}}$  to vary between 1900 ppb and 2200 ppb (enhancement of  $\sim 15\%$ ), and  $\phi_{\text{ff}}$  to vary between 0 (no fossil  $\text{CH}_4$  component) and 1 (no biogenic  $\text{CH}_4$  component), the simulated  $\Delta^{14}\text{CH}_{4\text{meas}}$  is displayed in Figure 3.9a.

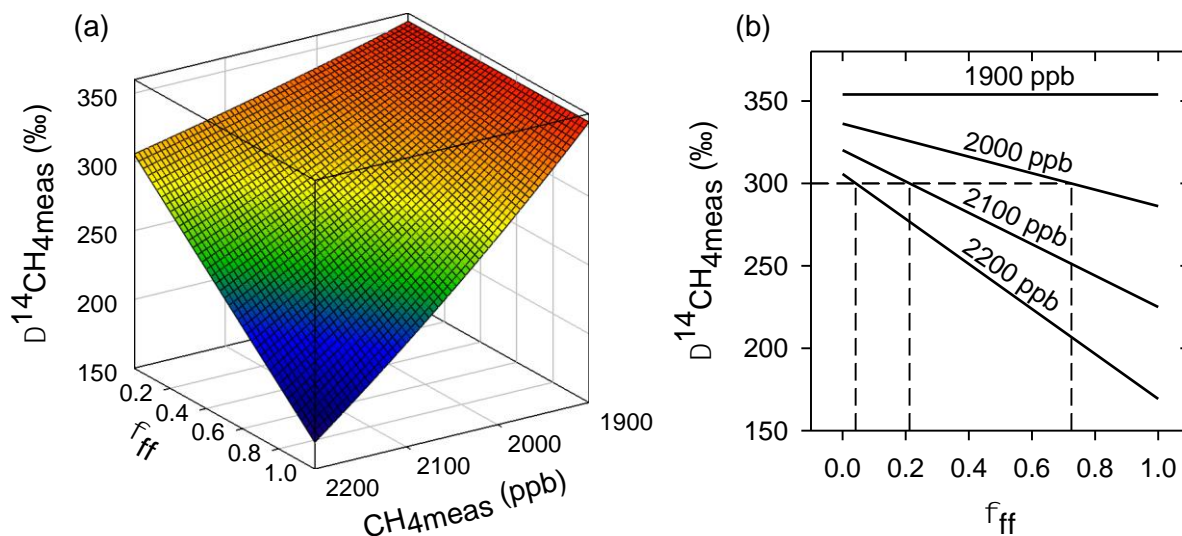


Figure 3.9 Simulation of natural variations of  $\Delta^{14}\text{CH}_4$  measured at a site (see Equation 3.9).  $\text{CH}_{4\text{meas}}$  is allowed to vary from 1900 ppb (mean  $\text{CH}_{4\text{bg}}$  at Jungfraujoch) and 2200 ppb (typical values at Bern).  $\phi_{\text{ff}}$  varies between 0 (pure biogenic  $\text{CH}_4$  source) and 1 (pure fossil  $\text{CH}_4$  source).  $^{14}\text{C}$  measurements at Jungfraujoch are used as references, i.e.  $\Delta^{14}\text{CH}_{4\text{bg}} = 354\text{‰}$  and  $\Delta^{14}\text{CH}_{4\text{bio}} = \Delta^{14}\text{CO}_{2\text{bg}} \approx 0\text{‰}$ . Local enhancements of  $\Delta^{14}\text{CH}_{4\text{meas}}$  due to  $^{14}\text{CH}_4$  releases from NPPs are not considered in the simulation.

The simulation shows that significant decreases of  $\Delta^{14}\text{CH}_{4\text{meas}}$  compared to  $\Delta^{14}\text{CH}_{4\text{bg}}$  should be measured at polluted sites, with a reduction from 354 to 169‰ if the  $\text{CH}_4$  excess at the site is +15% and purely fossil. Because biogenic sources of  $\text{CH}_4$  have a lower  $^{14}\text{C}$  content than background  $^{14}\text{CH}_4$ , their emissions will locally decrease  $\Delta^{14}\text{CH}_{4\text{meas}}$  too. However, the

sensitivity of  $\Delta^{14}\text{CH}_{4\text{meas}}$  to biogenic sources is approximately four times lower than the sensitivity to fossil sources, as the difference between  $\Delta^{14}\text{CH}_{4\text{meas}}$  and  $\Delta^{14}\text{CH}_{4\text{bg}}$  essentially depends on the disequilibrium of  $^{14}\text{CH}_4$  content between the sources ( $\Delta^{14}\text{CH}_{4\text{bio}} \approx 0\text{‰}$  and  $\Delta^{14}\text{CH}_{4\text{ff}} = -1000\text{‰}$ ) and the background ( $\Delta^{14}\text{CH}_{4\text{bg}} = 354\text{‰}$ ). Hence, if the  $\text{CH}_4$  excess at a site is  $+15\text{‰}$  and purely of a biogenic origin, it will only reduce  $\Delta^{14}\text{CH}_{4\text{meas}}$  from 350 to 306‰.

Different combinations of  $(\phi_{\text{ff}}, \text{CH}_{4\text{meas}})$  can lead to the same  $\Delta^{14}\text{CH}_{4\text{meas}}$ , therefore  $\text{CH}_{4\text{meas}}$  and  $\text{CH}_{4\text{bg}}$  need both to be measured for an unequivocal determination of  $\text{CH}_{4\text{ff}}$  and  $\text{CH}_{4\text{bio}}$ . This feature is exemplified in Figure 3.9b, where strong biogenic emissions ( $\phi_{\text{ff}} < 0.1$ ) or weak fossil emissions ( $\phi_{\text{ff}} > 0.7$ ) yield to the same measured  $\Delta^{14}\text{CH}_4$  value of 300‰. This graph also shows that the precision of calculated  $\phi_{\text{ff}}$  improves when the amount of excess  $\text{CH}_4$  is larger, as the sensitivity of  $\Delta^{14}\text{CH}_{4\text{meas}}$  to a change of  $\phi_{\text{ff}}$  increases accordingly. This effect carries an interesting consequence: for a known precision of  $\Delta^{14}\text{CH}_{4\text{meas}}$ , the precision of the estimation of  $\phi_{\text{ff}}$  will increase in regions where  $\text{CH}_4$  emissions are large, such as urban areas where mitigation strategies could be implemented (Hopkins et al., 2016).

The quality of the estimation of  $\text{CH}_{4\text{ff}}$  does not solely depend on the precision of  $\Delta^{14}\text{CH}_{4\text{meas}}$ , but also on the precision of  $\Delta^{14}\text{CH}_{4\text{bg}}$ ,  $\Delta^{14}\text{CO}_{2\text{bg}}$ ,  $\text{CH}_{4\text{bg}}$  and  $\text{CH}_{4\text{meas}}$  (see Equation 3.8). Thus, the  $\Delta^{14}\text{CH}_4$  measurement precision of the MPPS ( $\sim 10\text{‰}$ , see Table 2.1) should not be regarded as the only limiting factor, as the choice of the background site and its associated  $\text{CH}_4$  and  $\Delta^{14}\text{CH}_4$  values are crucial as well.

In Switzerland, almost 85% of  $\text{CH}_4$  emissions are attributed to the agricultural sector (Hiller et al., 2014; Henne et al., 2016). At Beromünster, the main source of  $\text{CH}_4$  is the ruminants near the tower (Satar et al., 2016). Hence, if the added  $\text{CH}_4$  at Beromünster is assumed to be exclusively biogenic (i.e.  $\phi_{\text{ff}} = 0$ ), the measured mean increase of  $\text{CH}_{4\text{meas}}$  compared to Jungfrauoch ( $+6\text{‰}$ ) would only lead to a difference of 20‰ between  $\Delta^{14}\text{CH}_4$  values at Jungfrauoch and Beromünster. The situation is different at Bern, as the  $\text{CH}_4$  mole fractions measured in the samples collected biweekly were on average 12% higher than at Jungfrauoch. As the sampling site is located in an urban area, larger fossil  $\text{CH}_4$  emissions are expected, mainly from fugitive emissions from the natural gas distribution and consumption, but also from fuel combustion, which is confirmed by the spatially explicit inventory of  $\text{CH}_4$  emissions reported by Hiller et al. (2014). However, it is not straightforward to get a prior estimate of  $\phi_{\text{ff}}$  at Bern, because a contribution from the agricultural sector cannot be excluded and fossil emissions from leaks in the gas distribution network are well mitigated in Switzerland (Henne et al., 2016; FOEN, 2017). By letting  $\phi_{\text{ff}}$  vary from 0 (pure biogenic component) to 1 (pure fossil component),  $\Delta^{14}\text{CH}_4$  values measured at Bern would be from 38 to 145‰ lower than background values. These findings emphasize that the  $^{14}\text{C}$  technique would reveal useful for an unequivocal attribution of the origin of pollution events when high  $\text{CH}_4$  mole fractions are measured at a site. As an example, Satar et al. (2016) noted some  $\text{CH}_4$  pollution spikes at Beromünster with  $\text{CH}_4$  enhancements of up to 25%, which they attributed to be likely coming

from grazing near the tower. For such large deviations from background  $\text{CH}_4$ , a  $^{14}\text{C}$  source apportionment would be very efficient and provide a reliable estimate of  $\phi_{\text{ff}}$ .

The simplified model presented here is very helpful, as it allows to estimate typical variations of  $\Delta^{14}\text{CH}_4$  which could be measured at different sites, with an expected very small depletion at Beromünster ( $-20\text{‰}$ ) and a larger depletion at Bern ( $-43$  to  $-166\text{‰}$ ). However, it is essential to keep in mind that it consists of an ideal hypothetical scenario, where the contribution of NPPs to  $\Delta^{14}\text{CH}_{4\text{meas}}$  is neglected (i.e.  $\alpha_{\text{NPP}} = 0$  in Equation 3.7). The fact that  $\Delta^{14}\text{CH}_4$  values measured at Bern were usually lower than at Beromünster cannot be solely explained by a depletion caused by fossil emissions as the deviations are too large. Furthermore, the observation of extremely high values at Beromünster confirms that the impact of NPPs is larger at that site. Neglecting the influence of NPPs would lead to the calculation of meaningless negative  $\text{CH}_{4\text{ff}}$  values for both sites. As mentioned by Eisma et al. (1994), Figure 3.9 shows that an underestimation of the contribution from NPPs would cause an underestimation of  $\text{CH}_{4\text{ff}}$  and a subsequent overestimation of  $\text{CH}_{4\text{bio}}$  (see Equation 3.6). Conversely, an overestimation will produce the opposite effects. Considering the large variations of  $\Delta^{14}\text{CH}_4$  observed at Beromünster and Bern, and the knowledge that  $^{14}\text{C}$  emissions from NPPs show a large temporal variability, accounting for the contribution of NPPs will always be associated with large uncertainties, which may impede any attempt of an atmospheric  $^{14}\text{CH}_4$  source apportionment in Switzerland.

Recently, Graven et al. (2019) simulated  $\Delta^{14}\text{CH}_4$  at several sites in California based on  $\text{CH}_4$  emission estimates, an atmospheric transport model and a mass balance model similar to the one previously described. Their simulations provide a good framework to help interpreting  $\Delta^{14}\text{CH}_4$  in atmospheric studies. Similarly to other studies of  $^{14}\text{CH}_4$  and  $^{14}\text{CO}_2$ , they included the impact of NPPs by assuming time-invariant emissions, as actual  $^{14}\text{C}$  emissions are not continuously monitored (Eisma et al., 1995; Berhanu et al., 2017). Unfortunately, the estimation of the contribution from NPPs at a sampling site is not only challenged by the reliability of meteorological data and the quality of the dispersion and transport model. Indeed, the large temporal variability of  $^{14}\text{C}$  emissions from NPPs holding a PWR might also be a limiting factor (Kunz, 1985; Eisma et al., 1995; Magnusson, 2007). More measurements of atmospheric  $\Delta^{14}\text{CH}_4$ , such as the ones reported in the present study, should help constraining the models used for the simulation of the influence of NPPs (Eisma et al., 1995).

In summary, a  $^{14}\text{C}$  source apportionment of  $\text{CH}_4$  is not well suited to regions moderately or strongly impacted by NPP releases, such as Europe or Asia, as the achievable precision for the estimation of  $\phi_{\text{ff}}$  will likely be limited by the choice of reference values and the capability to account accurately for the contribution of the NPPs. However, the easy collection of samples and the high throughput of the MPPS are particularly well suited to regions where large  $\text{CH}_4$  sources are expected but not clearly identified. As an example of application in regions where the influence of NPPs is low, detecting fugitive emissions from the fossil fuel industry in urban

areas might reveal a useful tool for the deployment of cost-effective mitigation plans (Schwietzke et al., 2016; Nisbet et al., 2019). Finally, the model used for the determination of the CH<sub>4</sub> fossil fraction could be refined: First, by considering the biospheric lag time between CO<sub>2</sub> uptake by photosynthesis and subsequent CH<sub>4</sub> emissions (Lassey et al., 2007a). Second, by including the possibility to account for intermediate age CH<sub>4</sub> sources, such as the example of an arctic lake releasing Pleistocene-aged carbon (Manning et al., 1990; Zimov et al., 1997).

### 3.4.2 Atmospheric <sup>14</sup>CO<sub>2</sub> — comparisons with <sup>14</sup>CH<sub>4</sub>

#### 3.4.2.1 Quality of the CO<sub>2</sub> extraction with the MPPS

The MPPS was primarily designed for the preparation of pure atmospheric CH<sub>4</sub> samples for <sup>14</sup>C analysis. However, a joint analysis of <sup>14</sup>CO<sub>2</sub> and <sup>14</sup>CH<sub>4</sub> from the same air sample is very valuable, as it allows the determination of common sources but also different origins, providing more information about the main drivers of these two GHGs at local and regional scales. As the CO<sub>2</sub> content from the Beromünster air samples was extracted with the MPPS and at the CEP, the <sup>14</sup>CO<sub>2</sub> results of the CEP extraction were used as a benchmark for the quality assessment of the MPPS extraction. The main results are summarized in Figure 3.10.

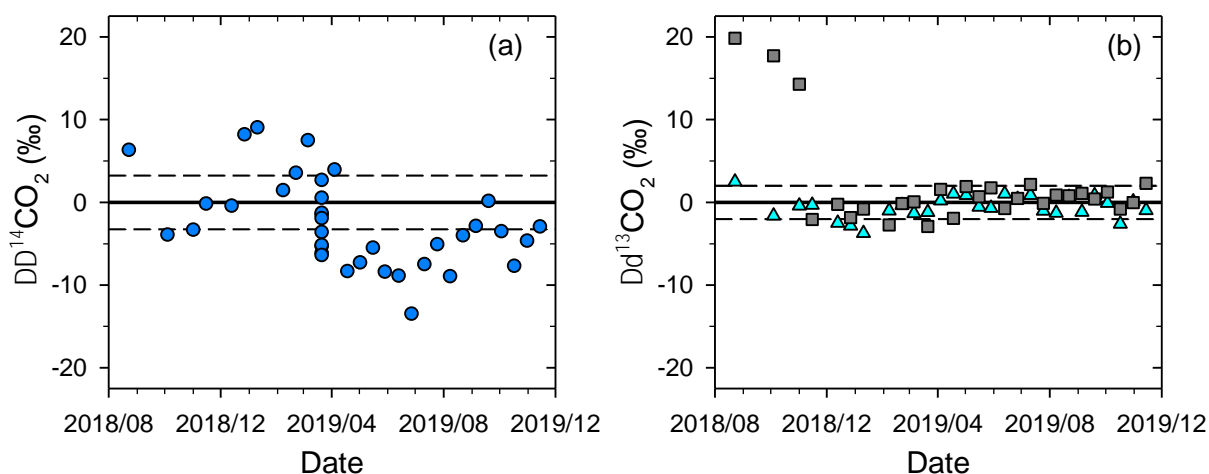


Figure 3.10 Quality assessment of the  $\Delta^{14}\text{CO}_2$  results obtained from the extraction of CO<sub>2</sub> with the MPPS (Beromünster samples). The horizontal dashed lines delimit the zone within error-propagated uncertainties of both measurements ( $1\sigma$ ). (a) Difference between the  $\Delta^{14}\text{CO}_2$  results for samples extracted with the MPPS and at the CEP. (b) Deviation of the  $\delta^{13}\text{CO}_2$  values from the AMS measurements with the corresponding IRMS results, for CO<sub>2</sub> extracted at the CEP (cyan triangles) and with the MPPS (grey squares).

The differences between the  $\Delta^{14}\text{CO}_2$  results obtained at the CEP and with the MPPS are shown in Figure 3.10a, including the 10 values from the overnight sampling (March 20–21, 2019). The  $\Delta^{14}\text{CO}_2$  results of the extraction with the MPPS are on average 2.6‰ lower than from the corresponding extraction at the CEP, which is within the average standard deviation of the differences ( $1\sigma$ ). However, the temporal evolution of the deviation is more of a concern:

since the beginning of 2019, the difference shifted from positive to negative values. The deviations are comparatively lower than the actual variations of the  $\Delta^{14}\text{CO}_2$  signal at Beromünster over time (see Figure 3.5), preserving the general evolution of the signal. However, they could considerably reduce the accuracy of a fossil fuel source apportionment based on the  $^{14}\text{C}$  method, as any error in the determination of  $\Delta^{14}\text{CO}_2$  will be propagated to the final result. Thus, the issue depicted in Figure 3.10a should be addressed, as it affects the reliability of the  $^{14}\text{CO}_2$  results obtained with the MPPS extraction.

A combination of many factors can contribute to the scatter and deviations reported in Figure 3.10a. The discrepancies reflected in the  $^{14}\text{CO}_2$  results could arise from differences during the sampling, the  $\text{CO}_2$  extraction and the AMS measurement. First, the samples extracted at the CEP do not physically originate from the same aluminum bags as the samples extracted with the MPPS, although they were successively collected with a common sampling system at Beromünster. Here, the observed discrepancies do likely not originate from fast temporal changes of atmospheric  $\Delta^{14}\text{CO}_2$  between the consecutive fillings of two bags. Indeed, the standard deviation of the triplicates collected between 2013 and 2017 and extracted at the CEP was usually between 0.2 and 3‰, with a mean standard deviation of the triplicates below 1‰. However, a small contribution from different sampling times to the scatter in the results may still happen, especially in spring and summer time. Indeed, these periods are associated with pronounced diurnal cycles and fast temporal changes of the  $\text{CO}_2$  mole fractions measured at the highest inlet of the Beromünster tower, which are caused by the strong convective vertical mixing of air masses in the morning (Satar et al., 2016; Berhanu et al., 2017). In addition, a contamination from some aluminum bags cannot be excluded, as it has not been accurately determined yet.

The general procedure for the extraction of  $\text{CO}_2$  with the MPPS and at the CEP is similar for both (see section 3.2.3.2). However, the  $\text{CO}_2$  recovery yield at the CEP (>99%) is much higher than with the MPPS (~70%), owing to a more efficient transfer of  $\text{CO}_2$  from the trap to the recovery flask. For such kinetic processes, isotopic fractionation may happen when the yield is lower than 100%. It is not really an issue for  $^{14}\text{C}$ -AMS measurements, as the  $^{14}\text{C}$  results are corrected for isotope fractionation in the data reduction process. However, large fractionations cannot be precisely accounted for and would lower the final precision of the  $^{14}\text{C}$  results (Fahrni et al., 2017). Figure 3.10b presents the AMS  $\delta^{13}\text{C}$  results, for  $\text{CO}_2$  extracted at the CEP (cyan triangles) and with the MPPS (grey squares). The values are displayed as deviations from a reference value, which is the corresponding IRMS measurement performed at the CEP. The three first samples extracted with the MPPS showed a significant isotopic fractionation in the recovered  $\text{CO}_2$  fraction, with an enrichment in  $^{13}\text{C}$  of up to 20‰. The fractionation was not caused by an incomplete scrubbing of  $\text{CO}_2$ , as the “Russian doll” trap has been previously tested and shows no significant  $\text{CO}_2$  breakthrough (see Chapter 2). Furthermore, Brenninkmeijer and Röckmann (1996) noticed that an incomplete trapping in this type of traps leads to a systematic isotopic depletion in  $^{13}\text{C}$ . During the early optimization tests of

CO<sub>2</sub> extraction with the MPPS, the recovery yield was very low (< 5%). It was attributed to the combination of an incomplete desorption of CO<sub>2</sub> from the three glass fiber thimbles nested in the inner part of the trap, and a substantial amount of air remaining in the line during the transfer of CO<sub>2</sub> from the trap to the flask. Although the three <sup>13</sup>C-enriched samples shown in Figure 3.10b were recovered using this poor technique, the isotopic enrichment did not happen during the transfer of CO<sub>2</sub> to the flask. Indeed, the CO<sub>2</sub> desorption from the glass fiber thimbles and the diffusion of CO<sub>2</sub> from the trap to the flask would both discriminate against the heavy isotopes, and therefore lead to a recovered fraction depleted in <sup>13</sup>C (Zeebe and Wolf-Gladrow, 2001). In fact, the CO<sub>2</sub> amounts recovered for these three samples were so small that they resulted in the graphitization of only 100–200 µg C. Significant <sup>13</sup>C enrichments of up to 20‰ in the graphitization process of small sample masses (< 400 µg C) have been already reported, which were attributed to an incomplete graphitization at low pressures (Alderliesten et al., 1997; van der Borg et al., 1997). The isotopic fractionation linked to the very poor recovery of CO<sub>2</sub> was solved by heating the trap to 90 °C, to fully desorb CO<sub>2</sub> from the glass fiber thimbles prior to the cryogenic transfer of CO<sub>2</sub> to the flask. Since then, the CO<sub>2</sub> samples extracted with the MPPS do not display any significant isotopic fractionation (see Figure 3.10b).

A contamination during the CO<sub>2</sub> extraction procedure cannot be excluded, although the glass fiber thimbles from the trap were thoroughly cleaned before and after each sample extraction, by heating the trap to 95 °C and flushing it with nitrogen. However, the air samples were first dried by means of a trap filled with calcium sulfate (drierite), which usage is questionable for the recovery of CO<sub>2</sub> as this type of drying agent may absorb CO<sub>2</sub> and lead to cross contamination between successive CO<sub>2</sub> extractions (Elia et al., 1986).

Finally, the samples extracted at the CEP and with the MPPS were usually not measured in the same magazine with the AMS. Thus, they did not undergo the same blank subtraction, standard normalization and correction for isotope fractionation. The day-to-day variability of the <sup>14</sup>C results obtained with the MICADAS was estimated to contribute to an additional uncertainty of 1.5‰ (Wacker et al., 2010a; Szidat et al., 2014). Hence, the deviations seen in Figure 3.10a are likely not explained by the day-to-day variability of the <sup>14</sup>C results, although the latter might slightly reduce the comparability of both extraction methods.

In summary, the discrepancies observed in Figure 3.10a are still not fully understood, and contamination tests will be made for the traps, the pumps and the bags. However, the intra-comparability of samples extracted with the MPPS is probably significantly better than the deviations between the two extraction methods. For example, if a contamination during the extraction procedure induces a bias towards lower  $\Delta^{14}\text{CO}_2$  results, as seen for the last sixteen samples extracted with the MPPS (see Figure 3.10a), the samples would be affected similarly as long as the procedure is kept the same.

### 3.4.2.2 $^{14}\text{CO}_2$ vs $^{14}\text{CH}_4$

The  $\Delta^{14}\text{CO}_2$  results of the biweekly point samplings at the three sites are considerably different from the  $\Delta^{14}\text{CH}_4$  results (see Figure 3.3 and Figure 3.2). The highest  $\Delta^{14}\text{CO}_2$  values were usually measured at Jungfrauoch, as this remote site is only weakly influenced by local and regional sources (Levin et al., 2010). Although the  $\Delta^{14}\text{CO}_2$  values at Jungfrauoch were significantly more stable than at Bern and Beromünster, some variations were observed as  $\Delta^{14}\text{CO}_2$  ranged between  $-9.4$  and  $+8.7\text{‰}$  in 2019, part of which stemming from natural variations, which will be described in section 3.4.4.1 together with the discussion of the long-term  $^{14}\text{CO}_2$  measurements at Beromünster. The unexplained part of the variability is imputed to the problems observed for the  $\text{CO}_2$  extraction with the MPPS, which were described in the previous section.

The  $^{14}\text{CO}_2$  depletions in the air samples collected at Beromünster and Bern with respect to the corresponding values at the background site Jungfrauoch are attributed to local and regional fossil fuel emissions, as biogenic emissions of  $\text{CO}_2$  have a  $^{14}\text{C}$  content close to atmospheric  $\text{CO}_2$  (Levin et al., 2003). The estimations of the fossil fuel  $\text{CO}_2$  component at Beromünster and Bern, which are displayed in Figure 3.6 and Figure 3.7, will be compared and discussed in sections 3.4.4.2 and 3.4.4.3.

Although GHG emissions are mainly anthropogenic in Switzerland,  $\text{CH}_4$  and  $\text{CO}_2$  do not share common sources, as most of  $\text{CH}_4$  emissions come from the agricultural sector, whereas fossil fuel emissions from the energy sector constitute the main  $\text{CO}_2$  source. In contrast, atmospheric  $^{14}\text{CH}_4$  and  $^{14}\text{CO}_2$  are both impacted by  $^{14}\text{C}$  emissions from NPPs. However, the atmospheric mole fraction of  $\text{CH}_4$  is below 2 ppm, whereas  $\text{CO}_2$  has a mole fraction over 400 ppm. Hence, for a similar  $^{14}\text{C}$  source strength, the impact of  $^{14}\text{C}$  releases from NPPs is more than 200 times larger on atmospheric  $^{14}\text{CH}_4$  than on atmospheric  $^{14}\text{CO}_2$ . The global contribution of NPPs on atmospheric  $^{14}\text{CH}_4$  and  $^{14}\text{CO}_2$  levels has been described in Chapter 1, explaining why background  $\Delta^{14}\text{CH}_4$  ( $\sim 350\text{‰}$ ) is significantly higher than background  $\Delta^{14}\text{CO}_2$  ( $\sim 0\text{‰}$ ). The difference of sensitivity of atmospheric  $^{14}\text{CH}_4$  and  $^{14}\text{CO}_2$  to NPP emissions is amplified at local and regional scales, where  $^{14}\text{C}$  discharges occasion large spatial and temporal variations of atmospheric  $^{14}\text{CH}_4$ , with some episodes of strong enhancement as reported by Eisma et al. (1994) and confirmed in this study. As an example, the samples collected at Beromünster in 2019 showed a mean  $\Delta^{14}\text{CH}_4$  enhancement of  $127\text{‰}$  compared to background values, which can be compared to the simulated mean  $\Delta^{14}\text{CO}_2$  enhancement of  $+1.6\text{‰}$  for the samples collected at Beromünster between 2013 and 2015 (Berhanu et al., 2017). However, this comparison should be taken with caution: First, because the actual mean  $\Delta^{14}\text{CH}_4$  enhancement in the samples collected at Beromünster caused by NPPs is undoubtedly larger than  $127\text{‰}$ , as biogenic and fossil  $\text{CH}_4$  sources tend to locally decrease the  $^{14}\text{C}$  content of atmospheric  $\text{CH}_4$ . Second, because the reported values stem from point measurements, which are heavily influenced by the provenance of air masses and the sporadic discharges from NPPs. With that

in mind, the values seem to lie in the order of magnitude one would expect from the respective impact of NPPs on  $^{14}\text{CH}_4$  and  $^{14}\text{CO}_2$ .

The situation is further compounded by the fact that at a sampling site,  $^{14}\text{CH}_4$  and  $^{14}\text{CO}_2$  results are usually not influenced by the same NPP, as PWRs release predominantly  $^{14}\text{CH}_4$  and BWRs vent almost exclusively  $^{14}\text{CO}_2$  (Kunz, 1985; Stenström et al., 1995). As a consequence, the  $^{14}\text{CO}_2$  enhancements simulated at Beromünster by Berhanu et al. (2017) were mainly attributed to the Mühleberg NPP, as it holds a BWR and is frequently situated upwind Beromünster (see Figure 3.1). As the Mühleberg NPP is located at only 12 km W from Bern, with the wind on the Swiss Plateau blowing regularly from SW, it can be expected that this NPP has a stronger influence on the  $^{14}\text{CO}_2$  content measured at Bern than at Beromünster. Hence, it is likely that some  $\Delta^{14}\text{CO}_2$  depletions measured at Bern were partially offset by the contribution of the Mühleberg NPP.

In contrast, atmospheric  $^{14}\text{CH}_4$  is mainly influenced by releases from NPPs holding a PWR, with the Gösgen NPP being the likely dominant source of  $^{14}\text{CH}_4$  excess at Beromünster and Bern. Although  $^{14}\text{CH}_4$  and  $^{14}\text{CO}_2$  releases do usually not originate from the same source, the highest  $\Delta^{14}\text{CH}_4$  and  $\Delta^{14}\text{CO}_2$  values measured at Bern were found in the same air sample, which was collected on June 14, 2019. According to CGER METEX, the air masses passed close to Gösgen a few hours before reaching Bern. As a result, the measured  $\Delta^{14}\text{CO}_2$  was +38.1‰, which is almost 40‰ higher than background  $\Delta^{14}\text{CO}_2$ . Considering that fossil fuel  $\text{CO}_2$  emissions at Bern contributed to a mean decrease of  $\Delta^{14}\text{CO}_2$  values of about -35‰ in 2019, it is likely that the  $^{14}\text{CO}_2$  bias imputed to the NPP was 40–120‰, which is large and prevents from any attempt to estimate the fossil fuel  $\text{CO}_2$  component at Bern on June 14. Although the Gösgen NPP might reveal at obvious culprit for the simultaneous enhancement of  $^{14}\text{CH}_4$  and  $^{14}\text{CO}_2$  observed at Bern on June 14, the reality is probably more complex. As previously explained, the impact of  $^{14}\text{C}$  releases from NPPs is more than 200 times larger on atmospheric  $^{14}\text{CH}_4$  than on  $^{14}\text{CO}_2$ , and Gösgen emits mainly  $^{14}\text{CH}_4$  as it holds a PWR. Thus, one would expect a  $\Delta^{14}\text{CH}_4$  value much higher than the measured  $\Delta^{14}\text{CH}_4$  of 632‰ to explain the  $\Delta^{14}\text{CO}_2$  enhancement observed. The concurrent increase of  $\Delta^{14}\text{CH}_4$  and  $\Delta^{14}\text{CO}_2$  recorded at Bern on June 14 might eventually have two different contributors, with the Gösgen NPP influencing  $^{14}\text{CH}_4$  and the Leibstadt NPP affecting  $^{14}\text{CO}_2$ , as the latter holds a BWR and was also situated upwind.

The discharges from NPPs affect significantly more the  $\Delta^{14}\text{CH}_4$  results, as confirmed by the measurements effectuated at the three sites in 2019. However, the measurements of June 14 at Bern confirm that NPPs can cause large biases on  $\Delta^{14}\text{CO}_2$  values as well, especially in hot spots of nuclear activities (Levin et al., 2003; Graven and Gruber, 2011; Vogel et al., 2013). The results showed that linking  $^{14}\text{C}$  sources to the  $^{14}\text{C}$  enhancements observed at a sampling site is a very challenging task, as the area of interest includes many  $^{14}\text{C}$  sources with their own release and atmospheric dispersion pattern. The impact of  $^{14}\text{C}$  emissions from Swiss NPPs on

atmospheric  $^{14}\text{CH}_4$  and  $^{14}\text{CO}_2$  will be further investigated in Chapter 4, which reports on a small study conducted in the vicinity of the Gösgen NPP in June 2019.

### 3.4.3 Diurnal variations and sampling duration

The overnight sampling at the three sites, the results of which are summarized in Figure 3.4, carried several objectives. First, to visualize how  $^{14}\text{CH}_4$  and  $^{14}\text{CO}_2$  vary along a diurnal cycle, if they show a common behavior and if the variations can be associated to diurnal variations of sources and vertical mixing processes. Second, to assess if the sampling time is critical for the biweekly collection of samples at each site. Finally, these results are used as a basis for a comparison between point sampling and time-integrated sampling techniques.

First and foremost, one should keep in mind that the diurnal cycle observed in Figure 3.4 is not representative of mean daily variations at the three sites, as the results are based on a single overnight measurement conducted between March 20 and March 21, 2019. Although 3–4 air samples can be extracted within a working day with the MPPS, radiocarbon measurements of  $\text{CH}_4$  and  $\text{CO}_2$  remain time consuming and expensive, which reduces the possibility to measure  $^{14}\text{CH}_4$  and  $^{14}\text{CO}_2$  with a high temporal resolution over long periods. Thus, several parameters had probably a large impact on the values measured during the two days: First, the meteorological conditions, mainly the wind speed and direction (Eisma et al., 1995). Second, the period of the year, influencing the strength of vertical mixing and the magnitude of individual sources of  $\text{CH}_4$  and  $\text{CO}_2$  (Levin et al., 2008; Bamberger et al., 2014; Satar et al., 2016). Third, eventual releases of  $^{14}\text{C}$  from NPPs, which are very variable in time (Kunz, 1985; Stenström et al., 1995). At Jungfraujoch, the wind was blowing from the south and intensified during the night. At Bern and Beromünster, the temperature went below 0 °C at night and there was a moderate wind coming from the north.

The general shape of the  $\Delta^{14}\text{CH}_4$  and  $\Delta^{14}\text{CO}_2$  results of the overnight sampling reflects well what has been observed at the three sites in 2019, with Jungfraujoch air displaying the lowest  $\Delta^{14}\text{CH}_4$  and the highest  $\Delta^{14}\text{CO}_2$ . There, both signals remained relatively stable throughout the diurnal cycle, which is what was expected for the sampling of free tropospheric air. However, the situation might have been different if the wind would have been strongly blowing from the north, as Jungfraujoch might have experienced an orographic lift of polluted air masses from the Swiss Plateau (Collaud Coen et al., 2011).

At Beromünster, a diurnal cycle was clearly visible for  $\text{CH}_4$  and  $\text{CO}_2$  mole fractions, with a maximum late morning and a minimum late afternoon (see Figure 3.11a). These diurnal variations, which are usually more pronounced in summer than in winter at Beromünster, are largely influenced by the strength of the vertical mixing before noon (Satar et al., 2016; Berhanu et al., 2017).  $\text{CH}_4$  and  $\text{CO}_2$  accumulate at night due to local and regional emissions, with a peak in the morning before a decrease caused by a convective mixing and an additional uptake of  $\text{CO}_2$  with the onset of photosynthesis. However, the  $\text{CH}_4$  variations were not driving

the  $\Delta^{14}\text{CH}_4$  values observed, as Figure 3.11b indicates no correlation between them. As shown in section 3.4.1.2, a relatively small variation of  $\text{CH}_4$  due to biogenic emissions should have a rather weak impact on the measured  $\Delta^{14}\text{CH}_4$  values, with expected variations in the range of 10–20‰ (see Figure 3.9). Therefore, the fluctuations of  $\Delta^{14}\text{CH}_4$  observed in Figure 3.4a are likely the result of temporal variations in the contribution of  $^{14}\text{CH}_4$  from NPPs. Conversely, the Keeling plot from Figure 3.11c reveals the presence of a fossil fuel  $\text{CO}_2$  source at Beromünster, as higher  $\text{CO}_2$  mole fractions were associated with lower  $^{14}\text{CO}_2$  contents. However, the rather low coefficient of determination ( $R^2 = 0.64$ ) and the intercept of  $-458\text{‰}$  ( $-1000\text{‰}$  for a pure fossil source) indicate that some respiration fluxes were also contributing to the  $\text{CO}_2$  fluctuations (Berhanu et al., 2017).

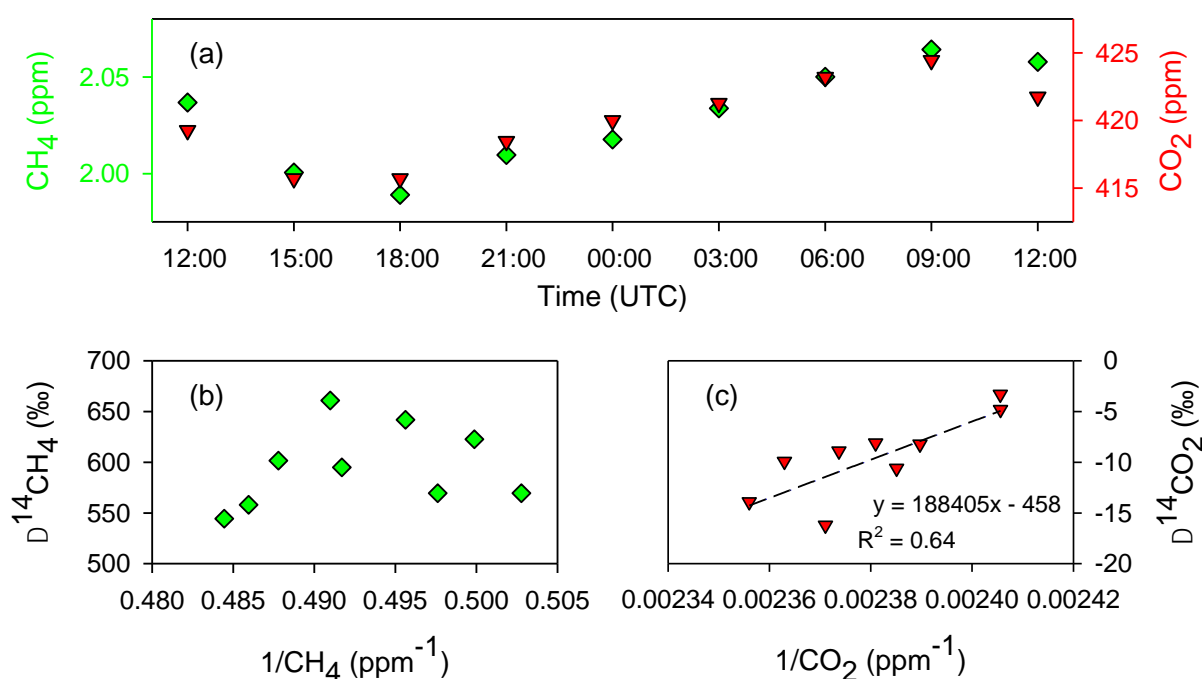


Figure 3.11 Diurnal variations of the concentrations and  $^{14}\text{C}$  contents of  $\text{CH}_4$  and  $\text{CO}_2$  at Beromünster during the overnight sampling from March 20 to March 21, 2019. (a)  $\text{CH}_4$  and  $\text{CO}_2$  mole fractions measured at the highest inlet during each sample collection. (b) Keeling plot of  $\Delta^{14}\text{CH}_4$ . (c) Keeling plot of  $\Delta^{14}\text{CO}_2$ . The temporal evolutions of  $\Delta^{14}\text{CH}_4$  and  $\Delta^{14}\text{CO}_2$  are shown in Figure 3.4.

Similarly to what has been observed at Beromünster, the  $\Delta^{14}\text{CH}_4$  signal at Bern did not reveal a clear diurnal cycle. However, the  $\text{CH}_4$  mole fractions inferred from the amounts of  $\text{CH}_4$  extracted indicated that  $\text{CH}_4$  was almost 15% higher early morning (06:00 UTC) than in the afternoon. Thus, the  $\text{CH}_4$  excess in the morning was probably not dominantly fossil, as 15% added fossil  $\text{CH}_4$  would have decreased the  $\Delta^{14}\text{CH}_4$  value by  $\sim 150\text{‰}$ . Unfortunately, the superposed  $\Delta^{14}\text{CH}_4$  fluctuations imputed to the contribution from NPPs do not allow an estimation of  $\text{CH}_{4\text{ff}}$  and  $\text{CH}_{4\text{bio}}$ . Unlike the  $\Delta^{14}\text{CH}_4$  results, the  $\Delta^{14}\text{CO}_2$  values measured at Bern showed a clear diurnal cycle, with observed depletions early morning and late afternoon

(see Figure 3.4b). Such diurnal cycles, which are commonly observed in urban areas, are mainly attributed to fossil fuel CO<sub>2</sub> emissions from domestic heating and road traffic (Kuc et al., 2003; Turnbull et al., 2015). Although the lack of a direct measurement of CO<sub>2</sub> mole fraction does not allow an apportionment of local CO<sub>2</sub> sources at Bern, the meteorological data and the typical emission patterns in urban areas allow a qualitative description of the diurnal evolution of atmospheric CO<sub>2</sub>. Emissions accumulated close to the surface during the night and the early morning, as the wind was weak and the temperature was below 0 °C, which created an inversion layer hindering the dispersion of pollutants. In the morning, an enhanced convective mixing and the rise of the wind caused a decrease of CO<sub>2</sub> mole fractions and a subsequent increase of  $\Delta^{14}\text{CO}_2$ . The smaller  $\Delta^{14}\text{CO}_2$  dip late afternoon was likely related to an augmentation of the road traffic (Lopez et al., 2013).

In summary, the overnight sampling showed that NPPs cause some temporal fluctuations of  $\Delta^{14}\text{CH}_4$  on a daily basis, although the amplitude of the fluctuations was significantly lower than the large variations observed in the biweekly collected samples (see Figure 3.2). Yet, the superposed fluctuations hampered an estimation of CH<sub>4ff</sub>, which was probably not very large at Beromünster and Bern, as fossil CH<sub>4</sub> emissions are well constrained in Switzerland (Hiller et al., 2014). As the overnight sampling was conducted a single time, potential larger temporal variations of the input from NPPs cannot be excluded as well. In contrast, the rather low influence of NPPs on <sup>14</sup>CO<sub>2</sub> levels allowed the distinction of clear  $\Delta^{14}\text{CO}_2$  diurnal cycles, especially in urban areas where fossil fuel emissions are large, with daily variations over 70‰ at Bern.

“Point sampling” (or grab sampling) refers to the collection of an air sample in a relatively short period, typically less than an hour, which is a technique widely used for atmospheric  $\Delta^{14}\text{CH}_4$  and  $\Delta^{14}\text{CO}_2$  analyses (e.g. Townsend-Small et al., 2012; Lopez et al., 2013; Berhanu et al., 2017). In contrast, “integrated sampling” designates the collection of air samples over long periods (typically days to weeks), which is a method frequently used for the monitoring of  $\Delta^{14}\text{CO}_2$  at background sites (Levin et al., 1985; Turnbull et al., 2017) and in some polluted sites such as Heidelberg (Levin et al., 1980; Gamnitzer et al., 2006). The primary reason why biweekly point samplings were used in the present study was practical: Jungfraujoch and Beromünster are not easily accessible, and important logistics would be required to install a reliable sampling system allowing the collection of air samples over a long period. Fortunately, point samplings carry some interesting advantages. As the signals are not averaged over long periods, the <sup>14</sup>CH<sub>4</sub> and <sup>14</sup>CO<sub>2</sub> values obtained are more representative of the potential variations of <sup>14</sup>CH<sub>4</sub> and <sup>14</sup>CO<sub>2</sub> at a specific site, in particular extreme values caused by sporadic <sup>14</sup>C releases from NPPs. For example, the <sup>14</sup>CH<sub>4</sub> values measured at Beromünster in 2018–2019 indicate that  $\Delta^{14}\text{CH}_4$  results of a field campaign in an area sensitive to discharges from NPPs should be taken with caution, as the results will highly depend on the specific contribution of NPPs during the sample collection. Moreover, the overnight results confirmed that point samplings should give the potential to track the temporal evolution of the

contribution of fossil and biogenic sources of CH<sub>4</sub> and CO<sub>2</sub> along a day, as long as the contribution of NPPs does not hide the desired signal. However, the aforementioned advantages of the point sampling technique are also drawbacks. Indeed, the biweekly and overnight samplings revealed that the measured  $\Delta^{14}\text{CH}_4$  and  $\Delta^{14}\text{CO}_2$  values were highly sensitive to the sampling time, the meteorological conditions, and the specific contribution from NPPs during the sample collection. For these reasons, integrated samples give a better representation of mean contributions and seasonal trends, and they suffer much less from temporal variations, such as fluctuations in the contribution from NPPs or diurnal cycles (Vogel et al., 2010).

In conclusion, a combination of both types of sample collection might provide complementary information (Vogel et al., 2010). The stable biweekly results from Jungfraujoch demonstrate that point samplings at background sites are probably sufficient, as long as the sampling time is wisely chosen to ensure that free tropospheric air is collected. In contrast, weekly or two-weekly integrated samplings are often a better choice at polluted sites, as they allow obtaining more representative results, which will less suffer from specific sampling conditions and the choice of sampling time. Moreover, integrated samples in areas where  $\Delta^{14}\text{CH}_4$  results are highly influenced by <sup>14</sup>C releases from NPPs should deliver valuable information concerning the average enhancement attributed to nuclear activities, which might be used to better constrain simulations. However, the overnight measurements showed that averaging  $\Delta^{14}\text{CH}_4$  and  $\Delta^{14}\text{CO}_2$  over time would considerably dampen the magnitude of the useful signal, as a significant part of the day was associated with rather low CO<sub>2</sub> and CH<sub>4</sub> excesses, and subsequent small  $\Delta^{14}\text{CH}_4$  and  $\Delta^{14}\text{CO}_2$  depletions. Integrating over time would therefore significantly decrease the sensitivity of the <sup>14</sup>C source apportionment method, in particular the achievable precision of the CH<sub>4</sub> fossil fraction ( $\phi_{\text{ff}}$ ) estimation (see Figure 3.9). Hence, additional point samplings during pollution peaks remain beneficial, as they should provide a good estimate of the relative contribution of fossil and biogenic sources during these events.

### 3.4.4 Long-term CO<sub>2ff</sub> at Beromünster – comparisons with an urban area

#### 3.4.4.1 The paramount choice of background $\Delta^{14}\text{CO}_2$ values

When small corrections for biases are neglected, Equation 3.4 indicates that the magnitude of the fossil fuel CO<sub>2</sub> component (CO<sub>2ff</sub>) is directly proportional to the difference between  $\Delta^{14}\text{CO}_{2\text{meas}}$  and  $\Delta^{14}\text{CO}_{2\text{bg}}$ . Thus, the choice of a corresponding background value for each  $\Delta^{14}\text{CO}_2$  measurement at Beromünster is an important step, as it could lead to significant biases if not wisely chosen. Figure 3.12 displays the monthly means of  $\Delta^{14}\text{CO}_2$  measured at Jungfraujoch (black circles). Today, the main driver of the long-term downward trend is the gradual dilution of atmospheric <sup>14</sup>CO<sub>2</sub> by the anthropogenic input of fossil fuel CO<sub>2</sub> since the beginning of the industrial revolution (Levin et al., 2008, 2010). The trend is modulated by an inter-annual variability of the <sup>14</sup>C production, which is mainly driven by the activity of the sun (Stuiver and Braziunas, 1998; Levin et al., 2010). Finally, the visible seasonal variations

are mainly due to stratosphere-troposphere exchanges, which are detailed by Naegler and Levin (2006).

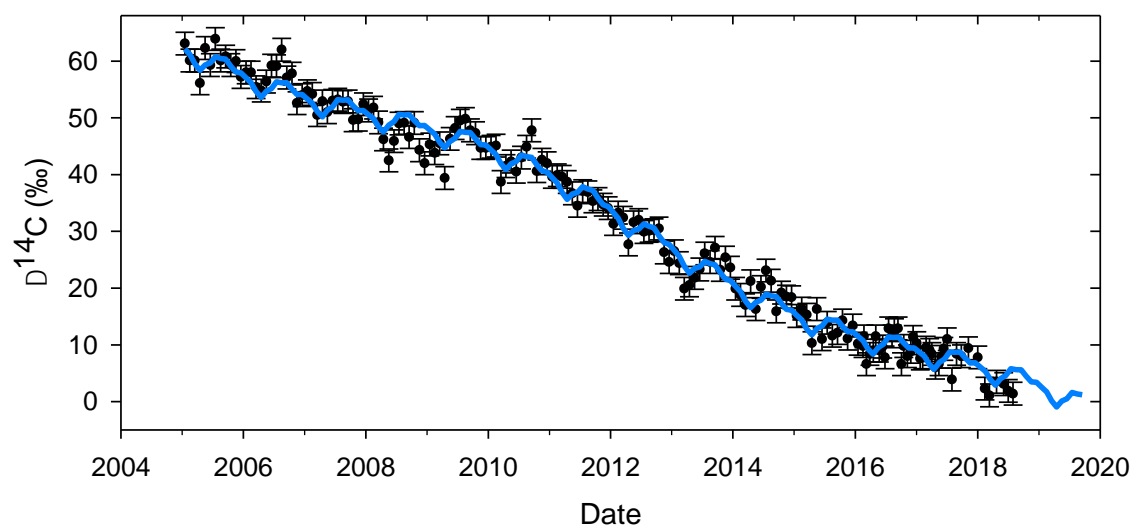


Figure 3.12 Black circles: Monthly means of two-weekly integrated  $\Delta^{14}\text{CO}_2$  at Jungfraujoch, including 2‰ measurement uncertainties ( $1\sigma$ ). Sources: Hammer and Levin (2017) and (ICOS RI, 2019). Blue curve: 3-components harmonic fit, including a linear trend ( $R^2 \approx 0.98$ ), a seasonal cycle and a 9-year solar cycle. The fit has an RMSE of 2.1‰. See text for details.

Although we have been measuring  $\Delta^{14}\text{CO}_2$  every second week at Jungfraujoch since December 2018, these results are not included in the dataset of background values, to preserve the consistency of the series as our results consisted of point measurements and suffered from the problems described in section 3.4.2.1. Thus, the  $\Delta^{14}\text{CO}_2$  values at Jungfraujoch were only available until July 2018, and it was necessary to extrapolate the dataset to get background reference values for the period August 2018 – July 2019. To mitigate possible biases when extrapolating  $\Delta^{14}\text{CO}_2$  values, it was decided to construct a model that fits the entire period 2005–2019, solely driven by three components based on the physical processes aforementioned (see blue curve in Figure 3.5 and Figure 3.12):

- **Linear trend:** the long-term trend of  $\Delta^{14}\text{CO}_2$  at Jungfraujoch for the period 2005–2018 is well described by a linear downward trend of  $-4.6\text{‰}$  per year ( $R^2 \approx 0.98$ ).
- **Inter-annual variability:** the residuals of the linear trend were used to detect an inter-annual variability, with a peak-to-peak amplitude of 6‰ and a period of 9 years. The amplitude, period and phase of this variability match well the expected variations of  $\Delta^{14}\text{CO}_2$  imputed to solar cycles, and this component was modeled by an exact sinusoidal function (Levin et al., 2010).
- **Seasonal cycle:** the seasonal component was calculated from the average detrended monthly variations observed between 2005 and 2018, resulting in a peak-to-peak amplitude of 4.2‰, a minimum in April and a maximum in September. The calculated

parameters of this component are consistent with the values observed by Levin et al. (2010), who found a peak-to-trough amplitude of 5‰ for the period 1995–2005.

The 3-component model has a root mean square error (RMSE) of 2.1‰, which is comparable to the  $1\sigma$  uncertainty of a single measurement (2‰). Only two samples from 2008 do not lie within a  $3\sigma$  range around the model, and the performance of the model is similar to the harmonic fit usually applied to Jungfraujoch background  $\Delta^{14}\text{CO}_2$  measurements for the estimation of  $\text{CO}_{2\text{ff}}$  (Levin and Kromer, 2004; Levin et al., 2008).

The leaf samples collected each year show a mean  $\Delta^{14}\text{CO}_2$  enhancement of 2.3‰ compared to the corresponding mean values at Jungfraujoch over the growing season. The small difference can be imputed to continental gradients of atmospheric  $\Delta^{14}\text{CO}_2$ , as Jungfraujoch is more remote from the sources of  $^{14}\text{C}$  (Graven and Gruber, 2011). As a comparison, the simulated mean enhancement at Beromünster caused by the NPPs was 1.6‰ for the period 2013–2015 (Berhanu et al., 2017). However, these biases remain very small and indicate that the influence of fossil fuel  $\text{CO}_2$  emissions and NPP  $^{14}\text{C}$  releases are not very significant at the leaf samples collection sites.

#### 3.4.4.2 $\text{CO}_{2\text{ff}}$ at Beromünster

The updated long-term trend of  $\Delta^{14}\text{CO}_2$  measurements at Beromünster revealed a mean difference of  $-6.5\text{‰}$  between Beromünster and the background site Jungfraujoch for the period 2013–2019, which is caused by regional and local emissions of fossil fuel  $\text{CO}_2$  (see Figure 3.5). There was no significant change in the trend after the period 2013–2015 analyzed by Berhanu et al. (2017), which showed a mean depletion of  $-6.3\text{‰}$ . The small increase of the difference between Beromünster and Jungfraujoch is solely due to the period mid-2018 to mid-2019, where no actual  $\Delta^{14}\text{CO}_2$  measurements were available at Jungfraujoch. It is therefore possible that the model used to represent background values was slightly overestimating actual Jungfraujoch  $\Delta^{14}\text{CO}_2$  values over this period. It should be mentioned that the calculated mean difference for the period 2013–2015 is significantly lower than the value of  $-9.9\text{‰}$  reported by Berhanu et al. (2017), the reason of which remains unclear and will need further investigation. The discrepancy cannot be explained by the choice of corresponding background  $\Delta^{14}\text{CO}_2$  values for each measurement at Beromünster, as it could affect individual differences but should not significantly alter the mean calculated depletion.

Owing to the absence of strong fossil fuel sources in the vicinity of the sampling site, the mean fossil fuel  $\text{CO}_2$  contribution at Beromünster was only 3.7 ppm between 2013 and 2019, which is less than 1% of excess  $\text{CO}_2$  of a fossil origin (see Figure 3.6b). This contribution is slightly lower than the mean  $\text{CO}_{2\text{ff}}$  of 4.3 ppm reported by Berhanu et al. (2017), because  $\text{CO}_{2\text{ff}}$  scales with the difference between background  $\Delta^{14}\text{CO}_2$  and the values measured at the site. The contribution from fossil fuel  $\text{CO}_2$  emissions was usually higher in winter, due to the combination of a weak vertical mixing and enhanced anthropogenic fossil fuel  $\text{CO}_2$  emissions

(Satar et al., 2016; Berhanu et al., 2017). During the cold season, a few spikes of CO<sub>2</sub> were observed, with a CO<sub>2</sub> mole fraction reaching 458 ppm on January 26, 2017 (see Figure 3.6a). This event was associated with a high CO<sub>2ff</sub> of 23.3 ppm, which can be explained by large fossil fuel CO<sub>2</sub> emissions as the sampling took place during a particularly cold day (−6 °C).

The mean  $\beta_{NPP}$  correction of 1.6‰ applied to the measured  $\Delta^{14}\text{CO}_2$  values at Beromünster corresponds to a typical bias of 0.7 ppm in the calculation of CO<sub>2ff</sub> (see Equation 3.4). Thus, if not accounted for, the NPPs contribute on average to an underestimation of CO<sub>2ff</sub> of 20% at Beromünster. However, conversely to Berhanu et al. (2017) we applied a mean correction for the contribution of NPPs, as simulations of their impact during each sample collection were not available. Although it should not significantly affect the calculation of the mean CO<sub>2ff</sub>, individual CO<sub>2ff</sub> results could be significantly biased. At worst, a correction of 1.6‰ instead of 8.4‰ (largest offset simulated by Berhanu et al. (2017)) would lead to an underestimation of CO<sub>2ff</sub> of about 3 ppm. Hence, applying a constant correction explains the few samples associated with slightly negative CO<sub>2ff</sub> values (see Figure 3.6b), for which the actual contribution from NPPs to the measured  $\Delta^{14}\text{CO}_2$  values was likely underestimated.

The biogenic CO<sub>2</sub> component (CO<sub>2bio</sub>) at Beromünster showed a large variability, with usually positive values in wintertime associated with respiration fluxes, and lower or negative values in summertime due to CO<sub>2</sub> uptake by photosynthesis (Satar et al., 2016; Berhanu et al., 2017). However, it should be noted that the values reported here do not consist of daily averages, as the biweekly air samplings lasted typically only 10–15 min. Thus, a substantial part of the variations can be imputed to the sensitivity of CO<sub>2bio</sub> and CO<sub>2ff</sub> to the variations of the meteorological conditions and the sampling time (between 9:00 and 13:00 UTC). The diurnal cycles of CO<sub>2</sub> were confirmed by the overnight sampling reported in Figure 3.11a, with a gradual accumulation of CO<sub>2</sub> in the morning, followed by a decrease in the afternoon due to vertical mixing and photosynthesis uptake. The cycles are usually more pronounced in summertime, explaining why a sampling in the afternoon instead of the morning could result in much lower values for CO<sub>2ff</sub> and CO<sub>2bio</sub> (Satar et al., 2016; Berhanu et al., 2017).

#### 3.4.4.3 CO<sub>2ff</sub> at Bern — comparisons with Beromünster

As no corrections for the impact of NPPs were applied for the calculation of CO<sub>2ff</sub> at Bern, the results reported in Figure 3.7 are minimum values, which likely provide an underestimation of the fossil fuel component at Bern during the biweekly air samplings. Indeed,  $\Delta^{14}\text{CO}_2$  measured at Bern on June 14 was very high (38.0 ‰), which corresponds to a CO<sub>2ff</sub> value of −16.3 ppm: this example shows that the <sup>14</sup>CO<sub>2</sub> content measured at Bern was probably enhanced by <sup>14</sup>CO<sub>2</sub> releases from NPPs, which were not accounted for when calculating CO<sub>2ff</sub> at Bern. This issue has already been addressed by Vogel et al. (2013), who noted that local <sup>14</sup>CO<sub>2</sub> emissions from NPPs in hotspots of nuclear activities may cause significant errors in the calculated fossil fuel derived CO<sub>2</sub>.

With a mean value of 15.2 ppm for the 19 air samples collected in 2019, CO<sub>2ff</sub> was significantly higher at Bern than at Beromünster (3.7 ppm), which is not surprising as urban areas contribute to almost 75% of global fossil fuel CO<sub>2</sub> emissions (Turnbull et al., 2019). However, the comparison with Beromünster is not straightforward, as CO<sub>2ff</sub> is only available for the period February to August 2019, which is not representative of a full year. In particular, CO<sub>2ff</sub> is expected to be significantly higher in urban areas during wintertime, as a combined consequence of enhanced domestic heating and reduced vertical mixing (Levin et al., 2008; Mitchell et al., 2018). The latter effect should have a strong impact for the comparison of CO<sub>2ff</sub> at Bern and Beromünster, as the sampling inlet at Bern is close to the ground, where CO<sub>2</sub> accumulates, whereas the sampling takes place at the top of a tower at Beromünster.

By virtue of its particular situation, CO<sub>2</sub> measured at Beromünster is influenced by emissions from the entire Swiss Plateau and has a rather weak contribution from local sources (Oney et al., 2015; Satar et al., 2016). Conversely, the sampling site at Bern catches a local signal with large diurnal variations, as indicated by the  $\Delta^{14}\text{CO}_2$  results of the overnight sampling (see Figure 3.4b). While the variations of CO<sub>2ff</sub> in Figure 3.7b are partially caused by the respective meteorological conditions and strength of local CO<sub>2</sub> sources, a significant part of the scatter is probably due to variations in the sampling time. Indeed, the CO<sub>2ff</sub> value reported in Figure 3.7b for the biweekly sampling at Bern on March 21 is 41.8 ppm, which corresponds to the sample collected between 7:00 and 8:00 local time during the overnight sampling. This value is the largest measured at Bern in 2019, which is probably a consequence of the very cold night and strong accumulation of pollutants close to the ground. However, the mean CO<sub>2ff</sub> calculated from the  $\Delta^{14}\text{CO}_2$  results of the overnight sampling is only 16.6 ppm when averaged over the entire diurnal cycle. These diurnal fluctuations of CO<sub>2ff</sub> in cities have been observed in other studies, highlighting that the sampling time is of paramount importance in an urban area (Gamnitzer et al., 2006; Turnbull et al., 2015). As pointed out by Vogel et al. (2010), only integrated samples can provide the true mean CO<sub>2ff</sub> at a site, which is particularly relevant in urban areas where daily fluctuations are more pronounced.

In a nutshell, the mean CO<sub>2ff</sub> calculated at Beromünster (3.7 ppm) and Bern (15.2 ppm) do probably not represent the true mean CO<sub>2ff</sub> at the respective sites for the following reasons: (1) the daily variability of CO<sub>2ff</sub>, which cannot be accounted for when sampling during only 10–60 minutes; and (2) the inter-daily variability of CO<sub>2ff</sub>, which challenges the representativeness of biweekly results. As the samples were usually collected in the morning, when CO<sub>2ff</sub> might be higher than daily averages, we suspect point (1) to cause an overestimation of the true mean CO<sub>2ff</sub> at a site, especially for the sampling site in Bern. Point (2) should not lead to a significant bias for the mean CO<sub>2ff</sub> at Beromünster, as the dataset covers 6 years of measurements. However, it reduces the confidence in the mean value at Bern, which is based on only 18 measurement points. With that in mind, our results are similar to the mean CO<sub>2ff</sub> values estimated by Levin et al. (2008) on the basis of integrated  $\Delta^{14}\text{CO}_2$  samples from two sampling sites in Germany. They reported a mean CO<sub>2ff</sub> of 1.31 ppm at

Schauinsland, a low polluted observatory situated in the Black Forrest, and a mean CO<sub>2ff</sub> of 10.96 ppm at Heidelberg, situated in a polluted region of the Rhine valley. When comparing with a larger city such as Paris, Vogel et al. (2013) estimated an average CO<sub>2ff</sub> of 20 ppm in February 2010, which is probably significantly higher than the true mean value at Bern.

Although the <sup>14</sup>C method constitutes the most straightforward technique to estimate CO<sub>2ff</sub> (Geels et al., 2007; Levin et al., 2008) it remains a time-consuming and expensive method, which limits the spatial and temporal resolutions achievable. In particular, we showed that the sampling time is of paramount importance, and that minimizing this factor could lead to misinterpretations. To overcome these drawbacks, some authors use measurements of SF<sub>6</sub> or CO as tracers for fossil fuel CO<sub>2</sub>, as they usually share a common anthropogenic source (Gamnitzer et al., 2006; Turnbull et al., 2006, 2015; Berhanu et al., 2017). Combined with regular <sup>14</sup>CO<sub>2</sub> analyses at a site, they allow a continuous monitoring of CO<sub>2ff</sub>. However, these tracers give rise to significant uncertainties in the estimation of CO<sub>2ff</sub>, as they are not uniquely co-emitted with fossil fuel CO<sub>2</sub> (Gamnitzer et al., 2006). A combination of point samplings, integrated samples and a wise use of tracers should provide the most useful information.

### 3.5 Conclusions and outlook

The suitability of the new methane preconcentration and purification setup for atmospheric <sup>14</sup>CH<sub>4</sub> and <sup>14</sup>CO<sub>2</sub> analyses has been demonstrated through the preparation and <sup>14</sup>C measurement of air samples collected in Switzerland. The first field samplings started in August 2018 and since January 2019, atmospheric air samples were biweekly collected and analyzed at three strategic sites in Switzerland: Beromünster (rural area), Bern (urban area) and Jungfrauoch (continental background).

We measured a mean  $\Delta^{14}\text{CH}_4$  of  $354 \pm 15\text{‰}$  at Jungfrauoch, which allowed addressing the lack of published values for background atmospheric  $\Delta^{14}\text{CH}_4$  since the early 2000s. The stability of the results confirmed the suitability of Jungfrauoch as a background continental reference for source apportionment of atmospheric <sup>14</sup>CH<sub>4</sub>, and the measured mean background  $\Delta^{14}\text{CH}_4$  is in very good agreement with the value of 350‰ inferred by Graven et al. (2019). Today, atmospheric CH<sub>4</sub> has a higher <sup>14</sup>C content than all the natural sources of CH<sub>4</sub>, which are responsible for local and regional depletions of  $\Delta^{14}\text{CH}_4$ . However, fossil and biogenic sources can still be differentiated by means of the <sup>14</sup>C method, as their respective dilution rates of atmospheric  $\Delta^{14}\text{CH}_4$  are very dissimilar. Unfortunately, the results from Beromünster and Bern showed that atmospheric  $\Delta^{14}\text{CH}_4$  is strongly impacted by <sup>14</sup>CH<sub>4</sub> releases from the nuclear industry, which is extensively developed in Europe. As a consequence, the considerable variability of  $\Delta^{14}\text{CH}_4$  at both sites was mainly driven by the variable contribution of NPPs, which hindered any attempt of CH<sub>4</sub> source apportionment.

The situation was quite different for atmospheric  $\Delta^{14}\text{CO}_2$ , which has been decreasing at a rate of about -3.5‰ per year between 2013 and 2019 at Jungfrauoch and Beromünster, as the

consequence of global anthropogenic fossil fuel CO<sub>2</sub> emissions. The <sup>14</sup>CO<sub>2</sub> results were considerably less affected by <sup>14</sup>C releases from NPPs, because CO<sub>2</sub> has a much larger atmospheric mole fraction than CH<sub>4</sub>. Hence, the biweekly point samplings allowed an estimation of CO<sub>2ff</sub> at Beromünster and Bern. The results revealed that the mean CO<sub>2ff</sub> did not noticeably change at Beromünster since 2013, indicating that there was probably no marked evolution of local and regional fossil sources. As expected from an urban area, CO<sub>2ff</sub> was significantly larger at Bern, with pronounced diurnal variations.

Despite some uncertainties associated with the large spatio-temporal variability of CH<sub>4</sub> sources (Bamberger et al., 2014; Hiller et al., 2014), the situation is relatively simple in Switzerland as CH<sub>4</sub> emissions are dominated by the agricultural sector and fossil CH<sub>4</sub> emissions in urban areas are well mitigated (Henne et al., 2016; FOEN, 2017). Future abatement strategies of anthropogenic emissions would be most effective in regions where CH<sub>4</sub> fluxes are large, and the <sup>14</sup>C method should be effective when the relative contribution of different sources remains unknown. We showed that if the survey area is affected by strong CH<sub>4</sub> sources and the impact from NPPs is low, the MPPS should provide an unequivocal tool to apportion the fossil and biogenic CH<sub>4</sub> fractions at local and regional scales. The sampling strategy enables the access to remote areas and does not require any equipment at the sampling site, as atmospheric air samples can be collected in aluminum bags with a small membrane pump powered by a car battery.

In addition to the biweekly point samplings at the three collection sites, integrated  $\Delta^{14}\text{CH}_4$  and  $\Delta^{14}\text{CO}_2$  measurements will be soon implemented at Bern. The results should provide an estimation of the average impact of NPPs on  $\Delta^{14}\text{CH}_4$ , and an assessment of the true mean CO<sub>2ff</sub> at the site. Finally, some unexpectedly high <sup>14</sup>CH<sub>4</sub> and <sup>14</sup>CO<sub>2</sub> results questioned the validity of using constant emissions from NPPs for the simulation of their contribution during a sample collection. As an attempt to answer this question, the next chapter reports on the impact of the Gösigen NPP on <sup>14</sup>CH<sub>4</sub> and <sup>14</sup>CO<sub>2</sub> levels in its vicinity, based on a case study during a revision period.

# 4. Impact of a nuclear power plant on atmospheric $^{14}\text{CH}_4$ and $^{14}\text{CO}_2$ – a case study in Switzerland

## 4.1 Preamble

Although nuclear power plants (NPPs) are not considered as relevant sources of greenhouse gases (van der Zwaan, 2013), they represent an important source of atmospheric  $^{14}\text{C}$  (Quay et al., 1999). As a result, the emissions of  $^{14}\text{CH}_4$  from NPPs since ca 1970 overcompensate the  $^{14}\text{C}$  dilution from fossil sources and the  $^{14}\text{C}$  content of atmospheric methane is rising (Lassey et al., 2007a, 2007b). Such a strong influence on  $^{14}\text{CH}_4$  levels, when compared to the rather low impact of nuclear activities on  $^{14}\text{CO}_2$  (Levin et al., 2010; Graven and Gruber, 2011), is explained by the relatively low atmospheric mole fraction of  $\text{CH}_4$  ( $< 2$  ppm) compared to the one of  $\text{CO}_2$  ( $> 400$  ppm).  $^{14}\text{C}$  is produced in nuclear reactors where water is used as a neutron moderator and a coolant. It is an activation product of  $^{17}\text{O}$  and  $^{14}\text{N}$  in the coolant, fuel and structural material (Kunz, 1985; Yim and Caron, 2006). The most widespread reactor types are the boiling water reactor (BWR) and the pressurized water reactor (PWR). While BWRs almost exclusively emit  $^{14}\text{C}$  as  $^{14}\text{CO}_2$ , gaseous effluents in PWRs are mostly in the form of  $^{14}\text{CH}_4$  (70–95%) due to the reducing conditions in the reactor coolant (Kunz, 1985; Uchirin et al., 1997; Yim and Caron, 2006; Lister and Uchida, 2015). At local and regional scales, NPPs are strong point source emitters of  $^{14}\text{C}$  (Eisma et al., 1995). This issue is well known with respect to  $^{14}\text{CO}_2$ , and several authors include simulations of the influence of NPPs for their estimations of the regional fossil fuel component of atmospheric  $\text{CO}_2$  (Graven and Gruber, 2011; Vogel et al., 2013; Berhanu et al., 2017). As  $^{14}\text{C}$  released from NPPs is not continuously monitored, the emissions are usually estimated using emission factors (EFs), which depend on the type of reactor and provide total emissions that scale with the electrical output of the NPPs (Kunz, 1985; Hertelendi et al., 1989; Eisma et al., 1995; Zazzeri et al., 2018). Unfortunately, the use of EFs is challenging as  $^{14}\text{C}$  emissions from NPPs are known to vary significantly for two reactors of the same type, but also that the emissions are very variable in time (Eisma et al., 1994; Magnusson, 2007; Graven and Gruber, 2011; Zazzeri et al., 2018).

In the Netherlands, some atmospheric measurements of  $^{14}\text{CH}_4$  showed very high  $^{14}\text{C}$  contents, more than three times over typical background values (Eisma et al., 1994). Such large values were primarily associated with the venting of volume control tanks during normal operation periods of NPPs; however, very high  $^{14}\text{CH}_4$  levels were also reported during shutdown and maintenance periods of the reactors (Kunz, 1985; Stenström et al., 1995; Vogel et al., 2013; Zazzeri et al., 2018). Furthermore, elevated  $^{14}\text{CH}_4$  contents were reported for air masses coming from areas where no  $^{14}\text{CH}_4$  emissions were expected, emphasizing the lack of knowledge of the spatial and temporal impacts of nuclear activities on atmospheric  $^{14}\text{CH}_4$  (Eisma et al., 1995).

Although the sporadic releases of  $^{14}\text{CH}_4$  from NPPs are not dose relevant, as plants and living organisms do not fix  $\text{CH}_4$ , their local and regional contributions to atmospheric  $^{14}\text{CH}_4$  levels remain poorly known. In regions where nuclear activities are significant, a good understanding of their impact on atmospheric  $^{14}\text{CH}_4$  is crucial, if  $^{14}\text{C}$  measurements shall be used as a tool for a  $\text{CH}_4$  source apportionment, in particular to allow an estimation of the fraction of  $\text{CH}_4$  of a fossil origin (Eisma et al., 1994; Lassey et al., 2007b; Graven et al., 2019).

The biweekly  $^{14}\text{CH}_4$  measurements at Beromünster and Bern, presented in Chapter 3, showed large variations and some very high values ( $F^{14}\text{C} \approx 4.00$ ), up to three times over the background level measured at the Jungfrauoch Research Station ( $F^{14}\text{C} \approx 1.37$ ). Such a high  $^{14}\text{CH}_4$  content can only be explained by the release of  $^{14}\text{CH}_4$  from nuclear activities, as all other sources of  $\text{CH}_4$  are directly related to atmospheric  $^{14}\text{CO}_2$ , which peaked at an  $F^{14}\text{C}$  value around 2.0 in the early sixties and decreased since then (Eisma et al., 1994). The Gösigen NPP is the most plausible culprit for the high  $^{14}\text{CH}_4$  content measured at Beromünster, as it holds a PWR and is the nearest NPP to the sampling site (~25 km NW of Beromünster). In Switzerland, the Eidgenössische Nuklearsicherheitsinspektorat (ENSI) is continuously measuring the emissions from the five national NPPs, providing free access to the levels of activity of the noble gases released through the stacks (<https://www.ensi.ch/de/dokumente/document-category/emi-daten/>). In addition,  $^{14}\text{CO}_2$  in the vicinity of the NPPs is also monitored via the collection of leave samples (FOPH, 2019). However,  $^{14}\text{CH}_4$  emissions and atmospheric levels are not measured, as  $^{14}\text{CH}_4$  is not associated with radiation-related health issues.

Since NPPs are strong point sources with very variable  $^{14}\text{C}$  emissions in time, sampling air during normal operation periods is unreliable, as the release events cannot be forecasted. However, the Swiss NPPs are revised once a year. During these maintenance periods, the reactors are shut down and the volume control tanks, the containment air and the gas decay tanks are vented, leading to a discharge of the gases dissolved in the reactor coolant and stored in the gas decay tanks. The study described in this chapter was conducted during the annual maintenance of the Gösigen NPP and reports on the impact of the revision on atmospheric  $^{14}\text{CH}_4$  and  $^{14}\text{CO}_2$  in its proximity. We collected air samples near the NPP and measured the  $^{14}\text{CH}_4$  and  $^{14}\text{CO}_2$  contents to assess the impact of nuclear activities at local and regional scales. To our best knowledge, atmospheric  $^{14}\text{CH}_4$  levels in the vicinity of a NPP during a revision have never been reported before.

## 4.2 Methods

### 4.2.1 Site description

The Gösgen NPP (47°21'57" N, 7°57'56" E, 382 m a.s.l.) is located in a rural area of the Swiss Plateau, along a loop of the Aare River (see Figure 4.1). In operation since 1979, the NPP holds a PWR with a net electrical output of 1010 MW and generates about 15% of Switzerland's electricity needs (KKG, 2015; SFOE, 2019). Gaseous effluents, which mainly consist of radioactive noble gases as well as volatile iodine compounds (e.g.  $^{133}\text{Xe}$ ,  $^{85}\text{Kr}$ ,  $^{41}\text{Ar}$ ,  $^{131}\text{I}$ ) and radiocarbon ( $^{14}\text{CH}_4$ ,  $^{14}\text{CO}_2$  and some  $\text{C}_n\text{H}_m$ ), are vented through a 99 m high chimney stack. The gases are mainly formed as fission and activation products in the reactor coolant. An air circulation system leads the radionuclides to gas decay tanks packed with activated carbon, to allow time for short-lived gaseous radionuclides to decay prior to discharge (Alonso, 2012). These gas releases through the chimney stack come from pressure-relief venting and purging of the containment air, but also venting of the gas decay tanks (Kunz, 1985). The activities of aerosols, iodine and noble gases are continuously monitored in the chimney stack by the ENSI. Unfortunately,  $^{14}\text{C}$  emissions at the Gösgen NPP are not directly measured, and the ENSI provides estimates of monthly  $^{14}\text{C}$  emissions in Gösgen, based on occasional measurements performed at the Beznau NPP, which holds a similar PWR. Thus, the reported values should be taken with caution, as  $^{14}\text{C}$  emissions of NPPs may differ significantly among sites holding the same reactor type (Graven and Gruber, 2011; Vogel et al., 2013).

Similarly to Beromünster, the prevailing wind direction in Gösgen is SW and sometimes NE, channeling between the Jura mountain range and the Alps (see Chapter 3). Therefore, the gaseous effluents from the NPP are usually not directly advected to Beromünster (see Figure 4.1), although the Gösgen NPP is located rather close to the Beromünster tall tower sampling site (~25 km).

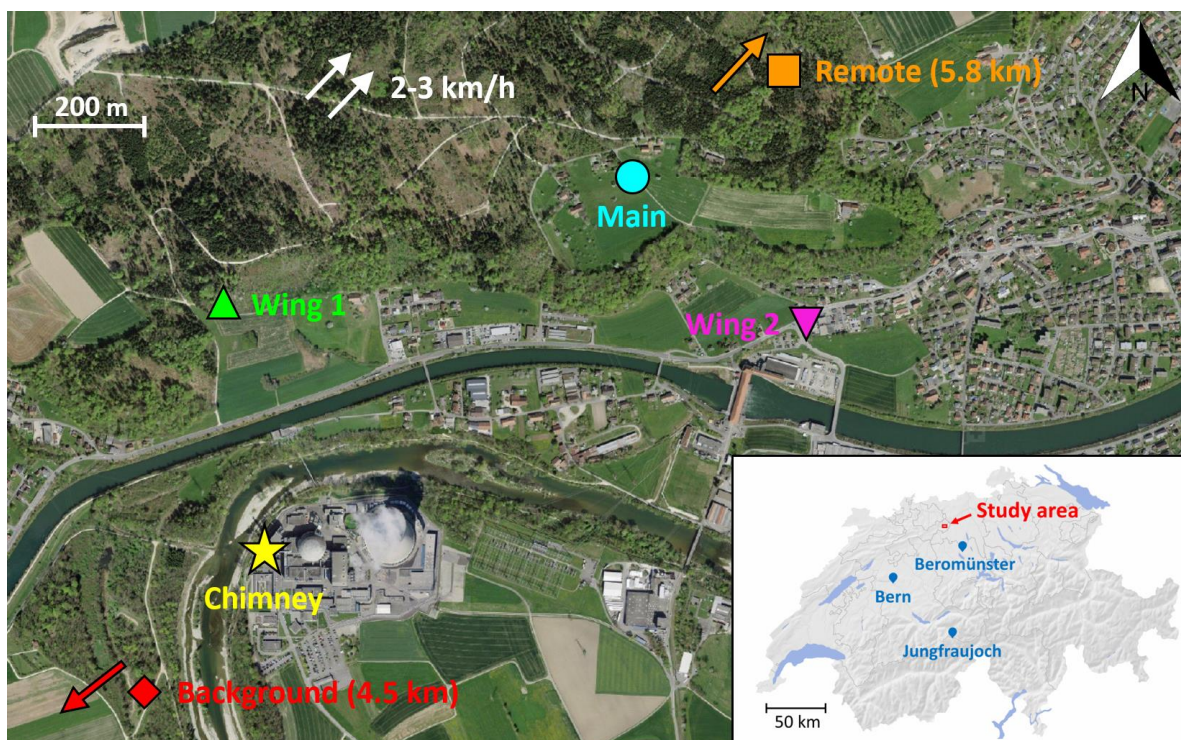


Figure 4.1 Geographical map of the study area around the Gösgen NPP, including the five sampling sites where air samples were collected on June 2, 2019 (symbols). The wind speed and direction during the study are shown (white arrows). The regular sampling sites, where atmospheric air samples are biweekly collected for  $^{14}\text{CH}_4$  and  $^{14}\text{CO}_2$  analyses (see Chapter 3), are displayed on the map of Switzerland (bottom right corner). See text below for the description of the Gösgen sampling sites. Source for the map: Google Maps.

## 4.2.2 Sampling

The revision of the Gösgen NPP took place between June 1 and June 19, 2019. The opening of the reactor cover was scheduled on June 2 at 6:30 (UTC), and most of the gaseous emissions were expected to occur within the next 8 hours<sup>2</sup>. Based on the wind forecast, which predicted a light SW wind (2–3 km/h), we collected air samples between 6:00 and 14:00 (UTC) at the following sites (see Figure 4.1):

- **“Background”**: positioned 4.5 km SW of the NPP, upwind ( $47^{\circ}20'28''$  N,  $7^{\circ}55'04''$  E, 463 m a.s.l.). Located on the edge of the woods.
- **“Main”**: positioned 1.2 km NE of the NPP, downwind ( $47^{\circ}22'24''$  N,  $7^{\circ}58'35''$  E, 460 m a.s.l.). Located on the slope of a hill facing the NPP, in an open field.
- **“Remote”**: positioned 5.8 km NE of the NPP, downwind ( $47^{\circ}24'14''$  N,  $8^{\circ}01'07''$  E, 500 m a.s.l.). Located on a small hill in an open area, next to a cow-filled field.
- **“Wing 1”**: positioned 0.5 km N of the NPP ( $47^{\circ}22'15''$  N,  $7^{\circ}57'49''$  E, 405 m a.s.l.). Located on the edge of the woods.

<sup>2</sup> Personal communication from the ENSI

- **“Wing 2”:** positioned 1.3 km ENE of the NPP (47°22’13” N, 7°58’53” E, 385 m a.s.l.). Located next to the main road of a small village.

In total, 18 aluminum bags were filled with 100-120 L air at ambient conditions, such as described in chapters 2 and 3. As it was located more than 4 km upwind from the NPP, the site “Background” was used as a background reference for atmospheric  $^{14}\text{CH}_4$  and  $^{14}\text{CO}_2$ . An air sample was collected at that site, prior to the expected onset of emissions associated with the opening of the reactor cover.

Site “Main” was the primary site, which was expected to catch the emission “plume” from the NPP, as it was ideally located 1.2 km downwind the NPP, almost at the same elevation as the chimney of the NPP. Indeed, such a distance from the chimney is in good accordance with previous studies on the enhancement of the  $^{14}\text{C}$  concentration in the vegetation near NPPs, which found maximum values between 0.5 and 2 km downwind the NPPs (Loosli and Oeschger, 1989; Stenström et al., 1996). At this location, air was continuously sampled by filling aluminum bags for 75 min each, at a flow rate of  $1.4 \text{ L min}^{-1}$ .

In addition to the fix sampling system assigned to site “Main”, a mobile setup was used to alternatively collect samples at the sites “Remote”, “Wing 1” and “Wing 2” (see Figure 4.1). For this purpose, a small membrane pump powered by a car battery was used to fill an aluminum bag within 20 min. Thus, while a bag was filled at site “Main”, two samples were alternatively collected at the site “Remote” and either site “Wing 1” or “Wing 2”. This strategy was adopted for two main reasons: First, to obtain some information about the dampening of the plume over distance, by comparing the results between site “Main” and site “Remote”, which are both situated downwind. Second, to gather some knowledge concerning the spatial distribution of the plume and its sensitivity to the topography and the wind direction by sampling at sites “Wing 1” and “Wing 2”. These two sites were also chosen to maximize the probability to catch the peak of  $^{14}\text{C}$  emissions, as the wind was weak and its direction was slightly changing throughout the day.

### 4.2.3 Analyses

Although the primary goal of the study was to measure atmospheric  $^{14}\text{CH}_4$ , the following analyses were conducted:

- **$^{14}\text{CH}_4$  and  $^{14}\text{CO}_2$ :** 45 L of each sample bag were used for the extraction of  $\text{CH}_4$  and  $\text{CO}_2$  for  $^{14}\text{C}$ -AMS in our laboratory. Methane was measured using the combination MPPS-GIS-AMS (gas measurement), whereas  $\text{CO}_2$  was recovered from the PRECON of the MPPS, graphitized and measured using the combination PRECON-CIS-AGE-AMS (see chapters 2 and 3).
- **$^{37}\text{Ar}$ :** With a half-life of 35.1 days, this inert gas released by NPPs is a useful tracer for studies of atmospheric transport and mixing processes (Loosli et al., 1973). It was

therefore an obvious candidate for the monitoring of the plume (Loosli et al., 1970). The remaining air from 3 sample bags was sent to the CEP for  $^{37}\text{Ar}$  analyses. There, argon was first extracted in a gas chromatography purification line (Riedmann and Purtschert, 2016) before  $^{37}\text{Ar}$  activity was measured by ultra-low level  $\beta$ -counting in an underground laboratory (Forster et al., 1992).

#### 4.2.4 Evaluation and correction of the data

The specific activities  $A$  (in  $\text{Bq kg}^{-1}$ ) were calculated from the  $\text{F}^{14}\text{C}$  results using the following formula (Stenström et al., 2011):

$$A = \text{F}^{14}\text{C} \cdot \left[ \frac{1 + \delta^{13}\text{C}}{0.975} \right]^2 \cdot e^{\frac{1950-y}{8267}} \cdot 226 \quad \text{Equation 4.1}$$

With  $\delta^{13}\text{C}$  being the isotopic signature (VPDB) measured with the AMS and  $y$  the year of measurement. The activity concentrations calculated from Equation 4.1 are per kg of pure carbon. To calculate the corresponding volume activities ( $\text{Bq m}^{-3}$ ) for  $^{14}\text{CH}_4$  and  $^{14}\text{CO}_2$ , the mole fractions of  $\text{CH}_4$  and  $\text{CO}_2$  in the air samples needed to be assessed. For each individual sample, the amount of  $\text{CH}_4$ -derived  $\text{CO}_2$  recovered from the preconcentration and purification of 45 L air was used for the calculation of  $\text{CH}_4$  mole fractions. As the amount of  $\text{CO}_2$  could not be precisely quantified with the MPPS (see Chapter 3), a conservative constant  $\text{CO}_2$  mole fraction of 400 ppm was used in the calculation of  $^{14}\text{CO}_2$  activity concentrations. This value is slightly lower than the mole fractions measured at Beromünster and Jungfraujoch on June 2 (~405–415 ppm), therefore the reported activities for  $^{14}\text{CO}_2$  may be slightly underestimated. Finally,  $^{14}\text{CH}_4$  and  $^{14}\text{CO}_2$  activities were corrected for their respective atmospheric background values. The air sample collected at the site “Background” had an  $\text{F}^{14}\text{C}$  of  $1.000 \pm 0.004$  for  $\text{CO}_2$  (see below in Table 4.1), which corresponds to a background activity of  $42.7 \pm 1.5 \text{ mBq m}^{-3}$ . As the  $^{14}\text{CH}_4$  content at that site was too high to be used as a reference ( $\text{F}^{14}\text{C} = 1.78$ , see below in Table 4.1), an  $\text{F}^{14}\text{C}$  value of 1.41 was used instead, corresponding to a background activity of  $0.30 \text{ mBq m}^{-3}$ . This value is the mean  $\text{CH}_4$   $\text{F}^{14}\text{C}$  content measured at the Beromünster tall tower between July 2018 and August 2019 (see Chapter 3). Despite its lower  $\text{F}^{14}\text{C}$  content, atmospheric  $^{14}\text{CO}_2$  has a much higher background activity than  $^{14}\text{CH}_4$ , because of its larger mole fraction in the atmosphere (~400 ppm and ~2 ppm for  $\text{CO}_2$  and  $\text{CH}_4$ , respectively).

The very large  $\text{F}^{14}\text{C}$  contents measured in the atmospheric  $\text{CH}_4$  samples (see below in Table 4.1), which were completely out of the range of values observed for environmental samples, induced some contamination and memory effects in the AMS. Although the origin of the problem could not be precisely determined, a contamination of the ion source and a saturation of the  $^{14}\text{C}$  detector are likely explanations (Schulze-König, 2010). As a result, the standards and blanks measured after the samples showed abnormally high  $^{14}\text{C}$  contents. This issue was

considered when calculating the  $F^{14}\text{C}$  uncertainties reported in Table 4.1. For the  $\text{CH}_4$  results, the relative uncertainty of a modern standard was multiplied by 2.5, giving an uncertainty of about 2.5%, and a conservative uncertainty of 8% was chosen for the largest  $F^{14}\text{C}$  content measured. For each  $F^{14}\text{C}$  result, the corresponding relative uncertainty was calculated from a linear scaling between 2.5% ( $F^{14}\text{C} = 1.34$ ) and 8% ( $F^{14}\text{C} = 4801$ ). Similarly, the relative uncertainties of the reported  $F^{14}\text{C}$  values of the  $\text{CO}_2$  samples were linearly scaled between 0.5% for a standard sample and 2% for the highest value measured (i.e.  $F^{14}\text{C} = 8.683$ ). The reported uncertainties of the background-corrected activities were estimated from the error-propagated uncertainties of the  $F^{14}\text{C}$  results, to which a 3% error was added. This additional uncertainty accounts for the quadratic contribution of a 2% error on the absolute  $\text{CH}_4$  and  $\text{CO}_2$  mole fractions at the measurement sites, and 2% uncertainty caused by the daily variations of  $\text{CO}_2$  and  $\text{CH}_4$  mole fractions.

## 4.3 Results and discussion

The  $^{14}\text{C}$  results for  $\text{CH}_4$  and  $\text{CO}_2$  are reported in Table 4.1 and displayed in Figure 4.2, to better visualize their temporal evolution. The graph includes measurements of the total noble gas activity in the stack, which corresponds to the average total  $\beta$  disintegrations measured every 10 min by two gas proportional counters. These values are published and updated monthly by the ENSI (<https://www.ensi.ch/de/dokumente/document-category/emi-daten/>) and were available only ~1 month after the air sampling.

### 4.3.1 Radioactive emissions at the stack

Figure 4.2a shows the radioactivity of the noble gases vented through the stack of the Gösgen NPP on June 2, 2019. As the gas flow rate through the chimney stack was kept relatively constant ( $45\text{--}48 \text{ m}^3 \text{ s}^{-1}$ ), emission rates are directly proportional to the activity concentrations reported in Figure 4.2. The detection limit of the gas proportional counters is  $3.2 \times 10^8 \text{ Bq h}^{-1}$ , which corresponds to an activity of  $\sim 2 \times 10^6 \text{ mBq m}^{-3}$ . Emissions over the detection limit are visible between 02:00 UTC and 11:30 UTC. The graph reveals two characteristic patterns: First, the activity level started to rise over baseline values at 02:00 UTC, peaked at a recorded value of  $2.03 \times 10^7 \text{ mBq m}^{-3}$  at 03:50 UTC and decreased to values close to baseline at 06:00 UTC. A second pattern of emissions occurred immediately after, with a sharp increase up to a maximum of  $5.41 \times 10^7 \text{ mBq m}^{-3}$  at 06:40 UTC, followed by damped oscillations of the activity level, which returned to baseline values at 11:30 UTC.

Table 4.1  $^{14}\text{C}$  activity near the Gösgen NPP on June 2, 2019, measured at the following sites (see Figure 4.1): “Background” (B), “Main” (M), “Remote” (R), “Wing 1” (W1) and “Wing 2” (W2). A total procedural blank of  $0.35 \pm 0.10 \mu\text{g C}$  with an  $F^{14}\text{C}$  of  $0.35 \pm 0.18$  and a cross contamination of 0.4% are considered for the  $\text{CH}_4$  results (see Table 2.1). The reported activities are background-corrected ( $0.30 \text{ mBq m}^{-3}$  for  $^{14}\text{CH}_4$  and  $42.7 \text{ mBq m}^{-3}$  for  $^{14}\text{CO}_2$ ). See text for the determination of the uncertainties ( $1\sigma$ ).

Site	Time* (UTC)	$\text{F}^{14}\text{C}$ ( $\text{CH}_4$ )	$^{14}\text{CH}_4$ activity ( $\text{mBq/m}^3$ )	$\text{F}^{14}\text{C}$ ( $\text{CO}_2$ )	$^{14}\text{CO}_2$ activity ( $\text{mBq/m}^3$ )	Activity ratio $^{14}\text{CO}_2/^{14}\text{CH}_4$
B	06:24	$1.78 \pm 0.04$	$0.08 \pm 0.03$	$1.000 \pm 0.004$	$0.0 \pm 2.1$	-
M	06:37	$489 \pm 15$	$109 \pm 7$	$1.426 \pm 0.008$	$18.4 \pm 2.6$	$0.17 \pm 0.03$
M	07:57	$2829 \pm 162$	$593 \pm 52$	$5.801 \pm 0.082$	$207 \pm 11$	$0.35 \pm 0.04$
M	09:17	$1428 \pm 59$	$283 \pm 20$	$4.594 \pm 0.054$	$153 \pm 8$	$0.54 \pm 0.05$
M	10:37	$878 \pm 30$	$181 \pm 12$	$2.315 \pm 0.016$	$56.5 \pm 4.0$	$0.31 \pm 0.03$
M	11:57	$120 \pm 3$	$23.3 \pm 1.3$	$1.143 \pm 0.005$	$6.37 \pm 2.25$	-
M	13:17	$85.7 \pm 2.2$	$17.2 \pm 1.0$	$1.085 \pm 0.005$	$4.22 \pm 2.19$	-
R	07:39	$881 \pm 31$	$182 \pm 12$	$1.629 \pm 0.009$	$27.5 \pm 2.9$	$0.15 \pm 0.02$
R	08:45	$2529 \pm 136$	$531 \pm 44$	$3.462 \pm 0.033$	$107 \pm 6$	$0.20 \pm 0.02$
R	10:10	$356 \pm 10$	$71.6 \pm 4.2$	$1.754 \pm 0.010$	$32.9 \pm 3.1$	$0.46 \pm 0.05$
R	11:30	$48.9 \pm 1.2$	$9.25 \pm 0.53$	$1.132 \pm 0.005$	$6.20 \pm 2.24$	-
R	12:52	$9.11 \pm 0.22$	$1.50 \pm 0.10$	$1.011 \pm 0.005$	$0.35 \pm 2.08$	-
W1	07:03	$16.3 \pm 0.4$	$3.21 \pm 0.19$	$1.013 \pm 0.005$	$0.53 \pm 2.09$	-
W1	09:21	$3.08 \pm 0.08$	$0.32 \pm 0.04$	$1.000 \pm 0.004$	$0.05 \pm 2.08$	-
W1	12:10	$11.4 \pm 0.3$	$1.95 \pm 0.12$	$1.115 \pm 0.005$	$5.58 \pm 2.22$	-
W2	08:14	$4801 \pm 384$	$993 \pm 109$	$8.683 \pm 0.173$	$328 \pm 19$	$0.33 \pm 0.04$
W2	10:50	$96.9 \pm 5.9$	$18.6 \pm 1.7$	$1.522 \pm 0.008$	$23.1 \pm 2.8$	$1.24 \pm 0.16$
W2	13:30	$9.85 \pm 0.24$	$1.63 \pm 0.11$	$1.012 \pm 0.005$	$1.11 \pm 2.10$	-

\* Middle time of each sample collection, which lasted 75 min at site “Main” and 20 min at the other sites.

The reactor cover was actually opened at about 6:30 UTC, and a flushing procedure was performed. The first broad peak is likely caused by the venting of the reactor containment air, which is not systematically performed during normal operation periods (Kunz, 1985). The damped oscillations of activity at the stack might be explained by successive purges of the radioactive gases in the different compartments of the NPP, particularly the gas decay tanks (Kunz, 1985; Stenström et al., 1995). The peak of discharge, corresponding to a noble gas activity of  $5.41 \times 10^7 \text{ mBq m}^{-3}$  in the stack, was at least 25 times over normal operation emissions. However, the reported baseline values correspond to the detection limit of the gas proportional counters and thus the actual background activity might have been significantly lower.

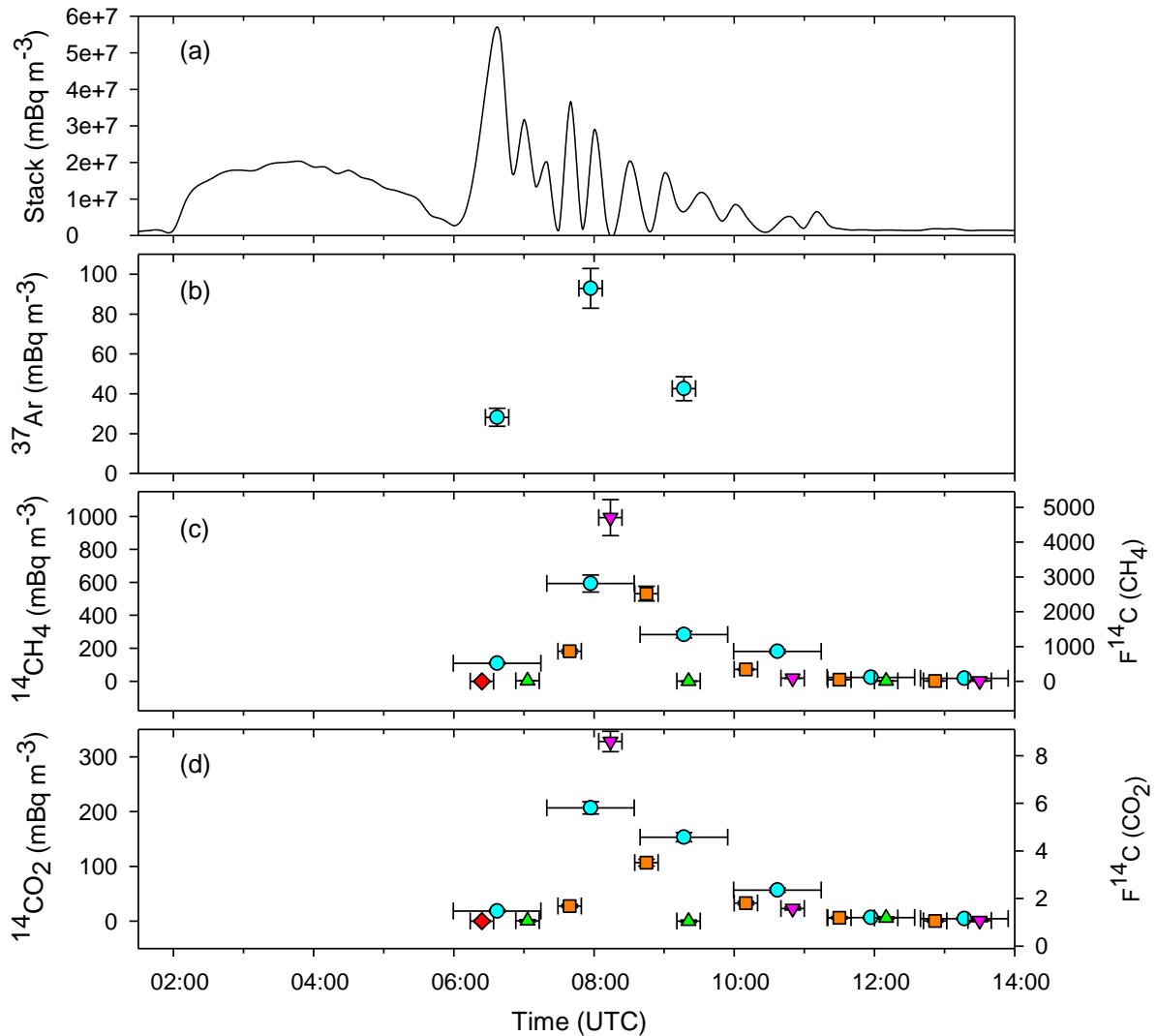


Figure 4.2 Activities ( $^{37}\text{Ar}$  and  $^{14}\text{C}$ ) at several sites in the vicinity of the Swiss Gösgen NPP during its yearly revision on June 2, 2019. The results are reported for air samples collected at five different sites (the locations are shown in Figure 4.1): “Background” (red diamonds), “Main” (cyan circles), “Remote” (orange squares), “Wing 1” (green triangles up) and “Wing 2” (pink triangles down). The horizontal error bars illustrate the air sampling duration and the vertical error bars show the error propagated  $1\sigma$  uncertainties. See Table 4.1 and text for more details. (a) Total noble gas activity in the chimney stack reported by the ENSI. (b)  $^{37}\text{Ar}$  activity. (c)  $^{14}\text{CH}_4$  activity (see Table 4.1). (d)  $^{14}\text{CO}_2$  activity (see Table 4.1).

#### 4.3.2 $^{14}\text{CH}_4$ at the sampling sites

The methane  $F^{14}\text{C}$  contents and corresponding activities measured near the NPP are listed in Table 4.1 and shown in Figure 4.2c. As previously mentioned, the discharge of gaseous effluents already started at 02:00 UTC, more than 4 hours before the sampling at the site “Background”, with is situated at less than 5 km upwind from the NPP. Hence, this first emission pattern is likely responsible for the slightly elevated  $^{14}\text{CH}_4$  content measured at that site ( $F^{14}\text{C} = 1.78$ ).

The first air sample from site “Main” (1.2 km downwind the NPP), collected between 5:59 and 7:15 UTC, already showed a very high  $^{14}\text{CH}_4$  content ( $F^{14}\text{C} = 489$ ). The concentrations kept increasing at that site and peaked at an  $F^{14}\text{C}$  value of 2829 during the second sampling (7:20–8:35 UTC), corresponding to a  $^{14}\text{CH}_4$  activity of  $593 \text{ mBq m}^{-3}$ , and then gradually decreased over time. The last sampling at site “Main”, which took place between 12:40 and 13:55 UTC, revealed that atmospheric air at 1.2 km from the NPP had still a very elevated  $^{14}\text{CH}_4$  content, with a measured  $F^{14}\text{C}$  value of  $\sim 86$ , which is about 60 times above background values measured at the Jungfraujoch research station in 2019 ( $F^{14}\text{C} \approx 1.37$ , see Chapter 2). Although the emissions from the stack had already returned to baseline values an hour before the last sampling at site “Main” was started, the relatively high  $^{14}\text{CH}_4$  concentration can be explained by a slow dispersion of the plume as the wind was weak. In other words, the last measurement likely corresponds to the tail of the emission plume. The sampling frequency at site “Main” was insufficient to monitor the dispersion and dilution in the environment of the complex emission pattern observed in the stack (see Figure 4.2a and Figure 4.2c). However, the general shape of  $^{14}\text{CH}_4$  concentrations at site “Main” over time is consistent with the total noble gas activity measured at the stack. Finally, it should be emphasized that the most striking result is the absolute values measured ( $F^{14}\text{C} = 86\text{--}2829$ ), which are very high in comparison to the  $^{14}\text{CH}_4$  concentrations observed at Bern, Beromünster and Jungfraujoch and reported in Chapter 3 ( $F^{14}\text{C} = 1.32\text{--}4.02$ ).

The  $^{14}\text{CH}_4$  content measured at site “Remote”, which was situated 5.8 km downwind the NPP, reveals a shape similar to the one observed at site “Main”. The signal at the remote site was slightly damped and delayed, due to dispersion and transport time, respectively. Surprisingly, the  $^{14}\text{CH}_4$  content at a distance of  $\sim 6$  km from the NPP was still very high, with an  $F^{14}\text{C}$  value of 2529 at 8:45 UTC, two hours after the peak of emissions reported by the NPP. At first sight, such a high value does not seem to be consistent with a normal dispersion of the plume. However, unlike at site “Main”, the samplings at site “Remote” lasted only 20 min and hence did not average the air content over a long period. As the wind speed was 2–3 km/h, blowing from the NPP towards site “Remote”, it is very likely that the sampling took place during the maximum of the plume. This result clearly indicates that such release events from NPPs have a wide spatial impact on atmospheric  $^{14}\text{CH}_4$ , and therefore strengthens the assumption that the relatively high values measured at Beromünster, located 25 km from Gösigen, were caused by  $^{14}\text{CH}_4$  discharges from NPPs.

The highest  $^{14}\text{CH}_4$  concentration ( $F^{14}\text{C} = 4801 \pm 384$ ) was measured at site “Wing 2”, between 08:04 and 08:24 UTC. This value corresponds to a  $^{14}\text{CH}_4$  activity of about  $1 \text{ Bq m}^{-3}$ , which is extremely high for atmospheric  $^{14}\text{CH}_4$  as it is over 3000 times higher than typical background values. Other authors already reported elevated  $^{14}\text{CH}_4$  values in the vicinity of NPPs, but they were just a few times over the concentration found at background sites (e.g. Eisma et al., 1995; Townsend-Small et al., 2012). This air sample was collected about 90 min after the main peak of activity at the chimney stack, at a distance of 1.3 km from the stack. Since there was almost

no wind at that moment, the timing between the two events is consistent with a normal dispersion of the plume. The slightly lower value measured at site “Main” ( $F^{14}\text{C} = 2829$ ) is thus most likely due to an averaging over a longer period, which creates a dampening of the peak.

Site “Wing 1”, located only 0.5 km north from the chimney, did not display very high values like the other locations ( $F^{14}\text{C} < 17$ ). The most plausible explanation is that the plume passed above this site. Indeed, the chimney has a height of 99 m and the vertical mixing was probably not strong enough for the plume to reach the ground at a horizontal distance of 500 m from the NPP. Even if the wind was rather weak (2–3 km/h), its direction might have also played a role as it was blowing toward sites “Main” and “Wing 2”.

### 4.3.3 $^{14}\text{CO}_2$ at the sampling sites

The  $\text{CO}_2$   $F^{14}\text{C}$  contents and corresponding activities measured near the NPP are presented in Table 4.1 and Figure 4.2d. The general pattern of  $^{14}\text{CO}_2$  results is very similar to the one of  $^{14}\text{CH}_4$  results reported above, which confirms that  $^{14}\text{CH}_4$  and  $^{14}\text{CO}_2$  shared a common source as they were co-emitted by the NPP. Therefore, the previous arguments explaining the measured  $^{14}\text{CH}_4$  at the sampling sites are valid for  $^{14}\text{CO}_2$  as well. However, in terms of absolute values, the measured  $F^{14}\text{C}$  values for  $^{14}\text{CO}_2$  are much lower than for  $^{14}\text{CH}_4$ , with a maximum value measured at site “Wing 2” of 8.68 and 4801, respectively. Although it will be shown that the NPP emitted more  $^{14}\text{CH}_4$  than  $^{14}\text{CO}_2$ , the discrepancy is mostly explained by the much larger mole fraction of  $\text{CO}_2$  in the atmosphere in comparison to the one of  $\text{CH}_4$ , which dilutes more the  $^{14}\text{C}$  discharges from NPPs (Lassey et al., 2007b; Graven et al., 2019).

Although less impressive than the measured  $^{14}\text{CH}_4$  contents, we measured a maximum enhancement of atmospheric  $^{14}\text{CO}_2$  concentration over natural levels of approximately 770% and 250% at ~1 km and ~6 km from the NPP, respectively. For the purpose of comparison, typical enhancements below 20% were reported for vegetation samples in the surroundings of NPPs (Loosli and Oeschger, 1989; Stenström et al., 1996). Similarly, air samples collected around several NPPs for a one-week period showed  $^{14}\text{CO}_2$  excesses usually well below 50% (Levin et al., 1988; Uchirin et al., 1997; Molnár et al., 2007; Dias et al., 2009). The leaves collected near the Gösgen NPP revealed a mean enhancement of ~4% in 2018 (FOPH, 2019), which is rather low because PWRs emit significantly less  $^{14}\text{CO}_2$  than BWRs (Kunz, 1985; Loosli and Oeschger, 1989). Thus, even though the Gösgen NPP is a relatively modest contributor to  $^{14}\text{CO}_2$  releases from the nuclear industry, the study presented here highlights the large impact of sporadic discharges, as the  $^{14}\text{CO}_2$  enhancements reported in this study are much larger than what was found in the literature.

As previously reported, background activities for  $^{14}\text{CO}_2$  and  $^{14}\text{CH}_4$  are  $42.7 \text{ mBq m}^{-3}$  and  $0.30 \text{ mBq m}^{-3}$ , respectively. Thus, the natural  $^{14}\text{CO}_2/^{14}\text{CH}_4$  activity ratio at background sites such as Jungfrauoch is around 150. The measured  $^{14}\text{CO}_2/^{14}\text{CH}_4$  activity ratios in the air

samples collected around the NPP are reported in Table 4.1. The activity ratios are not displayed when the  $^{14}\text{CO}_2$  activity was not significantly higher than background values, as the associated uncertainties are high. Since the  $^{14}\text{CO}_2$  and  $^{14}\text{CH}_4$  activities are background subtracted, the mean activity ratio should allow an estimation of the relative source strength for the emissions of  $^{14}\text{CO}_2$  and  $^{14}\text{CH}_4$  from the NPP. The  $^{14}\text{CH}_4$  and  $^{14}\text{CO}_2$  activities in each air sample collected, which are presented in Figure 4.3, show a good correlation with a  $^{14}\text{CO}_2/^{14}\text{CH}_4$  activity ratio of  $0.32 \pm 0.05$  estimated from a linear regression ( $R^2 = 0.93$ ). When neglecting a possible small contribution from higher alkanes (Kunz, 1985), the calculated activity ratio indicates that  $^{14}\text{CH}_4$  emissions from the NPP contributed to 73–79% of the total  $^{14}\text{C}$  emissions from the stack, the remaining 21–27% being released as  $^{14}\text{CO}_2$ . Such a value is in good agreement with reported  $^{14}\text{C}$  emissions from NPPs equipped with a PWR, which show that 70–95% of their  $^{14}\text{C}$  releases are in the form  $^{14}\text{CH}_4$  (Kunz, 1985; Uchrin et al., 1997; Yim and Caron, 2006). However, significant changes in the composition of released gases from the stack of PWR-type NPPs have been previously observed during outage periods, with sometimes a larger proportion of  $^{14}\text{CO}_2$  emitted than in normal operation periods (Kunz, 1985; Kristina Stenström et al., 1995; Uchrin et al., 1997). Hence, the measured  $^{14}\text{C}$  fraction of 21–27% for  $^{14}\text{CO}_2$  discharges from the Gösgen NPP likely constitutes an upper value, and the results of the present study confirm that most of the  $^{14}\text{C}$  emissions from this NPP are in the form  $^{14}\text{CH}_4$ .

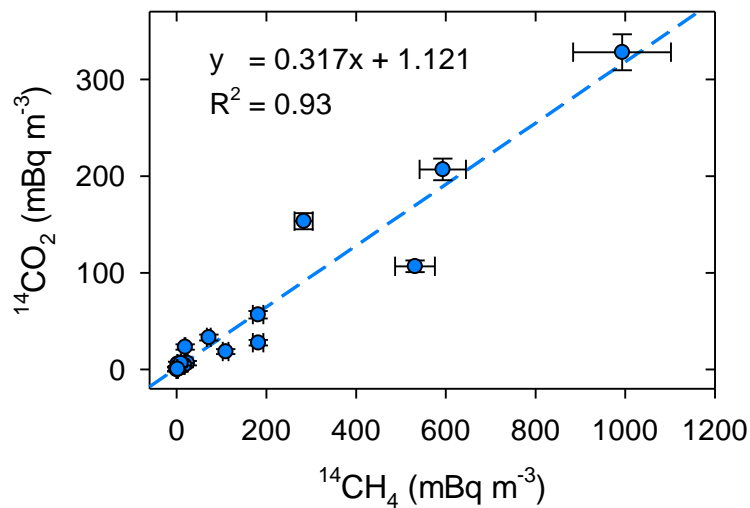


Figure 4.3 Determination of the mean  $^{14}\text{CO}_2/^{14}\text{CH}_4$  activity ratio of  $^{14}\text{C}$  emissions from the Gösgen NPP during the revision of June 2, 2019. The  $^{14}\text{CH}_4$  and corresponding  $^{14}\text{CO}_2$  results of the 18 air samples analyzed are displayed.

#### 4.3.4 $^{37}\text{Ar}$ at site “Main”

Atmospheric  $^{37}\text{Ar}$  is mainly produced in cosmic ray induced reactions with  $^{40}\text{Ar}$  (Gäggeler, 1995). The typical background concentration of atmospheric  $^{37}\text{Ar}$  in Switzerland is

~1–5 mBq m<sup>-3</sup> (Gäggeler, 1995; Riedmann and Purtschert, 2011). <sup>37</sup>Ar was analyzed for the three first air samples collected at site “Main”, from which high <sup>14</sup>C contents were measured (see Figure 4.2b). The 3 successive <sup>37</sup>Ar measurements between 6:00 UTC and 10:00 UTC were 28 ± 5 mBq m<sup>-3</sup>, 93 ± 10 mBq m<sup>-3</sup> and 43 ± 6 mBq m<sup>-3</sup>, respectively. These values are much higher than the natural <sup>37</sup>Ar concentration in the atmosphere, indicating that <sup>37</sup>Ar was actually co-emitted with <sup>14</sup>CH<sub>4</sub> and <sup>14</sup>CO<sub>2</sub> by the NPP and that the dispersion in the atmosphere was similar for the three gas species aforementioned. Indeed, the activity ratios <sup>37</sup>Ar/<sup>14</sup>CH<sub>4</sub> are between 15 and 25% for the three samples measured, which confirms a common source for <sup>37</sup>Ar and <sup>14</sup>CH<sub>4</sub>. However, it should be mentioned that the time resolution is rather low, especially at site “Main”. There, the samples were collected over a period of 75 min, which resulted in an averaging of the plume maximum. As suggested by the <sup>14</sup>CH<sub>4</sub> measurements at site “Wing 2”, it is very likely that the <sup>37</sup>Ar concentration at a distance of 1 km from the NPP peaked at values over 100 mBq m<sup>-3</sup>, which is 20–100 times over natural atmospheric <sup>37</sup>Ar levels.

### 4.3.5 Significance of the observed <sup>14</sup>C release event

#### 4.3.5.1 With respect to the Gösgen NPP itself

Our study revealed that large amounts of <sup>14</sup>CH<sub>4</sub> and <sup>14</sup>CO<sub>2</sub> were emitted during the revision of the Gösgen NPP, due to a release of radioactive gases that lasted approximately 10 hours. The discharge was responsible for extremely elevated <sup>14</sup>CH<sub>4</sub> and <sup>14</sup>CO<sub>2</sub> activities measured in the vicinity of the NPP, but also at a distance of ~6 km from the source. As a comparison, the maximum <sup>14</sup>CO<sub>2</sub> enhancement of 770% measured in the air was approximately 200 times larger than the mean <sup>14</sup>C enhancement of 4% in leave samples collected at the same distance from the NPP in 2018 (FOPH, 2019).

It is important to know if the discharge measured during the revision of the Gösgen NPP was exceptional in terms of intensity, in comparison with the sporadic discharges during normal operation periods and the total yearly emissions. As <sup>14</sup>C emissions were not directly measured at the stack, the monitoring of total noble gas activity by the ENSI was used as a proxy for <sup>14</sup>C emissions, as they are co-vented through the stack. The integration of the noble gas emissions over the period of the discharge (02:00–12:00 UTC) gives a total emission of about 21 GBq. The ENSI reports that the total noble gas emissions for June 2019 was below 240 GBq, a conservative upper limit that is probably larger than the real emissions. The problem arises from the low sensitivity of the noble gas detector, which prevents from knowing the actual emissions during normal operation periods. When using the value reported by the ENSI, the discharge observed on June 2 contributed to less than 9% of the total emissions from the month of June. When setting all the measures below the detection limit to half the value of the detection limit, the event on June 2 contributed to 14% of the monthly emissions. Finally, if we assume that the emissions are in reality much lower than the detection limit, the discharge contributed to 45% of the monthly discharge, which becomes a significant fraction of the total noble gas release. Thus, the discharge of June 2 contributed to 9–45% of

the total noble gas emission of June 2019. Although smaller in magnitude, it should also be noted that the month of June was particularly active in terms of emissions, with two other discharge events observed on June 4 and between June 18 and June 23 during the restart of the NPP.

The ENSI reports that the total noble gas emission from the Gösgen NPP in 2018 was below 2400 GBq, which would indicate that the release event from the NPP revision was responsible for ~1% of typical annual releases, which is only 3–4 times larger than average daily emissions. However, owing to the lack of knowledge of the actual annual emissions as previously explained, the contribution of June 2 is probably significantly underestimated. Hence, it is not fully clear what was the real contribution of the release event to the annual  $^{14}\text{C}$  emissions from the Gösgen NPP. However, Stenström et al. (1995) noticed that revision periods of PWRs significantly contribute to annual  $^{14}\text{C}$  emissions, with a revision period of 6 weeks amounting to 45% of the annual  $^{14}\text{C}$  discharge. We therefore suspect that the contribution of the revision period to annual  $^{14}\text{C}$  emissions of the Gösgen NPP was significantly higher than 1%, highlighting the temporal variability of this  $^{14}\text{C}$  source. Moreover, the revision of 2019 was not exceptional in terms of noble gas emissions, as the corresponding discharge during the beginning of the revision of 2018 was even slightly larger.

The emission of noble gases published by the ENSI shows that releases happen on average 1–2 times per month at the Gösgen NPP. These events, consisting of successive discharges over periods of one or two days, are probably caused by the venting of gas decay tanks (Kunz, 1985; Stenström et al., 1995). A typical example of discharge is shown in Figure 4.4. Although the maximum measured activity is almost one order of magnitude lower than what was observed during the revision of June 2 (see Figure 4.2a), the integrated emission over that period contributes to almost 50% of the total emissions observed in this study. Thus, sporadic discharges from NPPs outside revision periods should not be overlooked, as they probably have a strong local and regional impact on  $^{14}\text{CH}_4$  and  $^{14}\text{CO}_2$  over relatively short periods.

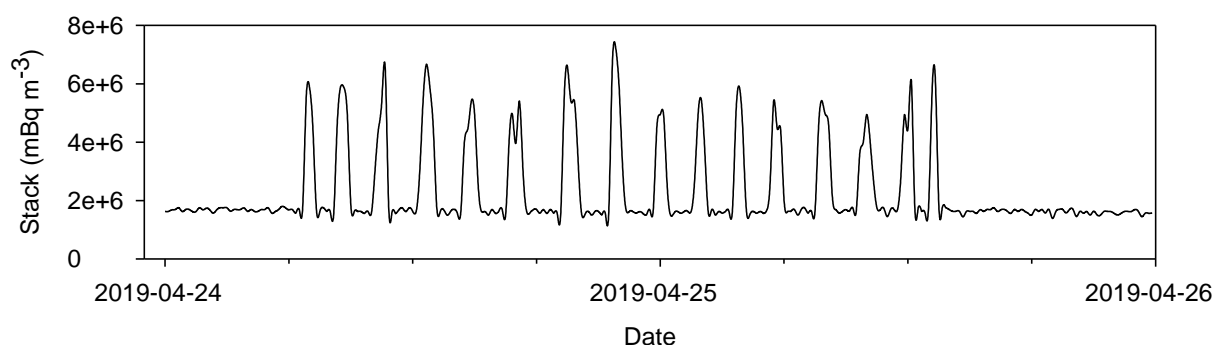


Figure 4.4 Discharge of noble gases through the chimney stack of the Gösgen NPP during a normal operation period. Source: ENSI.

#### 4.3.5.2 With respect to other nuclear sources of atmospheric $^{14}\text{C}$

Nuclear power plants holding a PWR are the main contributors to  $^{14}\text{CH}_4$  releases from nuclear industries (Hertelendi et al., 1989; Eisma et al., 1995). The study reported here highlights the very large temporal variability of  $^{14}\text{C}$  emissions, which impedes the use of constant EFs for such types of reactors. In contrast, NPPs equipped with a BWR reveal a very different contribution pattern: First, they are usually neglected as a  $^{14}\text{CH}_4$  source, as they emit almost exclusively  $^{14}\text{CO}_2$  (Kunz, 1985; Lassey et al., 2007a; Zazzeri et al., 2018). Second, their discharges are more continuous, and thus the  $^{14}\text{C}$  emission rate is proportional to the power level of the reactor (Stenström et al., 1995). Hence, although BWRs have a much larger global impact on atmospheric  $^{14}\text{CO}_2$  than PWRs, sporadic discharges from PWRs should not be overlooked, as the proportion of  $^{14}\text{C}$  released as  $^{14}\text{CO}_2$  varies between 5 and 30% depending on the particular plant (Kunz, 1985; Zazzeri et al., 2018), with a measured proportion of 21–27% in the current study (see Figure 4.3). Indeed, the air samples collected near the Gösigen NPP revealed that during a period of discharge  $^{14}\text{CO}_2$  enhancements of 250% are observed at a distance of 6 km from the NPP, which is more than 50 times larger than the typical  $^{14}\text{C}$  excess measured at the same distance of a NPP holding a BWR (Stenström et al., 1996).

Although there are only a handful of them in the world, nuclear reprocessing plants should not be neglected as they are the largest point sources of  $^{14}\text{C}$  (Zazzeri et al., 2018). Since  $^{14}\text{C}$  emissions from reprocessing plants are almost exclusively in the form of  $^{14}\text{CO}_2$ , these plants are not considered as sources of  $^{14}\text{CH}_4$  (IAEA, 2004). A maximum  $^{14}\text{C}$  excess of 350% was measured in biological samples in the vicinity of the Sellafield reprocessing plant in UK (McCartney et al., 1986). With an annual  $^{14}\text{C}$  discharge over 20 TBq, La Hague (France) accounts for ~15% of the global  $^{14}\text{C}$  emissions from nuclear activities, which is almost 100 times larger than the typical release of a NPP holding a PWR (Zazzeri et al., 2018). Fontugne et al. (2004) measured a  $^{14}\text{C}$  excess of up to 4236% in atmospheric  $\text{CO}_2$  samples collected at 1 km downwind the COGEMA-La Hague reprocessing plant, which is more than 5 times higher than the  $^{14}\text{CO}_2$  enhancement observed in this study. As for BWRs,  $^{14}\text{C}$  emissions from reprocessing plants can be considered as quasi-continuous over time, as they typically consist of 10–15 releases per day, which last 30–40 min each (Fontugne et al., 2004). Although reprocessing plants have an obvious very large regional impact on atmospheric  $^{14}\text{CO}_2$  levels, the closest reprocessing plant (La Hague) is situated at more than 700 km from Switzerland. Fortunately, simulations show that large  $^{14}\text{C}$  sources such as La Hague and Sellafield reprocessing plants should induce a mean  $^{14}\text{CO}_2$  enhancement below 0.3% in Switzerland (Graven and Gruber, 2011).

#### 4.3.6 Monitoring the $^{14}\text{C}$ emissions of NPPs

Although the use of EFs seems still relevant for NPPs holding a BWR, our observations clearly show that this approach can only fail for the simulation of  $^{14}\text{C}$  emissions from PWRs, as they mainly consist of sporadic discharges associated with the venting of gas decay tanks and

containment air (Stenström et al., 1995). Thus, the use of constant  $^{14}\text{C}$  emissions from PWRs leads most of the time to an overestimation of the strength of these sources, but also to a very large underestimation of  $^{14}\text{CH}_4$  and  $^{14}\text{CO}_2$  emissions during periods of release. The present study showed that the problem is amplified during maintenance periods, when  $^{14}\text{C}$  discharges are at their maximum but the reactor is shutdown, which according to the use of EFs corresponds to an absence of  $^{14}\text{C}$  releases (Stenström et al., 1995; Zazzeri et al., 2018).

To overcome the fact that  $^{14}\text{CH}_4$  and  $^{14}\text{CO}_2$  emissions from NPPs are only occasionally measured by nuclear safety organizations such as the ENSI, we showed that the noble gas activity in the stack could be used as a proxy for  $^{14}\text{C}$  emissions, as it is continuously monitored in the chimney stacks. Indeed, the gaseous species share a common pathway of emission in NPPs (Kunz, 1985), and the  $^{14}\text{C}$  and  $^{37}\text{Ar}$  contents in the air samples collected near the Gösgen NPP revealed a good temporal correlation with the measured activity of the nobles gases vented at the stack (see Figure 4.2). However, this information can only be used as an *a posteriori* evidence of an important  $^{14}\text{C}$  discharge from a specific NPP holding a PWR: First, because the noble gas emission data are not available in real time but only 1–2 months after their acquisition; and second, because such information is only qualitative, as  $^{14}\text{CH}_4$  and  $^{14}\text{CO}_2$  are not directly measured in the stack and the proportion of the gaseous effluents is not well known and may vary over time.

Very few studies report on direct measurements of  $^{14}\text{C}$  releases from NPPs (Hertelendi et al., 1989; Uchrin et al., 1997; Světlík et al., 2006). The purpose of such investigations was not for an assessment of the impact of  $^{14}\text{C}$  releases from NPPs on atmospheric  $^{14}\text{CH}_4$  and  $^{14}\text{CO}_2$  levels, but rather for an estimation of the radiation dose in the proximity of NPPs. As an example, Stenström et al. (1993) designed a sampler for the continuous sampling of stack air over periods of two weeks. The samples were analyzed for their  $^{14}\text{CO}_2$  and total  $^{14}\text{C}$  activities with an AMS. Although  $^{14}\text{C}$  emissions were averaged over periods of two weeks, the measurements allowed emphasizing the temporal variability of  $^{14}\text{C}$  releases from PWRs. Indeed, the measured  $^{14}\text{C}$  activity in the stack of the NPP varied between 2 and  $1132 \text{ Bq m}^{-3}$ , with a mean value of  $200 \text{ Bq m}^{-3}$  (Stenström et al., 1995). Unfortunately, it has been demonstrated in the present study that a higher time resolution is necessary for the monitoring of  $^{14}\text{C}$  releases from PWRs, and a daily assessment seems to constitute a minimum requirement. Therefore,  $^{14}\text{C}$ -AMS analysis does not seem to be a cost-effective solution for the monitoring of the  $^{14}\text{C}$  activity in the stacks of NPPs, as measurements are expensive and labor-intensive. An optical method based on laser spectroscopy has been recently proposed for on-site monitoring of  $^{14}\text{CH}_4$  and  $^{14}\text{CO}_2$  emissions of NPPs, with a single measurement lasting about 1.5 hours (Genoud et al., 2019). If future tests confirm that the technique is implementable in nuclear facilities, it might offer a valuable tool for simulations of the impact of NPPs in atmospheric studies.

### 4.3.7 Implications for $^{14}\text{CH}_4$ and $^{14}\text{CO}_2$ source apportionments

As presented in Chapter 3,  $^{14}\text{C}$  measurements of atmospheric  $\text{CH}_4$  and  $\text{CO}_2$  can be used as tracers for fossil emissions of these two major greenhouse gases. Local and regional  $^{14}\text{CH}_4$  and  $^{14}\text{CO}_2$  depletions caused by fossil emissions are expected to be in the order of a few percent (Levin et al., 2008; Berhanu et al., 2017; Graven et al., 2019). Unfortunately, the biweekly measurements of atmospheric  $^{14}\text{CH}_4$  at Bern and Beromünster showed that  $^{14}\text{C}$  releases from NPPs were the main drivers for the observed temporal variations of the signal, which hindered the detection of any potential depletion of  $^{14}\text{CH}_4$  caused by fossil  $\text{CH}_4$  emissions (Eisma et al., 1994; Townsend-Small et al., 2012). Measurements in the vicinity of the Gösgen NPP strongly emphasized that sporadic releases from NPPs with a PWR create a large spatial and temporal variability of  $^{14}\text{CH}_4$  and  $^{14}\text{CO}_2$  levels in their proximity. Wind speed and direction, topography and distance to the source have also a large influence on the actual contribution of NPP releases at a specific location, and a simple Gaussian model for the dispersion of the plume is often not valid (Stenström et al., 1996; Dias et al., 2009). For a meaningful simulation of the impact of  $^{14}\text{C}$  emissions of PWRs on atmospheric  $^{14}\text{CH}_4$  and  $^{14}\text{CO}_2$  levels observed at a site, the meteorological conditions but also the temporal variability of the  $^{14}\text{C}$  source should both be considered in atmospheric transport models. Because of using constant EFs, the contribution from PWRs is overestimated outside periods of release and strongly underestimated during discharge events.

The study showed that sporadic  $^{14}\text{C}$  discharges from PWRs have the potential to deeply impact atmospheric  $^{14}\text{CH}_4$  and  $^{14}\text{CO}_2$  at local and regional scales for relatively short periods. Although such events should not significantly alter the  $^{14}\text{CO}_2$  content of air samples integrated over long periods, they might substantially affect grab samples collected after a discharge. Unfortunately, atmospheric  $^{14}\text{CH}_4$  and  $^{14}\text{CO}_2$  could not be measured at the regular sampling sites during and immediately after the large discharge observed at Gösgen, but it is very likely that in the next hours and days following the release the  $^{14}\text{C}$  contents were abnormally elevated at these sites.

Eleven days after the revision of the Gösgen NPP, an air sample was collected at Jungfraujoch, which is located 90 km south from Gösgen. For the first time since the biweekly air sampling started at Jungfraujoch in December 2018,  $\text{CH}_4$  had an elevated  $F^{14}\text{C}$  value of 1.49, which is ~10% higher than all the previous values observed at this location (see Chapter 3). Back trajectory simulations with CGER METEX show that the air masses advected to Jungfraujoch during the sampling passed very close to the Gösgen NPP 5 hours before. Moreover, the emissions of noble gases reported by the ENSI confirm that a small episode of gaseous release took place at Gösgen on that same morning. Although both events cannot be linked with a high level of confidence, they underline that  $^{14}\text{CH}_4$  releases from NPPs have the potential to cause significant temporal variations of the atmospheric  $^{14}\text{CH}_4$  content at a remote site, which was supposed to be representative of background  $^{14}\text{CH}_4$ . The day after the sampling at

Jungfrauoch (June 14), the sample collected at Bern exhibited the highest  $^{14}\text{CH}_4$  and  $^{14}\text{CO}_2$  concentrations ever measured there, with  $F^{14}\text{C}$  values of 1.65 and 1.047 corresponding to  $^{14}\text{C}$  increases of about 53% and 7% compared to mean values measured at these sites, respectively. Back trajectory simulations are consistent with a contribution from air masses advected from the Gösigen NPP, and data from the ENSI confirm a small discharge. At first glance, the results do not seem to agree well with the Gösigen NPP being a common source for the observed enhancements of  $^{14}\text{CH}_4$  and  $^{14}\text{CO}_2$ , as the study confirmed that the impact of discharges from PWRs should be at least two orders of magnitude larger on atmospheric  $^{14}\text{CH}_4$  than on atmospheric  $^{14}\text{CO}_2$ . However, previous studies have shown that during maintenance periods of PWRs, a change to oxidizing conditions in the reactor coolant for cleaning purposes leads to a drastic alteration of the proportions of the gaseous species discharged, with the major fraction of  $^{14}\text{C}$  being emitted as  $^{14}\text{CO}_2$  (Kunz, 1985; Kristina Stenström et al., 1995). Hence, we cannot exclude that the Gösigen NPP was the culprit for the enhancement of both  $^{14}\text{CH}_4$  and  $^{14}\text{CO}_2$  at Bern, and this example highlights the need of a simultaneous monitoring of  $^{14}\text{CH}_4$  and  $^{14}\text{CO}_2$  emissions from PWRs. Finally,  $^{14}\text{C}$  emissions from France should not be neglected for atmospheric  $^{14}\text{C}$  measurements in Switzerland: First, because air masses are often advected from France via the westerly winds (Berhanu et al., 2017); and second, because France is one of the world largest emitters of  $^{14}\text{C}$ , as the country is equipped with 58 NPPs holding all a PWR (IAEA, 2017; Zazzeri et al., 2018). The large spatial and temporal variations of  $^{14}\text{CH}_4$  among the different sites near the Gösigen NPP, with maximum  $^{14}\text{CH}_4$  enhancements of about 340000% at 1 km and 180000% at 6 km, together with the inability to consistently link  $^{14}\text{CH}_4$  observations at Beromünster and Bern with specific  $^{14}\text{C}$  releases from NPPs, emphasize that  $^{14}\text{C}$  source apportionments of atmospheric  $\text{CH}_4$  will always be very challenging in regions with NPPs holding a PWR (Eisma et al., 1995).

Although atmospheric  $^{14}\text{CO}_2$  is much less sensitive to  $^{14}\text{C}$  emissions of NPPs than atmospheric  $^{14}\text{CH}_4$ , the study around Gösigen and a measurement at Bern showed that sporadic discharges from PWRs could lead to significant underestimations of the  $\text{CO}_2$  fossil fuel component at a sampling site. Fortunately, these events should not be very frequent, as they require the combination of a discharge and the transport of contaminated air masses to the sampling site. Nevertheless, abnormally high  $^{14}\text{CO}_2$  contents could be examined by checking if any noble gas discharge was detected in the stack of PWR-type NPPs. If  $^{14}\text{CO}_2$  and  $^{14}\text{CH}_4$  are jointly measured at a site, very high  $^{14}\text{CH}_4$  contents may be used as indicators of a potential contamination of atmospheric  $^{14}\text{CO}_2$ .

## 4.4 Conclusion

Radiocarbon analysis of atmospheric CH<sub>4</sub> and CO<sub>2</sub> is a valuable tool to apportion fossil and biogenic sources of these two greenhouse gases. Unfortunately, <sup>14</sup>C emissions from nuclear facilities are a major artefact of this technique, in particular for measurements of atmospheric <sup>14</sup>CH<sub>4</sub> levels, which are very sensitive to releases from NPPs. Whereas BWRs emit predominantly <sup>14</sup>CO<sub>2</sub> at a relatively constant rate, releases from PWRs consist of sporadic <sup>14</sup>C discharges predominantly in the form <sup>14</sup>CH<sub>4</sub>. There is very little known concerning the local and regional impacts of PWRs on atmospheric <sup>14</sup>C levels and some very high atmospheric <sup>14</sup>CH<sub>4</sub> contents measured at several sites in Switzerland motivated the study presented here. To maximize the probability to measure atmospheric <sup>14</sup>CH<sub>4</sub> and <sup>14</sup>CO<sub>2</sub> in the vicinity of a PWR during a discharge, we collected air samples during the beginning of a revision period of the Gösgen NPP, when the reactor cover is opened and the compartments of the NPP are purged.

The collection of air samples downwind the NPP allowed to visualize the temporal evolution of the plume, which could be clearly identified for <sup>14</sup>CH<sub>4</sub>, <sup>14</sup>CO<sub>2</sub> and <sup>37</sup>Ar. The results are in good agreement with previous studies in the stacks of PWRs, with <sup>14</sup>CH<sub>4</sub> accounting for 73–79% of the <sup>14</sup>C discharge, the remaining being emitted as <sup>14</sup>CO<sub>2</sub>. Measured <sup>14</sup>C concentrations were extremely high for <sup>14</sup>CH<sub>4</sub> and <sup>14</sup>CO<sub>2</sub>, peaking at F<sup>14</sup>C values of 4801 and 8.683, corresponding to activities about 3300 and 7.7 times over background values, respectively. The sampling at different locations near the NPP and at 6 km downwind showed that the dispersion of the plume is highly sensitive to weather conditions and topography, but also that <sup>14</sup>CH<sub>4</sub> and <sup>14</sup>CO<sub>2</sub> contents were still very high at the remote site.

Bearing in mind that the study presented here does not consist of a large-scale investigation of the impact of NPPs on atmospheric <sup>14</sup>CH<sub>4</sub> and <sup>14</sup>CO<sub>2</sub> levels, it still carries some relevant information for source apportionment of CH<sub>4</sub> and CO<sub>2</sub>. First, <sup>14</sup>C emissions of PWRs may be a major hindrance to <sup>14</sup>C source apportionments of atmospheric CH<sub>4</sub> in Switzerland, but also in other countries equipped with PWRs. Second, although BWRs emit approximately one order of magnitude more <sup>14</sup>CO<sub>2</sub> than PWRs on average (Graven and Gruber, 2011; Berhanu et al., 2017; Zazzeri et al., 2018), our observations near the Gösgen NPP revealed that large <sup>14</sup>C releases from PWRs have the potential to be the main contributors to atmospheric <sup>14</sup>CO<sub>2</sub> enhancements over relatively short periods. Unfortunately, <sup>14</sup>C emissions are not continuously monitored in the stacks of NPPs yet, with the consequence that simulations assume constant emissions over long periods. Such a strategy could lead to small overestimations of the fossil fuel CO<sub>2</sub> component at a sampling site, but also to substantial underestimations if <sup>14</sup>CO<sub>2</sub> discharges are advected to the measurement site.

Finally, we showed that noble gas emissions of NPPs can be used as indicators of large <sup>14</sup>C discharges, as they are usually continuously monitored in the stacks. Although the noble gases signal seems to indicate that the venting during the revision of the Gösgen NPP significantly

contributed to annual emissions, successive discharges over periods of 1–2 days are regularly observed. Unfortunately, the magnitude and the frequency of such discharges could greatly vary among several PWRs, depending on the type of reactor, the venting strategy and the presence of impurities in the reactor coolant (Kunz, 1985; Uchirin et al., 1997). Hence, a direct monitoring of  $^{14}\text{CH}_4$  and  $^{14}\text{CO}_2$  emissions from NPPs appears as a prerequisite for a better estimation of the local and regional impacts of NPPs on atmospheric  $^{14}\text{C}$  levels. However, the simulations will still be limited by the precision of atmospheric transport models.

The future evolution of  $^{14}\text{C}$  releases from the nuclear industry in various regions of the world remains unclear: while several NPPs are shut down in several countries, the construction of new NPPs in Asia and the threat of climate change might substantially increase the number of nuclear facilities in the coming years (van der Zwaan, 2013; Zazzeri et al., 2018). To mitigate the negative impact of NPPs in  $^{14}\text{C}$  source apportionments of  $\text{CH}_4$  and  $\text{CO}_2$ , the  $^{14}\text{C}$  emissions from NPPs could be captured at the source, before their venting through chimney stacks. Sun et al. (2018) evaluated the storage of  $^{14}\text{CH}_4$  in PCN-14 metal-organic frameworks, which are known as highly efficient  $\text{CH}_4$  adsorbents (Wu et al., 2010). Unfortunately, as  $^{14}\text{CH}_4$  emissions from NPPs are not dose relevant for human health, mitigation strategies will probably not arise as long as regulations do not exist.

## 5. $^{14}\text{C}$ -AMS lab intercomparison

### 5.1 Introduction

The demand for biogas as an alternative to fossil fuels and natural gas is currently increasing. Unlike other fuels, biogas is a renewable energy, which is produced from the biodegradation of raw materials such as agricultural waste, manure, plant material, sewage and food waste. Moreover, it is carbon-neutral as the carbon in biogas comes from organic matter that fixed atmospheric  $\text{CO}_2$  (Mohseni et al., 2012).

Biogas can substitute natural gas for cooking, heating, electrical generation and many other applications. As there is a growing market associated with incentives to promote the use of renewable energy resources, the verification of the biogenic carbon composition of produced biomethane, biofossil gas mixtures and of related  $\text{CO}_2$  emissions becomes more relevant (Palstra and Meijer, 2014). The  $^{14}\text{C}$  method is well suited for the determination of the biogenic and the fossil carbon fractions in fuels and flue gas, noted “bioC fraction” and “fossilC fraction”, respectively (Mohn et al., 2008; Palstra and Meijer, 2010). Indeed, the  $^{14}\text{C}$  content of biogenic carbon roughly reflects the  $^{14}\text{C}$  value of atmospheric  $\text{CO}_2$ , whereas fossil carbon is  $^{14}\text{C}$ -free.

In general, raw biogas samples contain a larger  $\text{CO}_2$  fraction than natural gas samples, with a proportion varying from a few percent up to 40% depending on the type of biogas producing plant (Rasi et al., 2007; Palstra and Meijer, 2014). As the  $\text{CO}_2$  fraction is jointly produced with  $\text{CH}_4$  from the raw material used for the production of biogas, it should show a similar  $^{14}\text{C}$  content than the  $\text{CH}_4$  fraction (Palstra and Meijer, 2014). To increase the efficiency of their product, biogas plants scrub most of the  $\text{CO}_2$  produced during the fermentation processes. Thus, their final product, called “upgraded biogas”, has a significantly reduced  $\text{CO}_2$  content (Weiland, 2010). Hence,  $^{14}\text{C}$  measurements of the biomethane fraction of raw biogas samples should provide a good estimate of the carbon composition of the final product.

The Centre for Isotope Research (ESRIG) from the University of Groningen (The Netherlands) initiated a  $^{14}\text{C}$ -AMS lab intercomparison among five European research groups. The intercomparison study is part of a Joint Research Project funded by the EU and carries several objectives. First, the verification of the reproducibility and accuracy of the  $^{14}\text{C}$ -based biogenic carbon fraction measurements for biogases and blends of biogas and natural gas, in the case where the laboratories apply their own combustion and AMS measurement methods. Second, the evaluation of possible factors influencing the results, such as specific laboratory methods and calculation methods. The results will help assessing, if further standardization of combustion and measurement methods is required for this specific application, to increase inter-laboratory reproducibility and accuracy. Finally, the findings of the intercomparison should be used in the development of a new standardized (ISO) test method for the biogenic carbon fraction measurement in biomethane or blends of biogas and natural gas.

The methane preconcentration and purification setup, described in Chapter 2, was primarily developed and optimized for the preparation of low concentration environmental CH<sub>4</sub> samples for radiocarbon analysis, such as atmospheric CH<sub>4</sub>. However, its flexibility enables the direct combustion of pure methane, biogas and natural gas samples. Moreover, the use of a preparative gas chromatography technique in the PURIF allows the separation of individual fractions from the gas mixtures, to gain more insight into the specific isotopic composition of the pure components. Thus, in addition to the total combustion of the gas samples received for the intercomparison, we isolated and measured pure CH<sub>4</sub>, CO<sub>2</sub>, C<sub>2</sub>H<sub>6</sub> and C<sub>3</sub>H<sub>8</sub> fractions. Unfortunately, the results and findings could not be compared to the results of the other participants of the intercomparison, as these are not available yet.

## 5.2 Methods

### 5.2.1 Samples

We received five different gaseous samples in 3 L Tedlar® gas sampling bags fitted with screw cap combo valves (samples A to E). Samples D and E were biogases, while samples A, B and C were blends of biogas and natural gas<sup>3</sup>. Sample A was a mixture of natural gas with sample E (biogas), whereas samples B and C were blends from a mixture of sample D (biogas) with natural gas. The natural gas used for the blends contained methane (89 mol%), CO<sub>2</sub> (3 mol%), ethane (4 mol%), propane (1.5 mol%), isobutane (0.3 mol%), n-butane (0.3 mol%) and pentane (0.2 mol%). In this chapter, all reported concentrations are given in mole fractions.

A gas syringe (Pressure-Lok Series A-2, 5 ml, VICI, USA) was used for the extraction of aliquots from each sample bag. Since several gas extractions were planned for each gasbag, the outlet tubes of the bags were used instead of the septa from the bags to keep the bags contamination-free after the extractions of aliquots. To do so, the outlet of each gasbag was connected to a union tee, of which one port was connected to a dead end fitted with a septum, and the other to a scroll pump. Thus, the line was first evacuated, then the bag outlet valve was opened and finally a gas aliquot was extracted with a syringe through the septum.

### 5.2.2 Total combustion of the gas samples

Since the five gas samples contained over 90% hydrocarbons, their elevated carbon content allowed producing graphite targets for the <sup>14</sup>C measurements, to get the best accuracy and precision available. Hence, 3 mL aliquots of each sample were combusted, graphitized and measured as solid targets with the MICADAS AMS. For this purpose, the PURIF (see Figure 2.2b) was slightly modified: (1) a union tee fitted with a septum on its side port was inserted in the external helium supply of the PURIF, just after MFC3; and (2) one of the six U-shaped collection traps of the PURIF was replaced by an empty U-shaped tube to avoid an irreversible

---

<sup>3</sup> Personal communication from the Centre for Isotope Research.

adsorption of low-volatile compounds onto the charcoal material. The aliquots were injected with a syringe through the septum of the union tee, and directly transferred through the empty U-shaped tube to the combustion oven. There, each aliquot was combusted at 950 °C in a He flow of 10 ml min<sup>-1</sup> for 10 min, following the standard procedure of the PURIF described in 2. The combustion product CO<sub>2</sub> could not be flame-sealed in a small glass ampoule as usually, because the typical amounts recovered were over 1000 µg C. To tackle this limitation, a new line was added to the CO<sub>2</sub> recovery part of the PURIF, which accepts 8 mm OD glass ampoules for the sealing of larger sample volumes.

### 5.2.3 Isolation of pure subfractions

As reported in Chapter 2, the PURIF of the MPPS allows the chromatographic purification of CH<sub>4</sub> and CO<sub>2</sub> from gas mixtures up to a volume of 10 mL, via a direct syringe injection of the samples into the inlet of the GC column. 3 mL of each gas mixture were processed through the PURIF to recover pure CH<sub>4</sub> and CO<sub>2</sub>, following the general procedure described in Chapter 2. The GC method was modified to ensure that higher alkanes, which have a relatively low volatility, would not remain stuck in the packed column and potentially contaminate the next sample. Thus, the inlet pressure was increased to 30 psig instead of 20 psig, resulting in a higher column flow and thus shorter retention times. Finally, the runtime was extended by 80 minutes at 280 °C, to guarantee that ethane, propane, isobutane, butane, and pentane would also elute from the column. For each gas sample, the pure CH<sub>4</sub> subfraction collected in a charcoal trap after the GC was first combusted and flame-sealed in a large glass ampoule. Then, the procedure was repeated for the CO<sub>2</sub> subfraction. However, as the samples contained only small amounts of CO<sub>2</sub> (~3%), the CO<sub>2</sub> recovery from the injection of 3 mL aliquots was yielding to a carbon amount of less than 40 µg, which is not sufficient for a CO<sub>2</sub> graphitization. Thus, the pure CO<sub>2</sub> fractions eluting from the GC column were flame-sealed in a small glass ampoule, as typically done for atmospheric CH<sub>4</sub> samples.

In addition to CH<sub>4</sub> and CO<sub>2</sub>, C<sub>2</sub>H<sub>6</sub> and C<sub>3</sub>H<sub>8</sub> subfractions in sample C were also isolated, as this sample contained the largest proportion of natural gas. While the purification of C<sub>2</sub>H<sub>6</sub> followed the general procedure for atmospheric CH<sub>4</sub> samples, C<sub>3</sub>H<sub>8</sub> was not volatile enough to allow its desorption from a charcoal trap at 95 °C. To overcome this issue, the C<sub>3</sub>H<sub>8</sub> subfraction eluting from the GC was first trapped at liquid nitrogen temperature in an empty U-shaped tube. The trap was then heated to 95 °C, and C<sub>3</sub>H<sub>8</sub> was combusted and recovered as usually. Similarly to the CO<sub>2</sub> subfractions, the two higher alkane fractions were flame-sealed in a small glass ampoule.

### 5.2.4 <sup>14</sup>C measurements

The procedure for the <sup>14</sup>C analyses of the total combustion and the pure CH<sub>4</sub> fraction of each gas sample followed the protocol for the measurement of atmospheric CO<sub>2</sub> samples, described in section 1.4.2.2. In short, the large CO<sub>2</sub> ampoules were cracked in a manual ampoule cracker

connected to the CIS, graphitized with the AGE and their  $^{14}\text{C}$  content was measured with the AMS. Conversely, the pure  $\text{CO}_2$ ,  $\text{C}_2\text{H}_6$  and  $\text{C}_3\text{H}_8$  fractions were directly measured as gas samples using the combination GIS-AMS. The typical precision achieved for a graphite measurement was 0.2–0.3%, and 0.8–1.0% for a direct gas measurement (Szidat et al., 2014).

## 5.3 Results and discussion

### 5.3.1 Composition

The chromatographic separation of the five gas samples is shown in Figure 5.1. The individual gas components eluted with respect to their respective volatility, with pentane presenting the longest retention time (90 min). For clarity, pentane that was not present in the biogas samples and barely detected in the blends of biogas and natural gas is not displayed. It should first be noted that a significant amount of air was visible in all the samples aliquots extracted from the gasbags, contributing to 7–10% of the gas volumes injected into the GC column. Although it is quite common to find some  $\text{N}_2$  and  $\text{O}_2$  in raw biogas (Rasi et al., 2007) and natural gas (Faramawy et al., 2016), such an air content was not expected for the biogas and natural gas samples of the study, as communicated by the initiators of the intercomparison. The contamination came from atmospheric air, which was added to the aliquots extracted from each gasbag. The culprits were found to be the septum screws from the bag outlets, which were not tightly connected to the valves of the bags, leaking air into the valves to the outlet tubes. Tightening the screw caps and keeping the sampling time as short as possible allowed to mitigate the air leakage. This issue, which also affected the results from other participants of the intercomparison, explains why the carbon amounts recovered after each sample combustion (1000–1400  $\mu\text{g C}$ ) were slightly lower than expected carbon content of the injection of 3 mL aliquots ( $\sim 1400 \mu\text{g C}$ ). Fortunately, this contamination with atmospheric air should not have any measurable influence on the  $^{14}\text{C}$  results, as  $\text{CO}_2$  is only  $\sim 415$  ppm in air. Indeed, it would correspond to a maximum of 6 ng modern carbon added to the aliquots, which has to be compared to the measured sample masses (60–1400  $\mu\text{g C}$ ).

As expected from pure biogas, sample D does not contain any higher alkanes. We were informed that sample E might incorporate a small amount of natural gas added at the biogas plant, which is confirmed by small  $\text{C}_x\text{H}_y$  peaks visible on the chromatogram (see Figure 5.1e). The  $\text{CO}_2$  fractions of the biogas samples are about 3%, which is quite low and indicates that the samples analyzed have already been upgraded at the plant (Awe et al., 2017).

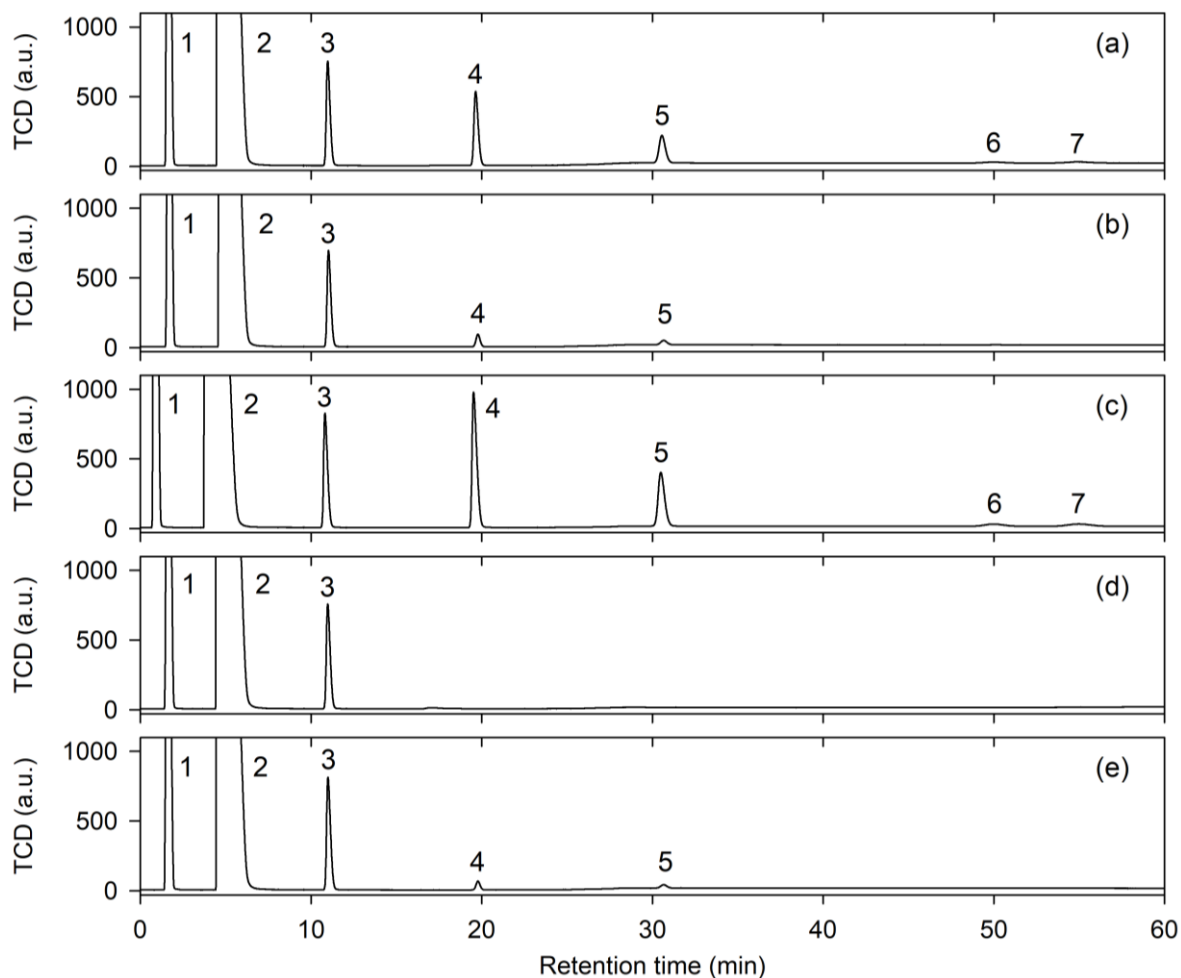


Figure 5.1 Chromatographic separation of 3 mL of each gaseous sample. The GC run lasted 100 min, with  $C_5H_{12}$  eluting after 90 min (not shown here). 1:  $N_2/O_2$ . 2:  $CH_4$ . 3:  $CO_2$ . 4:  $C_2H_6$ . 5:  $C_3H_8$ . 6:  $C_4H_{10}$  (isobutane). 7:  $C_4H_{10}$  (n-butane). (a) Sample A. (b) Sample B. (c) Sample C. (d) Sample D. (e) Sample E.

The estimation of the relative proportion of biogas and natural gas in samples A, B and C is not straightforward. The main reason is that the sensitivity of the TCD depends on the thermal conductivity of individual fractions and also on the carrier gas flow rate, the latter being not constant as the flow rate decreases during the GC run (see Chapter 2). Sample B, which is a mixture of biogas (sample D) and natural gas, seems to be mostly composed of biogas, as indicated by the very small  $C_2H_6$  and  $C_3H_8$  peaks. In contrast, samples A and C contain a larger fraction of natural gas. The relative proportion of natural gas in these two samples can be compared, as they both consist of blends of biogas, which include little to no higher alkanes, and natural gas from the same origin. Hence, the peak areas of  $C_2H_6$  and  $C_3H_8$  being twice as large in sample C as in sample A, it suggests that sample C contains approximately two times more natural gas than sample A. Those findings should be confirmed by  $^{14}C$  measurements of each gas sample, as biogas and natural gas are modern and  $^{14}C$ -free, respectively (Dijs et al., 2006).

### 5.3.2 Radiocarbon content

The  $^{14}\text{C}$  contents of the five samples are listed in Table 5.1. The results are reported for the total carbon fraction (total combustion), but also for the pure subfractions such as  $\text{CH}_4$ ,  $\text{CO}_2$ ,  $\text{C}_2\text{H}_6$  and  $\text{C}_3\text{H}_8$  alone.

Table 5.1  $^{14}\text{C}$  content of the five biogas and natural gas samples. The  $F^{14}\text{C}$  values of the pure subfractions separated with the MPPS are corrected for constant contamination ( $0.35 \pm 0.10 \mu\text{g C}$  with an  $F^{14}\text{C}$  of  $0.35 \pm 0.18$ ) and cross contamination ( $0.4 \pm 0.2\%$ ). The reported uncertainties ( $1\sigma$ ) include sample pretreatment and AMS measurement.

Sample	$F^{14}\text{C}$ (total)	$F^{14}\text{C}$ ( $\text{CH}_4$ )	$F^{14}\text{C}$ ( $\text{CO}_2$ )	$F^{14}\text{C}$ ( $\text{C}_2\text{H}_6$ )	$F^{14}\text{C}$ ( $\text{C}_3\text{H}_8$ )
A	$0.7289 \pm 0.0018$	$0.7631 \pm 0.0019$	$0.498 \pm 0.007$		
B	$0.9635 \pm 0.0023$	$0.9716 \pm 0.0023$	$0.641 \pm 0.007$		
C	$0.4597 \pm 0.0013$	$0.5007 \pm 0.0015$	$0.372 \pm 0.005$	$0.053 \pm 0.006$	$0.025 \pm 0.002$
D	$1.0127 \pm 0.0025$	$1.0178 \pm 0.0024$	$0.856 \pm 0.008$		
E	$0.9941 \pm 0.0024$	$0.9981 \pm 0.0023$	$0.880 \pm 0.008$		

The  $^{14}\text{C}$  results from the total combustion of the five gas samples confirm the findings from the chromatograms (see Figure 5.1). Hence, as expected from samples collected at a biogas plant, samples D and E present the highest  $^{14}\text{C}$  contents. Sample E was expected to contain a small amount of natural gas added at the biogas plant, which is confirmed by the slightly lower  $^{14}\text{C}$  content of sample E compared to sample D ( $F^{14}\text{C}$  values of 0.9941 and 1.0127, respectively). Samples A, B and C, which are blends of biogas and natural gas, display intermediate  $^{14}\text{C}$  values according to the fraction of natural and biogas in each gasbag. Sample C contains the largest proportion of natural gas ( $F^{14}\text{C} = 0.4597$ ), followed by sample A ( $F^{14}\text{C} = 0.7289$ ) and sample B ( $F^{14}\text{C} = 0.9635$ ), the latter including a very small amount of natural gas.

As expected from the large proportion of  $\text{CH}_4$  in the five gas samples ( $> 89\%$ ), the  $F^{14}\text{C}$  values of the final mixtures are close to the respective  $F^{14}\text{C}$  values of  $\text{CH}_4$  alone. The first measurement from the total combustion of sample C yielded to an  $F^{14}\text{C}$  of 0.4902 (not reported in Table 5.1). This value was surprisingly close to  $\text{CH}_4$  alone ( $F^{14}\text{C} = 0.5007$ ), as significant amounts of ethane, propane and butane from the natural gas component were expected to contribute to a decrease of the  $F^{14}\text{C}$  value of the total mixture (see Figure 5.1c). During the first tests of a total combustion of the gas samples, the gas aliquots were first loaded into a charcoal trap prior to their release and combustion. Unfortunately, less volatile components such as propane, butane, pentane and to some extent ethane were not fully desorbed from the trap and were therefore not combusted and recovered as  $\text{CO}_2$  (Ray and Box, 1950). To overcome this issue, the total combustions of samples A, B, C and E were repeated by replacing the charcoal trap with an empty U-tube, as described in section 5.2.2. For sample C, the  $^{14}\text{C}$  content of  $\text{CH}_4$  alone ( $F^{14}\text{C} = 0.507$ ) is significantly higher than the  $^{14}\text{C}$  content of the total gas mixture ( $F^{14}\text{C} = 0.4597$ ). As anticipated from natural gas components, ethane and propane

revealed to be fossil, with  $F^{14}\text{C}$  values of 0.053 and 0.025, respectively. These two values are slightly too elevated for pure fossil compounds, which is probably caused by the contribution from the larger bleeding of the GC column when eluting higher alkanes at 280 °C. Thus, it is confirmed that the presence of higher alkanes in sample C contributes to a significant lowering of the  $^{14}\text{C}$  content of the total mixture with respect to  $\text{CH}_4$  alone. Hence, the influence of higher alkanes on the final  $F^{14}\text{C}$  result of the total carbon content in the samples should not be overlooked. Indeed, even if they are in relatively small proportions, the molar contribution of  $\text{C}_2\text{H}_6$ ,  $\text{C}_3\text{H}_8$  and  $\text{C}_4\text{H}_{10}$  to the total carbon amount is 2, 3 and 4 times higher than the corresponding contribution of  $\text{CH}_4$  and  $\text{CO}_2$ , respectively. This example emphasizes the fact that the use of an improper loading or combustion method could yield to significant errors in the estimation of the biogenic carbon fraction of a biofossil gas mixture.

Interestingly, the  $\text{CO}_2$  fraction in both biogas samples has a lower  $F^{14}\text{C}$  value than the  $\text{CH}_4$  fraction. This observation is confirmed by the total  $^{14}\text{C}$  content of sample D ( $F^{14}\text{C} = 1.0127$ ), which is the result of the mixing of 97%  $\text{CH}_4$  ( $F^{14}\text{C} = 1.0178$ ) with 3%  $\text{CO}_2$  ( $F^{14}\text{C} = 0.856$ ). It is difficult to explain why  $\text{CO}_2$  has a lower  $^{14}\text{C}$  content than  $\text{CH}_4$ , as both fractions should originate from the same digested materials in biogas plants (Palstra and Meijer, 2014). Nevertheless, in this particular case, the bioC content of the gas sample determined from the  $^{14}\text{C}$  measurement of the total fraction could significantly differ from a bioC determination based on  $\text{CH}_4$  alone. The problem would be strengthened when measuring raw biogas samples, which often contain up to 40%  $\text{CO}_2$  (Rasi et al., 2007). The instigators of the intercomparison, who confirmed our finding concerning the lower  $^{14}\text{C}$  of the  $\text{CO}_2$  subfraction, will further investigate this surprising observation.

As both biogas and natural gas include  $\text{CO}_2$ , the  $F^{14}\text{C}$  values of the  $\text{CO}_2$  fractions for the three blends depend on the respective  $\text{CO}_2$  concentrations in the pure biogas and natural gas samples, their corresponding  $^{14}\text{C}$  content and the proportion of biogas and natural gas in the blends. This explanation stays valid for the  $\text{CH}_4$  fraction in the blends. As  $\text{CH}_4$  and  $\text{CO}_2$  are fossil in the natural gas component, the  $F^{14}\text{C}$  contents of  $\text{CH}_4$  and  $\text{CO}_2$  in the blends decrease when the proportion of natural gas increases (see Table 5.1).

### 5.3.3 Stable isotope composition

Stable isotope measurements provide useful information concerning the origin of biogas and natural gas samples, as different formation pathways are associated with a variety of isotopic signatures (Whiticar, 1999). Depending on the type of raw material and the biophysical conditions leading to their formation, biogas samples show a large variety of  $\delta^{13}\text{C}$  values (Palstra and Meijer, 2014; De Vrieze et al., 2018; Kufka et al., 2019). In general, biogas samples are more depleted in heavy isotopes than natural gas samples (Miller et al., 2002).

The  $\delta^{13}\text{C}$  results of the AMS, reported in Table 5.2, unveil some interesting aspects. First, the  $\delta^{13}\text{C}$  value of the  $\text{CH}_4$  fraction from the two biogas samples ( $\delta^{13}\text{C}\text{-CH}_4 \approx -64\text{‰}$ ) indicates a

rather strong depletion in heavy isotopes. In contrast, the CO<sub>2</sub> fractions of these two samples are strongly enriched ( $\delta^{13}\text{C-CO}_2 \approx +17\text{‰}$ ). Similar values have been reported for the biogas production in landfills (Laukenmann et al., 2010; Palstra and Meijer, 2014), where the bacterial reduction of CO<sub>2</sub> to CH<sub>4</sub> leads to an enrichment of the remaining fraction (Conrad, 2005; Zyakun et al., 2010). The  $\delta^{13}\text{C}$  content of pure natural gas could not be measured, as it was already mixed with biogas in samples A, B and C. However, the  $\delta^{13}\text{C}$  value of the blends generally increases when the proportion of natural gas increases, which indicates that the natural gas fraction is significantly more enriched in heavy isotopes than the biogenic fraction. Conversely, the CO<sub>2</sub> content from the natural gas component does not show a strong enrichment such as in biogas, as expected from its different formation process (Faramawy et al., 2016).

*Table 5.2 Stable isotope composition ( $\delta^{13}\text{C}$  vs VPDB) of the five samples (AMS results). The AMS  $\delta^{13}\text{C}$  values show a long-term standard uncertainty of 1.2‰ for graphite measurements (Szidat et al., 2014), and 1.9‰ for direct CO<sub>2</sub> measurements.*

Sample	Type	$\delta^{13}\text{C}_{\text{tot}}$ (‰)	$\delta^{13}\text{C-CH}_4$ (‰)	$\delta^{13}\text{C-CO}_2$ (‰)
A	Biogas + natural gas	-46.6	-60.6	-8.7
B	Biogas + natural gas	-60.0	-64.5	-1.0
C	Biogas + natural gas	-48.7	-51.6	-14.0
D	Biogas	-67.0	-64.5	+17.9
E	Biogas	-62.2	-64.0	+16.8

### 5.3.4 Biogenic carbon fraction

The biogenic carbon fraction ( $f_{\text{bioC}}$ ) of a gas sample is generally determined using Equation 5.1 (Mohn et al., 2008; Calcagnile et al., 2011; Palstra and Meijer, 2014):

$$f_{\text{bioC}} = \frac{F^{14}\text{C}_{\text{sample}}}{F^{14}\text{C}_{100\%\text{bioC}}} \quad \text{Equation 5.1}$$

With  $F^{14}\text{C}_{\text{sample}}$  the <sup>14</sup>C content of the sample and  $F^{14}\text{C}_{100\%\text{bioC}}$  the measured or estimated <sup>14</sup>C content of the pure biogenic gas that lies at the basis of the sample. The choice of an  $F^{14}\text{C}$  value as a reference for 100% biogenic is therefore crucial, as an incorrect value for 100% biogenic can lead to significant errors in the calculation of  $f_{\text{bioC}}$ . Unfortunately, the bioC and fossil fractions in biofossil gas mixtures are already mixed, which means that the <sup>14</sup>C content of the biogenic fraction cannot be measured and has to be estimated. As seen in section 1.4.3, large variations in atmospheric <sup>14</sup>CO<sub>2</sub> since the 1950s are observed, which are due to the combined influence of <sup>14</sup>C releases from bomb tests and the addition of <sup>14</sup>C-free fossil fuel CO<sub>2</sub> (Fellner and Rechberger, 2009; Levin et al., 2010; Turnbull et al., 2017). If the origin of the bioC fraction is known, the  $F^{14}\text{C}$  content of atmospheric CO<sub>2</sub> during the average year of growth of the plant materials is used to represent  $F^{14}\text{C}_{100\%\text{bioC}}$  (Palstra and Meijer, 2014).

In the particular case of the study presented here, sample D is pure biogas, which was mixed with natural gas to create the blends (samples B and C). Therefore, its measured  $^{14}\text{C}$  content ( $F^{14}\text{C} = 1.0127$ ) can be used as a reference for 100% biogenic when calculating the bioC fraction of samples B and C. Similarly, sample E was mixed with natural gas to form sample A. However, as sample E contains a small proportion of natural gas added at the biogas production plant, its measured  $^{14}\text{C}$  content ( $F^{14}\text{C} = 0.9941$ ) cannot be used for a 100% biogenic reference and the value from sample D was used instead.

Prior to the calculation of the bioC fraction of the five samples using Equation 5.1, an additional potential source of error should be considered. Indeed, the  $F^{14}\text{C}$  values (total fraction) reported in Table 5.1 are corrected for isotopic fractionation to a normalized value of  $-25\text{‰}$  (see Equation 1.4), using the measured  $\delta^{13}\text{C}$  value in the total carbon fraction present in the samples. Since natural gas is radiocarbon-free, the  $F^{14}\text{C}$  content of the gas mixture should not be corrected for isotopic fractionation that happened to the fossil fraction (Palstra and Meijer, 2014). Thus, the isotope fractionation correction should only correct for fractionation that happened to the bioC fraction alone, based on the  $\delta^{13}\text{C}$  value of the biogenic fraction. As explained previously, since pure biogas (sample D) has a  $\delta^{13}\text{C}$  value of  $-67\text{‰}$ , which is significantly lower than the  $\delta^{13}\text{C}$  value of the natural gas component (probably about  $-32\text{‰}$ ), the  $\delta^{13}\text{C}$  values in the blends differ from the  $\delta^{13}\text{C}$  value of the bioC fraction alone. Hence, the  $F^{14}\text{C}$  values of samples A, B, C and E should be corrected with respect to the  $\delta^{13}\text{C}$  value of the biogas component alone ( $-67\text{‰}$ ), instead of the measured  $\delta^{13}\text{C}$  values of the mixtures ( $\delta^{13}\text{C}_{\text{tot}}$  in Table 5.2). Knowing the fractionation factor associated with isotopic fractionation corrections when reporting  $F^{14}\text{C}$  values (see Equation 1.4), the  $^{14}\text{C}$  content of a sample ( $F^{14}\text{C}_{\delta^{13}\text{C}_{\text{bioC}}}$ ) corrected with respect to the  $\delta^{13}\text{C}$  value of the biogas component alone ( $\delta^{13}\text{C}_{\text{bioC}}$ ) is given by (Palstra and Meijer, 2014):

$$F^{14}\text{C}_{\delta^{13}\text{C}_{\text{bioC}}} = F^{14}\text{C}_{\delta^{13}\text{C}_{\text{tot}}} \cdot \left[ \frac{1 + \delta^{13}\text{C}_{\text{tot}}}{1 + \delta^{13}\text{C}_{\text{bioC}}} \right]^2 \quad \text{Equation 5.2}$$

With  $F^{14}\text{C}_{\delta^{13}\text{C}_{\text{tot}}}$  being the measured total  $^{14}\text{C}$  content of a sample (reported in the second column of Table 5.1). The bioC fractions ( $f_{\text{bioC}}$ ) of the five samples are given in Table 5.3, where  $f_{\text{bioC}_{\delta^{13}\text{C}_{\text{tot}}}}$  is the bioC fraction calculated with the  $F^{14}\text{C}$  results of the AMS ( $F^{14}\text{C}_{\delta^{13}\text{C}_{\text{tot}}}$ ), and  $f_{\text{bioC}_{\delta^{13}\text{C}_{\text{bioC}}}}$  is the bioC fraction calculated with the corrected  $F^{14}\text{C}$  value from Equation 5.2.

Table 5.3 Biogenic carbon fractions ( $f_{bioC}$ ) of the five gas samples, calculated from Equation 5.1, with fractionation corrections applied based on  $\delta^{13}C_{tot}$  ( $f_{bioC\_delta13C\_tot}$ ) and on  $\delta^{13}C_{bioC}$  ( $f_{bioC\_delta13C\_bioC}$ ). The results of sample D ( $F^{14}C = 1.0127$  and  $\delta^{13}C = -67\text{‰}$ ) are used as a reference for 100% biogenic in the calculation of the bioC fractions of the other gas samples. See text for details.

Sample	$\delta^{13}C_{tot}$ (‰)	$\delta^{13}C_{bioC}$ (‰)	$F^{14}C_{delta13C\_tot}$	$F^{14}C_{delta13C\_bioC}$	$f_{bioC\_delta13C\_tot}$ (%)	$f_{bioC\_delta13C\_bioC}$ (%)
A	-46.6	-67.0	0.7289	0.7611	72.0	75.2
B	-60.0	-67.0	0.9635	0.9780	95.1	96.6
C	-48.7	-67.0	0.4597	0.4780	45.4	47.2
D	-67.0	-67.0	1.0127	1.0127	100.0	100.0
E	-62.2	-67.0	0.9941	1.0044	98.2	99.2

The calculated bioC fractions are in good agreement with the respective compositions of the samples shown in Figure 5.1, with sample C containing roughly twice the amount of natural gas as sample A. In theory, the absolute deviation in the bioC fraction due to an incorrect fractionation correction (using  $\delta^{13}C_{tot}$  instead of  $\delta^{13}C_{bioC}$ ) increases with the difference between the  $\delta^{13}C$  values of the bioC and the fossilC fractions, and is maximal for samples with 50% bioC (Palstra and Meijer, 2014). Here, the largest absolute deviation between the corrected and uncorrected bioC fraction was found in sample A, with a difference of +3.2% between  $f_{bioC\_delta13C\_bioC}$  and  $f_{bioC\_delta13C\_tot}$ . As the fossil fraction ( $\delta^{13}C \approx -32\text{‰}$ ) is significantly less depleted in heavy isotopes than the bioC fraction ( $\delta^{13}C = -67\text{‰}$ ), actual bioC fractions in the gas mixtures are systematically underestimated if erroneous fractionation corrections are applied. One should however keep in mind that the study reported here represents an ideal case, were pure biogas (sample D) could be measured ( $F^{14}C$  and  $\delta^{13}C$ ) and used as a reference for the determination of the bioC fraction of the other four samples. When considering a biofossil gas mixture, the composition of the pure bioC fraction is often not available and has to be estimated, which can result in significant errors in the calculation of the bioC fraction as shown in Table 5.3 (Dijs et al., 2006; Palstra and Meijer, 2014).

## 5.4 Conclusion

The small intercomparison study reported in this chapter presented another application of  $^{14}C$  source apportionment, to estimate the biogenic carbon fraction in fuel mixtures containing biogas and natural gas, as biogas is a renewable source of energy associated with a growing demand. First, aliquots from the five gas samples were combusted and their radiocarbon contents were measured with the AMS. In addition, the versatility of the MPPS allowed an investigation of the individual components in each gas sample, which were isolated, combusted, recovered as pure  $CO_2$  and analyzed with the AMS.

The chromatographic separation of the gas mixtures allowed to detect the presence of natural gas in the samples, as ethane and other higher alkanes can be used as a tracers for natural gas

(Aydin et al., 2011; Simpson et al., 2012; Hausmann et al., 2016). The results highlight two common problems arising when trying to estimate the biogenic carbon fraction of samples consisting of a mixture of biogenic and fossil carbon. First, the choice of a  $^{14}\text{C}$  reference for 100% biogenic carbon, which is usually not known and needs an approximation, which reduces the precision of the estimation of the biogenic carbon fraction (Palstra and Meijer, 2014). Second, the study highlighted the potential bias associated with erroneous isotope fractionation corrections, which can be significant if the biogenic and fossil fractions of the gas samples have very dissimilar stable isotope compositions.

In addition to the challenges aforementioned, the biogas samples showed a significantly lower  $^{14}\text{C}$  content for the  $\text{CO}_2$  fraction than for the biomethane fraction, which is surprising as both fractions were expected to originate from a common organic material. The reason for such a low  $^{14}\text{CO}_2$  content remains unclear. If it is an artifact associated with the scrubbing of  $\text{CO}_2$  during the upgrade of raw biogas, the  $^{14}\text{C}$  measurement of the total carbon fraction will lead to an underestimation of the biogenic carbon fraction in the gas mixture. On the contrary, if raw biogas produced at the plant contains a proportion of  $\text{CO}_2$  from fossil origin, its removal during the upgrading process will result in an underestimation of the fossil fraction of the raw material used by the plant. As Palstra and Meijer (2014) pointed out, the knowledge of the origin and composition of the organic material is essential when trying to provide a robust estimate of the biogenic fraction of biofossil gas mixtures.

## 6. General conclusions and outlook

### 6.1 Summary of the achievements

Owing to the complexity of CH<sub>4</sub> sources, which are highly sensitive to human activities and climate change, the greenhouse gas CH<sub>4</sub> deserves special attention. Despite all efforts and tools implemented for its understanding, the recent evolution of atmospheric CH<sub>4</sub> keeps surprising us. Notwithstanding the challenges associated with the radiocarbon analysis of atmospheric CH<sub>4</sub>, it could be used to apportion fossil and modern sources at local and regional scales. In this framework, this thesis carried two objectives: First, the development of an analytical setup for the preparation of pure atmospheric CH<sub>4</sub> samples for <sup>14</sup>C analysis. Second, the validation of the setup and the source apportionment technique with the collection and radiocarbon measurement of atmospheric CH<sub>4</sub> samples.

The setup combines a CH<sub>4</sub> preconcentration line and a preparative GG technique, which together offer a maximum of flexibility, a rather short preparation time and high-quality results. The precision of the <sup>14</sup>C method for a source apportionment of atmospheric CH<sub>4</sub> is not only limited by the <sup>14</sup>C measurement precision, but also by potential contamination during the sample pretreatment and other sources of error such as the choice of a background reference and the influence of nuclear power plants. By sacrificing a bit of measurement precision via the direct measurement of gas samples with the AMS, we dramatically reduced the requested sample size from 1000 L to 20–60 L air. The benefits of such a strategy are numerous: First, the sample collection requires minimal equipment, which allows the sampling in areas devoid of any installation. Second, the size of the preconcentration line is considerably reduced compared to other typical CH<sub>4</sub> preparation setups, resulting in significantly shorter processing and cleaning procedures. The addition of a purification setup does not extend the total preparation time, as both setups can be used in parallel with the recovery of CO<sub>2</sub> from the preconcentration line when CH<sub>4</sub> is purified in the GC column. The use of a preparative GC technique ensures the recovery of pure CH<sub>4</sub> samples and allows a quality check of the overall performance of the pretreatment. The choice of small sample sizes allows reducing the preparation time by skipping the graphitization step, as the CH<sub>4</sub>-derived CO<sub>2</sub> samples are directly measured with the AMS. Finally, we showed that the purification setup can be used as a standalone for the preparation of pure CO, CH<sub>4</sub>, CO<sub>2</sub> and higher alkanes from higher concentration gas mixtures.

Since the beginning of 2019, we regularly collected atmospheric air samples at three strategic locations in Switzerland and performed a combined analysis of their <sup>14</sup>CH<sub>4</sub> and <sup>14</sup>CO<sub>2</sub> contents. The results from the Jungfrauoch Research Station revealed that in addition to being a suitable reference for continental background  $\Delta^{14}\text{CO}_2$ , the site is also well adapted for background  $\Delta^{14}\text{CH}_4$  as long as the sampling is performed when the PBL is low. A mean  $\Delta^{14}\text{CH}_4$

of 354‰ obtained at Jungfrauoch allowed us to address the lack of published measurements of background  $\Delta^{14}\text{CH}_4$  since the early 2000s. The  $\Delta^{14}\text{CO}_2$  values measured at Beromünster and Bern were compared to the background values from Jungfrauoch, which allowed an estimation of the fossil fuel  $\text{CO}_2$  component at these two locations. An update of the long-term  $\Delta^{14}\text{CO}_2$  measurements conducted at Beromünster revealed that regional sources of fossil fuel  $\text{CO}_2$  emissions did not significantly change since 2013. Fossil fuel  $\text{CO}_2$  emissions are larger in Bern, which was expected from the sampling in a city where local fossil sources are dominant. The comparison of  $\Delta^{14}\text{CO}_2$  and  $\Delta^{14}\text{CH}_4$  values measured at Beromünster and Bern shed light on the striking difference between the main drivers of the observed variations of the  $^{14}\text{C}$  content in these two gas species. In contrast to the  $\Delta^{14}\text{CO}_2$  signal, which displays depletions with respect to background values imputed to fossil fuel emissions, the  $\Delta^{14}\text{CH}_4$  signal is characterized by large fluctuations between background levels and very high values. The observed pattern is explained by the high sensitivity of atmospheric  $\Delta^{14}\text{CH}_4$  to  $^{14}\text{C}$  emissions from NPPs, because  $\text{CH}_4$  is much less abundant than  $\text{CO}_2$  in the atmosphere. As a result, the  $\Delta^{14}\text{CH}_4$  values obtained at Beromünster and Bern did not allow an estimation of regional fossil  $\text{CH}_4$  components under the current conditions. Indeed, any potential depletion of atmospheric  $\Delta^{14}\text{CH}_4$  due to fossil or biogenic emissions was hidden by the large scatter induced by the variable contribution from NPPs.

These frustrating  $^{14}\text{CH}_4$  results motivated the conduction of a small field study near the Gösgen NPP during a revision period, as NPPs holding a PWR emit  $^{14}\text{C}$  mainly as  $^{14}\text{CH}_4$  and potential large emissions are expected at the beginning of maintenance periods. With a measured atmospheric  $^{14}\text{CH}_4$  content up to about 1800 times over background levels at 6 km downwind the NPP, our results confirmed that PWRs are extremely large point source emitters. In regions equipped with PWRs, the combination of sporadic discharges over periods of a few hours to days and a dispersion of the plume in accordance with meteorological conditions are the main drivers to the variability of atmospheric  $^{14}\text{CH}_4$  levels at a specific location. In addition to being a major hindrance to the use of  $^{14}\text{CH}_4$  measurements for a  $\text{CH}_4$  source apportionment, the  $^{14}\text{C}$  discharge from the Gösgen NPP had also a very large impact on atmospheric  $^{14}\text{CO}_2$ , with a maximum  $^{14}\text{CO}_2$  content at 6 km downwind the NPP of more than 3 times over atmospheric background values. Such an enhancement is at least 2–3 orders of magnitude larger than average values found in biological samples at a similar distance to NPPs. Thus, although PWRs emit on average about ten times less  $^{14}\text{CO}_2$  than BWRs, large discharges over short periods turn them into very strong sources, which have the potential to create significant biases in the determination of the fossil fuel  $\text{CO}_2$  component at a site. These stunning results questioned the use of constant EFs for the simulation of the atmospheric  $^{14}\text{C}$  impact of PWRs and a continuous monitoring of  $^{14}\text{CH}_4$  and  $^{14}\text{CO}_2$  releases from PWRs seems a prerequisite for a meaningful consideration of their impact in  $^{14}\text{C}$  source apportionments of  $\text{CH}_4$  and  $\text{CO}_2$ . Although disappointing when applied in regions of nuclear activities, a small simulation showed that measurements of atmospheric  $^{14}\text{CH}_4$  with the setup presented in this thesis have

the potential to apportion biogenic and fossil emissions of CH<sub>4</sub>. It further revealed that the precision of the relative contributions of these two sources will improve with increasing emissions, i.e. for cases where mitigation strategies may be implemented.

Finally, the participation to a laboratory intercomparison presented another application of <sup>14</sup>C measurements as a source apportionment tool, for the evaluation of the biogenic carbon fraction in blends of biogas and natural gas. The flexibility of the setup was used to measure the <sup>14</sup>C content of individual subfractions of the gas mixtures, which allowed emphasizing the potential biases associated with the method.

## 6.2 Future technical developments

The development of an analytical setup is a permanent process, usually consisting of small modifications adding to the overall quality of the results. Two axes of improvement should be explored: ameliorations of existing features and adaptations to increase the versatility of the MPPS.

As the system is mostly operated manually, the modification or automation of individual steps should only be considered if they significantly contribute to an improvement of the overall quality, an increase of the sample throughput or a reduction of the operator's workload. As an obvious next step, it has been shown that the CO<sub>2</sub> recovery method needs improvements. First, the recovery should be complete to avoid isotopic fractionation effects and allow an estimation of the original CO<sub>2</sub> mole fraction in the air sample. To do so, the evacuation time of the RDT could be prolonged and CO<sub>2</sub> from the RDT should be flushed to a liquid-nitrogen-cooled U-trap equipped with inlet and outlet, as proposed by Brenninkmeijer and Röckmann (1996). Second, the CaSO<sub>4</sub> used for the drying of the air samples should be replaced by another desiccant such as SICAPENT® (P<sub>2</sub>O<sub>5</sub>) to avoid a parasitic absorption of CO<sub>2</sub> leading to a lower quality of the <sup>14</sup>CO<sub>2</sub> results.

Another amelioration of paramount importance is the possibility to measure the CH<sub>4</sub> mole fractions accurately. We showed in Chapter 3 that because all natural sources of CH<sub>4</sub> have a lower <sup>14</sup>C content than atmospheric air, the fossil fraction of recently added CH<sub>4</sub> in the measured air sample depends on both the <sup>14</sup>CH<sub>4</sub> depletion compared to a background reference and the amount of excess CH<sub>4</sub> in the air sample. Unfortunately, if not directly measured at the collection site (e.g. like at Beromünster), the CH<sub>4</sub> mole fraction in a sample is just estimated from the volume preconcentrated (typically 60 L) and the amount of CH<sub>4</sub>-derived CO<sub>2</sub> recovered in a glass ampoule. Indeed, the co-elution of CH<sub>4</sub> and Kr from the GC column impedes the determination of CH<sub>4</sub> mole fractions from the TCD peak area (see section 2.3.2.1). A first improvement might be to add a split to redirect a portion of the column eluate to an FID (e.g. 10%), as this type of detector is sensitive to hydrocarbons but not to noble gases. As the FID is a mass-sensitive device, it will not be affected by flow variations and should allow an estimation of the total amount of CH<sub>4</sub> in the preconcentrated samples. However, the

achievable precision will still be limited by the knowledge of the actual amount of sample processed through the preconcentration line and the CH<sub>4</sub> yield. An alternative is to use the FID as a standalone for the detection of CH<sub>4</sub> from calibrated volumes, such as a sample loop filled with an aliquot of the air sample. To get accurate results, CH<sub>4</sub> mole fractions should be measured with a dedicated gas analyzer in the original air sample. This task could be performed directly at the sampling site, as for Beromünster samples, or in the laboratory when starting a sample pretreatment.

The MPPS has been recently adapted to allow the preparation of pure CH<sub>4</sub> samples from CH<sub>4</sub>-rich environments such as wetlands or marine sediments, opening up new opportunities (Bantle, 2021). Combining information from radiocarbon and stable isotope analyses would be of great interest to obtain a signature of these CH<sub>4</sub> sources. However, the  $\delta^{13}\text{C}$  values obtained from AMS results do not meet the accuracy and precision required. If only interested in  $\delta^{13}\text{C}$  results, an aliquot of the CH<sub>4</sub>-derived CO<sub>2</sub> could be sealed in a small ampoule for an IRMS measurement prior to the recovery of the remaining CO<sub>2</sub> for <sup>14</sup>C analysis. If also interested in  $\delta\text{D}$  measurements, an aliquot of CH<sub>4</sub> should be collected before its combustion to CO<sub>2</sub>. Further tests need to be carried out to find the most reliable way to extract and store a CH<sub>4</sub> aliquot from the U-shaped collection traps after the GC. Unfortunately, co-eluting Kr is trapped together with CH<sub>4</sub> before the combustion process. Although Kr is known to interfere during  $\delta^{13}\text{C}$  measurements of CH<sub>4</sub> with an IRMS, it should not be the case for  $\delta\text{D}$  measurements after pyrolysis of CH<sub>4</sub> (Schmitt et al., 2013; Bock et al., 2017).

### 6.3 Further research

The biweekly <sup>14</sup>CH<sub>4</sub> and <sup>14</sup>CO<sub>2</sub> analyses conducted at Jungfraujoch, Beromünster and Bern since the beginning of 2019 will be continued. In addition to providing background reference values for regional CH<sub>4</sub> source apportionments, the continued  $\Delta^{14}\text{CH}_4$  measurements at Jungfraujoch will allow monitoring the global trend of atmospheric  $\Delta^{14}\text{CH}_4$ , which is mainly controlled by the respective strength of the NPP source, the fossil source and to a lesser extent the biogenic source (Lassey et al., 2007b). The collection of integrated samples over a period of 2–4 weeks will be implemented at Bern and Jungfraujoch. Along with the possibility to compare mean values with point sampling results, it should allow evaluating the possibility to install air samplers at other sites.

The large spatial and temporal variability of CH<sub>4</sub> emissions is a major hindrance to the estimation of the magnitude of individual sources, but also to the monitoring and forecasting of their evolution over long periods. Radiocarbon measurements might reveal a very useful additional tool in regions where remote sensing or observational networks detect large CH<sub>4</sub> emissions, but fail to estimate the relative contribution of each source. When different sources are identified, uncertainties could be reduced by an assessment of the source signatures (e.g.  $\Delta^{14}\text{CH}_4$  and  $\delta^{13}\text{C-CH}_4$ ) prior to the <sup>14</sup>C measurement of atmospheric CH<sub>4</sub> in the area.

Unfortunately, this thesis underlined that local and regional  $^{14}\text{C}$  source apportionments of atmospheric  $\text{CH}_4$  are strongly challenged by  $^{14}\text{C}$  emissions from NPPs. Thus, the technique should first be tested in regions where the impact of nuclear activities is low. As an example, the  $^{14}\text{C}$  tool might help detecting fugitive emissions from the natural gas supply in urban centers, which have been reported in other studies (Schwietzke et al., 2016; Plant et al., 2019). Africa and South America are good candidates, are they include some hotspots of emissions and do not host NPPs.

An alternative for the estimation of the  $\text{CH}_4$  and  $\text{CO}_2$  emissions from urban areas would be to measure upwind and downwind a city, which is a method that has been previously applied to apportion fossil fuel emissions from urban areas (Turnbull et al., 2015, 2019).

With the development of a new  $\text{CH}_4$  preconcentration and purification setup, this work is a key milestone for the practical use of atmospheric  $^{14}\text{C}$  measurements as an additional tool for a better understanding of regional  $\text{CH}_4$  sources. In combination with other monitoring and apportionment techniques, it should provide additional constraints on the  $\text{CH}_4$  budget and help tracking temporal changes of  $\text{CH}_4$  sources.

## 7. Bibliography

- Ahrens, D., Henson, R., 2015. *Meteorology today: An Introduction to Weather, Climate, and the Environment*, 11th ed. *Cengage Learning*.
- Alderliesten, C., Van Der Borg, K., De Jong, A.F.M., 1997. Contamination and Fractionation Effects in AMS-Measured  $^{14}\text{C}/^{12}\text{C}$  and  $^{13}\text{C}/^{12}\text{C}$  Ratios of Small Samples. *Radiocarbon* 40(1), 215–221. doi:10.1017/S0033822200018075.
- Allan, W., Lowe, D.C., Gomez, A.J., Struthers, H., Brailsford, G.W., 2005. Interannual variation of  $^{13}\text{C}$  in tropospheric methane: Implications for a possible atomic chlorine sink in the marine boundary layer. *J. Geophys. Res. D Atmos.* 110, D11306. doi:10.1029/2004JD005650.
- Alonso, A., 2012. Site selection and evaluation for nuclear power plants (NPPs), in: *Infrastructure and Methodologies for the Justification of Nuclear Power Programmes*. *Elsevier*, pp. 599–620. doi:10.1533/9780857093776.3.599.
- Anderson, E.C., Libby, W.F., Weinhouse, S., Reid, A.F., Kirshenbaum, A.D., Grosse, A. V., 1947. Radiocarbon from cosmic radiation. *Science* 105(2735), 576. doi:10.1126/science.105.2735.576.
- Arnold, J.R., Libby, W.F., 1949. Age determinations by radiocarbon content: Checks with samples of known age. *Science* 110(2869), 678–680. doi:10.1126/science.110.2869.678.
- Arrhenius, S., 1896. On the Influence of Carbonic Acid in the Air upon the Temperature of the Ground. *Philos. Mag. J. Sci.* 41(5), 237–276.
- Assan, S., Vogel, F.R., Gros, V., Baudic, A., Staufer, J., Ciais, P., 2018. Can we separate industrial  $\text{CH}_4$  emission sources from atmospheric observations? - A test case for carbon isotopes, PMF and enhanced APCA. *Atmos. Environ.* 187, 317–327. doi:10.1016/j.atmosenv.2018.05.004.
- Awe, O.W., Zhao, Y., Nzihou, A., Minh, D.P., Lyczko, N., 2017. A Review of Biogas Utilisation, Purification and Upgrading Technologies. *Waste and Biomass Valorization* 8(2), 267–283. doi:10.1007/s12649-016-9826-4.
- Aydin, M., Verhulst, K.R., Saltzman, E.S., Battle, M.O., Montzka, S.A., Blake, D.R., Tang, Q., Prather, M.J., 2011. Recent decreases in fossil-fuel emissions of ethane and methane derived from firn air. *Nature* 476(7359), 198–201. doi:10.1038/nature10352.
- Baltensperger, U., Gäggeler, H.W., Jost, D.T., Lugauer, M., Schwikowski, M., Weingartner, E., Seibert, P., 1997. Aerosol climatology at the high-alpine site Jungfraujoch, Switzerland. *J. Geophys. Res. Atmos.* 102(D16), 19707–19715. doi:10.1029/97JD00928.
- Bamberger, I., Stieger, J., Buchmann, N., Eugster, W., 2014. Spatial variability of methane: Attributing atmospheric concentrations to emissions. *Environ. Pollut.* 190, 65–74. doi:10.1016/j.envpol.2014.03.028.

- Bantle, M.C., 2021. Radiocarbon measurements of atmospheric methane samples. MSc. thesis. *University of Bern, Switzerland.*
- Bastviken, D., Cole, J., Pace, M., Tranvik, L., 2004. Methane emissions from lakes: Dependence of lake characteristics, two regional assessments, and a global estimate. *Global Biogeochem. Cycles* 18, GB4009. doi:10.1029/2004GB002238.
- Beer, J., McCracken, K., von Steiger, R., 2012. Production of Cosmogenic Radionuclides in Other Environmental Systems. doi:10.1007/978-3-642-14651-0\_11.
- Bergamaschi, P., Brenninkmeijer, C.A.M., Hahn, M., Röckmann, T., Scharffe, D.H., Crutzen, P.J., Elansky, N.F., Belikov, I.B., Trivett, N.B.A., Worthy, D.E.J., 1998. Isotope analysis based source identification for atmospheric CH<sub>4</sub> and CO sampled across Russia using the Trans-Siberian railroad. *J. Geophys. Res. Atmos.* 103(D7), 8227–8235. doi:10.1029/97JD03738.
- Berhanu, T.A., Szidat, S., Brunner, D., Satar, E., Schanda, R., Nyfeler, P., Battaglia, M., Steinbacher, M., Hammer, S., Leuenberger, M., 2017. Estimation of the fossil fuel component in atmospheric CO<sub>2</sub> based on radiocarbon measurements at the Beromünster tall tower, Switzerland. *Atmos. Chem. Phys.* 17(17), 10753–10766. doi:10.5194/acp-17-10753-2017.
- Blake, D.R., Mayer, E.W., Tyler, S.C., Makide, Y., Montague, D.C., Rowland, F.S., 1982. Global increase in atmospheric methane concentrations between 1978 and 1980. *Geophys. Res. Lett.* 9(4), 477–480. doi:10.1029/GL009i004p00477.
- Bloom, A.A., Exbrayat, J.F., Van Der Velde, I.R., Feng, L., Williams, M., 2016. The decadal state of the terrestrial carbon cycle: Global retrievals of terrestrial carbon allocation, pools, and residence times. *Proc. Natl. Acad. Sci. U. S. A.* 113(5), 1285–1290. doi:10.1073/pnas.1515160113.
- Bock, M., Schmitt, J., Beck, J., Seth, B., Chappellaz, J., Fischer, H., 2017. Glacial/interglacial wetland, biomass burning, and geologic methane emissions constrained by dual stable isotopic CH<sub>4</sub> ice core records. *Proc. Natl. Acad. Sci. U. S. A.* 114(29), E5778–E5786. doi:10.1073/pnas.1613883114.
- Bock, M., Schmitt, J., Behrens, M., Möller, L., Schneider, R., Sapart, C., Fischer, H., 2010. A gas chromatography/pyrolysis/isotope ratio mass spectrometry system for high-precision δD measurements of atmospheric methane extracted from ice cores. *Rapid Commun. Mass Spectrom.* 24(5), 621–633. doi:10.1002/rcm.4429.
- Bousquet, P., Ciais, P., Miller, J.B., Dlugokencky, E.J., Hauglustaine, D.A., Prigent, C., Van Der Werf, G.R., Peylin, P., Brunke, E.-G., Carouge, C., Langenfelds, R.L., Lathière, J., Papa, F., Ramonet, M., Schmidt, M., Steele, L.P., Tyler, S.C., White, J., 2006. Contribution of anthropogenic and natural sources to atmospheric methane variability. *Nature* 443(7110), 439–443. doi:10.1038/nature05132.
- Brass, M., Röckmann, T., 2010. Continuous-flow isotope ratio mass spectrometry method for carbon and hydrogen isotope measurements on atmospheric methane. *Atmos. Meas. Tech.* 3(6), 1707–1721. doi:10.5194/amt-3-1707-2010.

- Bräunlich, M., 2000. Study of atmospheric carbon monoxide and methane using isotopic analysis. PhD thesis. *University of Heidelberg, Germany*.
- Bréas, O., Guillou, C., Reniero, F., Wada, E., 2001. The global methane cycle: Isotopes and mixing ratios, sources and sinks. *Isotopes Environ. Health Stud.* 37(4), 257–379. doi:10.1080/10256010108033302.
- Brenninkmeijer, C.A.M., 1993. Measurement of the abundance of  $^{14}\text{C}$  in the atmosphere and the  $^{13}\text{C}/^{12}\text{C}$  and  $^{18}\text{O}/^{16}\text{O}$  ratio of atmospheric CO with applications in New Zealand and Antarctica. *J. Geophys. Res.* 98(D6), 10595–10614. doi:10.1029/93jd00587.
- Brenninkmeijer, C.A.M., 1991. Robust, High-Efficiency, High-Capacity Cryogenic Trap. *Anal. Chem.* 63(11), 1182–1184. doi:10.1021/ac00011a024.
- Brenninkmeijer, C.A.M., Röckmann, T., 1996. Russian Doll Type Cryogenic Traps: Improved Design and Isotope Separation Effects. *Anal. Chem.* 68(17), 3050–3053. doi:10.1021/ac960208w.
- Brock, F., Eastaugh, N., Ford, T., Townsend, J.H., 2019. Bomb-pulse Radiocarbon Dating of Modern Paintings on Canvas. *Radiocarbon* 61(1), 39–49. doi:10.1017/RDC.2018.55.
- Brown, T.A., Southon, J.R., 1997. Corrections for contamination background in AMS  $^{14}\text{C}$  measurements. *Nucl. Instruments Methods Phys. Res. B* 123(1–4), 208–213. doi:10.1016/S0168-583X(96)00676-3.
- Calcagnile, L., Quarta, G., D’Elia, M., Ciceri, G., Martinotti, V., 2011. Radiocarbon AMS determination of the biogenic component in CO<sub>2</sub> emitted from waste incineration. *Nucl. Instruments Methods Phys. Res. B* 269(24), 3158–3162. doi:10.1016/j.nimb.2011.04.020.
- Cambaliza, M.O.L., Shepson, P.B., Bogner, J., Caulton, D.R., Stirm, B., Sweeney, C., Montzka, S.A., Gurney, K.R., Spokas, K., Salmon, O.E., Lavoie, T.N., Hendricks, A., Mays, K., Turnbull, J., Miller, B.R., Lauvaux, T., Davis, K., Karion, A., Moser, B., Miller, C., Obermeyer, C., Whetstone, J., Prasad, K., Miles, N., Richardson, S., 2015. Quantification and source apportionment of the methane emission flux from the city of Indianapolis. *Elementa* 3, 000037. doi:10.12952/journal.elementa.000037.
- Cavallo, L.M., Mann, W.B., 1980. New National Bureau of Standards Contemporary Carbon-14 Standards. *Radiocarbon* 22(3), 962–963. doi:10.1017/S0033822200010377.
- Chanton, J.P., Bauer, J.E., Glaser, P.A., Siegel, D.I., Kelley, C.A., Tyler, S.C., Romanowicz, E.H., Lazrus, A., 1995. Radiocarbon evidence for the substrates supporting methane formation within northern Minnesota peatlands. *Geochim. Cosmochim. Acta* 59(17), 3663–3668. doi:10.1016/0016-7037(95)00240-Z.
- Chanton, J.P., Glaser, P.H., Chasar, L.S., Burdige, D.J., Hines, M.E., Siegel, D.I., Tremblay, L.B., Cooper, W.T., 2008. Radiocarbon evidence for the importance of surface vegetation on fermentation and methanogenesis in contrasting types of boreal peatlands. *Global Biogeochem. Cycles* 22, GB4022. doi:10.1029/2008GB003274.

- Cho, H.S., Moon, H.S., Kim, J.Y., 2012. Effect of quantity and composition of waste on the prediction of annual methane potential from landfills. *Bioresour. Technol.* 109, 86–92. doi:10.1016/j.biortech.2012.01.026.
- Ciais, P., Chris, S., Govindasamy, B., Bopp, L., Brovkin, V., Canadell, J., Chhabra, A., Defries, R., Galloway, J., Heimann, M., 2013. Carbon and other biogeochemical cycles. *Clim. Chang. 2013 Phys. Sci. Basis* 465–570.
- Collaud Coen, M., Weingartner, E., Furger, M., Nyeki, S., Prévôt, A.S.H., Steinbacher, M., Baltensperger, U., 2011. Aerosol climatology and planetary boundary influence at the Jungfraujoch analyzed by synoptic weather types. *Atmos. Chem. Phys.* 11(12), 5931–5944. doi:10.5194/acp-11-5931-2011.
- Conrad, R., 2005. Quantification of methanogenic pathways using stable carbon isotopic signatures: A review and a proposal. *Org. Geochem.* 36(5), 739–752. doi:10.1016/j.orggeochem.2004.09.006.
- Crutzen, P.J., 1995. On the Role of CH<sub>4</sub> in Atmospheric Chemistry: Sources, Sinks and Possible Reductions in Anthropogenic Sources. *Ambio* 24(1), 52–55.
- Crutzen, P.J., Aselmann, I., Seiler, W., 1986. Methane production by domestic animals, wild ruminants, other herbivorous fauna, and humans. *Tellus B* 38B(3–4), 271–284. doi:10.1111/j.1600-0889.1986.tb00193.x.
- Damon, P.E., Sternberg, R.E., 1989. Global Production and Decay of Radiocarbon. *Radiocarbon* 31(03), 697–703. doi:10.1017/S0033822200012297.
- De Vrieze, J., De Waele, M., Boeckx, P., Boon, N., 2018. Isotope Fractionation in Biogas Allows Direct Microbial Community Stability Monitoring in Anaerobic Digestion. *Environ. Sci. Technol.* 52(11), 6704–6713. doi:10.1021/acs.est.8b00723.
- Dean, J.F., Middelburg, J.J., Röckmann, T., Aerts, R., Blauw, L.G., Egger, M., Jetten, M.S.M., de Jong, A.E.E., Meisel, O.H., Rasigraf, O., Slomp, C.P., in't Zandt, M.H., Dolman, A.J., 2018. Methane Feedbacks to the Global Climate System in a Warmer World. *Rev. Geophys.* 56(1), 207–250. doi:10.1002/2017RG000559.
- Delmotte, M., Chappellaz, J., Brook, E., Yiou, P., Barnola, J.M., Goujon, C., Raynaud, D., Lipenkov, V.I., 2004. Atmospheric methane during the last four glacial-interglacial cycles: Rapid changes and their link with Antarctic temperature. *J. Geophys. Res.* 109, D12104. doi:10.1029/2003JD004417.
- Dias, C.M., Stenström, K., Bacelar Leão, I.L., Santos, R.V., Nicoli, I.G., Skog, G., Ekström, P., da Silveira Corrêa, R., 2009. <sup>14</sup>C<sub>2</sub> dispersion around two PWR nuclear power plants in Brazil. *J. Environ. Radioact.* 100(7), 574–580. doi:10.1016/j.jenvrad.2009.03.022.
- Dijs, I.J., van der Windt, E., Kaihola, L., van der Borg, K., 2006. Quantitative determination by <sup>14</sup>C analysis of the biological component in fuels. *Radiocarbon* 48(3), 315–323. doi:10.1017/S0033822200038777.

- Dlugokencky, E.J., Bruhwiler, L., White, J.W.C., Emmons, L.K., Novelli, P.C., Montzka, S.A., Masarie, K.A., Lang, P.M., Crotwell, A.M., Miller, J.B., Gatti, L. V., 2009. Observational constraints on recent increases in the atmospheric CH<sub>4</sub> burden. *Geophys. Res. Lett.* 36, L18803. doi:10.1029/2009GL039780.
- Dlugokencky, E.J., Nisbet, E.G., Fisher, R., Lowry, D., 2011. Global atmospheric methane: budget, changes and dangers. *Philos. Trans. R. Soc. A* 369(1943), 2058–2072. doi:10.1098/rsta.2010.0341.
- Donahue, D.J., Linick, T.W., Jull, A.J.T., 1990. Isotope-ratio and background corrections for accelerator mass spectrometry radiocarbon measurements. *Radiocarbon* 32(2), 135–142. doi:10.1017/S0033822200040121.
- Dumke, I., Faber, E., Poggenburg, J., 1989. Determination of stable carbon and hydrogen isotopes of light hydrocarbons. *Anal. Chem.* 61(19), 2149–2154. doi:10.1021/ac00194a007.
- Ehhalt, D.H., 1974. The atmospheric cycle of methane. *Tellus* 26(1–2), 58–70. doi:10.3402/tellusa.v26i1-2.9737.
- Ehhalt, D.H., Schmidt, U., 1978. Sources and sinks of atmospheric methane. *Pure Appl. Geophys.* 116(2–3), 452–464. doi:10.1007/BF01636899.
- Eisma, R., van der Borg, K., de Jong, A.F.M., Keskamp, W.M., Veltkamp, A.C., 1994. Measurements of the <sup>14</sup>C content of atmospheric methane in The Netherlands to determine the regional emissions of <sup>14</sup>CH<sub>4</sub>. *Nucl. Instruments Methods Phys. Res. B* 92(1–4), 410–412. doi:10.1016/0168-583X(94)96044-5.
- Eisma, R., Vermeulen, A.T., Van Der Borg, K., 1995. <sup>14</sup>CH<sub>4</sub> Emissions from Nuclear Power Plants in Northwestern Europe. *Radiocarbon* 37(2), 475–483. doi:10.1017/S0033822200030952.
- Elia, M., McDonald, T., Crisp, A., 1986. Errors in measurements of CO<sub>2</sub> with the use of drying agents. *Clin. Chim. Acta* 158(3), 237–244. doi:10.1016/0009-8981(86)90287-1.
- Etiope, G., 2015. Natural Gas Seepage. The Earth's Hydrocarbon Degassing. *Springer International Publishing*. doi:10.1007/978-3-319-14601-0.
- Etiope, G., Lassey, K.R., Klusman, R.W., Boschi, E., 2008. Reappraisal of the fossil methane budget and related emission from geologic sources. *Geophys. Res. Lett.* 35, L09307. doi:10.1029/2008GL033623.
- Etminan, M., Myhre, G., Highwood, E.J., Shine, K.P., 2016. Radiative forcing of carbon dioxide, methane, and nitrous oxide: A significant revision of the methane radiative forcing. *Geophys. Res. Lett.* 43(24), 12,614–12,623. doi:10.1002/2016GL071930.
- Eyer, S., Stadie, N.P., Borgschulte, A., Emmenegger, L., Mohn, J., 2014. Methane preconcentration by adsorption: A methodology for materials and conditions selection. *Adsorption* 20(5–6), 657–666. doi:10.1007/s10450-014-9609-9.

- Eyer, S., Tuzson, B., Popa, M.E., Van Der Veen, C., Röckmann, T., Rothe, M., Brand, W.A., Fisher, R., Lowry, D., Nisbet, E.G., Brennwald, M.S., Harris, E., Zellweger, C., Emmenegger, L., Fischer, H., Mohn, J., 2016. Real-time analysis of  $\delta^{13}\text{C}$ - And  $\delta\text{D-CH}_4$  in ambient air with laser spectroscopy: Method development and first intercomparison results. *Atmos. Meas. Tech.* 9(1), 263–280. doi:10.5194/amt-9-263-2016.
- Fahrni, S.M., Southon, J.R., Santos, G.M., Palstra, S.W.L., Meijer, H.A.J., Xu, X., 2017. Reassessment of the  $^{13}\text{C}/^{12}\text{C}$  and  $^{14}\text{C}/^{12}\text{C}$  isotopic fractionation ratio and its impact on high-precision radiocarbon dating. *Geochim. Cosmochim. Acta* 213, 330–345. doi:10.1016/j.gca.2017.05.038.
- Fahrni, S.M., Wacker, L., Synal, H.A., Szidat, S., 2013. Improving a gas ion source for  $^{14}\text{C}$  AMS. *Nucl. Instruments Methods Phys. Res. B* 294, 320–327. doi:10.1016/j.nimb.2012.03.037.
- Faramawy, S., Zaki, T., Sakr, A.A.E., 2016. Natural gas origin, composition, and processing: A review. *J. Nat. Gas Sci. Eng.* 34, 34–54. doi:10.1016/j.jngse.2016.06.030.
- Fellner, J., Rechberger, H., 2009. Abundance of  $^{14}\text{C}$  in biomass fractions of wastes and solid recovered fuels. *Waste Manag.* 29(5), 1495–1503. doi:10.1016/j.wasman.2008.11.023.
- FOEN, 2017. Switzerland's Greenhouse Gas Inventory 1990-2015, National Inventory Report 2017, Swiss Federal Office for the Environment. Bern.
- Fontugne, M., Maro, D., Baron, Y., Hatté, C., Hebert, D., Douville, E., 2004.  $^{14}\text{C}$  Sources and Distribution in the Vicinity of La Hague Nuclear Reprocessing Plant: Part I—Terrestrial Environment. *Radiocarbon* 46(2), 827–830. doi:10.1017/S0033822200035852.
- FOPH, 2019. Umweltradioaktivität und Strahlendosen in der Schweiz (2018), Federal Office of Public Health. Bern.
- Forster, M., Maier, P., Loosli, H.H., 1992. Current techniques for measuring the activity of  $^{37}\text{Ar}$  and  $^{39}\text{Ar}$  in the environment. IAEA, International Atomic Energy Agency (IAEA).
- Frankenberg, C., Meirink, J.F., Bergamaschi, P., Goede, A.P.H., Heimann, M., Körner, S., Platt, U., van Weele, M., Wagner, T., 2006. Satellite cartography of atmospheric methane from SCIAMACHY on board ENVISAT: Analysis of the years 2003 and 2004. *J. Geophys. Res. Atmos.* 111, D07303. doi:10.1029/2005JD006235.
- Gäggeler, H.W., 1995. Radioactivity in the Atmosphere. *Radiochim. Acta* 70–71, 345–353.
- Galimov, E.M., 1988. Sources and mechanisms of formation of gaseous hydrocarbons in sedimentary rocks. *Chem. Geol.* 71(1–3), 77–95. doi:10.1016/0009-2541(88)90107-6.
- Galli, I., Bartalini, S., Ballerini, R., Barucci, M., Cancio, P., De Pas, M., Giusfredi, G., Mazzotti, D., Akikusa, N., De Natale, P., 2016. Spectroscopic detection of radiocarbon dioxide at parts-per-quadrillion sensitivity. *Optica* 3(4), 385–388. doi:10.1364/OPTICA.3.000385.

- Gamnitzer, U., Karstens, U., Kromer, B., Neubert, R.E.M., Meijer, H.A.J., Schroeder, H., Levin, I., 2006. Carbon monoxide: A quantitative tracer for fossil fuel CO<sub>2</sub>? *J. Geophys. Res.* 111, D22302. doi:10.1029/2005JD006966.
- Garnett, M.H., Gulliver, P., Billett, M.F., 2016. A rapid method to collect methane from peatland streams for radiocarbon analysis. *Ecohydrology* 9(1), 113–121. doi:10.1002/eco.1617.
- Garnett, M.H., Hardie, S.M.L., Murray, C., 2011. Radiocarbon and Stable Carbon Analysis of Dissolved Methane and Carbon Dioxide from the Profile of a Raised Peat Bog. *Radiocarbon* 53(1), 71–83. doi:10.1017/S0033822200034366.
- Garnett, M.H., Hardie, S.M.L., Murray, C., Billett, M.F., 2013. Radiocarbon dating of methane and carbon dioxide evaded from a temperate peatland stream. *Biogeochemistry* 114(1–3), 213–223. doi:10.1007/s10533-012-9804-2.
- Garnett, M.H., Murray, C., Gulliver, P., Ascough, P.L., 2019. Radiocarbon Analysis of Methane at the NERC Radiocarbon Facility (East Kilbride). *Radiocarbon* 61(5), 1477–1487. doi:10.1017/RDC.2019.3.
- Geels, C., Gloor, M., Ciais, P., Bousquet, P., Peylin, P., Vermeulen, A.T., Dargaville, R., Aalto, T., Brandt, J., Christensen, J.H., Frohn, L.M., Haszpra, L., Karstens, U., Rödenbeck, C., Ramonet, M., Carboni, G., Santaguida, R., 2007. Comparing atmospheric transport models for future regional inversions over Europe - Part 1: Mapping the atmospheric CO<sub>2</sub> signals. *Atmos. Chem. Phys.* 7(13), 3461–3479. doi:10.5194/acp-7-3461-2007.
- Genoud, G., Lehmuskoski, J., Bell, S., Palonen, V., Oinonen, M., Koskinen-Soivi, M.-L., Reinikainen, M., 2019. Laser Spectroscopy for Monitoring of Radiocarbon in Atmospheric Samples. *Anal. Chem.* 91(19), 12315–12320. doi:10.1021/acs.analchem.9b02496.
- Geyh, M.A., 2001. Bomb Radiocarbon Dating of Animal Tissues and Hair. *Radiocarbon* 43(2B), 723–730. doi:10.1017/S0033822200041382.
- Gloor, M., Fan, S.M., Pacala, S., Sarmiento, J., 2000. Optimal sampling of the atmosphere for purpose of inverse modeling: A model study. *Global Biogeochem. Cycles* 14(1), 407–428. doi:10.1029/1999GB900052.
- Godwin, H., 1962. Half-life of Radiocarbon. *Nature* 195(4845), 984–984. doi:10.1038/195984a0.
- Golding, S.D., Boreham, C.J., Esterle, J.S., 2013. Stable isotope geochemistry of coal bed and shale gas and related production waters: A review. *Int. J. Coal Geol.* 120, 24–40. doi:10.1016/j.coal.2013.09.001.
- Graven, H., Hocking, T., Zazzeri, G., 2019. Detection of Fossil and Biogenic Methane at Regional Scales Using Atmospheric Radiocarbon. *Earth's Future* 7(3), 283–299. doi:10.1029/2018EF001064.
- Graven, H.D., Gruber, N., 2011. Continental-scale enrichment of atmospheric <sup>14</sup>CO<sub>2</sub> from the nuclear power industry: Potential impact on the estimation of fossil fuel-derived CO<sub>2</sub>. *Atmos. Chem. Phys.* 11(23), 12339–12349. doi:10.5194/acp-11-12339-2011.

- Gregg, J.S., Andres, R.J., Marland, G., 2008. China: Emissions pattern of the world leader in CO<sub>2</sub> emissions from fossil fuel consumption and cement production. *Geophys. Res. Lett.* 35, L08806. doi:10.1029/2007GL032887.
- Hahn, V., Högberg, P., Buchmann, N., 2006. <sup>14</sup>C - A tool for separation of autotrophic and heterotrophic soil respiration. *Glob. Chang. Biol.* 12(6), 972–982. doi:10.1111/j.1365-2486.2006.001143.x.
- Hammer, S., Friedrich, R., Kromer, B., Cherkinsky, A., Lehman, S.J., Meijer, H.A.J., Nakamura, T., Palonen, V., Reimer, R.W., Smith, A.M., Southon, J.R., Szidat, S., Turnbull, J., Uchida, M., 2017. Compatibility of Atmospheric <sup>14</sup>CO<sub>2</sub> Measurements: Comparing the Heidelberg Low-Level Counting Facility to International Accelerator Mass Spectrometry (AMS) Laboratories. *Radiocarbon* 59(3), 875–883. doi:10.1017/RDC.2016.62.
- Hammer, S., Levin, I., 2017. Monthly mean atmospheric Δ<sup>14</sup>CO<sub>2</sub> at Jungfraujoch and Schauinsland from 1986 to 2016. *heiDATA*, University of Heidelberg, Germany. doi:10.11588/data/10100.
- Hanson, P.J., Edwards, N.T., Garten, C.T., Andrews, J.A., 2000. Separating root and soil microbial contributions to soil respiration: A review of methods and observations. *Biogeochemistry* 48(1), 115–146. doi:10.1023/A:1006244819642.
- Hausmann, P., Sussmann, R., Smale, D., 2016. Contribution of oil and natural gas production to renewed increase in atmospheric methane (2007–2014): top–down estimate from ethane and methane column observations. *Atmos. Chem. Phys.* 16(5), 3227–3244. doi:10.5194/acp-16-3227-2016.
- Heimann, M., Reichstein, M., 2008. Terrestrial ecosystem carbon dynamics and climate feedbacks. *Nature* 451(7176), 289–292. doi:10.1038/nature06591.
- Henne, S., Brunner, D., Oney, B., Leuenberger, M., Eugster, W., Bamberger, I., Meinhardt, F., Steinbacher, M., Emmenegger, L., 2016. Validation of the Swiss methane emission inventory by atmospheric observations and inverse modelling. *Atmos. Chem. Phys.* 16(6), 3683–3710. doi:10.5194/acp-16-3683-2016.
- Hertelendi, E., Uchirin, G., Ormai, P., 1989. <sup>14</sup>C Release in Various Chemical Forms With Gaseous Effluents From the Paks Nuclear Power Plant. *Radiocarbon* 31(3), 754–761. doi:10.1017/S0033822200012352.
- Hesshaimer, V., Heimann, M., Levin, I., 1994. Radiocarbon evidence for a smaller oceanic carbon dioxide sink than previously believed. *Nature* 370(6486), 201–203. doi:10.1038/370201a0.
- Hiller, R. V., Bretscher, D., Delsontro, T., Diem, T., Eugster, W., Henneberger, R., Hobi, S., Hodson, E., Imer, D., Kreuzer, M., Künzle, T., Merbold, L., Niklaus, P.A., Rihm, B., Schellenberger, A., Schroth, M.H., Schubert, C.J., Siegrist, H., Stieger, J., Buchmann, N., Brunner, D., 2014. Anthropogenic and natural methane fluxes in Switzerland synthesized within a spatially explicit inventory. *Biogeosciences* 11(7), 1941–1960. doi:10.5194/bg-11-1941-2014.

- Hmiel, B., Petrenko, V. V., Dyonisius, M.N., Buizert, C., Smith, A.M., Place, P.F., Harth, C., Beaudette, R., Hua, Q., Yang, B., Vimont, I., Michel, S.E., Severinghaus, J.P., Etheridge, D., Bromley, T., Schmitt, J., Faïn, X., Weiss, R.F., Dlugokencky, E., 2020. Preindustrial  $^{14}\text{CH}_4$  indicates greater anthropogenic fossil  $\text{CH}_4$  emissions. *Nature* 578(7795), 409–412. doi:10.1038/s41586-020-1991-8.
- Hoefs, J., 2009. Stable Isotope Geochemistry, 6th ed. *Springer*.
- Hopkins, F.M., Ehleringer, J.R., Bush, S.E., Duren, R.M., Miller, C.E., Lai, C.-T., Hsu, Y.-K., Carranza, V., Randerson, J.T., 2016. Mitigation of methane emissions in cities: How new measurements and partnerships can contribute to emissions reduction strategies. *Earth's Future* 4(9), 408–425. doi:10.1002/2016EF000381.
- Houweling, S., Bergamaschi, P., Chevallier, F., Heimann, M., Kaminski, T., Krol, M., Michalak, A.M., Patra, P., 2017. Global inverse modeling of  $\text{CH}_4$  sources and sinks: An overview of methods. *Atmos. Chem. Phys.* 17(1), 235–256. doi:10.5194/acp-17-235-2017.
- Howarth, R.W., Santoro, R., Ingraffea, A., 2011. Methane and the greenhouse-gas footprint of natural gas from shale formations. *Clim. Change* 106(4), 679–690. doi:10.1007/s10584-011-0061-5.
- IAEA, 2017. IAEA Annual Report 2017, International Atomic Energy Agency. Vienna.
- IAEA, 2004. Management of Waste Containing Tritium and Carbon-14, Technical Reports Series No. 421. International Atomic Energy Agency. Vienna.
- ICOS RI, 2019. ICOS ATC  $^{14}\text{C}$  Release, Jungfraujoch (10.0 m), 2016-01-04–2018-07-16. <https://hdl.handle.net/11676/0yDrKllpdGVPtMsFIMSUEm1N>.
- IPCC, 2018. Global Warming of 1.5 °C. An IPCC Special Report on the impacts of global warming of 1.5 °C above pre-industrial levels and related global greenhouse gas emission pathways, in the context of strengthening the global response to the threat of climate change, sustainable development, and efforts to eradicate poverty. *In Press*.
- IPCC, 2013. Climate Change 2013: The Physical Science Basis. Contribution of Working Group I to the Fifth Assessment Report of the Intergovernmental Panel on Climate Change. *Cambridge University Press*, Cambridge, United Kingdom and New York, NY, USA.
- Jacob, D.J., Turner, A.J., Maasakkers, J.D., Sheng, J., Sun, K., Liu, X., Chance, K., Aben, I., McKeever, J., Frankenberg, C., 2016. Satellite observations of atmospheric methane and their value for quantifying methane emissions. *Atmos. Chem. Phys.* 16(22), 14371–14396. doi:10.5194/acp-16-14371-2016.
- Kai, F.M., Tyler, S.C., Randerson, J.T., Blake, D.R., 2011. Reduced methane growth rate explained by decreased Northern Hemisphere microbial sources. *Nature* 476(7359), 194–197. doi:10.1038/nature10259.

- Karhu, J., Tomberg, T., Senna Vieira, F., Genoud, G., Hänninen, V., Vainio, M., Metsälä, M., Hieta, T., Bell, S., Halonen, L., 2019. Broadband photoacoustic spectroscopy of  $^{14}\text{CH}_4$  with a high-power mid-infrared optical frequency comb. *Opt. Lett.* 44(5), 1142. doi:10.1364/ol.44.001142.
- Kessler, J.D., Reeburgh, W.S., 2005. Preparation of natural methane samples for stable isotope and radiocarbon analysis. *Limnol. Oceanogr. Methods* 3(9), 408–418. doi:10.4319/lom.2005.3.408.
- Kessler, J.D., Reeburgh, W.S., Valentine, D.L., Kinnaman, F.S., Peltzer, E.T., Brewer, P.G., Southon, J., Tyler, S.C., 2008. A survey of methane isotope abundance ( $^{14}\text{C}$ ,  $^{13}\text{C}$ ,  $^2\text{H}$ ) from five nearshore marine basins that reveals unusual radiocarbon levels in subsurface waters. *J. Geophys. Res. Ocean.* 113, C12021. doi:10.1029/2008JC004822.
- Ketterer, C., Zieger, P., Bukowiecki, N., Collaud Coen, M., Maier, O., Ruffieux, D., Weingartner, E., 2014. Investigation of the Planetary Boundary Layer in the Swiss Alps Using Remote Sensing and In Situ Measurements. *Boundary-Layer Meteorol.* 151(2), 317–334. doi:10.1007/s10546-013-9897-8.
- Kirschke, S., Bousquet, P., Ciais, P., Saunio, M., Canadell, J.G., Dlugokencky, E.J., Bergamaschi, P., Bergmann, D., Blake, D.R., Bruhwiler, L., Cameron-Smith, P., Castaldi, S., Chevallier, F., Feng, L., Fraser, A., Heimann, M., Hodson, E.L., Houweling, S., Josse, B., Fraser, P.J., Krummel, P.B., Lamarque, J.F., Langenfelds, R.L., Le Quéré, C., Naik, V., O’doherly, S., Palmer, P.I., Pison, I., Plummer, D., Poulter, B., Prinn, R.G., Rigby, M., Ringeval, B., Santini, M., Schmidt, M., Shindell, D.T., Simpson, I.J., Spahni, R., Steele, L.P., Strode, S.A., Sudo, K., Szopa, S., Van Der Werf, G.R., Voulgarakis, A., Van Weele, M., Weiss, R.F., Williams, J.E., Zeng, G., 2013. Three decades of global methane sources and sinks. *Nat. Geosci.* 6(10), 813–823. doi:10.1038/ngeo1955.
- KKG, 2015. Technology and Operation, Kernkraftswerk Gösgen-Däniken AG (KKG). Däniken.
- Klouda, G.A., Currie, L.A., Donahue, D.J., Jull, A.J.T., Naylor, M.H., 1986. Urban Atmospheric  $^{14}\text{CO}$  and  $^{14}\text{CH}_4$  Measurements by Accelerator Mass Spectrometry. *Radiocarbon* 28(2A), 625–633. doi:10.1017/S0033822200007815.
- Koven, C.D., Ringeval, B., Friedlingstein, P., Ciais, P., Cadule, P., Khvorostyanov, D., Krinner, G., Tarnocai, C., 2011. Permafrost carbon-climate feedbacks accelerate global warming. *Proc. Natl. Acad. Sci. U. S. A.* 108(36), 14769–14774. doi:10.1073/pnas.1103910108.
- Kuc, T., Rozanski, K., Zimnoch, M., Necki, J.M., Korus, A., 2003. Anthropogenic emissions of  $\text{CO}_2$  and  $\text{CH}_4$  in an urban environment. *Appl. Energy* 75(3–4), 193–203. doi:10.1016/S0306-2619(03)00032-1.
- Kufka, D., Bucha, M., Pleśniak, Ł., Jędrysek, M.O., 2019. Stable isotopes of C and H in methane fermentation of agriculture substrates at different temperature conditions. *Open Geosci.* 11(1), 471–481. doi:10.1515/geo-2019-0039.

- Kunz, C., 1985. Carbon-14 discharge at three light-water reactors. *Health Phys.* 49(1), 25–35. doi:10.1097/00004032-198507000-00002.
- Kuze, A., Suto, H., Shiomi, K., Kawakami, S., Tanaka, M., Ueda, Y., Deguchi, A., Yoshida, J., Yamamoto, Y., Kataoka, F., Taylor, T.E., Buijs, H.L., 2016. Update on GOSAT TANSO-FTS performance, operations, and data products after more than 6 years in space. *Atmos. Meas. Tech.* 9(6), 2445–2461. doi:10.5194/amt-9-2445-2016.
- Lal, D., Suess, H.E., 1968. The Radioactivity of the Atmosphere and Hydrosphere. *Annu. Rev. Nucl. Sci.* 18(1), 407–434. doi:10.1146/annurev.ns.18.120168.002203.
- Lassey, K.R., Etheridge, D.M., Lowe, D.C., Smith, A.M., Ferretti, D.F., 2007a. Centennial evolution of the atmospheric methane budget: What do the carbon isotopes tell us? *Atmos. Chem. Phys.* 7(8), 2119–2139. doi:10.5194/acp-7-2119-2007.
- Lassey, K.R., Lowe, D.C., Smith, A.M., 2007b. The atmospheric cycling of radiomethane and the “fossil fraction” of the methane source. *Atmos. Chem. Phys.* 7(8), 2141–2149. doi:10.5194/acp-7-2141-2007.
- Laukenmann, S., Polag, D., Heuwinkel, H., Greule, M., Gronauer, A., Lelieveld, J., Keppler, F., 2010. Identification of methanogenic pathways in anaerobic digesters using stable carbon isotopes. *Eng. Life Sci.* 10(6), 509–514. doi:10.1002/elsc.201000074.
- Lawrence, D.M., Koven, C.D., Swenson, S.C., Riley, W.J., Slater, A.G., 2015. Permafrost thaw and resulting soil moisture changes regulate projected high-latitude CO<sub>2</sub> and CH<sub>4</sub> emissions. *Environ. Res. Lett.* 10, 094011. doi:10.1088/1748-9326/10/9/094011.
- Le Mer, J., Roger, P., 2001. Production, oxidation, emission and consumption of methane by soils: A review. *Eur. J. Soil Biol.* 37(1), 25–50. doi:10.1016/S1164-5563(01)01067-6.
- Le Quéré, C., Andrew, R.M., Canadell, J.G., Sitch, S., Ivar Korsbakken, J., Peters, G.P., Manning, A.C., Boden, T.A., Tans, P.P., Houghton, R.A., Keeling, R.F., Alin, S., Andrews, O.D., Anthoni, P., Barbero, L., Bopp, L., Chevallier, F., Chini, L.P., Ciais, P., Currie, K., Delire, C., Doney, S.C., Friedlingstein, P., Gkritzalis, T., Harris, I., Hauck, J., Haverd, V., Hoppema, M., Klein Goldewijk, K., Jain, A.K., Kato, E., Körtzinger, A., Landschützer, P., Lefèvre, N., Lenton, A., Lienert, S., Lombardozzi, D., Melton, J.R., Metzl, N., Millero, F., Monteiro, P.M.S., Munro, D.R., Nabel, J.E.M.S., Nakaoka, S.I., O’Brien, K., Olsen, A., Omar, A.M., Ono, T., Pierrot, D., Poulter, B., Rödenbeck, C., Salisbury, J., Schuster, U., Schwinger, J., Séférian, R., Skjelvan, I., Stocker, B.D., Sutton, A.J., Takahashi, T., Tian, H., Tilbrook, B., Van Der Laan-Luijkx, I.T., Van Der Werf, G.R., Viovy, N., Walker, A.P., Wiltshire, A.J., Zaehle, S., 2016. Global Carbon Budget 2016. *Earth Syst. Sci. Data* 8(2), 605–649. doi:10.5194/essd-8-605-2016.
- Leith, F.I., Garnett, M.H., Dinsmore, K.J., Billett, M.F., Heal, K. V., 2014. Source and age of dissolved and gaseous carbon in a peatland-riparian-stream continuum: A dual isotope (<sup>14</sup>C and δ<sup>13</sup>C) analysis. *Biogeochemistry* 119(1–3), 415–433. doi:10.1007/s10533-014-9977-y.

- Leuenberger, M.C., Eyer, M., Nyfeler, P., Stauffer, B., Stocker, T.F., 2003. High-resolution  $\delta^{13}\text{C}$  measurements on ancient air extracted from less than  $10\text{ cm}^3$  of ice. *Tellus B* 55(2), 138–144. doi:10.1034/j.1600-0889.2003.01463.x.
- Levin, I., Bösinger, R., Bonani, G., Francey, R.J., Kromer, B., Münnich, K.O., Suter, M., Trivett, N.B.A., Wölfli, W., 1992. Radiocarbon in Atmospheric Carbon Dioxide and Methane: Global Distribution and Trends. *Radiocarb. After Four Decad.* 503–518. doi:10.1007/978-1-4757-4249-7\_31.
- Levin, I., Hammer, S., Kromer, B., Meinhardt, F., 2008. Radiocarbon observations in atmospheric  $\text{CO}_2$ : Determining fossil fuel  $\text{CO}_2$  over Europe using Jungfraujoch observations as background. *Sci. Total Environ.* 391(2–3), 211–216. doi:10.1016/j.scitotenv.2007.10.019.
- Levin, I., Hesshaimer, V., 2000. Radiocarbon – A Unique Tracer of Global Carbon Cycle Dynamics. *Radiocarbon* 42(1), 69–80. doi:10.1017/S0033822200053066.
- Levin, I., Kromer, B., 2004. The Tropospheric  $^{14}\text{CO}_2$  Level in Mid-Latitudes of the Northern Hemisphere (1959–2003). *Radiocarbon* 46(3), 1261–1272. doi:10.1017/S0033822200033130.
- Levin, I., Kromer, B., Barabas, M., Münnich, K.O., 1988. Environmental Distribution and Long-term Dispersion of Reactor  $^{14}\text{CO}_2$  Around Two German Nuclear Power Plants. *Health Phys.* 54(2), 149–156. doi:10.1097/00004032-198802000-00002.
- Levin, I., Kromer, B., Hammer, S., 2013. Atmospheric  $\Delta^{14}\text{CO}_2$  trend in Western European background air from 2000 to 2012. *Tellus, Ser. B Chem. Phys. Meteorol.* 65(1). doi:10.3402/tellusb.v65i0.20092.
- Levin, I., Kromer, B., Schmidt, M., Sartorius, H., 2003. A novel approach for independent budgeting of fossil fuel  $\text{CO}_2$  over Europe by  $^{14}\text{CO}_2$  observations. *Geophys. Res. Lett.* 30(23), 2194. doi:10.1029/2003GL018477.
- Levin, I., Kromer, B., Schoch-Fischer, H., Bruns, M., Münnich, M., Berdau, D., Vogel, J.C., Münnich, K.O., 1994. Delta  $^{14}\text{CO}_2$  Record from Vermunt, Austria, February 1959 – June 1983. doi:10.3334/CDIAC/ATG.028.
- Levin, I., Kromer, B., Schoch-Fischer, H., Bruns, M., Münnich, M., Berdau, D., Vogel, J.C., Münnich, K.O., 1985. 25 Years of Tropospheric  $^{14}\text{C}$  Observations in Central Europe. *Radiocarbon* 27(1), 1–19. doi:10.1017/S0033822200006895.
- Levin, I., Münnich, K.O., Weiss, W., 1980. The Effect of Anthropogenic  $\text{CO}_2$  and  $^{14}\text{C}$  Sources on the Distribution of  $^{14}\text{C}$  in the Atmosphere. *Radiocarbon* 22(2), 379–391. doi:10.1017/S003382220000967X.
- Levin, I., Naegler, T., Kromer, B., Diehl, M., Francey, R.J., Gomez-Pelaez, A.J., Steele, L.P., Wagenbach, D., Weller, R., Worthy, D.E., 2010. Observations and modelling of the global distribution and long-term trend of atmospheric  $^{14}\text{CO}_2$ . *Tellus B* 62(1), 26–46. doi:10.1111/j.1600-0889.2009.00446.x.

- Levin, I., Schuchard, J., Kromer, B., Münnich, K.O., 1989. The Continental European Suess Effect. *Radiocarbon* 31(3), 431–440. doi:10.1017/S0033822200012017.
- Libby, W.F., 1946. Atmospheric helium three and radiocarbon from cosmic radiation. *Phys. Rev.* 69(11–12), 671–672. doi:10.1103/PhysRev.69.671.2.
- Lister, D., Uchida, S., 2015. Determining water chemistry conditions in nuclear reactor coolants. *J. Nucl. Sci. Technol.* 52(4), 451–466. doi:10.1080/00223131.2014.973460.
- Loosli, H.H., Oeschger, H., Studer, R., Wahlen, M., Wiest, W. Atmospheric concentrations and mixing of argon-37. In: Stanley, R.E., Moghissi, A.A., 1973. Symposium on noble gases. September 24–28, 1973, Las Vegas, Nevada, United States.
- Loosli, H.H., Heimann, M., Oeschger, H., 1980. Low-Level Gas Proportional Counting in An Underground Laboratory. *Radiocarbon* 22(2), 461–469. doi:10.1017/S0033822200009772.
- Loosli, H.H., Oeschger, H., 1989.  $^{14}\text{C}$  in the Environment of Swiss Nuclear Installations. *Radiocarbon* 31(3), 747–753. doi:10.1017/S0033822200012340.
- Loosli, H.H., Oeschger, H., Wiest, W., 1970. Argon 37, argon 39, and krypton 81 in the atmosphere and tracer studies based on these isotopes. *J. Geophys. Res.* 75(15), 2895–2900. doi:10.1029/JC075i015p02895.
- Lopez, M., Schmidt, M., Delmotte, M., Colomb, A., Gros, V., Janssen, C., Lehman, S.J., Mondelain, D., Perrussel, O., Ramonet, M., Xueref-Remy, I., Bousquet, P., 2013. CO, NO<sub>x</sub> and  $^{13}\text{C}$  as tracers for fossil fuel CO<sub>2</sub>: Results from a pilot study in Paris during winter 2010. *Atmos. Chem. Phys.* 13(15), 7343–7358. doi:10.5194/acp-13-7343-2013.
- Lowe, D.C., Brenninkmeijer, C.A.M., Manning, M.R., Sparks, R., Wallace, G., 1988. Radiocarbon determination of atmospheric methane at Baring Head, New Zealand. *Nature* 332(6164), 522–525. doi:10.1038/332522a0.
- Lowe, D.C., Brenninkmeijer, C.A.M., Tyler, S.C., Dlugokencky, E.J., 1991. Determination of the isotopic composition of atmospheric methane and its application in the Antarctic. *J. Geophys. Res.* 96(D8), 455–467. doi:10.1029/91jd01119.
- MacFarling Meure, C., Etheridge, D., Trudinger, C., Steele, P., Langenfelds, R., Van Ommen, T., Smith, A., Elkins, J., 2006. Law Dome CO<sub>2</sub>, CH<sub>4</sub> and N<sub>2</sub>O ice core records extended to 2000 years BP. *Geophys. Res. Lett.* 33, L14810. doi:10.1029/2006GL026152.
- Magnusson, Å., 2007.  $^{14}\text{C}$  Produced by Nuclear Power Reactors - Generation and Characterization of Gaseous, Liquid and Solid Waste. PhD thesis. *Lund University, Sweden.*
- Manning, M.R., Lowe, D.C., Melhuish, W.H., Sparks, R.J., Wallace, G., Brenninkmeijer, C.A.M., McGill, R.C., 1990. The Use of Radiocarbon Measurements in Atmospheric Studies. *Radiocarbon* 32(1), 37–58. doi:10.1017/S0033822200039941.
- Marland, G., 2008. Uncertainties in accounting for CO<sub>2</sub> from fossil fuels. *J. Ind. Ecol.* 12(2), 136–139. doi:10.1111/j.1530-9290.2008.00014.x.

- Matsumoto, T., Han, L.F., Jaklitsch, M., Aggarwal, P.K., 2013. A Portable Membrane Contactor Sampler for Analysis of Noble Gases in Groundwater. *Ground Water* 51(3), 461–468. doi:10.1111/j.1745-6584.2012.00983.x.
- McCartney, M., Baxter, M.S., McKay, K., Scott, E.M., 1986. Global and Local Effects of  $^{14}\text{C}$  Discharges from the Nuclear Fuel Cycle. *Radiocarbon* 28(2A), 634–643. doi:10.1017/S0033822200007827.
- McIntyre, C.P., McNichol, A.P., Roberts, M.L., Seewald, J.S., von Reden, K.F., Jenkins, W.J., 2013. Improved Precision of Radiocarbon Measurements for  $\text{CH}_4$  and  $\text{CO}_2$  Using GC and Continuous-Flow AMS Achieved by Summation of Repeated Injections. *Radiocarbon* 55(2–3), 677–685. doi:10.1017/s0033822200057830.
- Melton, J.R., Wania, R., Hodson, E.L., Poulter, B., Ringeval, B., Spahni, R., Bohn, T., Avis, C.A., Beerling, D.J., Chen, G., Eliseev, A. V., Denisov, S.N., Hopcroft, P.O., Lettenmaier, D.P., Riley, W.J., Singarayer, J.S., Subin, Z.M., Tian, H., Zürcher, S., Brovkin, V., Van Bodegom, P.M., Kleinen, T., Yu, Z.C., Kaplan, J.O., 2013. Present state of global wetland extent and wetland methane modelling: Conclusions from a model inter-comparison project (WETCHIMP). *Biogeosciences* 10(2), 753–788. doi:10.5194/bg-10-753-2013.
- Middleton, R., 1983. A versatile high intensity negative ion source. *Nucl. Instruments Methods Phys. Res.* 214(2–3), 139–150. doi:10.1016/0167-5087(83)90580-X.
- Milkov, A. V., 2005. Molecular and stable isotope compositions of natural gas hydrates: A revised global dataset and basic interpretations in the context of geological settings. *Org. Geochem.* 36(5), 681–702. doi:10.1016/j.orggeochem.2005.01.010.
- Miller, J.B., Mack, K.A., Dissly, R., White, J.W.C., Dlugokencky, E.J., Tans, P.P., 2002. Development of analytical methods and measurements of  $^{13}\text{C}/^{12}\text{C}$  in atmospheric  $\text{CH}_4$  from the NOAA Climate Monitoring and Diagnostics Laboratory Global Air Sampling Network. *J. Geophys. Res.* 107(D13), 4178. doi:10.1029/2001JD000630.
- Mitchell, L.E., Lin, J.C., Bowling, D.R., Pataki, D.E., Strong, C., Schauer, A.J., Bares, R., Bush, S.E., Stephens, B.B., Mendoza, D., Mallia, D., Holland, L., Gurney, K.R., Ehleringer, J.R., 2018. Long-term urban carbon dioxide observations reveal spatial and temporal dynamics related to urban characteristics and growth. *Proc. Natl. Acad. Sci. U. S. A.* 115(12), 2912–2917. doi:10.1073/pnas.1702393115.
- Mohn, J., Guggenheim, C., Tuzson, B., Vollmer, M.K., Toyoda, S., Yoshida, N., Emmenegger, L., 2010. A liquid nitrogen-free preconcentration unit for measurements of ambient  $\text{N}_2\text{O}$  isotopomers by QCLAS. *Atmos. Meas. Tech.* 3(3), 609–618. doi:10.5194/amt-3-609-2010.
- Mohn, J., Szidat, S., Fellner, J., Rechberger, H., Quartier, R., Buchmann, B., Emmenegger, L., 2008. Determination of biogenic and fossil  $\text{CO}_2$  emitted by waste incineration based on  $^{14}\text{CO}_2$  and mass balances. *Bioresour. Technol.* 99(14), 6471–6479. doi:10.1016/j.biortech.2007.11.042.
- Mohseni, F., Magnusson, M., Görling, M., Alvfors, P., 2012. Biogas from renewable electricity – Increasing a climate neutral fuel supply. *Appl. Energy* 90(1), 11–16. doi:10.1016/j.apenergy.2011.07.024.

- Molnár, M., Bujtás, T., Svingor, É., Futó, I., Světlík, I., 2007. Monitoring of Atmospheric Excess  $^{14}\text{C}$  Around Paks Nuclear Power Plant, Hungary. *Radiocarbon* 49(2), 1031–1043. doi:10.1017/S0033822200042892.
- Mook, W.G., van der Plicht, J., 1999. Reporting  $^{14}\text{C}$  Activities and Concentrations. *Radiocarbon* 41(3), 227–239. doi:10.1017/S0033822200057106.
- Moriizumi, J., Nagamine, K., Iida, T., Ikebe, Y., 1998. Carbon isotopic analysis of atmospheric methane in urban and suburban areas: Fossil and non-fossil methane from local sources. *Atmos. Environ.* 32(17), 2947–2955. doi:10.1016/S1352-2310(98)00014-4.
- Naegler, T., Levin, I., 2009. Biosphere-atmosphere gross carbon exchange flux and the  $\delta^{13}\text{C}$  and  $\Delta^{14}\text{C}$  disequilibria constrained by the biospheric excess radiocarbon inventory. *J. Geophys. Res.* 114(D17), D17303. doi:10.1029/2008JD011116.
- Naegler, T., Levin, I., 2006. Closing the global radiocarbon budget 1945–2005. *J. Geophys. Res.* 111, D12311. doi:10.1029/2005JD006758.
- Neef, L., Van Weele, M., Van Velthoven, P., 2010. Optimal estimation of the present-day global methane budget. *Global Biogeochem. Cycles* 24, GB4024. doi:10.1029/2009GB003661.
- Némec, M., Wacker, L., Gäggeler, H., 2010. Optimization of the graphitization process at AGE-1. *Radiocarbon* 52(2–3), 1380–1393. doi:10.1017/S0033822200046464.
- Nisbet, E., Weiss, R., 2010. Top-Down Versus Bottom-Up. *Science* 328(5983), 1241–1243. doi:10.1126/science.1189936.
- Nisbet, E.G., Dlugokencky, E.J., Bousquet, P., 2014. Methane on the Rise—Again. *Science* 343(6170), 493–495. doi:10.1126/science.1247828.
- Nisbet, E.G., Dlugokencky, E.J., Manning, M.R., Lowry, D., Fisher, R.E., France, J.L., Michel, S.E., Miller, J.B., White, J.W.C., Vaughn, B., Bousquet, P., Pyle, J.A., Warwick, N.J., Cain, M., Brownlow, R., Zazzeri, G., Lanoisellé, M., Manning, A.C., Gloor, E., Worthy, D.E.J., Brunke, E.G., Labuschagne, C., Wolff, E.W., Ganesan, A.L., 2016. Rising atmospheric methane: 2007–2014 growth and isotopic shift. *Global Biogeochem. Cycles* 30(9), 1356–1370. doi:10.1002/2016GB005406.
- Nisbet, E.G., Manning, M.R., Dlugokencky, E.J., Fisher, R.E., Lowry, D., Michel, S.E., Myhre, C.L., Platt, S.M., Allen, G., Bousquet, P., Brownlow, R., Cain, M., France, J.L., Hermansen, O., Hossaini, R., Jones, A.E., Levin, I., Manning, A.C., Myhre, G., Pyle, J.A., Vaughn, B.H., Warwick, N.J., White, J.W.C., 2019. Very Strong Atmospheric Methane Growth in the 4 Years 2014–2017: Implications for the Paris Agreement. *Global Biogeochem. Cycles* 33(3), 318–342. doi:10.1029/2018GB006009.
- Nydal, R., Lövseth, K., 1965. Distribution of Radiocarbon from Nuclear Tests. *Nature* 206(4988), 1029–1031. doi:10.1038/2061029a0.
- Oney, B., Henne, S., Gruber, N., Leuenberger, M., Bamberger, I., Eugster, W., Brunner, D., 2015. The CarboCount CH sites: Characterization of a dense greenhouse gas observation network. *Atmos. Chem. Phys.* 15(19), 11147–11164. doi:10.5194/acp-15-11147-2015.

- Pack, M.A., Xu, X., Lupascu, M., Kessler, J.D., Czimczik, C.I., 2015. A rapid method for preparing low volume CH<sub>4</sub> and CO<sub>2</sub> gas samples for <sup>14</sup>C AMS analysis. *Org. Geochem.* 78, 89–98. doi:10.1016/j.orggeochem.2014.10.010.
- Palonen, V., Uusitalo, J., Seppälä, E., Oinonen, M., 2017. A portable methane sampling system for radiocarbon-based bioportion measurements and environmental CH<sub>4</sub> sourcing studies. *Rev. Sci. Instrum.* 88, 075102. doi:10.1063/1.4993920.
- Palstra, S.W.L., Meijer, H.A.J., 2014. Biogenic Carbon Fraction of Biogas and Natural Gas Fuel Mixtures Determined with <sup>14</sup>C. *Radiocarbon* 56(1), 7–28. doi:10.2458/56.16514.
- Palstra, S.W.L., Meijer, H.A.J., 2010. Carbon-14 based determination of the biogenic fraction of industrial CO<sub>2</sub> emissions – Application and validation. *Bioresour. Technol.* 101(10), 3702–3710. doi:10.1016/j.biortech.2009.12.004.
- Papa, F., Prigent, C., Aires, F., Jimenez, C., Rossow, W.B., Matthews, E., 2010. Interannual variability of surface water extent at the global scale, 1993–2004. *J. Geophys. Res. Atmos.* 115, D12111. doi:10.1029/2009JD012674.
- Petrenko, V. V., Severinghaus, J.P., Brook, E.J., Mühle, J., Headly, M., Harth, C.M., Schaefer, H., Reeh, N., Weiss, R.F., Lowe, D., Smith, A.M., 2008. A novel method for obtaining very large ancient air samples from ablating glacial ice for analyses of methane radiocarbon. *J. Glaciol.* 54(185), 233–244. doi:10.3189/002214308784886135.
- Petrenko, V. V., Smith, A.M., Schaefer, H., Riedel, K., Brook, E., Baggenstos, D., Harth, C., Hua, Q., Buizert, C., Schilt, A., Fain, X., Mitchell, L., Bauska, T., Orsi, A., Weiss, R.F., Severinghaus, J.P., 2017. Minimal geological methane emissions during the Younger Dryas-Preboreal abrupt warming event. *Nature* 548(7668), 443–446. doi:10.1038/nature23316.
- Petrenko, V. V., Smith, A.M., Brailsford, G., Riedel, K., Hua, Q., Lowe, D., Severinghaus, J.P., Levchenko, V., Bromley, T., Moss, R., Mühle, J., Brook, E.J., 2008. A New Method for Analyzing <sup>14</sup>C of Methane in Ancient Air Extracted from Glacial Ice. *Radiocarbon* 50(1), 53–73. doi:10.1017/S0033822200043368.
- Plant, G., Kort, E.A., Floerchinger, C., Gvakharia, A., Vimont, I., Sweeney, C., 2019. Large Fugitive Methane Emissions From Urban Centers Along the U.S. East Coast. *Geophys. Res. Lett.* 46(14), 8500–8507. doi:10.1029/2019gl082635.
- Prather, M.J., Holmes, C.D., Hsu, J., 2012. Reactive greenhouse gas scenarios: Systematic exploration of uncertainties and the role of atmospheric chemistry. *Geophys. Res. Lett.* 39, L09803. doi:10.1029/2012GL051440.
- Quay, P., Stutsman, J., Wilbur, D., Snover, A., Dlugokencky, E., Brown, T., 1999. The isotopic composition of atmospheric methane. *Global Biogeochem. Cycles* 13(2), 445–461. doi:10.1029/1998GB900006.
- Quay, P.D., King, S.L., Stutsman, J., Wilbur, D.O., Steele, L.P., Fung, I., Gammon, R.H., Brown, T.A., Farwell, G.W., Grootes, P.M., Schmidt, F.H., 1991. Carbon isotopic composition of atmospheric CH<sub>4</sub>: Fossil and biomass burning source strengths. *Global Biogeochem. Cycles* 5(1), 25–47. doi:10.1029/91GB00003.

- Rasi, S., Veijanen, A., Rintala, J., 2007. Trace compounds of biogas from different biogas production plants. *Energy* 32(8), 1375–1380. doi:10.1016/j.energy.2006.10.018.
- Ray, G.C., Box, E.O., 1950. Adsorption of Gases on Activated Charcoal. *Ind. Eng. Chem.* 42(7), 1315–1318. doi:10.1021/ie50487a021.
- Reimer, P.J., Austin, W.E.N., Bard, E., Bayliss, A., Blackwell, P.G., Bronk Ramsey, C., Butzin, M., Cheng, H., Edwards, R.L., Friedrich, M., Grootes, P.M., Guilderson, T.P., Hajdas, I., Heaton, T.J., Hogg, A.G., Hughen, K.A., Kromer, B., Manning, S.W., Muscheler, R., Palmer, J.G., Pearson, C., van der Plicht, J., Reimer, R.W., Richards, D.A., Scott, E.M., Southon, J.R., Turney, C.S.M., Wacker, L., Adolphi, F., Büntgen, U., Capano, M., Fahrni, S.M., Fogtmann-Schulz, A., Friedrich, R., Köhler, P., Kudsk, S., Miyake, F., Olsen, J., Reinig, F., Sakamoto, M., Sookdeo, A., Talamo, S., 2020. The IntCal20 Northern Hemisphere Radiocarbon Age Calibration Curve (0–55 cal kBP). *Radiocarbon* 62(4), 725–757. doi:10.1017/RDC.2020.41.
- Reimer, P.J., Baillie, M.G.L., Bard, E., Bayliss, A., Beck, J.W., Bertrand, C.J.H., Blackwell, P.G., Buck, C.E., Burr, G.S., Cutler, K.B., Damon, P.E., Edwards, R.L., Fairbanks, R.G., Friedrich, M., Guilderson, T.P., Hogg, A.G., Hughen, K.A., Kromer, B., 2004. Terrestrial Radiocarbon Age Calibration. *Radiocarbon* 46(3), 1029–1058.
- Reimer, P.J., Bard, E., Bayliss, A., Beck, J.W., Blackwell, P.G., Ramsey, C.B., Buck, C.E., Cheng, H., Edwards, R.L., Friedrich, M., Grootes, P.M., Guilderson, T.P., Haflidason, H., Hajdas, I., Hatté, C., Heaton, T.J., Hoffmann, D.L., Hogg, A.G., Hughen, K.A., Kaiser, K.F., Kromer, B., Manning, S.W., Niu, M., Reimer, R.W., Richards, D.A., Scott, E.M., Southon, J.R., Staff, R.A., Turney, C.S.M., van der Plicht, J., 2013. IntCal13 and Marine13 Radiocarbon Age Calibration Curves 0–50,000 Years cal BP. *Radiocarbon* 55(4), 1869–1887. doi:10.2458/azu\_js\_rc.55.16947.
- Riedmann, R.A., Purtschert, R., 2016. Separation of argon from environmental samples for Ar-37 and Ar-39 analyses. *Sep. Purif. Technol.* 170, 217–223. doi:10.1016/j.seppur.2016.06.017.
- Riedmann, R.A., Purtschert, R., 2011. Natural <sup>37</sup>Ar concentrations in soil air: Implications for monitoring underground nuclear explosions. *Environ. Sci. Technol.* 45(20), 8656–8664. doi:10.1021/es201192u.
- Rigby, M., Montzka, S.A., Prinn, R.G., White, J.W.C., Young, D., O'Doherty, S., Lunt, M.F., Ganesan, A.L., Manning, A.J., Simmonds, P.G., Salameh, P.K., Harth, C.M., Mühle, J., Weiss, R.F., Fraser, P.J., Steele, L.P., Krummel, P.B., McCulloch, A., Park, S., 2017. Role of atmospheric oxidation in recent methane growth. *Proc. Natl. Acad. Sci. U. S. A.* 114(21), 5373–5377. doi:10.1073/pnas.1616426114.
- Riley, W.J., Hsueh, D.Y., Randerson, J.T., Fischer, M.L., Hatch, J.G., Pataki, D.E., Wang, W., Goulden, M.L., 2008. Where do fossil fuel carbon dioxide emissions from California go? An analysis based on radiocarbon observations and an atmospheric transport model. *J. Geophys. Res.* 113, G04002. doi:10.1029/2007JG000625.

- Rinta, P., Bastviken, D., van Hardenbroek, M., Kankaala, P., Leuenberger, M., Schilder, J., Stötter, T., Heiri, O., 2015. An inter-regional assessment of concentrations and  $\delta^{13}\text{C}$  values of methane and dissolved inorganic carbon in small European lakes. *Aquat. Sci.* 77(4), 667–680. doi:10.1007/s00027-015-0410-y.
- Röckmann, T., 1998. Measurement and interpretation of  $^{13}\text{C}$ ,  $^{14}\text{C}$ ,  $^{17}\text{O}$  and  $^{18}\text{O}$  variations in atmospheric carbon monoxide. PhD thesis. *University of Heidelberg, Germany*.
- Röckmann, T., Eyer, S., Van Der Veen, C., Popa, M.E., Tuzson, B., Monteil, G., Houweling, S., Harris, E., Brunner, D., Fischer, H., Zazzeri, G., Lowry, D., Nisbet, E.G., Brand, W.A., Necki, J.M., Emmenegger, L., Mohn, J., 2016. In situ observations of the isotopic composition of methane at the Cabauw tall tower site. *Atmos. Chem. Phys.* 16(16), 10469–10487. doi:10.5194/acp-16-10469-2016.
- Rogelj, J., Den Elzen, M., Höhne, N., Fransen, T., Fekete, H., Winkler, H., Schaeffer, R., Sha, F., Riahi, K., Meinshausen, M., 2016. Paris Agreement climate proposals need a boost to keep warming well below 2 °C. *Nature* 534(7609), 631–639. doi:10.1038/nature18307.
- Ruff, M., Szidat, S., Gäggeler, H.W., Suter, M., Synal, H.A., Wacker, L., 2010. Gaseous radiocarbon measurements of small samples. *Nucl. Instruments Methods Phys. Res. B* 268(7–8), 790–794. doi:10.1016/j.nimb.2009.10.032.
- Ruff, M., Wacker, L., Gäggeler, H.W., Suter, M., Synal, H.-A., Szidat, S., 2007. A Gas Ion Source for Radiocarbon Measurements at 200 kV. *Radiocarbon* 49(2), 307–314. doi:10.1017/S0033822200042235.
- Salazar, G., Zhang, Y.L., Agrios, K., Szidat, S., 2015. Development of a method for fast and automatic radiocarbon measurement of aerosol samples by online coupling of an elemental analyzer with a MICADAS AMS. *Nucl. Instruments Methods Phys. Res. B* 361, 163–167. doi:10.1016/j.nimb.2015.03.051.
- Sanderson, M.G., 1996. Biomass of termites and their emissions of methane and carbon dioxide: A global database. *Global Biogeochem. Cycles* 10(4), 543–557. doi:10.1029/96GB01893.
- Sapart, C.J., Shakhova, N., Semiletov, I., Jansen, J., Szidat, S., Kosmach, D., Dudarev, O., van der Veen, C., Egger, M., Sergienko, V., Salyuk, A., Tumskey, V., Tison, J.-L., Röckmann, T., 2017. The origin of methane in the East Siberian Arctic Shelf unraveled with triple isotope analysis. *Biogeosciences* 14(9), 2283–2292. doi:10.5194/bg-14-2283-2017.
- Sapart, C.J., Van Der Veen, C., Vigano, I., Brass, M., Van De Wal, R.S.W., Bock, M., Fischer, H., Sowers, T., Buizert, C., Sperlich, P., Blunier, T., Behrens, M., Schmitt, J., Seth, B., Röckmann, T., 2011. Simultaneous stable isotope analysis of methane and nitrous oxide on ice core samples. *Atmos. Meas. Tech.* 4(12), 2607–2618. doi:10.5194/amt-4-2607-2011.
- Satar, E., Berhanu, T.A., Brunner, D., Henne, S., Leuenberger, M., 2016. Continuous  $\text{CO}_2/\text{CH}_4/\text{CO}$  measurements (2012–2014) at Beromunster tall tower station in Switzerland. *Biogeosciences* 13(9), 2623–2635. doi:10.5194/bg-13-2623-2016.

- Saunio, M., Bousquet, P., Poulter, B., Peregon, A., Ciais, P., Canadell, J.G., Dlugokencky, E.J., Etiope, G., Bastviken, D., Houweling, S., Janssens-Maenhout, G., Tubiello, F.N., Castaldi, S., Jackson, R.B., Alexe, M., Arora, V.K., Beerling, D.J., Bergamaschi, P., Blake, D.R., Brailsford, G., Brovkin, V., Bruhwiler, L., Crevoisier, C., Crill, P., Covey, K., Curry, C., Frankenberg, C., Gedney, N., Höglund-Isaksson, L., Ishizawa, M., Ito, A., Joos, F., Kim, H.-S., Kleinen, T., Krummel, P., Lamarque, J.-F., Langenfelds, R., Locatelli, R., Machida, T., Maksyutov, S., McDonald, K.C., Marshall, J., Melton, J.R., Morino, I., Naik, V., O&apos;Doherty, S., Parmentier, F.-J.W., Patra, P.K., Peng, C., Peng, S., Peters, G.P., Pison, I., Prigent, C., Prinn, R., Ramonet, M., Riley, W.J., Saito, M., Santini, M., Schroeder, R., Simpson, I.J., Spahni, R., Steele, P., Takizawa, A., Thornton, B.F., Tian, H., Tohjima, Y., Viovy, N., Voulgarakis, A., van Weele, M., van der Werf, G.R., Weiss, R., Wiedinmyer, C., Wilton, D.J., Wiltshire, A., Worthy, D., Wunch, D., Xu, X., Yoshida, Y., Zhang, B., Zhang, Z., Zhu, Q., 2016. The global methane budget 2000–2012. *Earth Syst. Sci. Data* 8(2), 697–751. doi:10.5194/essd-8-697-2016.
- Schaefer, H., Fletcher, S.E.M., Veidt, C., Lassey, K.R., Brailsford, G.W., Bromley, T.M., Dlugokencky, E.J., Michel, S.E., Miller, J.B., Levin, I., Lowe, D.C., Martin, R.J., Vaughn, B.H., White, J.W.C., 2016. A 21st-century shift from fossil-fuel to biogenic methane emissions indicated by <sup>13</sup>CH<sub>4</sub>. *Science* 352(6281), 80–84. doi:10.1126/science.aad2705.
- Schmitt, J., Seth, B., Bock, M., Van Der Veen, C., Möller, L., Sapart, C.J., Prokopiou, M., Sowers, T., Röckmann, T., Fischer, H., 2013. On the interference of Kr during carbon isotope analysis of methane using continuous-flow combustion-isotope ratio mass spectrometry. *Atmos. Meas. Tech.* 6(5), 1425–1445. doi:10.5194/amt-6-1425-2013.
- Schneider Von Deimling, T., Meinshausen, M., Levermann, A., Huber, V., Frieler, K., Lawrence, D.M., Brovkin, V., 2012. Estimating the near-surface permafrost-carbon feedback on global warming. *Biogeosciences* 9(2), 649–665. doi:10.5194/bg-9-649-2012.
- Schoell, M., 1988. Multiple origins of methane in the Earth. *Chem. Geol.* 71(1–3), 1–10. doi:10.1016/0009-2541(88)90101-5.
- Schulze-König, T., 2010. Advancements in biomedical radiocarbon mass spectrometry. PhD thesis. *ETH Zürich, Switzerland*. doi:10.3929/ethz-a-006226428.
- Schuur, E.A.G., Druffel, E.R.M., Trumbore, S.E., 2016. Radiocarbon and Climate Change. *Springer International Publishing*. doi:10.1007/978-3-319-25643-6.
- Schuur, E.A.G., McGuire, A.D., Schädel, C., Grosse, G., Harden, J.W., Hayes, D.J., Hugelius, G., Koven, C.D., Kuhry, P., Lawrence, D.M., Natali, S.M., Olefeldt, D., Romanovsky, V.E., Schaefer, K., Turetsky, M.R., Treat, C.C., Vonk, J.E., 2015. Climate change and the permafrost carbon feedback. *Nature* 520(7546), 171–179. doi:10.1038/nature14338.
- Schwietzke, S., Griffin, W.M., Matthews, H.S., Bruhwiler, L.M.P., 2014. Global bottom-up fossil fuel fugitive methane and ethane emissions inventory for atmospheric modeling. *ACS Sustain. Chem. Eng.* 2(8), 1992–2001. doi:10.1021/sc500163h.

- Schwietzke, S., Sherwood, O.A., Bruhwiler, L.M.P., Miller, J.B., Etiope, G., Dlugokencky, E.J., Michel, S.E., Arling, V.A., Vaughn, B.H., White, J.W.C., Tans, P.P., 2016. Upward revision of global fossil fuel methane emissions based on isotope database. *Nature* 538(7623), 88–91. doi:10.1038/nature19797.
- SFOE, 2019. Schweizerische Elektrizitätsstatistik 2018, Swiss Federal Office of Energy. Bern.
- Sherwood, O.A., Schwietzke, S., Arling, V.A., Etiope, G., 2017. Global Inventory of Gas Geochemistry Data from Fossil Fuel, Microbial and Burning Sources, version 2017. *Earth Syst. Sci. Data* 9(2), 639–656. doi:10.5194/essd-9-639-2017.
- Shindell, D., Kuylenstierna, J.C.I., Vignati, E., Van Dingenen, R., Amann, M., Klimont, Z., Anenberg, S.C., Muller, N., Janssens-Maenhout, G., Raes, F., Schwartz, J., Faluvegi, G., Pozzoli, L., Kupiainen, K., Höglund-Isaksson, L., Emberson, L., Streets, D., Ramanathan, V., Hicks, K., Oanh, N.T.K., Milly, G., Williams, M., Demkine, V., Fowler, D., 2012. Simultaneously mitigating near-term climate change and improving human health and food security. *Science* 335(6065), 183–189. doi:10.1126/science.1210026.
- Simpson, I.J., Andersen, M.P.S., Meinardi, S., Bruhwiler, L., Blake, N.J., Helmig, D., Sherwood Rowland, F., Blake, D.R., 2012. Long-term decline of global atmospheric ethane concentrations and implications for methane. *Nature* 488(7412), 490–494. doi:10.1038/nature11342.
- Solomon, S., Rosenlof, K.H., Portmann, R.W., Daniel, J.S., Davis, S.M., Sanford, T.J., Plattner, G.K., 2010. Contributions of stratospheric water vapor to decadal changes in the rate of global warming. *Science* 327(5970), 1219–1223. doi:10.1126/science.1182488.
- Sparrow, K.J., Kessler, J.D., 2017. Efficient collection and preparation of methane from low concentration waters for natural abundance radiocarbon analysis. *Limnol. Oceanogr. Methods* 15(7), 601–617. doi:10.1002/lom3.10184.
- Stadtman, T.C., 1967. Methane Fermentation. *Annu. Rev. Microbiol.* 21(1), 121–142. doi:10.1146/annurev.mi.21.100167.001005.
- Stenström, K., Erlandsson, B., Hellborg, R., Håkansson, K., Skog, G., Wiebert, A., 1993. Development of a method to measure the concentration of  $^{14}\text{C}$  in the stack air of nuclear power plants by accelerator mass spectrometry (AMS), Internal Report LJNFD6/(NFFR-3061 )/1 -31/(1993). Lund.
- Stenström, Kristina, Erlandsson, B., Hellborg, R., Wiebert, A., 1995.  $^{14}\text{CO}_2$  and total airborne  $^{14}\text{C}$  releases from a PWR and a BWR at Ringhals nuclear power plant measured with accelerator mass spectrometry, Internal Report NEI-SE--219. Lund.
- Stenström, K., Erlandsson, B., Hellborg, R., Wiebert, A., Skog, G., 1996. Environmental levels of carbon-14 around a Swedish nuclear power plant measured with accelerator mass spectrometry. *Nucl. Instruments Methods Phys. Res. B* 113(1–4), 474–476. doi:10.1016/0168-583X(95)01379-2.

- Stenström, K., Erlandsson, B., Hellborg, R., Wiebert, A., Skog, S., Vesanen, R., Alpsten, M., Bjurman, B., 1995. A one-year study of the total air-borne  $^{14}\text{C}$  effluents from two Swedish light-water reactors, one boiling water- and one pressurized water reactor. *J. Radioanal. Nucl. Chem. Artic.* 198(1), 203–213. doi:10.1007/BF02038258.
- Stenström, K.E., Skog, G., Georgiadou, E., Genberg, J., Johansson, A., 2011. A guide to radiocarbon units and calculations, Internal Report LUNFD6(NFFR-3111)/1-17/(2011). Lund.
- Stolper, D.A., Martini, A.M., Clog, M., Douglas, P.M., Shusta, S.S., Valentine, D.L., Sessions, A.L., Eiler, J.M., 2015. Distinguishing and understanding thermogenic and biogenic sources of methane using multiply substituted isotopologues. *Geochim. Cosmochim. Acta* 161, 219–247. doi:10.1016/j.gca.2015.04.015.
- Streets, D.G., Canty, T., Carmichael, G.R., De Foy, B., Dickerson, R.R., Duncan, B.N., Edwards, D.P., Haynes, J.A., Henze, D.K., Houyoux, M.R., Jacob, D.J., Krotkov, N.A., Lamsal, L.N., Liu, Y., Lu, Z., Martin, R. V., Pfister, G.G., Pinder, R.W., Salawitch, R.J., Wecht, K.J., 2013. Emissions estimation from satellite retrievals: A review of current capability. *Atmos. Environ.* 77, 1011–1042. doi:10.1016/j.atmosenv.2013.05.051.
- Stuiver, M., 1983. International Agreements and the Use of the New Oxalic Acid Standard. *Radiocarbon* 25(2), 793–795. doi:10.1017/S0033822200006159.
- Stuiver, M., Braziunas, T.F., 1998. Anthropogenic and solar components of hemispheric  $^{14}\text{C}$ . *Geophys. Res. Lett.* 25(3), 329–332. doi:10.1029/97GL03694.
- Stuiver, M., Polach, H.A., 1977. Discussion: Reporting of  $^{14}\text{C}$  data. *Radiocarbon* 19(3), 355–363.
- Stuiver, M., Quay, P.D., 1981. Atmospheric  $^{14}\text{C}$  changes resulting from fossil fuel  $\text{CO}_2$  release and cosmic ray flux variability. *Earth Planet. Sci. Lett.* 53(3), 349–362. doi:10.1016/0012-821X(81)90040-6.
- Suess, H.E., 1958. The Radioactivity of the Atmosphere and Hydrosphere. *Annu. Rev. Nucl. Sci.* 8(1), 243–256. doi:10.1146/annurev.ns.08.120158.001331.
- Suess, H.E., 1955. Radiocarbon concentration in modern wood. *Science* 122(3166), 415–417. doi:10.1126/science.122.3166.415-a.
- Sun, H., Zhang, J., Ouyang, C., Ren, Z., Li, J., 2018. Computational evaluation of the impact of metal substitution on the  $^{14}\text{CH}_4$  storage in PCN-14 metal-organic frameworks. *Catal. Today* 312, 168–173. doi:10.1016/j.cattod.2018.03.057.
- Světlík, I., Rulík, P., Michálek, V., Tomášková, L., Mizera, J., Molnár, M., Svingor, E., Futó, I., Pintér, T., Rulík, P., Michálek, V., 2006. Determination of  $^{14}\text{C}$  in grab samples of stack air from nuclear power plants, in: LSC 2005, Advances in Liquid Scintillation Spectrometry. *Radiocarbon*, pp. 417–422. doi:10.1007/s10582-006-0517-4.
- Synal, H.A., 2013. Developments in accelerator mass spectrometry. *Int. J. Mass Spectrom.* 349–350(1), 192–202. doi:10.1016/j.ijms.2013.05.008.

- Synal, H.A., Stocker, M., Suter, M., 2007. MICADAS: A new compact radiocarbon AMS system. *Nucl. Instruments Methods Phys. Res. B* 259(1), 7–13. doi:10.1016/j.nimb.2007.01.138.
- Szidat, S., Jenk, T.M., Gäggeler, H.W., Synal, H.-A., Fisseha, R., Baltensperger, U., Kalberer, M., Samburova, V., Wacker, L., Saurer, M., Schwikowski, M., Hajdas, I., 2004. Source Apportionment of Aerosols by  $^{14}\text{C}$  Measurements in Different Carbonaceous Particle Fractions. *Radiocarbon* 46(1), 475–484. doi:10.1017/S0033822200039783.
- Szidat, S., Jenk, T.M., Gäggeler, H.W., Synal, H.A., Hajdas, I., Bonani, G., Saurer, M., 2004. THEODORE, a two-step heating system for the EC/OC determination of radiocarbon ( $^{14}\text{C}$ ) in the environment. *Nucl. Instruments Methods Phys. Res. B* 223–224(SPEC. ISS.), 829–836. doi:10.1016/j.nimb.2004.04.153.
- Szidat, S., Jenk, T.M., Synal, H.A., Kalberer, M., Wacker, L., Hajdas, I., Kasper-Giebl, A., Baltensperger, U., 2006. Contributions of fossil fuel, biomass-burning, and biogenic emissions to carbonaceous aerosols in Zurich as traced by  $^{14}\text{C}$ . *J. Geophys. Res. Atmos.* 111, D07206. doi:10.1029/2005JD006590.
- Szidat, S., Salazar, G.A., Vogel, E., Battaglia, M., Wacker, L., Synal, H.-A., Türler, A., 2014.  $^{14}\text{C}$  Analysis and Sample Preparation at the New Bern Laboratory for the Analysis of Radiocarbon with AMS (LARA). *Radiocarbon* 56(2), 561–566. doi:10.2458/56.17457.
- Tarnocai, C., Canadell, J.G., Schuur, E.A.G., Kuhry, P., Mazhitova, G., Zimov, S., 2009. Soil organic carbon pools in the northern circumpolar permafrost region. *Global Biogeochem. Cycles* 23, GB2023. doi:10.1029/2008GB003327.
- Thornton, B.F., Wik, M., Crill, P.M., 2015. Climate-forced changes in available energy and methane bubbling from subarctic lakes. *Geophys. Res. Lett.* 42(6), 1936–1942. doi:10.1002/2015GL063189.
- Townsend-Small, A., Tyler, S.C., Pataki, D.E., Xu, X., Christensen, L.E., 2012. Isotopic measurements of atmospheric methane in Los Angeles, California, USA: Influence of “fugitive” fossil fuel emissions. *J. Geophys. Res. Atmos.* 117(D7), n/a-n/a. doi:10.1029/2011JD016826.
- Turnbull, J., Rayner, P., Miller, J., Naegler, T., Ciais, P., Cozic, A., 2009. On the use of  $^{14}\text{CO}_2$  as a tracer for fossil fuel  $\text{CO}_2$ : Quantifying uncertainties using an atmospheric transport model. *J. Geophys. Res. Atmos.* 114, D22302. doi:10.1029/2009JD012308.
- Turnbull, J.C., Fletcher, S.E.M., Ansell, I., Brailsford, G.W., Moss, R.C., Norris, M.W., Steinkamp, K., 2017. Sixty years of radiocarbon dioxide measurements at Wellington, New Zealand: 1954–2014. *Atmos. Chem. Phys.* 17(23), 14771–14784. doi:10.5194/acp-17-14771-2017.
- Turnbull, J.C., Karion, A., Davis, K.J., Lauvaux, T., Miles, N.L., Richardson, S.J., Sweeney, C., McKain, K., Lehman, S.J., Gurney, K.R., Patarasuk, R., Liang, J., Shepson, P.B., Heimburger, A., Harvey, R., Whetstone, J., 2019. Synthesis of Urban  $\text{CO}_2$  Emission Estimates from Multiple Methods from the Indianapolis Flux Project (INFLUX). *Environ. Sci. Technol.* 53(1), 287–295. doi:10.1021/acs.est.8b05552.

- Turnbull, J.C., Miller, J.B., Lehman, S.J., Tans, P.P., Sparks, R.J., Southon, J., 2006. Comparison of  $^{14}\text{CO}_2$ , CO, and SF<sub>6</sub> as tracers for recently added fossil fuel CO<sub>2</sub> in the atmosphere and implications for biological CO<sub>2</sub> exchange. *Geophys. Res. Lett.* 33, L01817. doi:10.1029/2005GL024213.
- Turnbull, J.C., Sweeney, C., Karion, A., Newberger, T., Lehman, S.J., Tans, P.P., Davis, K.J., Lauvaux, T., Miles, N.L., Richardson, S.J., Cambaliza, M.O., Shepson, P.B., Gurney, K., Patarasuk, R., Razlivanov, I., 2015. Toward quantification and source sector identification of fossil fuel CO<sub>2</sub> emissions from an urban area: Results from the INFLUX experiment. *J. Geophys. Res. Atmos.* 120(1), 292–312. doi:10.1002/2014JD022555.
- Turner, A.J., Frankenberg, C., Wennberg, P.O., Jacob, D.J., 2017. Ambiguity in the causes for decadal trends in atmospheric methane and hydroxyl. *Proc. Natl. Acad. Sci. U. S. A.* 114(21), 5367–5372. doi:10.1073/pnas.1616020114.
- Tyndall, J., 1861. On the absorption and radiation of heat by gases and vapours, and on the physical connexion of radiation, absorption, and conduction.—The bakerian lecture. *London, Edinburgh, Dublin Philos. Mag. J. Sci.* 22(146), 169–194. doi:10.1080/14786446108643138.
- Uchirin, G., Hertelendi, E., Volent, G., Slavik, O., Morávek, J., Kobal, I., Vokal, B., 1997.  $^{14}\text{C}$  Measurements at PWR-Type Nuclear Power Plants in Three Middle European Countries. *Radiocarbon* 40(1), 439–446. doi:10.1017/S0033822200018324.
- van der Borg, K., Alderliesten, C., de Jong, A.F.M., van den Brink, A., de Haas, A.P., Kersemaekers, H.J.H., Raaymakers, J.E.M.J., 1997. Precision and mass fractionation in  $^{14}\text{C}$  analysis with AMS. *Nucl. Instruments Methods Phys. Res. B* 123(1–4), 97–101. doi:10.1016/S0168-583X(96)00713-6.
- van der Laan-Luijkx, I.T., van der Laan, S., Uglietti, C., Schibig, M.F., Neubert, R.E.M., Meijer, H.A.J., Brand, W.A., Jordan, A., Richter, J.M., Rothe, M., Leuenberger, M.C., 2013. Atmospheric CO<sub>2</sub>,  $\delta(\text{O}_2/\text{N}_2)$  and  $\delta^{13}\text{CO}_2$  measurements at Jungfraujoch, Switzerland: results from a flask sampling intercomparison program. *Atmos. Meas. Tech.* 6(7), 1805–1815. doi:10.5194/amt-6-1805-2013.
- van der Zwaan, B., 2013. The role of nuclear power in mitigating emissions from electricity generation. *Energy Strateg. Rev.* 1(4), 296–301. doi:10.1016/j.esr.2012.12.008.
- Vogel, F.R., Hammer, S., Steinhof, A., Kromer, B., Levin, I., 2010. Implication of weekly and diurnal  $^{14}\text{C}$  calibration on hourly estimates of CO<sub>2</sub>-based fossil fuel CO<sub>2</sub> at a moderately polluted site in southwestern Germany. *Tellus, Ser. B Chem. Phys. Meteorol.* 62(5), 512–520. doi:10.1111/j.1600-0889.2010.00477.x.
- Vogel, F.R., Levin, I., Worthy, D.E.J., 2013. Implications for Deriving Regional Fossil Fuel CO<sub>2</sub> Estimates from Atmospheric Observations in a Hot Spot of Nuclear Power Plant  $^{14}\text{CO}_2$  Emissions. *Radiocarbon* 55(2–3), 1556–1572. doi:10.1017/s0033822200048487.
- Wacker, L., Christl, M., Synal, H.A., 2010a. Bats: A new tool for AMS data reduction. *Nucl. Instruments Methods Phys. Res. B* 268(7–8), 976–979. doi:10.1016/j.nimb.2009.10.078.

- Wacker, L., Fahrni, S.M., Hajdas, I., Molnar, M., Synal, H.A., Szidat, S., Zhang, Y.L., 2013. A versatile gas interface for routine radiocarbon analysis with a gas ion source. *Nucl. Instruments Methods Phys. Res. B* 294, 315–319. doi:10.1016/j.nimb.2012.02.009.
- Wacker, L., Němec, M., Bourquin, J., 2010b. A revolutionary graphitisation system: Fully automated, compact and simple. *Nucl. Instruments Methods Phys. Res. B* 268(7–8), 931–934. doi:10.1016/j.nimb.2009.10.067.
- Wahlen, M., 1993. The global methane cycle. *Annu. Rev. Earth Planet. Sci.* 21, 407–426. doi:10.1146/annurev.ea.21.050193.002203.
- Wahlen, M., Tanaka, N., Henry, R., Deck, B., Zeglen, J., Vogel, J.S., Southon, J., Shemesh, A., Fairbanks, R., Broecker, W., 1989. Carbon-14 in methane sources and in atmospheric methane: The contribution from fossil carbon. *Science* 245(4915), 286–290. doi:10.1126/science.245.4915.286.
- Walter, K.M., Chanton, J.P., Chapin, F.S., Schuur, E.A.G., Zimov, S.A., 2008. Methane production and bubble emissions from arctic lakes: Isotopic implications for source pathways and ages. *J. Geophys. Res. Biogeosciences* 113, G00A08. doi:10.1029/2007JG000569.
- Walter, K.M., Smith, L.C., Chapin, F.S., 2007. Methane bubbling from northern lakes: Present and future contributions to the global methane budget. *Philos. Trans. R. Soc. A Math. Phys. Eng. Sci.* 365(1856), 1657–1676. doi:10.1098/rsta.2007.2036.
- Walter, K.M., Vas, D.A., Brosius, L., Chapin, F.S., Zimov, S.A., Zhuang, Q., 2010. Estimating methane emissions from northern lakes using ice-bubble surveys. *Limnol. Oceanogr. Methods* 8(11), 592–609. doi:10.4319/lom.2010.8.0592.
- Walter, K.M., Zimov, S.A., Chanton, J.P., Verbyla, D., Chapin, F.S., 2006. Methane bubbling from Siberian thaw lakes as a positive feedback to climate warming. *Nature* 443(7107), 71–75. doi:10.1038/nature05040.
- Warwick, N.J., Bekki, S., Law, K.S., Nisbet, E.G., Pyle, J.A., 2002. The impact of meteorology on the interannual growth rate of atmospheric methane. *Geophys. Res. Lett.* 29(20), 1947. doi:10.1029/2002gl015282.
- Weiland, P., 2010. Biogas production: Current state and perspectives. *Appl. Microbiol. Biotechnol.* 85(4), 849–860. doi:10.1007/s00253-009-2246-7.
- Wenger, A., Pugsley, K., O’Doherty, S., Rigby, M., Manning, A.J., Lunt, M.F., White, E.D., 2019. Atmospheric radiocarbon measurements to quantify CO<sub>2</sub> emissions in the UK from 2014 to 2015. *Atmos. Chem. Phys.* 19(22), 14057–14070. doi:10.5194/acp-19-14057-2019.
- Whiticar, M.J., 1999. Carbon and hydrogen isotope systematics of bacterial formation and oxidation of methane. *Chem. Geol.* 161(1), 291–314. doi:10.1016/S0009-2541(99)00092-3.
- Winckler, G., Aeschbach-Hertig, W., Holocher, J., Kipfer, R., Levin, I., Poss, C., Rehder, G., Suess, E., Schlosser, P., 2002. Noble gases and radiocarbon in natural gas hydrates. *Geophys. Res. Lett.* 29, 1423. doi:10.1029/2001GL014013.

- Wu, H., Simmons, J.M., Liu, Y., Brown, C.M., Wang, X. Sen, Shengqian, M., Peterson, V.K., Southon, P.D., Kepert, C.J., Zhou, H.C., Yildirim, T., Zhou, W., 2010. Metal-organic frameworks with exceptionally high methane uptake: Where and how is methane stored? *Chem. - A Eur. J.* 16(17), 5205–5214. doi:10.1002/chem.200902719.
- Yim, M.-S., Caron, F., 2006. Life cycle and management of carbon-14 from nuclear power generation. *Prog. Nucl. Energy* 48(1), 2–36. doi:10.1016/j.pnucene.2005.04.002.
- Zazzeri, G., Yeomans, E.A., Graven, H.D., 2018. Global and regional emissions of radiocarbon from nuclear power plants from 1972 to 2016. *Radiocarbon* 60(4), 1068–1081. doi:10.1017/RDC.2018.42.
- Zeebe, R., Wolf-Gladrow, D., 2001. CO<sub>2</sub> in Seawater: Equilibrium, Kinetics, Isotopes. *Elsevier Oceanography Series 65, Elsevier*.
- Zhang, B., Chen, G.Q., 2014. China's CH<sub>4</sub> and CO<sub>2</sub> emissions: Bottom-up estimation and comparative analysis. *Ecol. Indic.* 47, 112–122. doi:10.1016/j.ecolind.2014.01.022.
- Zhang, T., Barry, R.G., Knowles, K., Heginbottom, J.A., Brown, J., 2008. Statistics and characteristics of permafrost and ground-ice distribution in the Northern Hemisphere. *Polar Geogr.* 31(1–2), 47–68. doi:10.1080/10889370802175895.
- Zhang, Y., Ren, H., Sun, Y., Cao, F., Chang, Y., Liu, S., Lee, X., Agrios, K., Kawamura, K., Liu, D., Ren, L., Du, W., Wang, Z., Prévôt, A.S.H., Szidat, S., Fu, P., 2017. High Contribution of Nonfossil Sources to Submicrometer Organic Aerosols in Beijing, China. *Environ. Sci. Technol.* 51(14), 7842–7852. doi:10.1021/acs.est.7b01517.
- Zimov, S.A., Voropaev, Y. V., Semiletov, I.P., Davidov, S.P., Prosiannikov, S.F., Chapin, F.S., Chapin III, M.C., Trumbore, S., Tyler, S., 1997. North Siberian Lakes: A Methane Source Fueled by Pleistocene Carbon. *Science* 277(5327), 800–802. doi:10.1126/science.277.5327.800.
- Zondervan, A., Meijer, H.A.J., 1996. Isotopic characterisation of CO<sub>2</sub> sources during regional pollution events using isotopic and radiocarbon analysis. *Tellus B* 48(4), 601–612. doi:10.1034/j.1600-0889.1996.00013.x.
- Zyakun, A.M., Muravyev, A.I., Baskunov, B.P., Laurinavichius, K.S., Zakharchenko, V.N., Peshenko, V.P., Lykov, I.N., Shestakova, G.A., 2010. Estimation of microbial methane generation and oxidation rates in the municipal solid waste landfill of Kaluga city, Russia. *Isotopes Environ. Health Stud.* 46(1), 78–90. doi:10.1080/10256010903388527.

# 8. Appendices

## 8.1 Detailed performance parameters of the MPPS

The data presented here refer to the individual measurements used to assess the averaged performance parameters of the MPPS, which are summarized in Table 2.1.

### Constant contamination

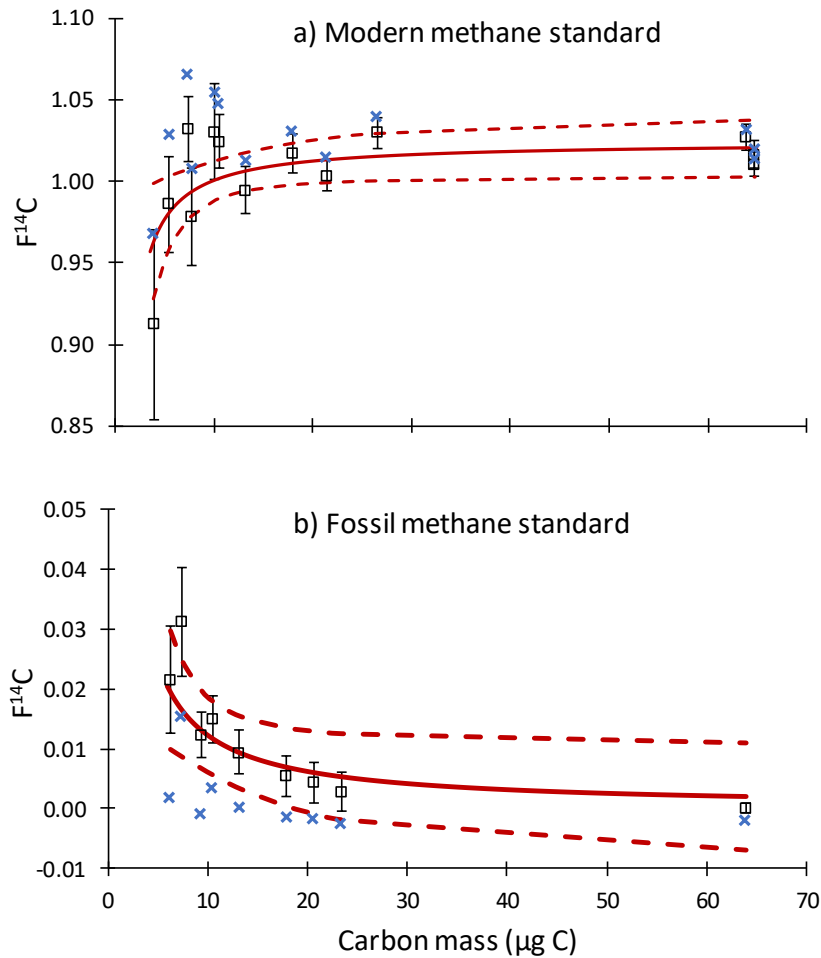


Figure 8.1 Constant contamination of the MPPS (procedural blank). Black open squares: measured  $F^{14}\text{C}$  values with  $1\sigma$  uncertainties. Red lines: Statistical “drift” model, including  $1\sigma$  confidence bands (dashed red lines). Blue crosses: corrected  $F^{14}\text{C}$  values, using the drift model.

## Cross contamination

The contamination from the previous sample ( $\phi$ ), deduced from the successive  $^{14}\text{C}$  measurements of modern and fossil methane samples processed through the MPPS, is evaluated using a simple mass balance equation:

$$\phi = \frac{m_{b1}}{m_s} \cdot \frac{R_{b1} - R_{b2}}{R_s}$$

With  $(m_s, R_s)$ ,  $(m_{b1}, R_{b1})$  and  $(m_{b2}, R_{b2})$  the carbon masses and  $F^{14}\text{C}$  values of the modern sample, the first blank and the second blank, respectively.

Table 8.1 Determination of the MPPS cross contamination by successive preconcentration, purification and  $^{14}\text{C}$  measurement of modern and fossil methane samples.

Sample code	Sample type	Material	$^{14}\text{C}$ measured ( $F^{14}\text{C}$ )	Mass ( $\mu\text{g C}$ )
BE-9339.1.1	Modern $\text{CH}_4$	Modern methane standard	$1.016 \pm 0.008$	59.2
BE-9340.1.1	Fossil $\text{CH}_4$	Standard gas mixture	$0.022 \pm 0.004$	19.5
BE-9341.1.1	Fossil $\text{CH}_4$	Standard gas mixture	$0.011 \pm 0.004$	18.7
BE-9342.1.1	Modern $\text{CH}_4$	Modern methane standard	$1.010 \pm 0.008$	59.2
BE-9343.1.1	Fossil $\text{CH}_4$	Standard gas mixture	$0.022 \pm 0.004$	20.3
BE-9344.1.1	Fossil $\text{CH}_4$	Standard gas mixture	$0.011 \pm 0.003$	18.7

## Repeatability and accuracy

Table 8.2 System repeatability and accuracy for the  $^{14}\text{C}$  measurements of atmospheric methane samples, which have been preconcentrated and purified using the MPPS.

Sample code	Sample type	Material	$^{14}\text{C}$ measured ( $F^{14}\text{C}$ )	Mass ( $\mu\text{g C}$ )
BE-9307.1.1	Atmospheric $\text{CH}_4$	Pressurized air sample	$1.544 \pm 0.014$	66.6
BE-9308.1.1	Atmospheric $\text{CH}_4$	Pressurized air sample	$1.535 \pm 0.012$	70.5
BE-9345.1.1	Atmospheric $\text{CH}_4$	Pressurized air sample	$1.538 \pm 0.012$	69.3
BE-9346.1.1	Atmospheric $\text{CH}_4$	Pressurized air sample	$1.547 \pm 0.011$	70.5
BE-9347.1.1	Atmospheric $\text{CH}_4$	Pressurized air sample	$1.522 \pm 0.011$	70.5
BE-9348.1.1	Atmospheric $\text{CH}_4$	Pressurized air sample	$1.549 \pm 0.011$	71.7
BE-9322.1.1	Modern $\text{CH}_4$	Modern methane standard	$1.011 \pm 0.008$	64.7
BE-9323.1.1	Modern $\text{CH}_4$	Modern methane standard	$1.016 \pm 0.008$	64.7
BE-9324.1.1	Modern $\text{CH}_4$	Modern methane standard	$1.027 \pm 0.008$	63.9

## Yield

Table 8.3 Methane yield of individual air samples preconcentrated and purified using the MPPS. The samples were collected in 200 L Al bags at the Beromünster tall tower, Switzerland. During each sample collection, the  $CH_4$  mole fraction was measured with a PICARRO gas analyzer and used to infer the theoretical amount of  $CH_4$  injected into the MPPS. The  $CH_4$  yield of individual samples is finally calculated by comparing the amount of  $CH_4$ -derived  $CO_2$  recovered into a glass ampoule to the original amount of  $CH_4$  processed through the setup.

Sampling date	Original $CH_4$ ( $\mu\text{g C}$ )	$CH_4$ -derived $CO_2$ ( $\mu\text{g C}$ )	$CH_4$ yield (%)
26.07.2018	63.8	65.8	103.5
08.08.2018	63.9	63.9	100.3
23.08.2018	65.3	65.8	101.0
06.09.2018	67.0	66.6	99.8
20.09.2018	65.6	65.4	100.0
04.10.2018	66.4	67.8	102.5
18.10.2018	69.2	69.3	100.5
01.11.2018	64.4	65.8	102.5
15.11.2018	68.2	67.8	99.7
29.11.2018	63.0	64.7	103.1
27.12.2018	62.5	61.9	99.3
10.01.2019	66.4	66.6	100.6
07.02.2019	63.8	64.7	101.8
21.02.2019	62.8	63.9	102.2

## 8.2 $\Delta^{14}\text{CH}_4$ and $\Delta^{14}\text{CO}_2$ at Beromünster, Bern and Jungfrauoch

Table 8.4  $\Delta^{14}\text{CH}_4$  measurements at Beromünster, Bern and Jungfrauoch. Results are corrected for constant contamination ( $0.35 \pm 0.10 \mu\text{g C}$  with an  $F^{14}\text{C}$  of  $0.35 \pm 0.18$ ) and cross contamination ( $0.4 \pm 0.2\%$ ). The reported uncertainties ( $1\sigma$ ) include sample pretreatment and AMS measurement.

Collection date	Beromünster		Bern		Jungfrauoch	
	Sample ID	$\Delta^{14}\text{CH}_4$ (‰)	Sample ID	$\Delta^{14}\text{CH}_4$ (‰)	Sample ID	$\Delta^{14}\text{CH}_4$ (‰)
26.07.2018	BE-9666	$344 \pm 11$				
08.08.2018	BE-9667	$396 \pm 12$				
23.08.2018	BE-9668	$371 \pm 12$				
06.09.2018	BE-9669	$477 \pm 12$				
20.09.2018	BE-9670	$441 \pm 12$				
04.10.2018	BE-9672	$366 \pm 12$				
18.10.2018	BE-9673	$332 \pm 12$	BE-9663	$344 \pm 13$		
01.11.2018	BE-9674	$398 \pm 12$	BE-9671	$392 \pm 12$		
15.11.2018	BE-10257	$319 \pm 12$	BE-10255	$334 \pm 13$		
29.11.2018	BE-10258	$368 \pm 12$	BE-10256	$330 \pm 12$		
13.12.2018	BE-10263	$395 \pm 12$	BE-10259	$335 \pm 12$	BE-10260 <sup>a</sup>	$348 \pm 12$
27.12.2018	BE-10264	$355 \pm 12$				
10.01.2019	BE-10265	$1063 \pm 16$	BE-10261 <sup>b</sup>	$422 \pm 12$	BE-10262	$354 \pm 12$
24.01.2019	BE-10269	$2984 \pm 29$	BE-10267 <sup>b</sup>	$468 \pm 11$	BE-10268	$364 \pm 12$
07.02.2019	BE-10563	$386 \pm 10$	BE-10561 <sup>b</sup>	$324 \pm 10$	BE-10562	$333 \pm 10$
21.02.2019	BE-10566	$358 \pm 10$	BE-10564 <sup>b</sup>	$313 \pm 10$	BE-10565	$327 \pm 10$
06.03.2019	BE-10569	$338 \pm 10$	BE-10567 <sup>b</sup>	$383 \pm 10$	BE-10568 <sup>b</sup>	$351 \pm 10$
21.03.2019	BE-10674	$601 \pm 11$	BE-10683	$507 \pm 10$	BE-10664	$344 \pm 10$

Table 8.4 (continued)

Collection date	Beromünster		Bern		Jungfrauoch	
	Sample ID	$\Delta^{14}\text{CH}_4$ (‰)	Sample ID	$\Delta^{14}\text{CH}_4$ (‰)	Sample ID	$\Delta^{14}\text{CH}_4$ (‰)
04.04.2019	BE-10688	385 ± 10	BE-10686 <sup>b</sup>	342 ± 10	BE-10687	359 ± 10
18.04.2019	BE-10904	421 ± 12	BE-10902 <sup>a</sup>	358 ± 11	BE-10903	348 ± 11
02.05.2019	BE-10907	449 ± 12	BE-10905 <sup>b</sup>	369 ± 11	BE-10906	346 ± 11
16.05.2019	BE-10910	360 ± 12	BE-10908 <sup>b</sup>	342 ± 11	BE-10909	363 ± 11
29.05.2019	BE-11106	1065 ± 15	BE-11104 <sup>c</sup>	349 ± 11	BE-11105 <sup>b</sup>	350 ± 11
13.06.2019	BE-11153	451 ± 12	BE-11151 <sup>b</sup>	632 ± 13	BE-11152	478 ± 12
27.06.2019	BE-11541	428 ± 11	BE-11539 <sup>b</sup>	582 ± 12	BE-11540	340 ± 11
11.07.2019	BE-11545	375 ± 11	BE-11543 <sup>b</sup>	366 ± 11	BE-11544	357 ± 11
25.07.2019	BE-11548	845 ± 14	BE-11546 <sup>b</sup>	480 ± 11	BE-11547	535 ± 12
08.08.2019	BE-11551	394 ± 11	BE-11549 <sup>b</sup>	348 ± 11	BE-11550	353 ± 11
22.08.2019	BE-12720	420 ± 12	BE-12718 <sup>b</sup>	365 ± 11	BE-12719	369 ± 12
05.09.2019	BE-12723	359 ± 12	BE-12722 <sup>b</sup>	397 ± 12	BE-12721	395 ± 12
19.09.2019	BE-12726	369 ± 12	BE-12725 <sup>b</sup>	362 ± 12	BE-12724	346 ± 12
03.10.2019	BE-12729	407 ± 12	BE-12728 <sup>b</sup>	354 ± 12	BE-12727	383 ± 11
17.10.2019	BE-12733	362 ± 11	BE-12732 <sup>b</sup>	316 ± 12	BE-12730	358 ± 12
31.10.2019	BE-12735	399 ± 12	BE-12736 <sup>b</sup>	450 ± 13	BE-12734	350 ± 12
14.11.2019	BE-12738	355 ± 12	BE-12737 <sup>b</sup>	728 ± 14		

<sup>a</sup> Sample collected one day before the collection date.

<sup>b</sup> Sample collected one day after the collection date.

<sup>c</sup> Sample collected two days after the collection date.

Table 8.5  $\Delta^{14}\text{CO}_2$  measurements at Beromünster, Bern and Jungfrauoch. The AMS measurement uncertainties ( $1\sigma$ ) are reported.

Collection date	Beromünster		Bern		Jungfrauoch	
	Sample ID	$\Delta^{14}\text{CO}_2$ (‰)	Sample ID	$\Delta^{14}\text{CO}_2$ (‰)	Sample ID	$\Delta^{14}\text{CO}_2$ (‰)
23.08.2018	BE-10295	$1.3 \pm 7.4$				
04.10.2018	BE-10298	$-3.4 \pm 7.5$				
01.11.2018	BE-10300	$-5.3 \pm 6.5$				
15.11.2018	BE-10301	$-1.2 \pm 2.8$				
13.12.2018	BE-10232	$-7.2 \pm 2.4$	BE-10303	$-42.4 \pm 7.1$	BE-10302 <sup>a</sup>	$6.4 \pm 2.6$
27.12.2018	BE-10305	$13.4 \pm 3.7$				
10.01.2019	BE-10306	$0.7 \pm 3.7$			BE-10307	$7.5 \pm 3.1$
24.01.2019					BE-10324	$0.6 \pm 2.4$
07.02.2019	BE-10327	$-0.3 \pm 2.4$	BE-10325 <sup>b</sup>	$-40.4 \pm 2.3$	BE-10326	$8.7 \pm 2.4$
21.02.2019	BE-10572	$-3.1 \pm 2.3$	BE-10570 <sup>b</sup>	$-39.4 \pm 2.3$	BE-10571	$-1.6 \pm 2.4$
06.03.2019	BE-10575	$-7.1 \pm 2.4$	BE-10573 <sup>b</sup>	$-7.7 \pm 2.4$	BE-10574 <sup>b</sup>	$-8.7 \pm 2.4$
21.03.2019	BE-10638	$-13.5 \pm 2.3$	BE-10647	$-90.1 \pm 2.1$	BE-10731	$1.1 \pm 2.4$
04.04.2019	BE-10913	$4.6 \pm 2.3$	BE-10911 <sup>b</sup>	$-30.8 \pm 2.3$	BE-10912	$-9.4 \pm 2.3$
18.04.2019	BE-10916	$-18.6 \pm 2.3$	BE-10914 <sup>a</sup>	$-43.0 \pm 2.3$	BE-10915	$-4.1 \pm 2.3$
02.05.2019	BE-10919	$-10.2 \pm 2.3$	BE-10917 <sup>b</sup>	$-32.8 \pm 2.3$	BE-10918	$-2.2 \pm 2.3$
16.05.2019	BE-10922	$-17.0 \pm 2.3$	BE-10920 <sup>b</sup>	$-63.4 \pm 2.2$	BE-10921	$-6.4 \pm 2.3$
29.05.2019	BE-11094	$0.0 \pm 2.2$	BE-11092 <sup>c</sup>	$-22.3 \pm 2.2$	BE-11093 <sup>b</sup>	$-4.4 \pm 2.3$
13.06.2019	BE-11188	$-7.3 \pm 2.2$	BE-11186 <sup>b</sup>	$38.0 \pm 2.3$	BE-11187	$-3.0 \pm 2.3$
27.06.2019	BE-11446	$-11.6 \pm 2.2$	BE-11444 <sup>b</sup>	$-40.0 \pm 2.2$	BE-11445	$0.9 \pm 2.2$

Table 8.5 (continued)

Collection date	Beromünster		Bern		Jungfrauoch	
	Sample ID	$\Delta^{14}\text{CO}_2$ (‰)	Sample ID	$\Delta^{14}\text{CO}_2$ (‰)	Sample ID	$\Delta^{14}\text{CO}_2$ (‰)
11.07.2019	BE-11450	$-8.7 \pm 2.2$	BE-11448 <sup>b</sup>	$-22.3 \pm 2.2$	BE-11449	$-0.2 \pm 2.2$
25.07.2019	BE-11598	$-7.5 \pm 2.3$	BE-11596 <sup>b</sup>	$-10.5 \pm 2.3$	BE-11597	$-4.7 \pm 2.3$
08.08.2019	BE-11601	$-9.8 \pm 2.3$	BE-11599 <sup>b</sup>	$-12.2 \pm 2.3$	BE-11600	$0.4 \pm 2.3$
22.08.2019	BE-11661	$-7.6 \pm 2.3$	BE-11659 <sup>b</sup>	$-40.5 \pm 2.3$	BE-11660	$3.1 \pm 2.3$
05.09.2019	BE-11807	$-0.6 \pm 2.3$	BE-11806 <sup>b</sup>	$-18.5 \pm 2.3$	BE-11805	$0.3 \pm 2.3$
19.09.2019	BE-11810	$4.6 \pm 2.3$	BE-11809 <sup>b</sup>	$-20.4 \pm 2.3$		
03.10.2019	BE-11813	$-3.3 \pm 2.3$	BE-11812 <sup>b</sup>	$-40.0 \pm 2.3$	BE-11811	$2.8 \pm 2.3$
17.10.2019	BE-12754	$0.1 \pm 2.4$	BE-12755 <sup>b</sup>	$-26.4 \pm 2.3$	BE-12753	$-1.4 \pm 2.4$
31.10.2019	BE-12758	$-21.0 \pm 2.3$	BE-12759 <sup>b</sup>	$-62.8 \pm 2.3$	BE-12757	$1.2 \pm 2.3$
14.11.2019	BE-12761	$-3.7 \pm 2.3$	BE-12760 <sup>b</sup>	$-22.7 \pm 2.3$		

<sup>a</sup> Sample collected one day before the collection date.

<sup>b</sup> Sample collected one day after the collection date.

<sup>c</sup> Sample collected two days after the collection date.

Table 8.6  $\Delta^{14}\text{CH}_4$  results from the overnight sampling of atmospheric air.

Collection date / time (UTC)	Beromünster		Bern		Jungfraujoch	
	Sample ID	$\Delta^{14}\text{CH}_4$ (‰)	Sample ID	$\Delta^{14}\text{CH}_4$ (‰)	Sample ID	$\Delta^{14}\text{CH}_4$ (‰)
20.03.2019 / 12:00	BE-10668	661 ± 12	n/a	n/a	BE-10658	341 ± 10
20.03.2019 / 15:00	BE-10669	623 ± 11	BE-10678	568 ± 11	BE-10659	329 ± 10
20.03.2019 / 18:00	BE-10670	570 ± 11	BE-10679	505 ± 11	BE-10660	342 ± 11
20.03.2019 / 21:00	BE-10671	569 ± 11	BE-10680	485 ± 10	BE-10661	346 ± 10
21.03.2019 / 00:00	BE-10672	642 ± 11	BE-10681	497 ± 11	BE-10662	346 ± 10
21.03.2019 / 03:00	BE-10673	595 ± 11	BE-10682	519 ± 11	BE-10663	351 ± 10
21.03.2019 / 06:00	BE-10674	602 ± 11	BE-10683	506 ± 10	BE-10664	343 ± 10
21.03.2019 / 09:00	BE-10675	545 ± 11	BE-10684	537 ± 10	BE-10665	346 ± 11
21.03.2019 / 12:00	BE-10676	558 ± 11	BE-10685	533 ± 11	BE-10666	353 ± 10

Table 8.7  $\Delta^{14}\text{CO}_2$  results from the overnight sampling of atmospheric air.

Collection date / time (UTC)	Beromünster		Bern		Jungfrauoch	
	Sample ID	$\Delta^{14}\text{CO}_2$ (‰)	Sample ID	$\Delta^{14}\text{CO}_2$ (‰)	Sample ID	$\Delta^{14}\text{CO}_2$ (‰)
20.03.2019 / 12:00	BE-10632	$-10.1 \pm 2.3$	n/a	n/a	BE-10623	$-2.1 \pm 2.4$
20.03.2019 / 15:00	BE-10633	$-4.8 \pm 2.4$	BE-10642	$-16.8 \pm 2.3$	BE-10624	$-4.1 \pm 2.4$
20.03.2019 / 18:00	BE-10634	$-11.0 \pm 2.4$	BE-10643	$-37.2 \pm 2.3$	BE-10625	$0.0 \pm 2.4$
20.03.2019 / 21:00	BE-10635	$-9.5 \pm 2.4$	BE-10644	$-25.6 \pm 2.3$	BE-10626	$0.1 \pm 2.4$
21.03.2019 / 00:00	BE-10636	$-13.5 \pm 2.3$	BE-10645	$-30.8 \pm 2.3$	BE-10627	$-4.7 \pm 2.4$
21.03.2019 / 03:00	BE-10637	$-14.1 \pm 2.3$	BE-10646	$-45.8 \pm 2.3$	BE-10628	$0.7 \pm 2.4$
21.03.2019 / 06:00	BE-10638	$-13.5 \pm 2.3$	BE-10647	$-90.1 \pm 2.1$	BE-10731	$1.1 \pm 2.4$
21.03.2019 / 09:00	BE-10639	$-15.8 \pm 2.3$	BE-10648	$-30.4 \pm 2.3$	BE-10629	$4.2 \pm 2.4$
21.03.2019 / 12:00	BE-10640	$-22.6 \pm 2.3$	BE-10649	$-19.1 \pm 2.3$	BE-10630	$1.0 \pm 2.4$

# Acknowledgements

I always thought a PhD project resembles to a marathon. However, I know learned that no matter how long and hard is the way to the finishing line, there is always a final (long-lasting) sprint to overcome. I could never have successfully finished this PhD thesis without the help, support and guidance of many persons. I would therefore like to thank:

Sönke, for giving me the opportunity to carry out this project in your group. I am grateful for your guidance throughout these years and the share of your extended knowledge in the field of radiocarbon analysis. Thank you for your understanding and support when times were hard.

My sincere gratitude goes to Dr. Alfred Bretscher, whose passion for science and commitment to the protection of the environment allowed the funding of the present work through the Dr. Alfred Bretscher Scholarship.

Thomas, thank you so much accepting to be my examiner. I always enjoyed coming to your lab as a Master student, and really appreciate we could keep the collaboration throughout my PhD project.

Markus, for the fruitful collaboration with the air sampling at Beromünster and the provision of  $^{14}\text{CO}_2$  data. Very special thanks to you and the International Foundation High Altitude Research Stations Jungfrauoch and Gornergrat (HFSJG) for giving me the opportunity to collect some atmospheric air samples every second week at the Jungfrauoch Research Station!

Michael L., for our great collaboration in the design and testing of the purification setup. It was undoubtedly a fruitful teamwork!

Michael B., for the help with the building of the setups, the technical advice and teaching on how to assemble a system. We are now experts in steel tubing bending! Thank you also for the help with the graphitization of  $\text{CO}_2$  samples.

Gary, for the support with the AMS measurements and the many scientific discussions we had all over the years.

Dipayan and Carina, for the precious help in the early stages of the development of the preconcentration setup. Thank you also for sending me the charcoal trap and the help with the design of the Russian Doll trap!

Célia, for the great help during all these years... As my former supervisor during my Master, you supported my application for this PhD project and you kept giving me invaluable advice when I was in Switzerland.

Martin, for pointing out my French accent and helping me in its “mitigation”. Our many political discussions were really challenging my poor awareness... Believe me or not, today I have an opinion: you were very helpful for the overnight sampling at Jungfrauoch!

Edith, for the joining the sampling nearby the nuclear power plant, an early Sunday morning! I really appreciated this successful survey! Thank you for not letting the plants in my office die during my vacation!

The former members of the group and colleagues from Andi’s group and the PSI, for all the great moments we had together, over a cup of coffee, a pizza or in the Alps! I will quite for sure forget some of you, so don’t blame an old man please: Benjamin, Chiara, Dimitri, Jogy, Ling, Matthias, Mohamed, Ronnie, Sara, Selina, Severin, Sven, Tabea, ...

Rüdiger, for the collection of air samples at Beromünster and the noble gases measurements.

The custodians of the JFJ Research Station Christine & Ruedi and Joan & Martin. Thanks for all the support, the kind words and the interesting discussions! You work in such a beautiful place!

René, for teaching me how to design and assemble electronic boxes for the displaying and stirring of MFCs and pressure sensors! Your crash course on welding and soldering was invaluable!

Yves, for the participation to the Gösigen sampling and our fruitful technical discussions. Huge thanks for the proofreading! We now both know that MFCs are perfidious and that water vapor is not our friend... Long live the heating guns!

Sanne, for the given opportunity to participate to a laboratory  $^{14}\text{C}$  intercomparison, but also for unveiling another application of the setup.

All the employees from the “Werkstatt”, the “Materialausgabe” and the “Hausdiensts”. You were always very helpful, efficient and generous! Always a kind word or a smile! Merci vilmal!

Finalement mais avant tout, un énorme merci à mes familles belge et suisse pour avoir toujours cru en moi tout au long de ces années ! Le chemin fut long et parsemé d’embûches... Merci de ne m’avoir jamais laissé tomber !

# Declaration of consent

On the basis of Article 18 of the PromR Phil.-nat. 19

Name/First Name: Espic Christophe

Registration Number: 00-809-558

Study program: Climate Sciences

Bachelor       Master       Dissertation

Title of the thesis: Radiocarbon analysis of atmospheric methane: A new setup to unravel regional methane sources

Supervisor: Prof. Dr. Sönke Szidat

I declare herewith that this thesis is my own work and that I have not used any sources other than those stated. I have indicated the adoption of quotations as well as thoughts taken from other authors as such in the thesis. I am aware that the Senate pursuant to Article 36 paragraph 1 litera r of the University Act of September 5th, 1996 and Article 69 of the University Statute of June 7th, 2011 is authorized to revoke the doctoral degree awarded on the basis of this thesis.

For the purposes of evaluation and verification of compliance with the declaration of originality and the regulations governing plagiarism, I hereby grant the University of Bern the right to process my personal data and to perform the acts of use this requires, in particular, to reproduce the written thesis and to store it permanently in a database, and to use said database, or to make said database available, to enable comparison with theses submitted by others.

Braine-le-Château, 12.12.2021

Place/Date

Signature

# Curriculum vitae

Last name	Espic
First name	Christophe
Country of birth	Switzerland
Date of birth	24 June 1981
08/1997 – 06/2000	<b>“High School”</b> , option: paramedic, Gymnase d’Yverdon, Switzerland.
10/2000 – 09/2001	<b>Special Mathematics Course (CMS)</b> , EPFL, Switzerland.
10/2001 – 09/2005	<b>Bachelor in “Electrical and Electronics Engineering”</b> , EPFL, Switzerland.
10/2005 – 03/2007	<b>Master in “Electrical and Electronics Engineering”</b> , specialization: “Signal processing”, EPFL, Switzerland. Master thesis: “ <i>Stabilization of the wavelength of a laser on a sub-Doppler absorption line</i> ”.
07/2007 – 08/2013	<b>Seller</b> in a food store, Belgium
09/2013 – 08/2015	<b>Master in “Environmental Science and Management”</b> , Université Libre de Bruxelles (ULB), Belgium. Master thesis: “ <i>The role of lake ice on methane cycle unraveled by stable isotopes</i> ”
09/2015 – 01/2022	<b>Ph.D. in “Climate Sciences”</b> , University of Bern, Switzerland. Supervisor: Prof. Dr. Sönke Szidat Examinator: Prof. Dr. Thomas Röckmann

## Publications

**Espic, C.**, Liechti, M., Battaglia, M., Paul, D. Röckmann, T., Szidat, S., 2019. Compound-specific radiocarbon analysis of atmospheric methane: A new preconcentration and purification setup. *Radiocarbon* 61(5), 1461-1476.

Sliz, M.U., Hofmann, B.A., Leya, I., **Espic, C.**, Szidat, S., 2020. An update on the performance of the *in situ* <sup>14</sup>C extraction line at the University of Bern. *Radiocarbon* 62(5), 1371–1388.

Wang, Y., Paul, S. M., Jocher, M., **Espic, C.**, Alewell, C., Szidat, S., Leifeld, J., 2021. Soil carbon loss from drained agricultural peatland after coverage with mineral soil. *Science of The Total Environment* 800, 149498.